Towards Transition Metal-Catalyzed Hydration of Olefins; Aquo Ions, and Pyridylphosphine-Platinum and Palladium Complexes

By

YUN XIE

B.Sc. Peking University, 1983

A THESIS SUBMITTED IN PARTIAL FULFILLMENT OF THE

REQUIREMENTS FOR THE DEGREE OF

DOCTOR OF PHILOSOPHY

in

THE FACULTY OF GRADUATE STUDIES

(Department of Chemistry)

We accept this thesis as confirming to the

required standard

THE UNIVERSITY OF BRITISH COLUMBIA

July, 1990

15 1

In presenting this thesis in partial fulfilment of the requirements for an advanced degree at the University of British Columbia, I agree that the Library shall make it freely available for reference and study. I further agree that permission for extensive copying of this thesis for scholarly purposes may be granted by the head of my department or by his or her representatives. It is understood that copying or publication of this thesis for financial gain shall not be allowed without my written permission.

Department of Chemistry

The University of British Columbia
Vancouver, Canada

Date Aug. 23, 90

DE-6 (2/88)

ABSTRACT

This thesis work resulted from an on-going project in this laboratory focusing on the hydration of olefins, using transition metal complexes as catalysts, with the ultimate aim of achieving catalytic asymmetric hydration, for example:

$$(HO_2C)CH{=}CH(CO_2H) \longrightarrow (HO_2C)CH_2\text{-}\overset{*}{C}H(OH)(CO_2H)$$

($\overset{*}{C}$ = chiral carbon atom).

Initially, the hydration of maleic to malic acid, catalyzed by $Cr(H_2O)_6^{3+}$ at 100°C in aqueous solution was studied, including the kinetic dependences on Cr^{3+}, maleic acid and pH. A proposed mechanism involving 1:1 complexes of Cr^{3+} with the maleato and malato monoanions is consistent qualitatively with the kinetic data. This Cr system was, however, ineffective for hydration of prochiral olefins, and the work became a minor component of the thesis and is described in the last chapter.

Emphasis was switched to the study of water-soluble phosphine systems based on Pd and Pt. The major part of this thesis describes the synthesis and characterization, principally by ^1H, $^{31}P\{^1H\}$ and $^{195}Pt\{^1H\}$ NMR spectroscopies, of: square-planar complexes of the type $MX_2(PPh_{3-n}py_n)_2$ (M = Pd, Pt; X = halides; n = 1, 2, 3); the binuclear species $M_2X_2(\mu\text{-}PPh_{3-n}py_n)_2$ (head-to-tail, HT) and $Pt_2I_2(\mu\text{-}PPh_{3-n}py_n)_2$ (head-to-head, HH; n = 1, **10a**, n = 2, **10b** and n = 3, **10c**); and the $Pt(PPh_2py)_3$, **27a**, and $Pt(Ppy_3)_3$, **26c**, complexes. The reactivities of the binuclear complexes toward acetylenes, and the Pt(0) species toward O_2, olefins, HCl and MeI, are also described.

With use of $PPhpy_2$ within the binuclear phosphine-bridged species, the P atom incidentally becomes chiral. The diastereomers of **10b** were isolated and characterized by $^{31}P\{^1H\}$ NMR spectral data.

All the isolated binuclear complexes react in CH_2Cl_2 with dimethylacetylene-dicarboxylate, DMAD, to form an A-frame insertion product. The HH or HT configuration of the precursor is maintained in every case except for **10b** and **10c** which form initially an HH-DMAD adduct that slowly isomerizes to the corresponding HT-DMAD adduct. Detailed

$^{31}P\{^1H\}$ NMR spectroscopic studies show that the presence of a properly positioned pyridyl group promotes the isomerization by forming a detectable chelated P-N intermediate, and that insertion of DMAD precedes chelation.

The reactions of $Pt_2I_2(\mu\text{-}PPh_{3-n}py_n)_2$ (HH) (n = 1, 2, 3) with DMAD in CH_2Cl_2 are kinetically first-order in both [Pt_2] and [DMAD] for the insertion step, and first-order in [Pt_2] and zero-order in [DMAD] for the isomerization step. The activation parameters for the insertion step are consistent with oxidative addition to a binuclear system. A proposed mechanism is fully supported by $^{31}P\{^1H\}$ and $^{195}Pt\{^1H\}$ NMR spectral data.

Complex **26c**, reacts in CH_2Cl_2 or $CDCl_3$ with limited oxygen to give $Pt(Ppy_3)_3(O_2)$, which may contain an end-on superoxo structure as judged by an IR band at 1114 cm^{-1}. Complex **26c**, under 1 atm O_2, forms the 'expected' peroxo species $Pt(Ppy_3)_2O_2$.

Complexes **26c** and **27a**, react with the olefins (maleic anhydride, acrylonitrile, methacrylonitrile and crotonitrile) to give the square-planar species $Pt(PPh_{3-n}py_n)_2(\eta^2\text{-olefin})$. The square-planar geometry infers strong π-back donation from metal to olefin, a state which is probably undesirable for the purpose of olefin activation toward hydration. Indeed, complex $Pt(PPh_2py)_2(\eta^2\text{-maleic anhydride})$, **47a**, shows no olefin hydration product when heated at 80°C in aqueous NaOH solution.

Trans-$Pt(H)Cl(PPh_2py)_2$, **50a**, was prepared from **27a** and gaseous HCl in THF; **50a** in acetone-d_6, reacts with acrylonitrile to give cis-$PtCl(CH_2CH_2CN)(PPh_2py)_2$, but in the presence of aqueous NaOH at 80°C, **50a** was inactive for hydration of acrylonitrile to either β-cyanoethanol or acrylamide.

Table of Contents

CHAPTER THREE: STRUCTURES OF M(II) AND M(I) (M = Pd, Pt) PYRIDYL-PHOSPHINE COMPLEXES AND THEIR SOLUTION CHEMISTRY

CHAPTER FOUR: REACTIVITIES OF THE HEAD-TO-HEAD ISOMERS OF $Pt_2I_2(\mu\text{-}PN_3)_2$ COMPLEXES TOWARD DIMETHYLACETYLENEDICARBOXYLATE AND TOWARD PHOSPHINE

CHAPTER FIVE: PREPARATIONS AND REACTIVITIES OF PYRIDYLPHOSPHINE PLATINUM(0) COMPLEXES

List of Tables

Page

List of Figures

List of Schemes

ABBREVIATIONS AND SYMBOLS

The following list of abbreviations and symbols will be employed in this thesis.

Å	Ångstrom (s) (10^{-10} metre)
A	absorbance
Ar	aryl
aq.	aqueous
anal. calcd.	analysis calculated
atm	atmosphere (1 atm = 760 mmHg)
br	broad, in NMR spectroscopy
^{n}Bu	normal butyl
BINAP	2,2'-bis(diphenylphosphino)-1,1'-dinaphthyl
BPPM	(2S,4S)-N-(tert-butoxycarbonyl)-4-(diphenylphosphino)-2-[(diphenylphosphino)-methyl]pyrrolidine
BPPFOH	1-[(s)-1'2-(diphenylphosphino)ferrocenyl]ethanol
BMPP	benzylmethylphenylphosphine
Ch.	chapter
COD	1,5-cyclooctadiene
cm	centimetre
conc.	concentration
^{o}C	degree Celsius
^{13}C	carbon-13 isotope
^{13}C{^{1}H}	proton broad band decoupled carbon-13 NMR spectroscopy
CAMP	cyclohexylanisolylmethylphosphine
Cy	cyclohexyl
CP	cross polarization in solid state NMR spectroscopy
d	doublet, in NMR spectroscopy

dba	dibenzylideneacetone
DMAD	dimethylacetylenedicarboxylate, ($CH_3OOCC{\equiv}CCOOCH_3$)
DEFM	diethylfumarate, (trans-$C_2H_5OOCCH{=}CHCOOC_2H_5$)
DEMA	diethylmaleate, (cis-$C_2H_5OOCCH{=}CHCOOC_2H_5$)
dppm	bis(diphenylphosphino)methane
dmpm	(dimethylphosphino)methane
DMA·HCl	N, N'-dimethylacetamide hydrochloride
DIOP	4,5-bis[(diphenylphosphino)methyl]-2,2-dimethyl-1,3-dioxolane
e.e	enantiomeric excess
e.u.	entropy unit, cal $mol^{-1}K^{-1}$
en	ethylenediamine
equiv.	equivalent
Eq.	equation
Et	ethyl (C_2H_5-)
Et_2O	diethyl ether
FT	Fourier transform
FA	fumarate dianion
Fig.	figure
g	gram (s)
GC	gas chromatography
HH	head-to-head
HT	head-to-tail
H_2MA	maleic acid
HMA	maleate monoanion
H_2FA	fumaric acid
HFA	fumarate monoanion
H_2mal	malic acid
Hmal	malate monoanion

h	hour (s)
HEDTA	trianion of ethylenediaminetetraacetic acid
Hz	Hertz, cycles per second
$\Delta H^{\neq}$	activation enthalpy
IR	infrared spectroscopy
J	coupling constant
k	rate constant
K	equilibrium constant
k_{obs}	observed rate constant
Kcal	kilocalories
^{o}K	degree Kelvin
lit.	literature
L	ligand, litre(s)
ln	natural logarithm
MA	maleate dianion, or maleic anhydride
mal	malate dianion
M	metal, or molarity (moles per liter)
m.p.	melting point
m	multiplet, in NMR spectroscopy
mg	milligram(s)
mL	milliliter(s)
mmol	millimole(s)
Me	methyl (CH_3-)
MCPBA	m-chloroperbenzoic acid
min	minute(s)
MAS	magic angle spinning in solid state NMR spectroscopy
MPP	methyl propiolate, MeOOCC≡CH
nm	nanometre(s)

NMR	nuclear magnetic resonance spectroscopy
ol	olefin
^{31}P	phosphorus-31 isotope
$^{31}P\{^{1}H\}$	proton broad band decoupled phosphorus NMR spectroscopy
^{195}Pt	platinum-195 isotope
$^{195}Pt\{^{1}H\}$	proton broad band decoupled platinum NMR spectroscopy
Ph	phenyl (C_6H_5-)
i-Pr	iso-propyl
ppm	parts per million
PPh_3	triphenylphosphine
PR_3	trialkylphosphine
py	pyridine
PN_1	2-(diphenylphosphino)pyridine, PPh_2py, $P(C_6H_5)_2(2\text{-}C_5H_4N)$
PN_2	bis(2-pyridyl)phenylphosphine, $PPhpy_2$, $P(C_6H_5)(2\text{-}C_5H_4N)_2$
PN_3	tris(2-pyridyl)phosphine, Ppy_3, $P(2\text{-}C_5H_4N)_3$
PN_n	(2-pyridyl)phosphines
q	quartet, in NMR spectroscopy
ref.	reference
RLi	organolithium
RMgX	Grignard reagent
r.t.	room temperature
r.d.s	rate determining step
sh	shoulder in UV/visible spectroscopy
Sect.	section
$\Delta S^{\neq}$	activation entropy
s	second
t	time, triplet in NMR spectroscopy
temp.	temperature

THF	tetrahydrofuran
TLC	thin layer chromatography
TMS	tetramethylsilane
TCNE	tetracyanoethylene
UV/vis	ultra-violet/visible spectroscopy
λ	wavelength, in nm
μ	bridging coordination mode
ν	wavenumber in infrared (cm^{-1})
ε	extinction coefficient, $M^{-1}cm^{-1}$; or dielectric constant
Λ_M	equivalent molar conductivity ($\Omega^{-1}mol^{-1}cm^2$)
η	hapticity
[ ]	concentration
$\{^1H\}$	proton broad band decoupled

ACKNOWLEDGEMENTS

I wish to thank Professor B. R. James for his guidance and encouragement throughout the preparation of this thesis. I would also like to thank the members of this group for their helpful comments and discussions. Sincere gratitude is due to my husband, Gang, whose encouragement and understanding were a constant support throughout the work.

The CGP Award (1984 -1985) from the State Education Commission of the People's Republic of China is also acknowledged.

Chapter 1

Introduction

1.1. Overview of homogeneous catalysis

Advances in the field of homogeneous catalysis have been particularly impressive since the discovery of the potent alkene hydrogenation catalyst, $RhCl(PPh_3)_3$, by Wilkinson's group in 1965. In spite of the problems in separating the product from the catalyst, homogeneous catalysts are utilized in many important industrial processes, including the Wacker process (oxidation of olefin to aldehyde or ketone), the Oxo process (hydroformylation of olefin), the Monsanto process (carbonylation of methanol), and the Ziegler process (olefin polymerization).[1 - 5] Growing interests in industrial application of homogeneously catalyzed processes have stimulated research in the area called heterogenization of homogeneous catalysts. The approaches toward heterogenization, which are currently under active study, include direct immobilization of homogeneous catalysts on inert supports and application of phase transfer catalysts. In the former approach, the catalyst is attached to an insoluble support (including inorganic supports, such as silica and zeolites, and organic supports, such as organic polymers). In the second approach, a tetraalkylammonium salt, such as benzyltriethylammonium chloride, is used to transport the catalyst to the organic phase and to keep the catalyst in the aqueous phase when the reaction is complete. By either of these approaches, the major disadvantage of product separation in homogeneous catalysis is compensated by the advantages of heterogeneous catalysis. A new generation of catalysts — heterogenized homogeneous catalysts — could have a much wider industrial application and represent a revolutionary progress in the field of catalysis.[6 - 10]

The field of homogeneous catalysis ranges from simple acid-base catalysis to more complicated enzyme catalysis. In this thesis, transition metal catalysts are of interest. The principal reasons why transition metals contribute the essential ingredient in a wide range of catalyst systems are: the bonding ability of transition metal to a catholic choice of ligands, the variability of oxidation states accessible by the transition metals, and the variability of

coordination sites accessible by the ligands. Delicate combinations of ligand steric and electronic effects influence strongly the structure and reactivity of the catalytically active species. Most reactions in homogeneous catalysis using transition metal complexes can be described by virtue of fundamental reactions of coordination and organometallic chemistry. These reactions, including ligand substitution, oxidative addition, reductive elimination and migratory insertion, occur in a logical sequence bringing about the necessary transformation in a catalytic cycle. Each species in the catalytic cycle obeys, in general, the sixteen- or eighteen-electron rule. These species may not all be detected by spectroscopic methods; however, characterization of the detected species often provides valuable information on the mechanism involved. Knowledge of catalytic mechanism is very essential because it will serve as a guide for tailoring a catalyst intentionally to meet the special need of more sophisticated organic synthesis in the research laboratory as well as in the fine chemical industry.[3]

1.2. Objective of this thesis

As one interest of our group is in bleaching and delignification chemistry of pulp, we became aware of the need for developing new chemistry for the bleaching of high-yield pulp (i.e. containing a large amount of lignin fragment* from chemical pulping) because current Cl_2-bleaching processes raise concern in the environment as a result of the formation of toxic chloro-organic materials, and because the sulfite-bleached pulp is prone to re-oxidation by air which leads to yellowing†.[11 - 15] It is certainly of interest to study what olefin hydration would do in regard to reduction of the chromophoric group. If the hydration of the C=C bond could be

*Basic units of lignin (ref. 15).

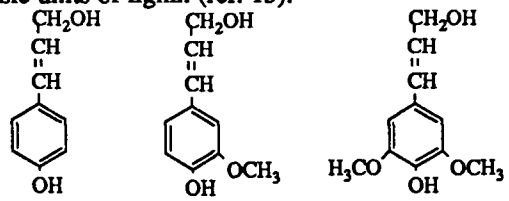

p-coumatyl alcohol | coniferyl alcohol | sinapyl alcohol

†Origin of color: (1) formation of carbonyl-olefinic double bond conjugation; (2) formation of alkali metal complex with chromophoric and auxochromic groups which are the products of oxidation of the phenolic group (ref. 11). The principal objective of pulp bleaching is the reduction or removal of the color constituents (ref. 16).

done catalytically, the chemistry could be useful for the utilization of lignin rich pulp in the paper making industry.

When this work began in 1985, there had been examples in the literature of olefin hydration to give alcohols catalyzed in solution by both non-phosphine or phosphine transition metal complexes. A few examples are presented here, while a more comprehensive coverage is given in Sect. 1.4. Chromium trichloride hexahydrate ($CrCl_3 \cdot 6H_2O$) activates hydration of maleic acid at 170°C.[17] Several α,β-unsaturated nitriles were hydrated using platinum phosphine catalysts in a side-reaction during nitrile hydration to the amide.[18-20] Addition of water to non-activated C=C bonds in 1,3-dienes was catalyzed by a palladium(0) triphenylphosphine complex in the presence of CO_2.[21, 22] Jensen and Trogler later claimed successful direct hydration of the C=C bond in both simple olefins and in α,β-unsaturated nitriles catalyzed by trans-$Pt(H)Cl(PMe_3)_2$,[23] although the reproducibility remains controversial.[24]

The initial objective of this thesis work was to realize catalytic hydration of olefins, particularly activated ones such as fumaric acid, by either non-phosphine or phosphine transition metal complexes. Limited success with some non-phosphine aquo metal ions (Ch. 6) led to the exploration of several pyridylphosphine palladium and platinum complexes (Ch. 3, 4, 5), and indeed the syntheses and characterizations of these pyridylphosphine complexes form the major part of this thesis. Their potential as hydration catalysts of olefins was investigated.

1.3. Alcohol manufacture and synthesis of asymmetric alcohols

Current industrial alcohol manufacturing is largely based on the Oxo process and the aldol process, using ethylene or propene as feedstocks; these processes are catalyzed homogeneously by organometallic complexes.[25] The Oxo process produces straight chain alcohol, while the aldol process gives branched alcohol.

Oxo process:

$$RCH{=}CH_2 + CO + H_2 \xrightarrow{cat.} R(CH_2)_2CHO \xrightarrow{H_2} R(CH_2)_3OH$$

cat. = Co, Rh metal complexes

Aldol process:

$$2CH_3(CH_2)_2CHO \xrightarrow{base} CH_3CH_2CH_2CH{=}\underset{CH_2CH_3}{C}CHO + H_2O$$

$$CH_3CH_2CH_2CH{=}\underset{CH_2CH_3}{C}CHO + 2H_2 \xrightarrow{cat.} CH_3(CH_2)_3\underset{CH_2CH_3}{C}HCH_2OH$$

cat. = Co, Rh, Ru metal complexes

Scheme 1.1. Major processes in industrial alcohol production (ref.25).

Another industrial synthesis of an aliphatic alcohol directly from olefin is via hydration catalyzed by solid phosphoric acid (H_3PO_4) in the vapour phase, the process requiring severe reaction conditions;[26, 27] the corrosion of the reactor, and deactivation of catalyst due to elimination of phosphoric acid during operation, have limited the application of the methods. Research developments in catalytic hydration of olefins on ion-exchanged zeolites (including exchange with metal ions and proton) under mild operating conditions are currently under active investigation by many researchers worldwide and provide a promising alternative to the direct hydration.[28 - 37]

In laboratory organic syntheses, the hydroxyl group can be introduced by either hydroboration or mercuration of alkenes.[38, 39] The anti-Markovnikov alcohol is formed from hydroboration of alkene followed by oxidation of the alkylborane intermediate, as illustrated below:

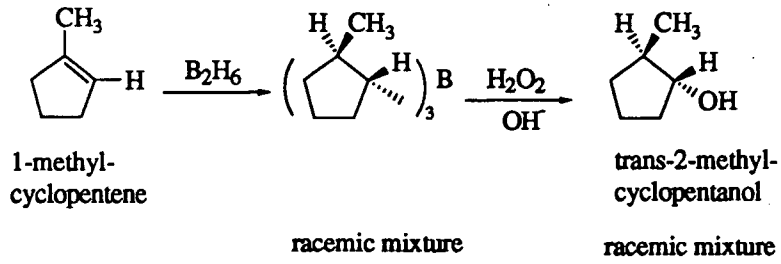

Scheme 1.2. Regioselective synthesis of alcohol via hydroboration of alkene.

The addition of diborane to alkene is rapid and quantitative, while oxidation of alkylborane gives highly regioselective alcohol with the OH situated on the less hindered carbon atom. Use of a modified chiral borane, such as a pinene derivative, gives for example 67-70% e.e of exo-norborneol from norbornene after the oxidation:[39, 40]

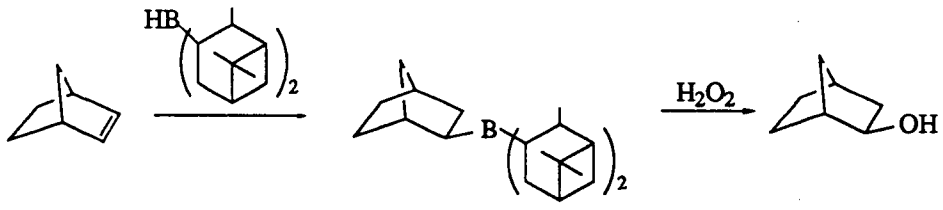

Scheme 1.3. Asymmetric synthesis of an alcohol via a chiral borane (ref.40). The example for asymmetric synthesis of 2-butanol from cis-butene given in ref. 40 appears to be erroneous.

As an alternative to acid-catalyzed hydration of olefins in solution, mercuration of the alkene, followed by sodium borohydride reduction of the intermediate hydroxyalkyl mercuric salt, produces the Markovnikov alcohol with the OH group on the more sterically hindered carbon atom (Scheme 1.4).[38] Asymmetric synthesis of an alcohol using modified mercuric salts is less successful, a tartaric acid complex of mercury(II) giving about 32% e.e in hydration of styrene (Scheme 1.5).[41]

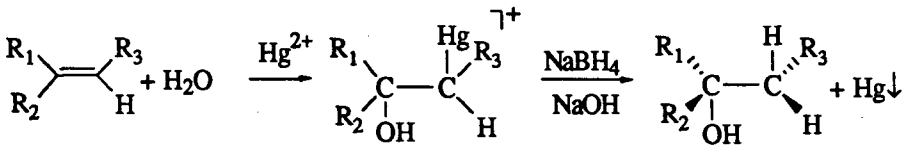

Scheme 1.4. Alcohol formation via mercuration of alkene.

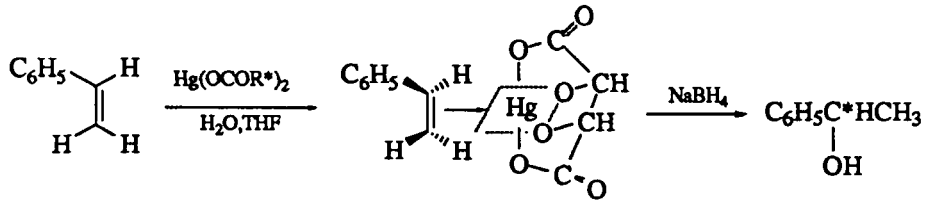

Scheme 1.5. Asymmetric synthesis of alcohol via a carboxylate complex of Hg(II) (ref. 41).

Unfortunately, both the hydroboration and mercuration reactions are stoichiometric and have limited uses in laboratory synthesis, and they are not suitable for industrial scale synthesis. Because of the importance of chiral alcohols in the fine chemical industry, as well as in laboratory synthesis of chiral alcohol ligands for asymmetric induction,[42] asymmetric synthesis of alcohols has been pursued by many research groups using catalytic hydrogenation of ketones[43 - 51] or catalytic hydrosilylation of ketones followed by hydrolysis.[52- 58] Chiral alcohol synthesis with 50% e.e from a prochiral olefin has also been realized via catalytic hydrosilylation of the olefin, followed by stoichiometric oxidation by MCPBA, using dichloro[(R)-N,N-dimethyl-1-[(S)-2-(diphenylphosphino)ferrocenyl]ethylamine]palladium(II) as the hydrosilylation catalyst.[59]

Homogeneous asymmetric hydrogenation of ketones has generally been less fruitful than for the olefinic substrates in terms of enantiomeric excess and the predictability of product configuration. The optical yields of the alcohol products normally range from 5~40% normally; a few ketones that are reduced with over 80% e.e. have a second functionality, such as keto or hydroxyl, at the α or β position capable of interacting with the metal centre, although the chelation has not yet been substantiated during the course of hydrogenation. The best homogeneous catalysts[60] are complexes of rhodium with 1-[(S)-1'2-(diphenylphosphino)ferrocenyl]ethanol (BPPFOH),[49] 4,5-bis[(diphenylphosphino)methyl]-2,2-dimethyl-1,3-dioxolane (DIOP),[50] and (2S,4S)-N-(tert-butoxycarbonyl)-4-(diphenylphosphino)-2-[(diphenylphosphino)methyl]pyrolidine (BPPM),[51] and of ruthenium with 2,2'-bis(diphenylphosphino)-1,1'-dinaphthyl (BINAP).[43] The understanding of specific catalyst-substrate interactions which give rise to the high enantioselectivity is far from clear. On the other hand, asymmetric reduction of ketone via initial hydrosilylation is better understood. Although PtL^*Cl_2 [L*= benzylmethyl-

phenylphosphine, (+)BMPP] was the first catalyst reported to catalyze hydrosilylation of ketonic substrates,[52] rhodium is again found to be the most effective metal, giving higher conversion and asymmetric induction. The optical yield for hydrosilylation of simple ketones is, in general, higher than for the corresponding hydrogenation reaction. The results from many studies show that the steric requirements for a match of the chiral ligand, hydrosilane and ketone are of critical importance for success of the asymmetric induction (Scheme 1.6).

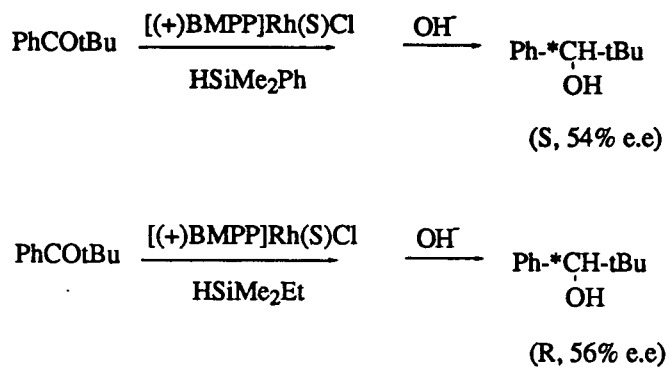

Scheme1.6. Hydrosilylation of a prochiral ketone catalyzed by a Rh complex, S = solvent (ref.58); the importance of matching the ligand, hydrosilane and ketone is demonstrated by the fact that a change of phenyl to ethyl group on the hydrosilane results in a change of the absolute configuration of the major optical isomer.

The catalytic cycle for the asymmetric hydrosilylation of prochiral ketones using Rh complexes involves four basic steps (Scheme 1.7): (a) oxidative addition of hydrosilane to the metal centre, (b) coordination of ketone, (c) insertion of carbonyl into the Si-M bond to form an α-siloxyalkylrhodium hydride, and (d) reductive elimination of the optically active silyl ether.[58, 61] As the stereorelationship of ligand, silane and ketone has become clearer, the enantiomeric excesses have improved; the highest e.e of 97.6% was achieved in the hydrosilylation of acetophenone using a rhodium diamine complex.[55]

The rapid developments in catalytic reduction of ketones via hydrogenation or hydrosilylation have perhaps led to an impediment in research on olefin hydration. Further, despite the great amount of work done in the hydrogenation/hydrosilylation areas, the results are still lacking in certain aspects — the rates for ketone reduction are much slower than those for

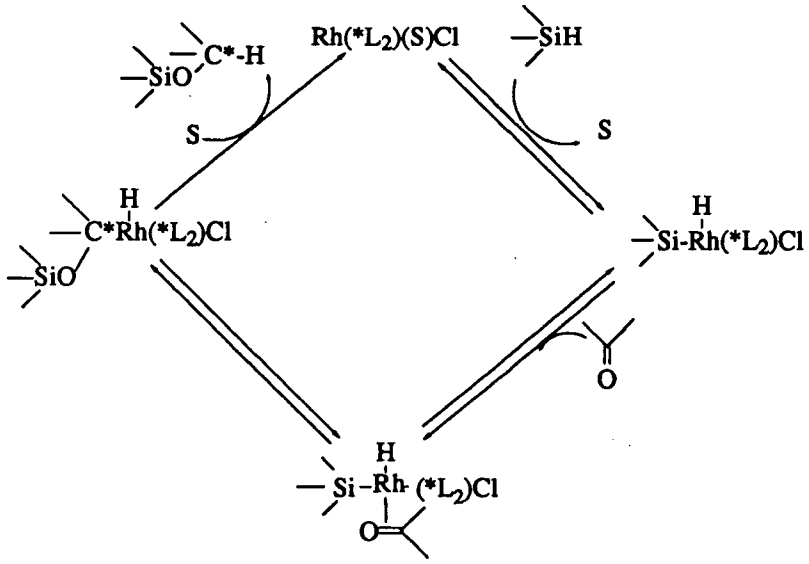

Scheme 1.7. Mechanism of hydrosilylation of a ketone; S = solvent, $*L_2$ = a chiral, bidentate ligand (modified from ref. 61).

olefins, and the number of ketones which give a high optical yield is far smaller than that of olefins.[42, 43, 47, 48, 60, 61] Direct catalytic hydration of olefins, using transition metal complexes, leading to asymmetric synthesis of alcohols is still well worth pursuing.

The only systems, which effect asymmetric hydration of olefins directly, are those of a biologically active enzyme, such as fumarase, aconitase and enoyl-CoA-hydratase (Scheme 1.8).[63] Specific substrate-enzyme interactions, are believed to play key role in these systems, although the detailed mechanisms of these hydration processes are not well understood.[63] The aconitase system is iron-dependent.[63]

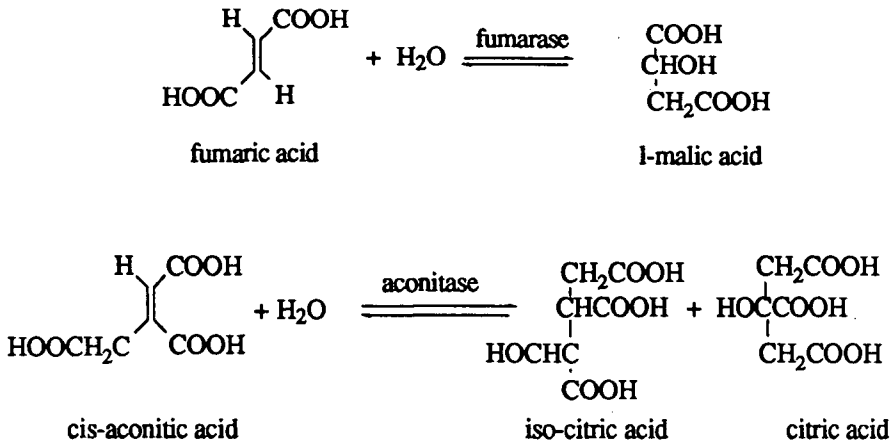

Scheme 1.8. Examples of enzyme-catalyzed hydration of biologically important olefins.

1.4. Feasibility of catalytic hydration by transition metal complexes

Hydration of olefins is a thermodynamically favourable process[64] and, in principle, transition metal complexes capable of activating water and/or olefin can catalyze the conversion of olefin to alcohol.[65] Three possible catalytic cycles will be dealt with: the first one (Scheme 1.9a) involves oxidative addition of water by a low valent metal complex, followed by coordination of olefin and then its insertion into the M-OH bond, and finally reductive elimination of the hydroxyalkyl-hydride as alcohol; the second one (Scheme 1.9b) involves coordination of an olefin followed by nucleophilic attack at the olefin by external OH^- and then protonation of the metal-carbon bond to give alcohol; alternatively the protonation could go via oxidative addition to give a Pt(II) hydride with subsequent reductive elimination of the hydroxyalkyl-hydride; the third one (Scheme 1.9c) involves oxidative addition of water, insertion of olefin into the M-H bond followed by reductive elimination of alkyl-hydroxyl to form an alcohol. All three possible catalytic cycles will be commented upon in later sections (Sect. 1.4.1-1.4.5), and also comparisons between catalytic hydration, hydrocyanation, and the Wacker process, will be discussed.

The following sections (Sect. 1.4.1-1.4.4) are divided according to the four major steps in the catalytic cycles, separate accounts being given on the possibility of the individual step. Following a review of the bond strengths of the M-C and M-O bonds, and thermodynamic consideration with respect to reductive elimination, a summary of the feasibility of catalytic hydration will be presented at the end of Sect. 1.4.4.

1.4.1 Activation of water

Transition metals interact with water molecules in the following fashions: coordination of a water molecule to a metal centre of higher oxidation state promotes the deprotonation of the water (Eq. 1.1), and oxidative addition of a water molecule to a low valent transition metal

$$M(H_2O)^{n+1} \rightleftharpoons M(OH)^{n+} + H^+ \qquad (1.1)$$

$$M^0 + H_2O \rightleftharpoons M^{II}(H)OH \qquad (1.2)$$

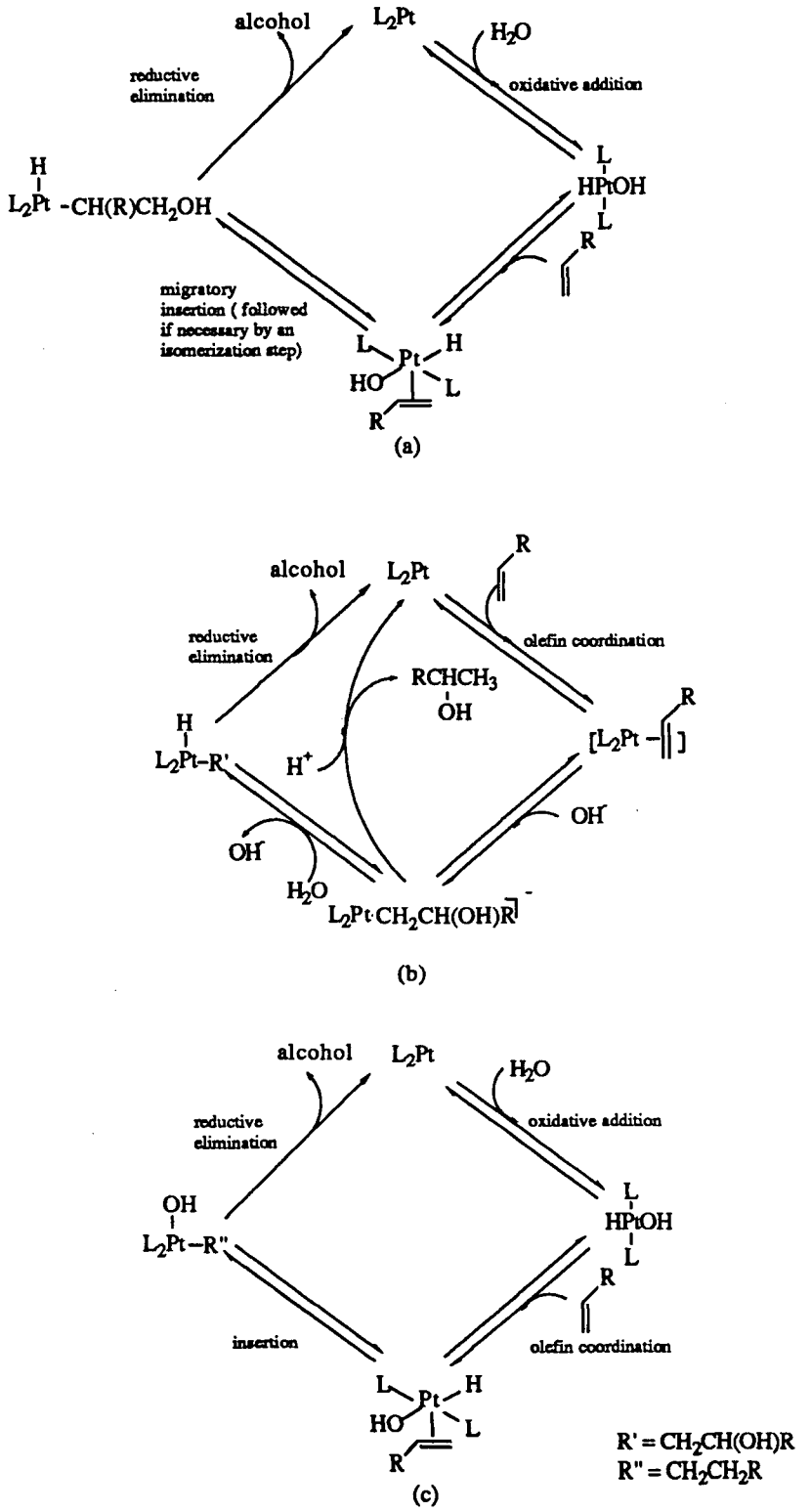

Scheme 1.9. Possible mechanistic pathways for catalytic hydration using, for example, a platinum metal complex;[23] oxidative addition of H_2O is written as giving trans species (Sect.1.4.1).

complex gives a hydridohydroxo species (e.g., Eq. 1.2). The chemistry exemplified in Eq. 1.1 has been recognized since the early days of aqueous solution chemistry while that of the latter is relatively new, within last twenty years. In aqueous solution, the proton dissociation constant or hydrolysis constant of a transition metal aquo complex increases several orders of magnitude with respect to that of free water; the higher the charge of the central ion, the more acidic the coordinated water becomes.[66] As a result of a strong M-OH interaction, the electron density is largely drawn to the metal and the basicity of hydroxide drops accordingly. On the other hand, oxidative addition of water to low-valent metal complexes is generally believed to promote the basicity of the OH group. Oxidative addition of protic compounds to low-valent transition metal complexes has been known for many years to give a metal hydride species,[67] and water has been shown in several cases to add oxidatively to give M(H)OH species, in which the hydroxo group can be coordinated or present as an associated anion. Within the coordinated OH species, both cis- and trans- geometry have been revealed. The cis-hydridohydroxo complexes are more stable thermodynamically;[68] however, trans addition products are more evident. Very few cases of cis addition have been reported. The early transition metal complexes of M(H)OH type tend to dimerize and form a bridging oxo species, and are thus less useful for the purpose of hydration. The only example of an early transition metal monomeric M(H)OH species is a hafnium permethylated cyclopentadienyl (Cp*) complex, which is not formed directly from an oxidative addition of H_2O but from an exchange reaction of $Hf(H)(NH_3)Cp^*$ with H_2O.[69] Complexes of the cis-M(H)OH type, formed directly from oxidative addition of H_2O, are cis-$Os(H)(OH)(PMe_3)_4$[70] and cis-$Ir(H)(OH)(PMe_3)_4(PF_6)$.[68] The iridium compound, which has been characterized crystallographically, is both air and thermally stable and does not eliminate water even at 200°C.[68] The more reactive oxidative adduct is of the type trans-M(H)OH. As a result of the strong trans influence of hydride,[71] the nucleophilicity of OH is greatly enhanced, and the basicity and nucleophilicity of the OH group have been recognized in several catalytic processes. Trans oxidative addition of water has been seen for several group VIII transition metal complexes. The $Os_3(CO)_{12}$ complex reacts with H_2O at 200°C giving $Os_3(H)(OH)(CO)_{10}$;[72] $[Rh(en)_2]^+$, electrochemically produced from $[RhCl_2(en)_2]^+$ in aqueous

solution, adds water to give $[Rh(H)(OH)(en)_2]^+$, which has been isolated as the tetraphenylborate salt.[73] The rhodium phosphine complexes, $Rh(H)[P(i\text{-}Pr)_3]_3$ and $Rh_2(H)_2(\mu\text{-}N_2)(PCy_3)_4$, are capable of activating H_2O/D_2O via oxidative addition for an H-D exchange process in aromatic compounds via orthometallated species.[74] The key intermediate in the Water Gas Shift (WGS) reaction catalyzed by $Rh(H)(PEt_3)_3$ or $Rh(H)(PEt_3)_4$ was found to be $[Rh(H)(PEt_3)_3]OH$.[75] The non-phosphine complex, $Ru(HEDTA)(CO)^-$ (HEDTA = trianion of ethylenediaminetetraacetic acid), was recently discovered by Khan et al. to catalyze the WGS reaction efficiently under mild conditions (20 ~ 80°C, 1 ~ 35 atm CO); kinetic investigations indicate that oxidative addition of water to form trans-$Ru(H)(OH)(CO)(HEDTA)^-$ is the rate limiting step.[76] The complex trans-$[Ru(H)(OH)(S)(PPh_3)_2]$ (S = THF, H_2O), reported by Wilkinson's group, is however formed by substituting a Cl^- with OH^-;[77] this hydridohydroxo species readily undergoes reductive elimination of H_2O under vacuum in dry solvents. The possibility that $Ru(CO)_2(PPh_2py)_3$ (where py represents a 2-pyridyl substituent) might form a Ru(H)(OH) species was examined by Prystay, but a dihydride formed instead.[78] The platinum tertiary phosphine derivatives, PtL_n [L = $P(i\text{-}Pr)_3$, n = 2, 3], catalyze the conversion of CO and H_2O to CO_2 and H_2, and D-H exchange in water via a Pt(H)OH intermediate; hydration of nitriles to amides, and olefins to alcohols, has also been investigated using the same systems.[79-83] The $IrCl(PCy_3)_2$ complex was found by James et al. to react reversibly with H_2O in CH_3CN form the unstable $Ir(H)(OH)Cl(CH_3CN)(PCy_3)_2$ species.[84] It is interesting to point out that oxidative addition of water has so far been limited to the second and third row group VIII metal complexes.

1.4.2. Activation of olefins toward nucleophilic attack by hydroxide, and migratory insertion of olefin into an M-OH bond

An olefin is electron-rich and generally prone to attack by an electrophile, such as H^+, Br^+, etc. However, upon complexation to an appropriate electron-deficient metal centre, the olefin ligand becomes subject to nucleophilic attack, because the electron-density of the olefin is now shifted towards the metal centre via a σ- M-olefin bond (Scheme 1.10).

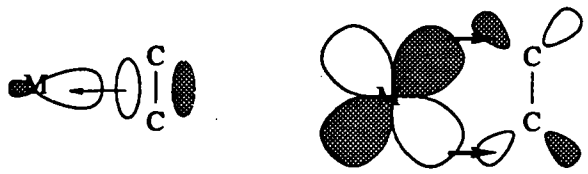

Scheme 1.10. Interactions between metal and olefin.

Transition metal complexes capable of activating an olefin must be in a relatively high oxidation state and have a number of associated electron withdrawing ligands, such as carbon monoxide, which will stabilize the negative charge resulting from an external nucleophilic attack.[85] The most characteristic reaction of a coordinated olefin complex is the attack of nucleophile to produce a σ-alkyl metal complex. Two basic modes of attack are possible and are distinguishable by both their stereo- and regiochemistry. Trans attack, from the face opposite the metal by a nucleophile (Nuc^-) without prior coordination, is commonly observed with the Nuc^- attack occurring predominantly at the more substituted olefin terminus:[85]

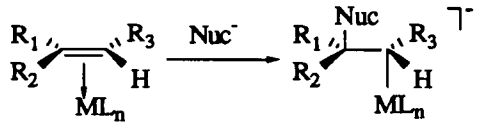

Cis attack, by a previously coordinated nucleophile, from the same side as the metal, appears as the net insertion of olefin into the M-Nuc bond. The cis attack normally occurs at the less substituted olefin terminus.[85] In both processes, a major competing reaction is the displacement of olefin by the nucleophile, particularly if the nucleophile is a good ligand for the metal, as illustrated below (Scheme 1.11).[85]

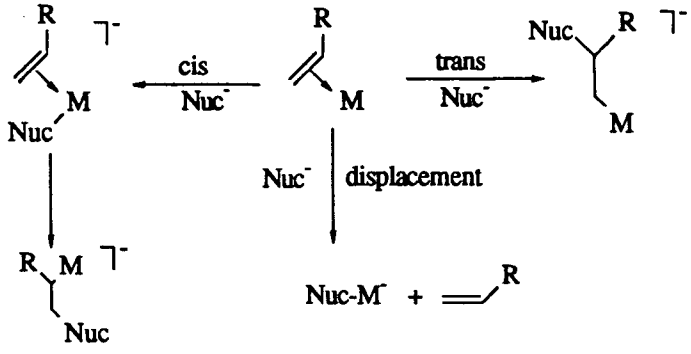

Scheme 1.11. Possible reactions for a coordinated olefin with nucleophile.

Hydroxide has long been perceived as a weak ligand for a late-transition-metal because of the mismatch of hard ligand base with soft metal acid.[86, 87] Before 1986, the success of the Wacker process had been attributed to the weak coordination of hydroxide to Pd, so that displacement of olefin did not compete with OH^- attack at the olefin.[88] Bryndza and his coworkers have since investigated the relative bond strength of M-H, M-O, M-N and M-C bonds through equilibrium studies and found them to be $M\text{-}C_{(sp)} > M\text{-}O > M\text{-}H > M\text{-}C_{(sp^3)} > M\text{-}N$,[64] indicating that the M-O bond is not intrinsically weak. Studies on the thermochemistry of the late transition metal hydroxide, alkoxide, and amide complexes further revealed that the bond strength of M-OH was 15 Kcal/mol greater than that of M-OMe.[89] The stability of the M-OAr bond (M = Pd^{II}, Ni^{II}) with respect to the M-Me bond has been demonstrated by Yamamoto et al. by the preferential insertion of CO into the M-Me bond in some chelating diphosphine complexes.[90, 91] On the other hand, insertion of CO and/or olefin into the M-OMe rather than the M-Me bond is more common in platinum(II) phosphine complexes.[65, 92 - 94] The higher reactivity of the M-OMe bond compared to the M-Me bond toward CO and/or olefin in these examples has been attributed to kinetic lability.[89] In fact, Yamamoto's group reported recently that reaction of CO with mixed alkyl alkoxo (not aryloxo) Pd^{II} and Ni^{II} complexes results in the formation of an alkoxycarbonyl, instead of an acetyl, before reductive elimination of an ester takes place.[95] These low valent metal alkoxide complexes display high reactivity, quite different from that of the high valent earlier group metal alkoxides.[96]

Migratory insertion of olefin into a Pt-OH bond was proposed by Jensen and Trogler as one option in a scheme for catalytic 1-hexene hydration, although there was no proof of a formation of a hydroxyalkyl intermediate.[23] Tetrafluroethylene has been shown to insert into a Pt-OMe bond,[65] but there are no data on reactivity with a Pt-OH species. The thermodynamics of olefin insertion into an M-OH bond are as favourable as those of the uncatalyzed olefin hydration, as inferred by the relative bond strengths of M-OH and $M\text{-}CH_2CH_2OH$.[89] The olefin insertion step may not be actually observed in catalysis by spectroscopic methods and the

hydroxyalkyl insertion product may not be isolable but, nevertheless, the insertion product is energetically accessible, and therefore a viable catalytic intermediate.

1.4.3. Reductive elimination of alkyl-hydride and alkyl-hydroxy moieties

Reductive elimination, the reverse of oxidative addition, is accompanied by a decrease in coordination number and lowering of metal oxidation state, and is of interest because the process leads to the formation of bonds between two ligands; this is particularly important in most homogeneously catalyzed reactions for it frees the organic product at the end of cycle. For reductive elimination to occur, the cis geometry is required; usually the reductive elimination of trans disposed ligands requires a preceding isomerization to a cis disposition. A trans hydrido(cyanomethyl)platinum(II) species, for instance, undergoes isomerization by photolysis before acetonitrile is produced by reductive elimination of the cis hydrido/cyanomethyl groups:[97]

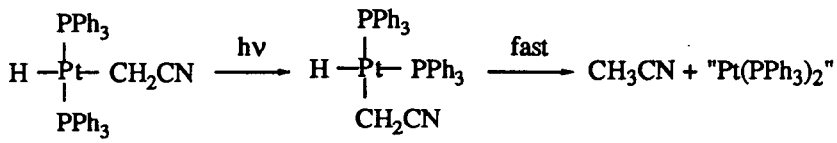

Reductive elimination from hydrido(alkyl) metal complexes has been well documented, whereas that from a hydroxo(alkyl) is very rare. The cis-$Pt(H)MeL_2$ and the cis-$Pt(H)(CH_2CF_3)(PPh_3)_2$ complexes have been shown to eliminate CH_4 and 1,1,1-trifluoroethane at -25°C, respectively.[98, 99] The relative rate of reductive elimination of hydrido-R is related to the metal-ligand (R) bond strength, and decreases in the order R = CH_3CO > CH_3 > $PhCH_2$ > CF_3.[100, 101] It is not surprising that M(H)(R'OH) species should eliminate alcohol more readily than does M(OH)R'. Indeed, as noted in the literature, many hydroxo(alkyl) complexes appear to be very stable;[19, 102] the corresponding alkoxo(alkyl) complex is, in certain cases, also resistant to reductive elimination.[103]

1.4.4. Olefin hydration catalyzed by metal phosphine complexes

The only such transition metal hydration catalysts reported thus far are trans-hydridochlorobis(trimethylphosphine)platinum(II), trans-$Pt(H)Cl(PMe_3)_2$ and the tris(iso-

propyl)phosphineplatinum(0) species, $Pt[P(i\text{-}Pr)_3]_3$. The former catalyst was claimed to catalyze the hydration of an unsaturated terminal olefin such as 1-hexene to the primary alcohol with a reasonable turnover rate at moderate temperatures.[23b] It was also found by the same research group, in a study of the catalytic hydration of acrylonitrile to amide, that in a side-reaction the α,β-unsaturated olefinic bond was hydrated at a competitive rate.[23a] In the presence of base, trans-$Pt(H)Cl(PMe_3)_2$ was converted to a hydridoaquobisphosphineplatinum(II) species. The reported turnover rates were 6.9 h^{-1} at 60°C for n-hexanol, and 8.3 h^{-1} at 100°C for n-dodecanol:

$$RCH{=}CH_2 \xrightarrow[\substack{R=CH_3(CH_2)_3,\ 60^\circ C \\ R=CH_3(CH_2)_9,\ 100^\circ C}]{\substack{Pt(H)Cl(PMe_3)_2/NaOH \\ (PhCH_2)Et_3NCl}} RCH_2CH_2OH$$

The proposed mechanism is similar to cycle (a) given on page 10, and basically consists of oxidative addition of H_2O, coordination of olefin followed by OH^- attack at the coordinated olefin to form a hydroxyalkyl complex, and reductive elimination of alcohol; catalyst is regenerated by oxidative addition of H_2O to PtL_2 (L = PMe_3). A kinetic study showed that the rate of olefin hydration was independent of $[OH^-]$ when present in excess, and first-order in the alkene concentration. Water replacement by olefin was said to be the rate limiting step. Deuterium labelling using D_2O showed exclusive β-deuterium incorporation, indicative of reductive elimination occurring at the end of cycle; deuterium scrambling or olefin isomerization was not observed, ruling out olefin insertion into the Pt-H bond which is often reversible.[103] The complex did not catalyze the hydration of an internal olefin such as 2-hexene, or 3-hexene. The β-hydrogen elimination from hydroxyalkyl, which occurs very readily in oxidation of olefins catalyzed by Pd^{II} to form ketone or aldehyde, does not compete with a trans to cis isomerization step which leads to the formation of alcohol. The primary alcohol formed in the reaction was better accounted for by olefin insertion into the Pt-OH bond, rather than OH external attack which would predominantly produce a secondary alcohol (Sect.1.4.2). A five-coordinate, square

pyramid intermediate may be involved before insertion. A controversy has arisen, however, concerning the olefin insertion step and the question of alcohol formation. The original authors claimed that slow insertion into Pt-H by the olefin did not compete with the insertion into Pt-OH which eventually led to the alcohol formation. On the contrary, some ^{1}H and ^{31}P NMR spectroscopic studies conducted by Ramprasad et al. showed that trans-$[Pt(H)(PMe_3)_2(1\text{-hexene})]^+$ was formed at -54°C and was only stable below -30°C.[24] Significant decomposition of the hydride/olefin complex occurred at -12°C and resulted in total isomerization of the 1-hexene, with no alcohol being detected. Formation of trans-$Pt(H)OH(PMe_3)_2$, a key intermediate in Trogler's cycle, by adding $NMe_4^+OH^-\cdot 5H_2O$ to trans-$[Pt(H)(PMe_3)_2(1\text{-hexene})]^+$ at -59°C, was confirmed by ^{1}H NMR spectroscopy, but no primary alcohol was formed on gradually warming the mixture to room temperature.[24]

Yoshida et al. have reported olefin hydration using $Pt[P(i\text{-}Pr)_3]_n/H_2O$ (n = 2, 3) systems[18] via a pathway similar to cycle (a) in Scheme 1.9. Although $Pt(OH)RL_2$ has also been reported as a catalyst precursor for the hydration of the olefinic bond in acrylonitrile,[19] the poor reproducibility suggested the involvement of a hydride impurity.[104]

Platinum is so far the only metal with coordinated phosphines showing promise for catalytic hydration. The chemistry related to mechanistic aspects still remains to be explored. Within the three cycles shown in Scheme 1.9, the metal-hydride in cycle (a) seems to be essential for product liberation at the end of catalytic cycle; meanwhile, the presence of both metal hydride and hydroxide initiates a major competition for olefin insertion; in cycle (b), there is no precedence for an $PtRL_2$ complex to undergo protonation of the alkyl by a H_2O molecule; in order to complete the catalytic cycle, an extra step may be required to cleave the Pt-C bond;[88] in cycle (c), the major concern is that the $Pt(OH)RL_2$ complex is probably stable to reductive elimination.[19, 64, 101] The challenge of finding an effective catalyst remains.

1.4.5. Olefin hydration catalyzed by metal non-phosphine complexes

Catalytic activation of olefinic substrates by non-phosphine transition metal complexes was pioneered by Halpern and coworkers in the early 1960s, when maleic, fumaric and acrylic acids were catalytically hydrogenated in aqueous acid solutions containing chlororuthenate(II) species.[105] The formation of a Ru^{II}-olefin complex, which later reacted with hydrogen, was demonstrated; in the case of maleic acid, a 1:1 olefin complex was confirmed spectrophotometrically and the stability constant was measured to be $5x10^3$ M^{-1} (aq. 3M HCl, 20°C). Further studies[106] using D_2 and D_2O demonstrated that the hydrogen atoms which added to the double bond originated from the aqueous solvent rather than hydrogen gas. However, no hydration product was revealed. The same group reported the catalytic hydration of acetylenic compounds by Ru^{III} chlorides in aqueous acid solution.[107] Acetylene, methylacetylene and ethylacetylene were converted under mild conditions to acetylaldehyde, acetone and methyl ethyl ketone, respectively. In the mechanism proposed for hydration of acetylene, a coordinated hydroxo ligand underwent migratory insertion into the coordinated acetylene, and the resulting hydroxyalkene group was cleaved off $Ru^{III}$by a proton to give the corresponding product, 'vinyl alcohol', which rearranged to acetaldehyde.[107] Aqueous acid solutions of some rhodium(III) chloro complexes, $[Rh(H_2O)_{6-n}Cl_n]^{(n-3)-}$, were also found later to be active for acetylene hydration.[108] Hydration of fluoroolefins was also observed in the aqueous Ru^{II}-3M HCl system, under conditions similar to those for hydrogenation of the olefinic acids; hydration was thus competitive with hydrogenation of the C=C bond in fluoro- or 1,1-difluoroethylene even under 1 atm H_2, so that only acetaldehyde and acetic acid, respectively, were detected following hydrolysis of the hydroxyfluorides.[109] Thus, chlororuthenate(II) species can function as a hydration catalyst for fluoroethylene as well as a hydrogenation catalyst for olefinic acids. Scheme 1.12 was the suggested mechanism of the olefin hydration process.[109]

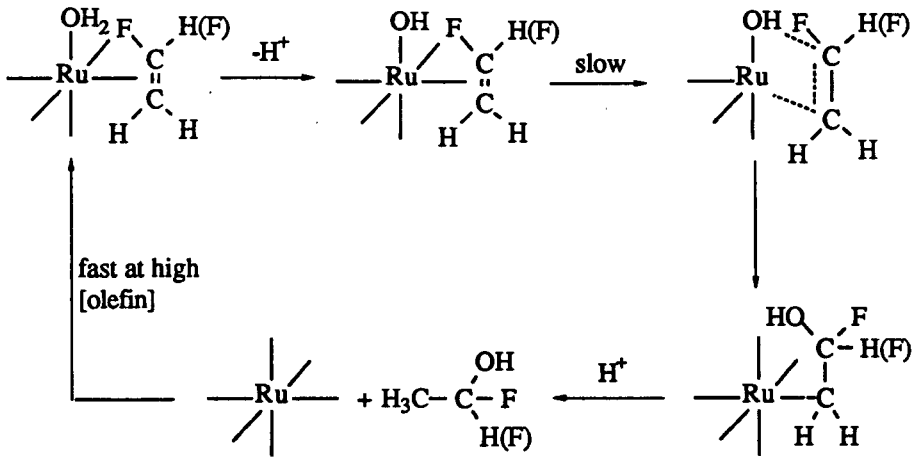

Scheme 1.12. The proposed mechanism for catalytic hydration of fluoroethylene by Ru^{2+}.[109]

The unique reactivity of fluoroethylenes in this Ru(II) system is not fully understood, but the suggestions were that fluoroolefins stabilize Ru^{II} sufficiently to prevent the reduction (e.g. under H_2) to metal, while the high electronegativity of fluorine promotes the nucleophilicity of the coordinated OH which attacks the olefin bond leading to a β-hydroxyalkyl intermediate. This reaction is a true olefin hydration catalyzed by a non-phosphine transition metal complex. Another example found in the literature in the late 1960s is that reported by Bzhasso and Pyatnitskii who found that $CrCl_3 \cdot 6H_2O$ catalyzes the hydration of maleic acid at 170°C.[17] Formation of a $[C\text{-}Cr]^{3+}$ cation analogous to a carbonium ion was suggested to play a crucial role in the catalysis. Matching a metal complex catalyst with a substrate under suitable conditions was the initial major aim of this thesis project, although the goal has not yet been achieved. In Chapter 6, a kinetic study of the Cr^{3+}/maleic acid system is described.

1.4.6. A comparison of catalytic hydrocyanation and hydration of olefins, and olefin oxidation via hydration

Hydrogen cyanide has a bond dissociation energy of 123 Kcal/mol, which is very close to that of water, 119 Kcal/mol,[110] and it is beneficial to compare activation of hydrogen cyanide with activation of water. Hydrocyanation is one of the most successful homogeneously catalyzed reactions in chemical industry, the catalysis utilizing Ni(0) phosphite and Pd(0) phosphine

complexes. Asymmetric induction has been achieved in a $Pd(DIOP)_2$ system with up to 40% e.e.[111] The mechanism of catalytic hydrocyanation using nickel complexes has been reported recently in detail,[112 - 114] whereas studies on the Pd-catalyzed reaction are still at a preliminary stage. Some similarities between systems using Ni and Pd catalysts have been revealed.[112] Nickel-catalyzed hydrocyanation has been shown to involve oxidative addition of hydrogen cyanide, coordination of olefin followed by olefin insertion into the Ni-H bond, and reductive elimination of alkyl cyanide.[112 - 116] The relative order of oxidative addition and olefin coordination may be reversed depending on the alkene; isomerization of olefin often takes place in the olefin insertion step because of its reversibility which may lead to the formation of linear and branched nitriles. Addition of a Lewis acid has been demonstrated to promote the formation of the linear nitrile.[113] Oxidative addition of HCN is shown to be cis, and olefin is shown to insert into the M-H bond exclusively.[115] The reductive elimination of alkyl cyanide is facile. Oxidative addition of H_2O can give either cis or trans hydridohydroxo species. There is little information on the reactivity of the cis type toward olefin insertion, while in the trans type olefin appears to insert readily into an M-OH bond.[23] Although insertion of olefin into the Pt-H bond of Pt(H)OH species was observed by Ramprasad et al., no reductive elimination of alkyl-hydroxide to give alcohol formation was detected.[24]

Oxidation of olefins to aldehyde or ketones has been catalyzed successfully by a $Pd^{II}/O_2/CuCl_2$ system in the Wacker process. Olefin is hydroxylated but, because of the β-hydride elimination, no alcohol is formed. The order of olefin reactivity is $CH_2{=}CH_2$ > $RCH{=}CH_2$ > $R_1CH{=}CHR_2$, geminal di-substituted, tri-substituted and tetra-substituted olefins, and electrophilic olefins generally do not coordinate sufficiently well to permit further chemistry.[117] The olefin, once coordinated to palladium, is generally subject to nucleophilic attack by OH^- or H_2O, which occurs rapidly at the more substituted position. The α-alkylpalladium species then formed is unstable and undergoes rapid, spontaneous β-hydride elimination to form an OH-substituted olefin which isomerizes to ketone. The Pd(0) formed after β-hydride elimination is oxidized to Pd^{II} by $O_2/CuCl_2$ and is continually used as catalyst. The

success of the Wacker process for formation of acetaldehyde from ethylene indicates that alcohol formation in this system is not attainable.

1.5. Chemistry of pyridylphosphines

1.5.1. Developments in synthesis of pyridylphosphines

Phosphines with substituted benzene rings and heteroaromatic groups, such as pyridine, were first reported by Davis and Mann,[118] and the synthetic strategy was further developed by Mann and Watson.[119] The overall yield of pyridylphosphine production, $PPh_{3-n}py_n$ (abbreviated as PN_n, n = 1, 2, 3; py represents the 2-py moiety throughout this thesis), was very poor because the use of a Grignard reagent created problems in product separation, so that extensive purification procedures including vacuum distillation were required. The introduction of 2-lithiopyridine by Wibaut et al.[120] provided an alternative route for pyridylphosphine synthesis. A revised experimental procedure using lithiopyridine was laid out by Plazek and Tyka[121] and has been adopted with minor modifications in more recent years by several research groups.[122 - 125]

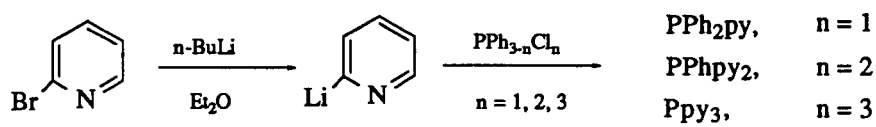

Scheme 1.13. Synthetic route for 2-pyridylphosphines via lithiopyridine.

Because of the instability of lithiopyridine above -60°C, the yield of this one pot synthesis is normally around 40 ~ 50%. PPh_2py (PN_1) and $PPhpy_2$ (PN_2) can also be made via a lithiophenylphosphine route, which is sometimes complicated by the coupling reaction of metallated phosphine; nevertheless, the yields are often comparable with those using lithiopyridine. Lithiophenylphosphine can be prepared by reacting lithium metal with PPh_3,[126], PPh_2Cl or $PPhCl_2$[127], or from reaction of methyllithium with diphenylphosphine,[128] as in equations (1.3) to (1.6)

$$PPh_3 + 2Li \longrightarrow PPh_2Li + PhLi \quad (1.3)$$

$$PPh_2Cl + 2Li \longrightarrow PPh_2Li + LiCl \quad (1.4)$$

$$PPhCl_2 + 4Li \longrightarrow PPhLi_2 + 2LiCl \quad (1.5)$$

$$PPh_2H + MeLi \longrightarrow PPh_2Li + CH_4 \quad (1.6)$$

$$PPh_3 + Na/NH_3 \longrightarrow PPh_2Na + PhNH_2 \quad (1.7)$$

Tolmachev et al. reported that triphenylphosphine could be metallated using sodium in liquid ammonia, Eq. (1.7), with the yield of PPh_2py being 50~60%.[129] A minor modification of the experimental conditions of Plazek and Tyka's method was used in the present work, giving an average yield of 40~56% for the three phosphines (Ch. 2).

1.5.2. Coordination chemistry of pyridylphosphines

Since a 1965 breakthrough in the field of homogeneous catalysis made by Wilkinson's group, who used $RhCl(PPh_3)_3$ as a catalyst to hydrogenate alkenes at 25°C and 1atm H_2 in organic solvents, attention has focused on tertiary phosphines as ligands in catalyst design. Phosphines are, in fact, found to be the most popular ligands in many catalytic systems, and it is not surprising that phosphine chemistry has flourished ever since. Triphenylphosphine is the most exhaustively studied phosphine; 2-pyridylphosphines, $PPh_{3-n}py_n$, appear to be a good choice for systematic studies on the electronic effect of pyridine on the phosphine, because the geometry of a pyridylphosphine remains relatively constant with respect to triphenylphosphine.[130] Equally important and significant are the heteropolydentate characteristics of these pyridylphosphines, which could be highly desirable in areas such as catalysis, asymmetric synthesis and organometallic stereochemistry.[131] Pyridylphosphine, as a heteropolydentate ligand, is more attractive perhaps than the chelating diphosphines and polyphosphines because the binding characteristic of phosphorus and nitrogen allow for a more rationalized design of a catalyst.

Pyridylphosphines, however, received little attention until the late 1970s and, in fact, the X-ray crystallographic structure of Ppy_3 was only done in 1988,[132] forty-four years after it was

first made. The binding options offered by these 2-pyridylphosphines are shown in the following diagram (Scheme 1.14).

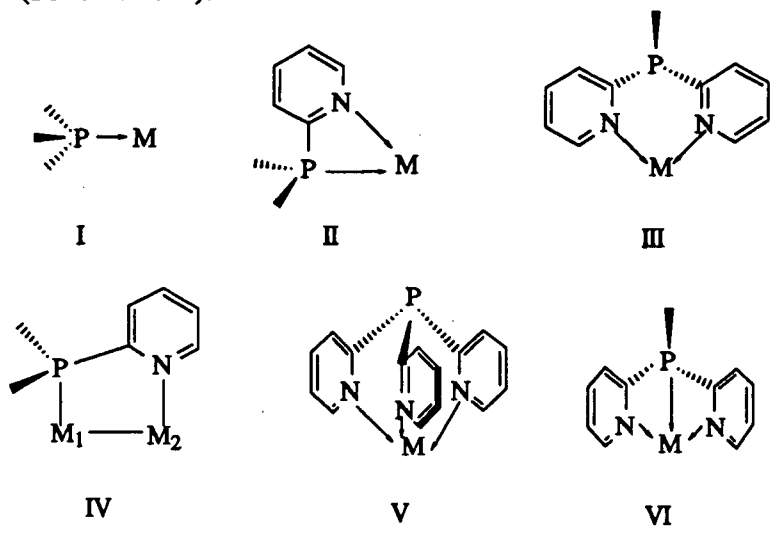

Scheme 1.14. Possible coordination modes of pyridylphosphines to transition metals.

Transition metals (Group VIB -VIII, IB) form complexes with 2-pyridylphosphines of the various structures I - V shown in Scheme 1.14. Although there is no example of an isolated type VI compound reported in the literature, this coordination mode is nevertheless possible from electronic and steric points of view,[122, 133] and it has been proposed to coexist in solution with type I (square planar) and type II (square pyramid) complexes in the case of the trans-$RhCl_2(CO)(PN_2)$ and trans-$RhCl_2(CO)(PN_3)$.[133] The most common coordination mode among the second and the third row transition metal 2-pyridylphosphine complexes is type I; i.e. only the phosphorus donor coordinates, for example, $Mo(CO)_4(PN_1)_2$,[134] $PdX_2(PN_n)_2$ (n = 1;[128] n = 2 and 3, Ch. 3), and $PtX_2(PN_n)_2$ (n = 1; [135] n = 2 and 3, Ch. 3). Cu, Ag and Au form $M(X)PN_n$ species (X = halides) which have unusually short M-P distances; under suitable conditions M(X)P is believed to aggregate to form a cluster.[136] The chelating coordination type II is found in some isolated Pt^{II} ($[PtI(PN_1)_2]PF_6$),[135] $RuCl_2(CO)_2(PN_1)$[137] and U^{III} ($U(BH_4)_3(PN_1)_2$) complexes,[138] and also is present in solution for several type I complexes as indicated by ^{31}P NMR data (Ch. 3). The U^{III} complex is shown by X-ray crystallography to be 13-coordinate with three BH_4^- ligands being tridentate and two chelating phosphines being

coplanar with one of the boron atoms.[138] Tetrahedral $CoCl_2(PN_2)$ is a type III compound, the phosphorus lone-pair not interacting with the central metal atom as shown by crystallographic data.[139] The unsymmetrical bridging mode in type IV is another common coordination mode for both hetero and homo binuclear complexes; examples include $Pd_2X_2(PN_n)_2$ (Ch. 3), $PdMo(\mu\text{-}CO)(CO)_2(\mu\text{-}PN_1)_2$,[134] $Re_2Cl_4(\mu\text{-}PN_1)_3$[140], $RhPtCl_3(CO)(PN_1)$ (head-to-tail, HT)[141], $Rh_2Cl_2(\mu\text{-}CO)(\mu\text{-}PN_1)_2$ (HT)[142], and $RhPdCl_3(CO)(\mu\text{-}PN_1)_2$ (HT).[143] Because of the different softness of phosphorus and nitrogen donors, M_1 and M_2 can be linked together even if they are of different hardness. The tridentate mode via three nitrogen atoms in type V is common among the first row transition divalent metals, as in $[M(\eta^3\text{-}PN_3)_2](ClO_4)_2$,[122, 144] and a Ru^{II} complex can also be formed of the same structure.[124]

The interesting coordination chemistry of these phosphine ligands has been extended to their oxides of both the phosphine and pyridine. Phosphine oxides have found practical applications in selective extraction processes for the platinum metals.[145] Formation of $(OPN_1)PtBr_4$, containing a five-member chelating structure as in (a),[146] demonstrates the affinity of pyridylphosphine oxides for platinum in a high oxidation state. Pyridylphosphine P, N-oxide is a 1,3-bifunctionalized ligand as in (b), structurally similar to ligands containing monophosphoryl and carbonyl groups, or carbonyl and phosphine oxide groups which are good extractant ligands for lanthanide and actinide ions.[147, 148] The ligand $OP(Ph)_2(Opy)$ was made in an attempt to replace these extractants so that selective extraction of uranium as $UO_2(NO_3)_2[OP(Ph)_2(Opy)]$ could be carried out. The structure of the uranium complex contains a six-member ring arranged in a distorted boat form.[149]

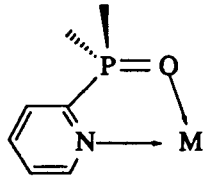

5-member ring
(a)

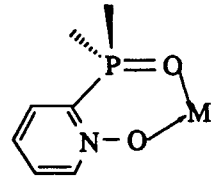

6-member ring
(b)

1.5.3. Reactivity of the coordinated pyridylphosphines and catalytic activities of their metal complexes

The pyridylphosphine complexes are also interesting in their distinctive reactivity. The triply bonded dirhenium(II) complex $Re_2Cl_4(PN_1)_3$ readily undergoes HCl elimination in the presence of base to give the ortho-metallated complex $Re_2Cl_3(PN_1)_2[PPh(o\text{-}C_6H_4)py]$;[139, 140] the base can be the 2-(diphenylphosphino) pyridine ligand itself. This is reported to be the first example of ortho-metallation occurring at a metal-metal multiple bond. When $Ru_3(CO)_{11}(PN_1)$ is heated under reflux in methanol, the spontaneous cleavage of a phosphorus-carbon bond of 2-(diphenylphosphino)pyridine takes place to give a doubly bridged phosphido ligand with the pyridyl nitrogen coordinated to the third ruthenium, while a bridging benzoyl group is formed by migratory insertion of a phenyl group onto a terminal carbonyl group.[150] A similar phosphorus-carbon bond cleavage reaction for triphenylphosphine occurs, but at a much higher temperature, at the boiling point of xylene for some Mn, Rh and Os clusters.[151]

A few catalytic aspects of pyridylphosphine complexes have also been investigated, but mechanistic studies of the catalysis are non-existent. The catalyst precursor in most cases is formed *in situ*; for instance, when a mixture of $Pd(OAc)_2$, PN_1, p-Me-C_6H_4-SO_3H, and propyne is heated at 45°C in methanol under 60 bar CO pressure, methylmethacrylate was obtained with 99% selectivity at a very high turnover rate (20,000 h^{-1}).[152] Catalytic homologation from methanol to ethanol can also be achieved at 155~180°C under 200~300 bar syn-gas ($CO:H_2$ = 1:1) pressure using a ruthenium pyridylphosphine catalyst, the selectivity being over 30% with 60 ~ 74% conversion.[153] A rhodium complex containing tripyridylphosphine formed *in situ* from $Rh_2(CH_3COO)_4$ catalyzes the conversion of a water and carbon monoxide mixture to hydrogen and carbon dioxide, the water gas shift (WGS) reaction.[154] The only example of a catalytic process using a well-defined catalyst precursor, $RhH(CO)(PPh_3)(PN_3)_2$, is the hydroformylation of 1-hexene at low CO and H_2 pressures in the presence of excess PN_3; no mechanistic detail was given by the authors.[125]

Pyridylphosphine complexes thus exhibit many differences in their coordination chemistry, reactivity and catalytic activity from those of the triphenylphosphine analogs. In this thesis, efforts in revealing these aspects of pyridylphosphine complexes are presented.

1.6. Scope of this thesis

The water solubility of the tris-2-pyridylphosphine palladium complex, $Pd_2Cl_2(\mu\text{-}PN_3)_2$ (HT) **11c**, appeared to be an asset for the complex as a candidate for a hydration catalyst, and the complex attracted our attention since it was discovered earlier in our group by Lee and Yang.[155] To our knowledge, few neutral tertiary phosphine complexes, excluding those with highly polar substituents ($-SO_3H$, $-CO_2H$, -OH, and $-NH_2$) in the phosphine molecules,[156] are soluble in water.[74, 75, 79 - 84, 157] Cis-$PdCl_2(PN_3)_2$ was later found in the present work to have even better solubility in water than the binuclear complex. The solution behaviours are discussed in Chapter 3. Some monomeric and binuclear metal pyridylphosphine complexes of palladium and platinum were synthesized via methods based on literature procedures for 2-(diphenylphosphino)pyridine derivatives described in Chapter 2, and structurally characterized by $^{31}P\{^1H\}$, $^{31}C\{^1H\}$ and ^1H NMR spectroscopic methods (Ch. 3). The molecule structure of $Pt_2Cl_2(\mu\text{-}PN_2)_2$ (HT) (1S, 2S) was determined crystallographically (Ch. 3). The diastereoisomers $Pt_2I_2(\mu\text{-}PN_2)_2$ (HH) (1S, 2S) and $Pt_2I_2(\mu\text{-}PN_2)_2$ (HH) (1S, 2R) were successfully separated by preparative TLC (Ch. 2) but, unfortunately, the high symmetry of the single crystals grown precluded crystallographic characterization. None of the M(I) or M(II) pyridylphosphine halide complexes binds olefin in organic solvents or in aqueous solution. The binuclear head-to-head (HH) or head-to-tail (HT) complexes $M_1M_2X_2(\mu\text{-}PN_n)_2$ ($M_1 = M_2 =$ Pd, or Pt; M_1 = Pd, M_2 = Pt; X = Cl, Br, I; n = 1, 2, 3) form a bridging adduct with dimethylacetylenedicarboxylate (DMAD). The isolated products bear the HT-configuration in most cases, except in $Pt_2I_2(\mu\text{-}PN_1)_2$ (HH) where the HH-configuration is maintained (Ch. 4). Kinetic and spectroscopic studies on the reactions of $Pt_2I_2(\mu\text{-}PN_n)_2$ (HH) (n = 1, 2, 3) with DMAD are presented in Chapter 4: a five-coordinate Pt(II) intermediate with chelating pyridine is

proposed based on $^{31}P\{^1H\}$ NMR data, while a destabilization effect of a non-bridging pyridine substituent plays a crucial role in isomerization of the HH DMAD adduct to the HT adduct. Isomerization of the HH to HT form of the binuclear complex $Pt_2I_2(\mu\text{-}PN_3)_2$ in the presence of excess phosphine PN_3 was also investigated by $^{31}P\{^1H\}$ NMR in some detail, and the findings are included in Chapter 4. Some platinum(0) pyridylphosphine complexes were then synthesized by modifying literature methods reported for the well known PPh_3 analogues (Ch. 2). Reactions of these Pt(0) complexes with HCl, O_2, and olefins were studied, differences in reactivity from their triphenylphosphine analogs being noticed. The discussion on some failed attempts at catalytic hydration using the palladium and platinum pyridylphosphine complexes is presented in Chapter 5. In Chapter 6, the results of a kinetic study on maleic acid hydration catalyzed by $Cr(H_2O)_6^{3+}$ ion is presented. Despite complications in the Cr^{3+} system, the results suggest that the major pathway proposed previously for stoichiometric aquation is also followed in the catalytic hydration process.

References

1. Collman, J.P.; Hegedus, L.S.; Norton, J.R.; Finke, R.G. *Principles and Applications of Organotransition Metal Chemistry,* 2nd ed.; University Science Books: Mill Valley, CA, 1987; Ch.10.

2. Masters, C. *Homogeneous Transition Metal Catalysis — A Gentle Art;* Chapman and Hall: London, 1981; Chs.1, 2.

3. Nakamura, A.; Tsutsui, M. *Principles and Applications of Homogeneous Catalysis;* John Wiley & Sons: New York, 1980; Chs.1, 2.

4. Dickson, R.S. *Homogeneous Catalysis with Compounds of Rhodium and Iridium;* Ugo, R., James, B.R., Eds.; Reidel: Dordrecht, 1985; Ch.1.

5. Parshall, G.W. *Homogeneous Catalysis;* John Wiley & Sons: New York, 1980.

6. Hartley, F.R. *Supported Metal Complexes;* Ugo, R., James, B.R., Eds.; Reidel: Dordrecht, 1985; Ch.1.

7. Iwasawa, Y., Ed. In *Tailored Metal Catalysts;* Ugo, R., James, B.R., Eds.; Reidel: Dordrecht, 1986; Ch.1.

8. Bond, G.C. *Heterogeneous Catalysis,* 2nd ed.; Oxford University Press: Oxford, 1987.

9. Stiles, A.B., Ed. *Catalyst Support and Supported Catalyst: Theoretical and Applied Concepts;* Butterworths: Boston, 1987.

10. Bleach, B.E. In *Applied Industrial Catalysis;* Bleach, B.E., Ed.; Academic Press: New York, 1983; Vol.1, Ch.1.

11. MacDonald, R.G., Ed. *The Pulp of Wood;* McGraw-Hill: New York, 1969; Vol.1.

12. Wahren, D. *Paper Technology: Compendium after Lectures — Part 1. Fundamentals;* Bonano, E.J., Ed.; Institute of Paper Chemistry: Appleton, WI., 1980.

13. *Pulp and Paper Manufacture—Sulfite Science and Technology, 3rd ed.;* Joint Textbook Committee of the Paper Industry: Montreal, 1983.

14. Nissan, A.H., Ed. *Future Technical Needs and Trends in the Paper Industry;* TAPPI: Atlanta, GA, 1973.

15. Crawford, R.L. *Lignin Biodegradation and Transformation;* John Wiley &Sons: New York, 1980; p.8.

16. Ref. 11, p.662.

17. (a) Bzhasso, N.A.; Pyatnitskii, M.P. *Zh. Prikl. Zhim.*, **1969**, *42*, 1610. (b) Bzhasso, N.A.; Pyatnitskii, M.P. *Izv. Vyssh. Ucheb. Zaved., Pishch. Tehch. Tekhnol.*, **1967**, *5*, 207 through *C.A.*, **1968**, *68*, 39013k.

18. Yoshida, T.; Matsuda, T.; Okano, T.; Kitani, T.; Otsuka, S. *J. Am. Chem. Soc.*, **1979**, *101*, 2027.

19. Arnold, D.P.; Bennett, M.A. *J. Organomet. Chem.*, **1976**, *199*, 119.

20. Bennett, M.A.; Yoshida, T. *J. Am. Chem. Soc.* , **1973**, *95*, 3030.

21. Inoue, Y.; Sato, M.; Satake, M.; Hashimoto, H. *Bull. Chem. Soc. Jpn.*, **1983**, *56*, 637.

22. Atkins, K.E.; Walker, W.E.; Manyik, R.M. *J. Chem. Soc. Chem. Commun.*, **1971**, 330.

23. (a) Jensen, C.M.; Trogler, W.C. *J. Am. Chem. Soc.*, **1986**, *108*, 723. (b) Jensen, C.M.; Trogler, W.C. *Science* (Washington, DC) **1986**, *233*, 1069.

24. Ramprasad, D.; Yue, H.J.; Marsella, J.A. *Inorg. Chem.*, **1988**, *27*, 3151.

25. *Encyclopedia of Chemical Technology*, 3rd. ed.; Wiley: New York, 1978; Vol.1, pp.716-754.

26. Onone, Y.; Mizutani, Y.; Akiyanma, S.; Izumi, Y.; Ihara, H. *Shokubai*, **1976**, *18*, 180 through *C.A.*, **1977**, *86* , 170747s.

27. Wiseman, P. *An Introduction to Industrial Organic Chemistry;* Applied Science: London, 1979.

28. Eguchi, K.; Tokiai, T.; Kimura, Y.; Arai, H. *Chem. Lett.* , **1986**, 567.

29. Tojo, M.; Fukuoka, Y. *Jpn Patent*, JP 61/234946 A2 ,1987 through *C.A.*, **1987**,*106* , 158285p.

30. Eguchi, K.; Tokiai, T.; Arai, H. *Appl. Catal.*, **1987**, *34*, 275.

31. Mitsui, O.; Nakagawa, K. *Jpn. Patent* , JP 63/154633 A2, 1988 through *C.A.*, **1989**, *110* , 134782e.

32. Arai, H.; Sekizawa, K. *Jpn. Patent*, JP 63/ 218251 A2 ,1988 through *C.A.*, **1989**, *110*, 78064h.

33. Mitsui, O.; Nakagawa, K. *Jpn. Patent* , JP 63/ 1556736 A2 ,1988 through *C.A.*, **1989**, *110*, 38661u.

34. Mtkins, M.P. *Eur. Patent*, Appl. EP 210793 A1, 1987 through *C.A.*, **1987**, *106*, 122902y.

35. Francois, F.F.F.; Moudafi, L.; Vera Pacheco, M.; Nicolas, S.; Dufresme, P.; Gueguen, C. *Belg. Patent* , BE 904797 A1, 1986 through *C.A.*, **1987**, *106*, 69118u.

36. Okumura, S.; Kamiyama, S.; Furukawa, H.; Kaneko, K. *Eur. Patent*, Appl. EP. 127486 A1, 1984 through *C.A.*, **1985**, *102*, 148714f.

37. Tsybulevskii, A.M.; Kondrat'ev, V.A.; Tolkacheva, C.N.; Novikova,, C.A.; Mortikov, E.S.; Minachev, Kh. M.; Breshchenko, E.M.; Lipkind, B.A. *U.S.S. R. Patent*, SU 803969, 1981 through *C.A.*, **1981**, *94*, 163378j.

38. Streitwieser, A. Jr.; Heathcock, C.H. *Introduction to Organic Chemistry*, 2nd ed.; MacMillan: New York, 1981; pp.311, 315.

39. Brown, H.C. *Boranes in Organic Chemistry;* Cornell University Press: Ithaca, New York, 1972; p.285.

40. Brown, H.C.; Lue, N.R.de; Rabalka, H.C.; Hegecock, H.C., Jr. *J. Am. Chem. Soc.* , **1976**, *98*, 1290.

41. Sugita, T.; Yamasaki, Y.; Itaoh, O.; Ichikawa, K. *Bull. Chem. Soc. Jpn.*, **1974**, *47*, 1945.

42. Kagan, H.B. In *Asymmetric Synthesis;* Morrison, J.D., Ed.; Academic Press: Orlando, 1985; Vol.5. Ch.1.

43. Kitamura, M.; Ohkuma, T.; Inoue, S.; Sayo, N.; Kumobayashi, H.; Akutagawa, S.; Chta,T.; Takaya, H.; Noyori, R. *J. Am. Chem. Soc.*, **1988**, *110*, 629.

44. Hatat, C.; Karim, A.; Kokel, N.; Mortreux, A.; Petit, F. *Tetrahedron Lett.*, **1988**, *29*, 3675.

45. Takahashi, H.; Morimoto, T.; Achiwa, K. *Chem. Lett.*, **1987**, 855.

46. Akira, T.; Harada, T.; Hiraki, Y.; Murakami, S. *Bull. Chem. Soc. Jpn.*, **1983**, *56*, 1414.

47. James, B.R.; Joshi, A.M.; Kvintovics, P.; Morris, R.H.; Thorburn, I.S. In *Catalysis of Organic Reactions;* Eds. Blackburn, D.W.; Marcel Dekker: New York, 1990; Ch.2.

48. Heil, B.; Markó, L.; Törös, S. In *Homogeneous Catalysis with Metal Phosphine Complexes;* Ed. Pignolet, L.H.; Plenum Press: New York, 1983; p.317.

49. Hayashi, T.; Katsumure, A.; Konishi, M.; Kumada, M. *Tetrahedron Lett.* **1979**, 425.

50. Törös, S.; Kollar, F.; Heil, B.; Markó, L. *J. Organomet. Chem.,* **1982**, *232*, C17.

51. (a) Ojima, I.; Kogura, T.; Terasaki, T.; Achiwa, K. *J. Org. Chem.,* **1978**, *43*, 3444. (b) Achiwa, K.; Kogure, T.; Ojima, I. *Tetrahedron Lett.,* **1977**, 4431.

52. Yamamoto, K.; Hayashi, T.; Kumada, M. *J. Organomet. Chem.,* **1972**, *46*, C65.

53. Nishiyama, H.; Sakaguchi, H.; Nakamura, T.; Horihata, M.; Kondo, M.; Itoh, K. *Organometallics*, **1989**, *8*, 846.

54. Noyori, R.; Ohkuma, T.; Kitamura, M.; Takaya, H.; Sayo, N.; Kumobayashi, H.; Akutagawa, S. *J. Am. Chem. Soc.* , **1987**, *109*, 5856.

55. (a) Brunner, H.; Becker, R.; Reipel, G. *Organometallics,* **1984**, *3*, 1354. (b) Brunner, H.; Kürtzinger, A. *J. Organomet. Chem.,* **1988**, *346*, 413.

56. Payne, N.C.; Stephan, D.W. *Inorg. Chem.,* **1982**, *21*, 182.

57. Hayashi, T.; Mise, T.; Fukushima, M.; Kagotani, M.; Wagashima, N.; Hamada, Y.; Matsumoto, A.; Kawakami, S.; Konishi, M.; Yamamoto, K.; Kumada, M. *Bull. Chem. Soc. Jpn.,* **1980**, *53*, 1138.

58. Ojima, I.; Kogura, T.; Kumagai, M.; Horiuchi, S.; Sato, T. *J. Organomet. Chem.,***1976**, *122*, 83.

59. Hayashi, T.; Tamao, K.; Katsuro, Y.; Nakae, Y.; Kumada, M. *Tetrahedron Lett.* , **1980**, *21*, 1871.

60. Koenig, K.E. In *Asymmetric Synthesis;* Morrison, J.D., Ed.; Academic Press: Orlando, 1985; Vol.5, Ch.3.

61. Hayashi, T.; Yamamoto, K.; Kasuga, K.; Omizu, H.; Kumada, M. *J. Organomet. Chem.,* **1976**, *113*, 127.

62. Ojima, I.; Hirai, K. In *Asymmetric Synthesis;* Morrison, J.D., Ed.; Academic Press: Orlando, 1985; Vol.5, Ch.4.

63. Bohinski, R.C. *Modern Concepts in Biochemistry,* 5th ed; Allyn & Bacon: Boston, 1987; pp.540-544.

64. Bryndza, H.E.; Fong, I.K.; Paciello, R.A.; Tam, W.; Bercaw, J.E. *J. Am. Chem. Soc.,* **1987**, *109*, 1444.

65. (a) Bryndza, H.E. *Organometallics* , **1985**, *4*, 406. (b) *Idem*, **1985**, *4*, 1686.

66. Basolo, F.; Pearson, R.G. *Mechanisms of Inorganic Reactions—A Study of Metal Complexes in Solution,* 2nd. ed.; John Wiley & Sons: New York, 1967; pp.31-32.

67. Muetterties, E.L. *Transition Metal Hydrides;* Marcel Dekker: New York, 1971.

68. Milstein, D.; Calabrese, J.C.; Williams, I.D. *J. Am. Chem. Soc.,* **1986**, *108,* 6387.

69. Hillhouse, G.L.; Bercaw, J.E. *J. Am. Chem. Soc.,* **1984**, *106,* 5472.

70. Gotzig, R.; Werner, R. Werner, H. *J. Organomet. Chem.,* **1985**, *290,* 99.

71. Appleton, T.G.; Clark, H.C.; Manzer, L.E. *Coord. Chem. Rev.* , **1973**, *10,* 355.

72. Eady, O.R.; Johnson, B.F.G.; Lewis, J. *J. Chem. Soc. Dalton Trans.,* **1977**, 838.

73. Gillard, R.D.; Heaton, B.T.; Vaughan, D.H. *J. Chem. Soc. A.,* **1970**, 3126.

74. Yoshida, T.; Okano, T.; Saito, K.; Otsuka, S. *Inorg. Chim. Acta* , **1980**, *44,* L135.

75. Yoshida, T.; Okano, T.; Ueda, Y.; Otsuka, S. *J. Am. Chem. Soc.,* **1981**, *103,* 3411.

76. Khan, M.M.T.; Halligudi, S.B.; Skukla, S. *Angew. Chem., Int. Engl. Ed.,* **1988**, *27,* 1735.

77. Chaudret, B.N.; Cole-Hamilton, D.J.; Nohr, R.S.; Wilkinson, G. *J. Chem. Soc. Dalton Trans.,* **1972**, 1546.

78. Prystay, M.C. *B.Sc. thesis,* University of British Columbia,1988; p.13.

79. Gerlach, D.H.; Kane, A.R.; Parshall, G.W.; Muetterties, E.L. *J. Am. Chem. Soc.,* **1971**, *93,* 3543.

80. Yoshida, T.; Matsuda, T.; Okano, T.; Kitani, T.; Otsuka, S. *J. Am. Chem. Soc.* , **1976**, *98,* 850.

81. Yoshida, T.; Matsuda, T.; Okano, T.; Kitani, T.; Otsuka, S. *J. Am. Chem. Soc.* , **1979**, *101,* 2027.

82. Yoshida, T.; Ueda, Y.; Otsuka, S. *J. Am. Chem. Soc.,* **1978**, *100,* 3941.

83. Yoshida, T.; Otsuka, S. In *Catalytic Aspects of Metal Phosphine Complexes,* ACS Symposium Series 196; American Chemical Society: Washington, DC, 1982; Ch.8.

84. James, B.R.; Preece, M.; Robinson, S.D. In *Catalytic Aspects of Metal Phosphine Complexes,* ACS Symposium Series 196; American Chemical Society: Washington, DC, 1982; Ch.9.

85. Ref. 1, p.410.

86. Pearson, R.G. *J. Am. Chem. Soc.*, **1963**, *85*, 3533.

87. Pearson, R.G. *J. Chem. Educ.*, **1968**, *45*, 643.

88. Ref. 1, pp.412-414.

89. Bryndza, H.E.; Tam. W. *Chem. Rev.*, **1988**, *88*, 1163.

90. Yamamoto, T.; Kohara, T.; Yamamoto, A. *Bull. Chem. Soc. Jpn.*, **1981**, *54*, 2161.

91. Komiya, S.; Akai, Y.; Tanaka, K.; Yamamoto, T.; Yamamoto, A. *Organometallics*, **1985**, *4*, 1130.

92. Bennett, M.A.; Yoshida, T. *J. Am. Chem. Soc.*, **1978**, *100*, 1750.

93. Michelin, R.A.; Napoli, M.; Ros, R. *J. Organomet. Chem.*, **1979**, *175*, 239.

94. Bryndza, H.E.; Calabrese, J.C.; Wreford, S.S. *Organometallics*, **1984**, *3*, 1603.

95. Kim, Y-J.; Osakada, K.; Sugita, K.; Yamamoto, T.; Yamamoto, A. *Organometallics*, **1988**, *7*, 2182.

96. Newman, L.J.; Bergman, R.G. *J. Am. Chem. Soc.*, **1985**, *107*, 5314.

97. Sostero, S.; Traversso, O.; Ros, R.; Michelin, R.A. *J. Organomet. Chem.*, **1978**, *246*, 325.

98. Halpern, J.; Sen, A.; Abis, L. *J. Am. Chem. Soc.*, **1978**, *100*, 2915.

99. Michelin, R.A.; Faglia, S.; Ugualiati, P. *Inorg. Chem.*, **1983**, *22*, 1831.

100. Ref. 1, p.332.

101. (a) Brown, M.P.; Puddephatt, R.J.; Upton, C.E.E.; Lavington, S.W. *J. Chem. Soc., Dalton Trans.*, **1974**, 1613. (b) Evitt, E.R.; Bergman, R.G. *J. Am. Chem. Soc.*, **1980**, *102*, 7003.

102. Appleton, T.G.; Bennett, M.A. *Inorg. Chem.*, **1978**, *17*, 738.

103. Benard, K.A.; Atwood, J.D. *Organometallics*, **1987**, *6*, 1133.

104. Ref. 89, footnote 147.

105. Halpern, J.; Harrod, J.F.; James, B.R. *J. Am. Chem. Soc.*, **1961**, *83*, 753.

106. Halpern, J.; Harrod, J.F.; James, B.R. *J. Am. Chem. Soc.*, **1966**, *88*,, 5150.

107. Halpern, J.; James. B.R. Kemp, A.L.W. *J. Am. Chem. Soc.,* **1961,** *83,* 4097.

108. James, B.R.; Rempel, G.L. *J. Am. Chem. Soc.,* **1969,** *91,* 863.

109. James, B.R.; Louie, J. *Inorg. Chim. Acta,* **1969,** *3,* 568.

110. McMillen, D.F.; Golden, D.M. *Ann. Rev. Phys. Chem.,* **1982,** *33,* 493.

111. Hodgson, M.; Parker, D.; Taylor, R.J.; Ferguson, G. *Organometallics* , **1988,** *7,* 1761.

112. Tolman, C.A.; McKinney, R.J.; Seidel, W.C.; Bruliner, J.D.; Stevens, W.R. *Adv. Catal.,* **1985,** *33,* 1.

113. Tolman, C.A.; Seidel, W.C.; Bruliner, J.D.; Domaille, P.J. *Organometallics* , **1984,** *3,* 33.

114. McKinney, R.J.; Roe, D.C. *J. Am. Chem. Soc.,* **1986,** *108,* 5167.

115. James, B.R. In *Comprehensive Organometallic Chemistry;* Wilkinson, G., Stone, F.G.A., Abel, E.W., Eds.; Pergamon Press: Oxford, 1982; Vol. 8 , Ch.51, p.353.

116. Ref. 1, pp.568-571.

117. Ref. 1, p.826.

118. Davies, W.C.; Mann, F.G. *J. Chem. Soc.,* **1944,** 276.

119. Mann, F.G.; Watson, J. *J. Org. Chem.,* **1948,** *13,* 502.

120. Wibaut, J.P.; Jonge, A.P.de; Voort, H.G.P. van der; Otto, P.P.H.L. *Rec. Trans. Chim.,* **1951,** *70,* 1054 through *C.A.,* **1952,** *46,* 11197d.

121. Plazek, E.; Tyka, R. *Zeszyty Nauk. Politech. Wroclaw., Chem.,* **1957,** *4,* 79 through *C.A.,***1958,** *52,* 20156c.

122. Boggess, R.K.; Zatko, D.A. *J. Coord. Chem.,* **1975,** *4,* 217.

123. Ch. 2 of this thesis.

124. Keene, F.R.; Snow, M. R.; Stephenson, P.J.; Tiekink, E.R.T. *Inorg. Chem.,* **1988,** *27,* 2040.

125. Kurtev, K.; Ribola, D.; Jones, R.A.; Cole-Hamilton, D.J.; Wilkinson, G. *J. Chem. Soc. Dalton Trans.* , **1980,** 55.

126. Bianco, V.P.; Boronzo, S. *Inorg. Synth.* **1976,** *16,* 161.

127. Newkome, G.R.; Hager, D.C. *J. Am. Chem. Soc.*, **1978**, *100*, 5567.

128. Maisonnet, A.; Farr, J.P.; Olmstead, M.M.; Hunt, C.T.; Balch, A.L. *Inorg. Chem.*, **1982**, *21*, 3961.

129. Tolmachev, A.A.; Kozlov, E.S.; Pinchuk, A.M. *Zh. Obshck. Khim.*, **1984**, *54*, 971.

130. Wajda-Hermanowicz, K.; Pruchnik, F.R. *Transition Met. Chem.*, **1988**, *13*, 22.

131. Meek, D.W. Ref. 48, p.257.

132. Keene, F.R.; Snow, M.R.; Tiekink, E.R.T. *Acta Crystallogr., Sect. C: Cryst. Struct. Commun.*, **1988**, *44*, 757.

133. Wajda-Hermanowicz, K.; Pruchnik, F.R. *Transition Met. Chem.*, **1988**, *13*, 101

134. Zhang, Z.; Wang, H.; Wang, H-G.; Wang, R. *J. Organomet. Chem.*, **1986**, *314*, 357.

135. Farr, J.P.; Olmstead, M.M.; Hunt, C.H.; Balch, A.L. *Inorg. Chem.*, **1983**, *22*, 3387.

136. Alcock, N.W.; Moore, P.; Lampe, P.A.; Mok, K.F. *J. Chem. Soc. Dalton Trans.*, **1982**, 207.

137. Olmstead, M.M.; Maisonnat, A.; Farr, J.P.; Balch, A.L. *Inorg. Chem.*, **1981**, *20*, 4060.

138. Wasserman, H.J.; Moody, D.C.; Paine, R.T.; Ryne, K.R.; Saluzar, K.V. *J. Chem. Soc. Chem. Commun.*, **1984**, 537.

139. Ehrlish, M.G.; Fronczek, F.R.; Watkins, G.R.; Newkome, G.R.; Hager, D.C. *Acta Crystallogr., Sect. C: Cryst. Struct. Commun.*, **1984**, *40*, 78.

140. (a) Barder, T.J.; Cotton, F.A.; Powell, G.L.; Tetrick, S.M.; Walton, R.A. *J. Am. Chem. Soc.*, **1984**, *106*, 1323. (b) Barder, T.J.; Tetrick, S.M.; Walton, R.A.; Cotton, F.A.; Powell, G.C. *J. Am. Chem. Soc.*, **1983**, *105*, 4090.

141. Farr, J.P.; Olmstead, M.M.; Wood, F.E.; Balch, A.L. *J. Am. Chem. Soc.*, **1983**, *105*, 792.

142. Farr, J.P.; Olmstead, M.M.; Hunt, C.H.; Balch, A.L. *Inorg. Chem.*, **1981**, *20*, 1182.

143. Farr, J.P.; Olmstead, M.M.; Balch, A.L. *J. Am. Chem. Soc.*, **1980**, *102*, 6654.

144. Boggess, R.K.; Huges, J.W.; Chew, C.W.; Kemper, J.J. *J. Inorg. Nucl. Chem.*, **1981**, *43*, 939.

145. Lomakina, L.N.; Ignat Va, T.I.; Pisareve, S.A.; Ya Medved, T.; Kabachnik, M.I. *Zh. Anal. Khim.*, **1980**, *35*, 86.

146. Wood, F.E.; Olmstead, M.M.; Farr, J.P.; Balch, A.L. *Inorg. Chim. Acta* , **1985**, *97*, 77.

147. Navrail, J.D.; Schulz, W.W.; Talbot, A.E. *Actinide Recovery from Waste and Low Grade Resource;* Harwood Academic: New York, 1982.

148. Schulz, W.W.; Narail, J.D. In *Recent Developments in Separation Science* ; Li, N.N., Ed.; CRC: Boca Raton, Fla., 1982; p.31.

149. Mecabe, D.J.; Russell, A.A; Karthikeyan, S.; Paine, R.T. Ryan, R.R.; Smith, B. *Inorg. Chem.*, **1987**, *26*, 1230.

150. Lugan,N.; Lavigne, G.; Bonnet, J.J. *Inorg. Chem.*, **1987**, *26*, 585.

151. Garrou, P.E. *Chem. Rev.*, **1985**, *85*, 171.

152. Drent, E. *Eur. Patent,* Appl. Ep 271144 A2, 1988 through *C.A.*, **1989**, *110*, 232239c.

153. Lindner, E.; Rauleder, H.; Wegner, P. *Z. Naturforsch., B: Anorg. Chem., Org. Chem.*, **1984**, *39 B*, 1224.

154. Pruchnik, F.P.; Kuczewska-Patrzalek, G.; Wajda-Hermanowicz, K. *Pol. Patent,* Pl. 128,190 ,1984 through *C.A.*, **1986**, *104*, 209509h.

155. Lee, C-L.; Yang, Y-P.; James, B.R. Unpublished results.

156. Joó, F.; Tóth, Z. *J. Mol. Catal.*, **1980**, *8*, 369.

157. (a) Kullberg, M.L.; Kubiak, C.P. *Organometallics,* **1984**, *3*, 632. (b) Kullberg, M.L.; Kukiak, C.P. *C1 Mol. Chem.*, **1984**, *1*, 171. (c) Kullerg, M.L.; Lemke, F.R.; Powell, D.R., Kubiak, C.P. *Inorg. Chem.*, **1985**, *4*, 3589.

Chapter 2

General Experimental Procedures

2.1. Materials

Spectral or reagent grade solvents, such as dichloromethane, benzonitrile, and diethyl ether, etc., were obtained from the commercial suppliers, Aldrich, Eastman, Fisher, or BDH. Where necessary, dichloromethane was dried over phosphorus pentoxide and distilled under nitrogen prior to use. Hexanes, THF, benzene and toluene were dried with sodium/ benzophenone ketyl and distilled just before use. Chloroform was purified by passing through an Alumina (neutral, Fisher Scientific) column. Methanol and ethanol were refluxed over alkoxides formed by reaction of Mg turnings with alcohol initiated by trace amount of I_2, and were distilled under nitrogen.

Deuterated solvents used in the present study, acetone-d_6, chloroform-d_1, toluene-d_8, dichloromethane-d_2, and benzene-d_6, were obtained from Merck Frosst Canada Inc., and degassed by three to six "freeze-pump-thaw" cycles for anaerobic NMR studies.

Anhydrous HCl(g) was supplied by BDH Chemical Co. Ethylene (CP Grade) was used as supplied from Matheson Gas Co. Argon, nitrogen, and oxygen (99.99%) were supplied by Union Carbide of Canada Ltd. All gases were used without purification.

Platinum and palladium were supplied on loan from Johnson Matthey Ltd. as $(PtCl_2)_n$, K_2PtCl_4 and $(PdCl_2)_n$. Chromium trichloride hexahydrate, $CrCl_3{\cdot}6H_2O$, was purchased from Aldrich Chemical Co. Potassium dichromate, $K_2Cr_2O_7$ (Aldrich), was used as supplied.

Diphenylchlorophosphine (PPh_2Cl) and dichlorophenylphosphine ($PPhCl_2$) were purchased from Aldrich chemical Co. and distilled before use. Phosphorus trichloride, PCl_3, was supplied by Mallinckrodt chemical Co., and was purified by distillation at 70 - 72°C after 30 min of vigorous reflux under N_2. 2-Bromopyridine, purchased from Aldrich, was purified by

stirring with NaOH pellets overnight at room temperature and then distilling from CaO under vacuum prior to use. 2-Chloropyridine (Aldrich Chemical Co.) was used without purification. Dimethylacetylenedicarboxylate, DMAD, supplied by Aldrich, was distilled under vacuum for kinetic studies only. Acrylonitrile, methacrylonitrile, crotonitrile and diethyl maleate (Aldrich) were distilled over CaO under reduced pressure and kept in the fridge. n-Butyllithium (1.60 M in hexane) and methyllithium (1.56 M in ether) were used as supplied from Aldrich. Dibenzylideneacetone, dba, was synthesized by a literature method.[1] Anhydrous hydrazine and the hydrate (reagent grades) were supplied by MCB Co. and used without further purification. Maleic acid and fumaric acid, purchased from Fisher Scientific Co., were recrystallized twice from water. Aconitic acid, mesaconic acid, R, S-malic acid and maleic anhydride were supplied by Aldrich and used without further purification.

2.2. General instrumentation

Visible absorption spectra were recorded on a thermostated (± 0.1°C) Perkin-Elmer 552A spectrophotometer, using spectral quartz cells of 1 or 10 mm path length. Absorbance data for kinetic experiments were obtained either from the digital display on the instrument at the wavelength of interest, or taken from the repetitive scanning spectra. Times were recorded either directly from a Lab-chron 1400 timer for faster reactions (10 - 20 s between readings), or by a built-in timer for slower reaction (3 to 90 min between readings). For recording visible spectra under anaerobic condition, the one type of cell shown in Fig. 2.1 was employed. The details of sample preparation and time recording for the kinetic studies will be described in Chapter 4, Sect. 4.2.

Infrared spectra were recorded on a Nicolet 5DX-FT or a Perkin-Elmer 598 spectrophotometer calibrated with the 1601 cm^{-1} peak of polystyrene film. Nujol mulls between KBr or CsI plates were normally used for solid state IR, while KRS-5 plates (42% TlBr + 58% TlI, Harshaw Chem. Co.) were used for the cis-$PdCl_2(PN_3)_2$ and cis-$PtCl_2(PN_3)_2$ species. A KBr solution cell with path length 0.1 mm was used for solution IR samples.

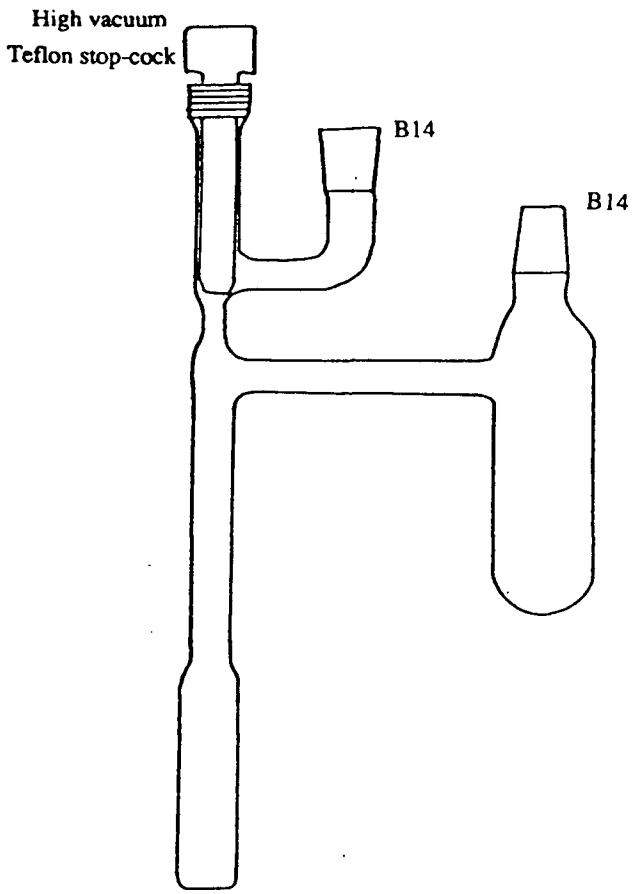

Fig. 2.1. Schematic representation of a spectral cell.

Nuclear magnetic resonance spectra were obtained on a Varian XL-300 MHz spectrometer using 5 mm NMR tubes. ^{1}H chemical shifts were recorded in ppm relative to external TMS, and ^{13}C chemical shifts were relative to external TMS or the $CDCl_3$ solvent peak at 77.1 ppm. All ^{31}P chemical shifts, both in solution and in solid state, were referenced to external 85% H_3PO_4. The ^{195}Pt chemical shifts were referenced to the absolute resonance frequency of ^{195}Pt which itself is relative to the ^{1}H resonance of TMS; at 100 MHz, $\Xi Pt = 21.4$ MHz,[2, 3] or 64.2 MHz on the Varian XL-300 spectrometer. This Pt reference is -4535 ppm upfield from the $PtCl_6^{2-}$ standard[4] which is frequently cited in the literature. Solid state $^{31}P\{^{1}H\}$ NMR spectra were recorded on a Bruker CXL-100 MHz instrument using a cross polarization and magic angle spinning FT programme. The high-frequency-positive convention, recommended by IUPAC, has been used in reporting all chemical shifts. Simulation of ^{31}P and

^{195}Pt NMR spectra were performed using the Bruker software PANIC85 on BDS-1000, or UBCPANIC on ASPECT-2000. The fit of the simulation was based on matching the individual peak positions of the experimental and calculated spectra.

Melting points of phosphine ligands were determined using a 6548-J17 microscope equipped with a Thomas model 40 micro, hot stage, melting point apparatus. GC analyses for organic compounds (in Ch. 5) were performed with an Hewlett-Packard 5890A instrument using a thermal conductivity detector and a 6-ft Porapak-Q column. Conductivity measurements were recorded in a cell (Fisher Scientific Co., cell constant 1.0) connected to a Beckman Serfass conductance bridge. pH-Titrations were carried out in aqueous media using a Corning 12 pH-meter and a combination glass electrode; care was taken to ensure that each reading recorded represented equilibrium conditions. The atmosphere was kept CO_2-free by bubbling presaturated N_2 through the solution. The temperature was maintained constant within 0.2°C by a water-bath equipped with a thermocouple.

Elemental analyses were performed by Mr. P. Borda of this department. The X-ray crystal structure determination of $Pt_2Cl_2(\mu\text{-}PN_2)_2$ (HT) was carried out by Dr. S.J. Rettig of this department.

2.3. Preparation of Pt and Pd starting materials

2.3.1. Dichlorobis(benzonitrile)-palladium(II) and -platinum(II)

The precursors $PdCl_2(PhCN)_2$ and $PtCl_2(PhCN)_2$ were prepared by standard methods described in the literature [5] using $(PdCl_2)_n$ and $(PtCl_2)_n$, respectively.

The $PtCl_2(PhCN)_2$ compound was also synthesized from K_2PtCl_4 by reaction with benzonitrile in a biphasic system. Some K_2PtCl_4 (2.0 g, 4.8 mmol) was dissolved in a minimum amount of water to which 30 mL of benzonitrile was added, and the mixture was then heated on a steam bath until the aqueous layer turned colourless. The yellow benzonitrile solution of $PtCl_2(PhCN)_2$ was separated from the aqueous layer while still hot and then left at

-20°C overnight. The yellow crystals that separated were collected by filtration, washed carefully with Et_2O, and dried in vacuo at 80°C; yield 1.2 g (55%). Anal. calcd. for $C_{14}H_{10}N_2Cl_2Pt$: C 35.61, H 2.13, N 5.93; found: C 35.77, H 2.11, N 5.96.

2.3.2. Cis-dichloro(1, 5-cyclooctadiene)platinum(II)

The cis-$PtCl_2$(COD) complex was prepared by a published procedure,[6] the purity being ascertained by elemental analysis; yield 76%. Anal. calcd. for $C_8H_{12}Cl_2Pt$: C 25.68, H 3.23; found: C 26.02, H 3.45.

2.3.3. Tris(dibenzylideneacetone)dipalladium(0), $Pd_2(dba)_3$

The title compound, $Pd_2(dba)_3$, was prepared by a modified literature procedure;[7] the benzonitrile precursor was used instead of $[PdCl_2]_n$. To a reaction flask containing 150 mL MeOH was added $PdCl_2(PhCN)_2$ (2.3 g, 6 mmol), dba (4.6 g, 19.0 mmol) and sodium acetate (3.9 g, 47.5 mmol). The mixture was refluxed for 1 h and then cooled to r.t. The precipitated product was filtered, washed with H_2O and acetone successively, and dried in vacuo to give a reddish purple solid; yield 4.0 g (73%). This compound was redissolved in hot $CHCl_3$ (130 mL) and reprecipitated with diethyl ether (100 mL) to yield the solvated, dark purple, microcrystalline compound $Pd_2(dba)_3 \cdot CHCl_3$. Anal. calcd. for $C_{51}H_{42}O_3Pd_2 \cdot CHCl_3$: C 60.34, H 4.19; found: C 59.87, H 4.01.

2.3.4. Bis(dibenzylideneacetone)platinum(0), $Pt(dba)_2$

The $Pt(dba)_2$ complex was prepared according to a literature procedure.[8] A hot aqueous solution (5 mL) of K_2PtCl_4 (1.0 g, 2.4 mmol) was added to a well stirred, refluxing solution of dba (1.6 g, 6.7 mmol) and sodium acetate (2.6 g, 32 mmol) in EtOH (50 mL) under N_2. The solution rapidly turned dark green and was left refluxing for 5 h (10 min in the original procedure). The mixture was cooled and the resulting black precipitate was filtered off. The crude product was run through a silica gel column using CH_2Cl_2. The purple eluent was

collected, and evaporated to dryness, and the resulting solid dried in vacuo; yield 0.97 g (61%). Anal. calcd. for $C_{34}H_{28}O_2Pt$: C 61.53, H 4.25; found: C 60.97, H 4.41.

2.4. Preparation of 2-Pyridylphosphines

Syntheses of $PPh_{3-n}py_n$, or PN_n (n = 1, 2, 3), were carried out under N_2 using conventional bench-top techniques for manipulation of air-sensitive compounds.[9] The phosphines, for convenience, are designated as PN_1, PN_2, and PN_3, respectively, according to the number of incorporated pyridyl substituents. These abbreviations will be used throughout this thesis.

2.4.1. 2-(Diphenylphosphino)pyridine

The ligand PPh_2py, or PN_1, was previously prepared in this group following the reported procedure[10] via diphenylphosphine, PPh_2H, which was itself made according to a literature method.[11] Diphenylphosphine is a bad smelling, toxic compound and is very air-sensitive. All the manipulations were carried out in an efficient fumehood. The yield of the PN_1 production step is 80%, while the overall yield from PPh_3 is 56%. The reaction procedure is outlined in the following equations:

$$PPh_3 \xrightarrow[+2Li]{THF,\ r.t.} PPh_2Li + PhLi \xrightarrow[-2LiOH]{2H_2O} PPh_2H + PhH$$

$$PPh_2H \xrightarrow[-CH_4]{THF,\ r.t.} PPh_2Li \xrightarrow[-LiCl]{2\text{-chloropyridine}} PPh_2py$$

An alternative route was via the procedure used to make PN_3, but using PPh_2Cl (80 mmol) in place of PCl_3 (see below); white crystals of PN_1 were obtained after recrystallization, yield 45 - 50%. The latter preparation is preferred because it requires a shorter reaction time and simpler work-up procedure. Anal. calcd. for $C_{17}H_{14}NP$: C 77.54, H 5.36, N 5.32; found: C

76.92, H 5.37, N 5.14. M.p. 84.5 - 86°C; lit. 82° [10] and 85°C.[12] $^{31}P\{^1H\}$ NMR data ($CDCl_3$, r.t.): -3.28 (s).

2.4.2. Bis(2-pyridyl)phenylphosphine

The ligand $PPhpy_2$ (PN_2) was prepared by the method described in the next section for Ppy_3, but using $PPhCl_2$ (40 mmol) instead of PCl_3. White crystals were obtained after recrystallization from acetone-petroleum ether (b.p. 30 - 60°C), yield 53 - 60%.

Anal. calcd. for $C_{16}H_{13}N_2P$: C 72.71, H 4.96, N 10.60; found: C 72.90, H 4.99, N 10.43. $^{31}P\{^1H\}$ NMR data ($CDCl_3$, r.t.): -1.98 (s). M.p. 96.7 - 98.3°C; lit. 96°C.[12]

2.4.3. Tris(2-pyridyl)phosphine

The ligand Ppy_3 (PN_3) was prepared by a modified version of a procedure described in the literature.[13]

A 50 mL of n-butyllithium (1.6 M in hexane, 80 mmol) was transferred to a flask containing 50 mL of diethyl ether at -100°C. 2-Bromopyridine (8 mL, 80 mmol) was introduced and then the mixture was stirred vigorously at -100°C for 4 h until the colour turned to deep red. Liquid PCl_3 (2.3 mL, 27 mmol) in Et_2O (15 mL) was then added dropwise via a syringe with vigorous stirring of the reaction solution. A light brown slurry was obtained. Before being warmed to r.t. gradually, the reaction mixture was stirred at -90°C for another 2 h. The mixture was extracted with degassed H_2SO_4 (2M, 2x100mL), and the aqueous layer collected. The aqueous solution was then made alkaline by adding saturated NaOH at 0°C and stirred, whereupon yellow crystals were deposited. The collected yellow crystals were washed thoroughly with H_2O and then acetone:H_2O (1:1), and recrystallized from acetone-petroleum ether (1:1) and dried in vacuo; yield 30 - 46%.

Anal. calcd. for $C_{15}H_{12}N_3P$: C 67.91, H 4.56, N 15.84; found: C 68.10, H 4.45, N 15.87. $^{31}P\{^1H\}$ data ($CDCl_3$, r.t.): -0.05 (s). M.p. 114.5 - 116°C; lit. 115° [12] and 111 - 113°C.[14, 15]

2.5. Preparation of Pt(II) and Pd(II) complexes of 2-pyridylphosphines

2.5.1. Cis-dihalobis(2-pyridyl)phosphineplatinum(II), **1a - 1c**

The complexes cis-$PtCl_2(PN_n)_2$, n = 1 (**1a***), 2 (**1b**) and 3 (**1c**), were obtained by reacting a yellow CH_2Cl_2 solution (50 mL) of cis-$PtCl_2$ $(PhCN)_2$ (~ 1.0 g, 3.76 mmol) with a colourless solution of 2.0 equivalent of PN_n (n = 1 - 3) in CH_2Cl_2 (15 mL). The reaction mixture was stirred for 1 h at r.t, and the resulting colourless solution was concentrated to ~ 15 mL before Et_2O (20 mL) was added to complete the precipitation. The white solid (**1a - 1c**) were collected by filtration and washed by Et_2O; yield ~90%. These compounds can also be made using cis-$PtCl_2$(COD) in place of cis-$PtCl_2(PhCN)_2$. The elemental analyses of compounds **1a - 1c** are listed in Table 2.1, while the $^{31}P\{^1H\}$ NMR data are listed in Table 3.1.

Table 2.1. Elemental Analyses of Cis-$PtX_2(PN_n)_2$ Complexes

Complexes	C		H		N	
	calcd.	found	calcd.	found	calcd.	found
$C_{34}H_{28}N_2Cl_2P_2Pt$, **1a**	51.52	51.32	3.56	3.67	3.54	3.29
$C_{34}H_{28}N_2I_2P_2Pt$, **3a**	41.86	42.03	2.89	3.05	2.87	2.60
$C_{32}H_{26}N_4Cl_2P_2Pt$, **1b**	48.36	46.44	3.30	3.32	7.05	6.66
$C_{32}H_{26}N_4I_2P_2Pt$, **3b**	39.32	38.94	2.68	2.74	5.73	5.57
$C_{30}H_{24}N_6Cl_2P_2Pt$, **1c**	45.23	45.46	3.04	2.94	10.55	10.51
$C_{30}H_{24}N_6Br_2P_2Pt$, **2c**	40.23	40.55	2.73	2.83	9.49	9.28
$C_{30}H_{24}N_6I_2P_2Pt$, **3c**	36.77	36.53	2.47	2.46	8.58	8.41

The complexes cis-$PtX_2(PN_n)_2$ (X = Br, n = 3 (**2c**); X = I, n = 1 (**3a**), 2 (**3b**) and 3 (**3c**)) were made by metathesis of cis-$PtCl_2(PN_n)_2$ with the appropriate NaX. Complex **1a** (0.20 g, 0.250 mmol), **1b** (0.20 g, 0.250 mmol) or **1c** (0.20 g, 0.251 mmol) was suspended in

* **a, b** and **c** will be used throughout this thesis to label complexes containing PN_1, PN_2 and PN_3 phosphine, respectively.

CH_2Cl_2 (20 mL), and about a five-fold excess of NaX dissolved in a minimum amount of water was added to the suspension. A small amount of MeOH (5 mL) was introduced to homogenize the mixture, which was then stirred at r.t. for about 1 h. The solution turned to pale or bright yellow for bromide or iodide, respectively, and was then concentrated to about 8 mL; the product precipitated was collected by filtration, washed extensively with H_2O and MeOH, and dried in vacuo; yields ~85%.

The elemental analyses of compounds **2c** and **3a** - **3c** are also listed in Table 2.1; the $^{31}P\{^1H\}$ NMR data are given in Table 3.1. Compounds $PtCl_2(PN_1)_2$, **1a**, and $PtI_2(PN_1)_2$, **3a**, have been reported previously by Farr et al.[16]

2.5.2. Dihalobis(2-pyridylphosphine)palladium(II), **4-6**

Most of the complexes under this heading have been made before, except **5b** and **6b**. $PdCl_2(PN_1)_2$, **4a**, and $PdCl_2(PN_2)_2$, **4b**, were reported by Balch's group[17] and Newkome's group[18] respectively. The others were made in our own group via a simple substitution of the coordinated benzonitrile groups by the corresponding phosphine;[19] however, these complexes were not characterized in terms of geometry and the elemental analyses were not satisfactory. Therefore, complexes **4c**, **5a** - **5c**, and **6a** - **6c** were prepared by the following procedures and characterized; **4a** and **4b** were also prepared. The $^{31}P\{^1H\}$ NMR data of the complete series are listed in Table 3.2.

Compounds $PdCl_2(PN_n)_2$ (**4a** - **4c**) were made by dissolving $PdCl_2(PhCN)_2$ (300 mg, 0.781 mmol) in CH_2Cl_2 (20 mL), and adding to this reddish-brown solution two equivalents of PN_n (n = 1 - 3) dissolved in a minimum amount of CH_2Cl_2 (7 mL). After the solution mixture was stirred at r.t. for 30 min, a yellow solid slowly precipitated; Et_2O (40 mL) was added to complete the precipitation. Species **4a** - **4c** were purified after dissolution and reprecipitation from CH_2Cl_2/Et_2O twice and dried in vacuo; yields ~95%.

The compounds $PdX_2(PN_n)_2$ (X = Br, I; n = 1 - 3, **5a** - **5c** and **6a** - **6c**) were prepared through the same method of metathesis as used for **2c** and **3b**, **3c**; yields 85 - 90%. The

elemental analyses of **4c**, **5a** - **5c**, and **6a** - **6c**, and the visible spectral data of **4a** - **4c**, **5a** - **5c**, and **6a** - **6c**, are summarized in Tables 2.2 and 2.3, respectively.

Table 2.2. Elemental Analyses of $PdX_2(PN_n)_2$ Complexes

Complexes	C		H		N	
	calcd.	found	calcd.	found	calcd.	found
$C_{34}H_{28}N_2Cl_2P_2Pd$, **4a**	58.01	57.89	4.01	4.27	3.98	4.20
$C_{34}H_{28}N_2Br_2P_2Pd$, **5a**	51.51	51.42	3.56	3.53	3.53	3.42
$C_{34}H_{28}N_2I_2P_2Pd$, **6a**	46.05	45.94	3.18	3.09	3.16	2.99
$C_{32}H_{26}N_4Cl_2P_2Pd$, **4b**	54.45	54.67	3.71	3.99	7.94	7.88
$C_{32}H_{26}N_4Br_2P_2Pd$, **5b**	48.36	46.84	3.30	3.52	7.05	6.71
$C_{32}H_{26}N_4I_2P_2Pd$, **6b**	43.24	41.85	2.95	2.82	6.31	6.59
$C_{30}H_{24}N_6Cl_2P_2Pd$, **4c**	50.90	50.62	3.42	3.34	11.87	11.90
$C_{30}H_{24}N_6Br_2P_2Pd$, **5c**	45.22	44.55	3.04	3.00	10.55	9.94
$C_{30}H_{24}N_6I_2P_2Pd$, **6c**	40.45	39.90	2.72	2.65	9.44	9.51

Table 2.3. Visible Spectral Data of $PdX_2(PN_n)_2$ Complexes [a]

Complexes	λ_{max} (εx10^{-3})
4a	340(13.2)
5a	363(9.73)
6a	425(3.11)
4b	337(6.21)
5b	362(6.63)
6b	421(3.62)
4c	338(3.42)
5c	362(4.13)
6c	428(3.03)

(a) Measured in CH_2Cl_2, at r.t.; λ in nm and ε in $M^{-1}cm^{-1}$.

2.6. Preparation of homo- and hetero-binuclear platinum(I) and palladium(I) complexes of pyridylphosphines

2.6.1. Dihalobis(2-pyridylphosphine)diplatinum(I) (head-to-tail, HT), **7 - 9**

The complexes $Pt_2X_2(\mu\text{-}PN_n)_2$(HT) (X = Cl, n = 1 (**7a**), 2 (**7b**), 3 (**7c**); X = Br, n = 3 (**8c**)) were made using a modified literature procedure.[16] A purple $CHCl_3$ solution (60 mL) of $Pt(dba)_2$ (0.25 g, 0.38 mmol) was added dropwise to a $CHCl_3$ solution (40 mL) of the corresponding cis-$PtX_2(PN_n)$ complex, **1a** - **1c**, or **2c** (0.38 mmol), and the mixture was then refluxed under N_2 for 5 h. TLC was performed every 30 min until the $Pt(dba)_2$ had all been consumed. The $CHCl_3$ solvent was completely removed on the rotary evaporator, and the crude product mixture was redissolved in CH_2Cl_2. The solution was then charged on to a silica gel column, and 2% MeOH in CH_2Cl_2 was used as eluent. The reddish-orange eluate following the yellow dba band was collected. An orange (**7a** - **7c**) or brownish-orange solid (**8c**) was obtained after solvent evaporation, respectively. The products were recrystallized from CH_2Cl_2/Et_2O (1:1), and dried in vacuo; yield 50 - 60%. The complex $Pt_2Cl_2(\mu\text{-}PN_1)_2$ (HT), **7a**, was previously made by Balch's group.[16]

The $Pt_2Cl_2(\mu\text{-}PN_2)_2$(HT) (**7b**) sample separated by column chromatography (~3 mg) was dissolved in CH_2Cl_2 (1.0 mL), on top of which MeOH (1.0 mL) was carefully placed. The red, hexagonal flakey single crystals of $Pt_2Cl_2(\mu\text{-}PN_2)_2$(HT) (1S, 2S) (see Sect. 3.2.3) for X-ray diffraction analysis were thus grown by the slow diffusion of MeOH into the CH_2Cl_2 solution at 5°C.

Complexes $Pt_2I_2(\mu\text{-}PN_n)_2$ (HT), n = 2 (**9b**) or 3 (**9c**), were prepared by metathesis of $Pt_2Cl_2(\mu\text{-}PN_n)_2$ (**7b** or **7c**) with NaI, using the method described for **3c** (Sect. 2.5.1). The products were obtained as pure HT form in nearly quantitative yield. Analytical data of the HT isomers of $Pt_2X_2(\mu\text{-}PN_n)_2$ are given in Table 2.4, and $^{31}P\{^1H\}$ NMR data in Table 3.5.

2.6.2. Diiodobis(2-pyridylphosphine)platinum(I) (head-to-head, HH), **10**

Complexes $Pt_2I_2(\mu\text{-}PN_n)_2$(HH), n = 1 (**10a**), 2 (**10b**) and 3 (**10c**), were synthesized by the procedure described for $Pt_2X_2(\mu\text{-}PN_n)_2$ (HT), X = Cl (**7c**) and Br (**8c**); see Sect. 2.6.1. The reactions were completed within 30 min to 1 h. The crude product was separated from free dba by column chromatography as described in Sect. 2.6.1. Pure HH isomer of $Pt_2I_2(\mu\text{-}PN_1)_2$, **10a**, was isolated (silica gel, CH_2Cl_2) from the first chromatography separation, while a mixture of HH and HT isomers was obtained for $Pt_2I_2(\mu\text{-}PN_2)_2$, **10b**, and $Pt_2I_2(\mu\text{-}PN_3)_2$, **10c**, with the HH isomer being a major product (HH/HT ~ 80%) (silica gel, 2% MeOH in CH_2Cl_2); the yield of **10a** was 60%, and the yields of **10b** (+ **9b**) and **10c** (+ **9c**) were ~ 65%.

Table 2.4. Elemental Analyses of $Pt_2X_2(\mu\text{-}PN_n)_2$ Complexes

Complexes	C		H		N	
	calcd.	found	calcd.	found	calcd.	found
$C_{34}H_{28}N_2Cl_2P_2Pt_2$, **7a** (HT)	41.35	41.60	2.86	2.96	2.84	3.15
$C_{34}H_{28}N_2I_2P_2Pt_2$, **10a** (HH)	34.89	34.77	2.41	2.30	2.39	2.13
$C_{32}H_{26}N_4Cl_2P_2Pt_2$, **7b** (HT)[a, b]	38.83	37.37	2.65	2.93	5.66	5.23
$C_{32}H_{26}N_4I_2P_2Pt_2$, **9b** (HT)[b]	32.78	32.42	2.23	2.25	4.78	4.60
$C_{32}H_{26}N_4I_2P_2Pt_2$, **10b** (HH)[b]	32.78	33.16	2.23	2.54	4.78	4.45
$C_{30}H_{24}N_6Cl_2P_2Pt_2$, **7c** (HT)	36.34	36.46	2.44	2.50	8.48	8.39
$C_{30}H_{24}N_6Br_2P_2Pt_2$, **8c** (HT)	33.34	33.20	2.24	2.34	7.78	7.72
$C_{30}H_{24}N_6I_2P_2Pt_2$, **9c** (HT)	30.67	30.69	2.06	2.14	7.15	6.96
$C_{30}H_{24}N_6I_2P_2Pt_2$, **10c** (HH)	30.67	30.65	2.06	2.01	7.15	7.08

(a) This compound is hygroscopic. The X-ray crystal structure is done for the (1S, 2S) diastereomer (Chapter 3, Fig. 3.11). (b) Mixture of diastereomers is analyzed.

The **10b** and **9b** mixture (0.28 g, 0.24 mmol), obtained after initial column chromatography (silica gel, 2% MeOH in CH_2Cl_2), was separated as three bands using a preparatory TLC plate (2 mm silica gel, 2% MeOH in CH_2Cl_2, 5 runs). The first band contained

10b.2/10b.3 (83 mg, 30%), the second band contained **10b.1** (92 mg, 33%), and the third band contained **9b** (36 mg, 13%). Complexes **10b.1**, **10b.2** and **10b.3** are optical isomers (see Sect. 3.2.3).

The red, single crystals of **10b.1** and **10b.2/10b.3** were grown by the same diffusion method as described for **7b** (Sect. 2.6.1) in CH_2Cl_2 (1.0 mL) and MeOH (1.0 mL) at 5°C. Compound **10b.1** grew as twin crystals on three occasions, and the **10b.2/10b.3** mixture grew as highly disordered single crystals.

Complex $Pt_2I_2(\mu\text{-}PN_3)_2(HH)$, **10c**, was obtained pure by fractional crystallization from CH_2Cl_2 and MeOH. The HT isomer **9c** was presumably more soluble and was left in the mother solution. The orange solid that came out from the solution after overnight standing in a freezer was the desired isomer.

Analytical data of the HH isomers **10a** to **10c** are listed in Table 2.4, and the $^{31}P\{^1H\}$ NMR data are given in Chapter 3 (Table 3.6). Compound $Pt_2I_2(\mu\text{-}PN_1)_2(HH)$, **10a**, has been made previously by Balch's group.[16] The spectroscopic data of **10a**, prepared in the present study, are in good agreement with the literature values.

Reaction of **10c** with greater than a two-fold excess of phosphine PN_3 yields a new tetrakisphosphine binuclear platinum species. The procedure for the isolation of the tetraphenylborate salt of this binuclear species, $[Pt_2(\mu\text{-}PN_3)_2(PN_3)_2](BPh_4)_2$, **41.2**, is described here. To an orange solution of **10c** (30 mg, 0.03 mmol) in CH_2Cl_2 (20 mL) was added solid PN_3 (30 mg, 0.11 mmol), and the mixture was stirred at r.t. for 15 min under air until the orange colour faded to nearly colourless. Water (15 mL) was added to extract the ionic species that had formed; to the extract was added excess $NaBPh_4$ (0.1 g, 0.3 mmol) in MeOH (5 mL). The bright yellow precipitate that formed was collected by filtration, purified by reprecipitation from acetone using Et_2O, and dried in vacuo; yield 55 mg (88%). Anal. calcd. for $C_{108}H_{88}N_{12}B_2P_4Pt_2$: C 62.07, H 4.24, N 8.04; found: C 62.43, H 4.35, N 7.94. UV/Vis.

(acetone, r.t.): λ_{max} = 336, 424 nm; ε_{max} = 1.6x10^4, 1.1x10^4 M^{-1}cm^{-1}. Molar conductivity (CH_3CN, r.t.): 204.3 Ω^{-1}mol^{-1}cm^2 at 1.9x10^{-3} M. ^{31}P and ^{195}Pt NMR: see Sect. 4.4.

2.6.3. Dihalobis(2-pyridylphosphine)dipalladium(I) (HT) (X = Cl, Br, I), **11 - 13**

Most of the binuclear palladium(I) HT isomers have been made before, except $Pd_2X_2(\mu\text{-}PN_2)_2$, X = Cl (**11b**), Br (**12b**), or I (**13b**). Complex $Pd_2Cl_2(\mu\text{-}PN_1)_2$, **11a**, was made by Maisonnat et al.[20] and complexes $Pd_2X_2(\mu\text{-}PN_n)_2$ (n = 1, X = Br (**12a**) and I (**13a**); n = 3, X = Cl, (**11c**), Br (**12c**), and I (**13c**)) were made previously in this laboratory.[19] The X-ray crystal structure of $Pd_2I_2(\mu\text{-}PN_n)_2$, **13c**, revealed the HT phosphine arrangement.[16] However, it was uncertain whether the rest of the binuclear palladium complexes were also adopting the same arrangement. In an effort to clear up the ambiguity regarding the relative orientation of these pyridylphosphine complexes, the complete series **11** to **13**, **a** to **c** inclusive (Table 2.5), were made according to the following procedure.

A dark violet, CH_2Cl_2 solution (20 mL) of $Pd_2(dba)_3{\cdot}CHCl_3$ (0.22 g, 0.21 mmol) was added slowly into a suspension of $PdX_2(PN_n)_2$ (0.42 mmol) in CH_2Cl_2 (20 mL). The resulting solution was stirred at r.t. for about 1 h until the suspended solid was all dissolved. The solution was concentrated to 10 mL, and Et_2O (10 mL) was added slowly to yield the desired products, which were reprecipitated from CH_2Cl_2 (15 mL) and Et_2O (10 mL) two or three times, and dried under vacuum; yield ~90%. The elemental analyses and the visible spectral data are summarized in Tables 2.5 and 2.6.

The $^{31}P\{^1H\}$ NMR data of the complete series are listed in Chapter 3 (Table 3.8). The structural characterization of these binuclear compounds, with emphasis on the diastereomers present, is discussed in Chapter 3.

Table 2.5. Elemental Analyses of $Pd_2X_2(\mu\text{-}PN_n)_2$ (HT) Complexes

Complexes	C calcd.	C found	H calcd.	H found	N calcd.	N found
$C_{34}H_{28}N_2Cl_2P_2Pd_2$, **11a**	51.40	51.17	3.48	3.25	3.46	3.73
$C_{34}H_{28}N_2Br_2P_2Pd_2$, **12a**	45.42	45.31	3.14	3.15	3.11	2.95
$C_{34}H_{28}N_2I_2P_2Pd_2$, **13a**	41.11	41.47	2.84	3.07	2.82	2.76
$C_{32}H_{26}N_4Cl_2P_2Pd_2{\cdot}2CH_2Cl_2$, **11b**[a]	44.17	44.06	3.37	3.23	6.24	6.27
$C_{32}H_{26}N_4Br_2P_2Pd_2$, **12b**	42.65	42.30	2.91	2.80	6.22	6.34
$C_{32}H_{26}N_4I_2P_2Pd_2$, **13b**	38.62	37.60	2.63	2.78	5.63	5.29
$C_{30}H_{24}N_6Cl_2P_2Pd_2$, **11c**	44.25	44.28	2.97	3.01	10.32	10.26
$C_{30}H_{24}N_6Br_2P_2Pd_2$, **12c**	39.90	39.63	2.68	2.70	9.31	9.00
$C_{30}H_{24}N_6I_2P_2Pd_2$, **13c**	36.14	36.08	2.43	2.40	8.43	8.20

(a) The chlorine analysis was done for this particular compound: calcd. 15.80, found 16.00.

Table 2.6. Visible Spectral Data of $Pd_2X_2(\mu\text{-}PN_n)_2$(HT) Complexes [a]

Complexes	λ_{max} (εx10^{-3})	
12a	348(13.7)	483(7.92)
13a	379(13.4)	540(10.8)
11b	333(10.8)	462(9.47)
12b	345(15.0)	476(9.90)
13b	376(15.3)	530(13.7)
11c	335(12.0)	460((8.43)
12c	348(11.6)	475(10.3)
13c	376(9.7)	525(11.7)

(a) Measured in CH_2Cl_2; the wavelength λ is in nm and the molar absorptivity ε is in $M^{-1}cm^{-1}$.

2.6.4. Dihalobis[tri(2-pyridyl)phosphine]palladium(I)platinum(I) (HT), **14c - 16c**

Complexes $PtPdX_2(\mu\text{-}PN_3)_2$ (HT) (X = Cl (**14c**), Br (**15c**) and I (**16c**)) were prepared by reaction of the appropriate cis-$PtX_2(PN_3)_2$ with $Pd_2(dba)_3{\cdot}CHCl_3$ using the same conditions described for the syntheses of $Pt_2X_2(\mu\text{-}PN_n)_2$ (HT) (Sect. 2.6.1). Head-to-tail isomers were formed exclusively. Analytical data are given in Table 2.7, while the $^{31}P\{^1H\}$ NMR data are given in Chapter 3, Table 3.7.

Table 2.7. Elemental Analyses of $PtPdX_2(\mu\text{-}PN_3)_2$ (HT) Complexes

Complexes	C		H		N	
	calcd.	found	calcd.	found	calcd.	found
$C_{30}H_{24}N_6Cl_2P_2PdPt$, **14c**	39.90	39.96	2.68	2.75	9.31	9.03
$C_{30}H_{24}N_6Br_2P_2PdPt$, **15c**	36.63	35.59	2.44	2.54	8.47	8.16
$C_{30}H_{24}N_6I_2P_2PdPt$, **16c**	33.17	33.37	2.23	2.46	7.74	7.40

2.7. Preparation of the DMAD A-frame adducts

An excess amount of DMAD (0.2 mL, 1.6 mmol) was added to a 20 mL CH_2Cl_2 solution containing (0.1 g, 0.1 mmol) of the appropriate $Pt_2I_2(\mu\text{-}PN_n)_2$ (HT) or (HH) (n = 1 - 3) complexes at r.t. The reaction mixture was stirred for about 15 min until the colour of solution turned from orange to yellow. The volume of solution was then reduced on a rotary evaporator to about 3 mL, when the orange solid that deposited was collected, and washed with Et_2O (3x10 mL) to get rid of excess DMAD. The products $Pt_2I_2(\mu\text{-DMAD})(\mu\text{-}PN_1)_2$ (HH) (**17**), $Pt_2I_2(\mu\text{-DMAD})(\mu\text{-}PN_2)_2$ (HT) (**18**), and $Pt_2I_2(\mu\text{-DMAD})(\mu\text{-}PN_3)_2$ (HT) (**19**),were dried at 80°C in vacuo; yield 95%. The complexes $Pt_2Cl_2(\mu\text{-DMAD})(\mu\text{-}PN_3)_2$, **20**, and $PtPdCl_2(\mu\text{-DMAD})(\mu\text{-}PN_3)_2$, **21**, were also isolated in this way. A methylpropiolate (MPP) A-frame adduct, **22**, was formed from **9c** *in situ* in an NMR tube by adding the acetylene to a $CDCl_3$ solution (0.8 mL) of **9c**. $^{31}P\{^1H\}$ NMR data of **22**, together with those of the isolated complexes, **17 - 21**, inclusive are listed in Table 4.1.

The palladium DMAD adducts were also prepared from the $Pd_2X_2(\mu\text{-}PN_n)_2$ precursors, in the same manner as the platinum adducts (Sect. 2.6.3). The compound $Pd_2Cl_2(\mu\text{-}PN_1)_2$, which was found not to react with CO,[20] reacts with DMAD, yielding an orange solid $Pd_2Cl_2(\mu\text{-}DMAD)(\mu\text{-}PN_1)_2$, **23**. The corresponding PN_2 complexes $Pd_2Cl_2(\mu\text{-}DMAD)(\mu\text{-}PN_2)_2$ (HT), **24**, and $Pd_2I_2(\mu\text{-}DMAD)(\mu\text{-}PN_2)_2$ (HT), **25**, are also among those isolated and characterized. The elemental analyses of **17** - **21** and **23** - **25** are presented in Table 2.8.

Table 2.8. Elemental Analyses of DMAD Insertion Products

complex	C		H		N	
	calcd.	found	calcd.	found	calcd.	found
$C_{40}H_{34}N_2I_2O_4P_2Pt_2$, **17**	36.60	36.45	2.61	2.65	2.13	2.01
$C_{38}H_{32}N_4I_2O_4P_2Pt_2$, **18**	34.72	34.88	2.45	2.41	4.26	4.50
$C_{36}H_{30}N_6I_2O_4P_2Pt_2$, **19**	32.84	32.80	2.30	2.14	6.38	6.16
$C_{36}H_{30}N_6Cl_2O_4P_2Pt_2$, **20**	38.14	38.11	2.67	2.86	7.42	7.17
$C_{36}H_{30}N_6Cl_2O_4P_2PdPt$, **21**	41.37	41.27	2.89	2.99	8.04	7.91
$C_{40}H_{34}N_2Cl_2O_4P_2Pd_2$, **23**	50.45	50.68	3.60	3.51	2.94	3.09
$C_{38}H_{32}N_4Cl_2O_4P_2Pd_2$, **24**	47.72	47.59	3.38	3.50	5.87	5.69
$C_{38}H_{32}N_4I_2O_4P_2Pd_2$, **25**	40.13	39.87	2.84	2.68	4.93	5.04

2.8. Preparation of Pt(0) complexes of pyridylphosphines and their derivatives from reactions with olefin, hydrogen chloride and methyl iodide

Experimental procedures similar to those described for the preparation of triphenylphosphine Pt(0) complexes[5] were adopted for syntheses of the pyridylphosphine Pt(0) derivatives. Some modifications in the experimental conditions were made. All reactions and subsequent manipulations were performed under anaerobic conditions, using conventional techniques for handling air-sensitive compounds.[9]

2.8.1. Tetrakis(tripyridylphosphine)platinum(0), **26c**

(1) A saturated aqueous solution of K_2PtCl_4 (0.50 g, 1.2 mmol; in 5 mL) was added to a refluxing THF solution (20 mL) containing KOH (0.13 g, 2.4 mmol) and five equivalents of PN_3 (2.92 g, 11 mmol). The mixture was refluxed for about 10 min, and the resulting orange solution was cooled to r.t., when the water and THF layers separated. The THF was pumped off, and the yellow precipitate that had formed in the aqueous layer upon cooling was extracted with CH_2Cl_2 (10 mL); this CH_2Cl_2 solution was subsequently transferred via a cannula tube to another flask where the extract was dried over $MgSO_4$ for 2 h. The drying agent was filtered off, and hexane was introduced to the CH_2Cl_2 filtrate until the precipitate reformed again; the solid was collected, washed thoroughly with hexane, and recrystallized from CH_2Cl_2/hexane (v/v 1:1) to give a yellow solid, which was dried in vacuo at r.t.; yield 0.65 g, 43%.

(2) A benzene suspension of cis-$PtCl_2(PN_3)_2$ (0.30 g, 0.38 mmol; in 30 mL) with PN_3 ligand (0.30 g, 1.14 mmol) was refluxed at 80°C. Hydrazine hydrate in benzene (10% by vol) was added dropwise to the mixture with vigorous stirring until all the white solid had dissolved. The yellow solution thus formed was refluxed for another 10 min and then cooled to 5°C. The yellow solid that formed upon concentration of the solution to 10 mL was collected by filtration and redissolved in CH_2Cl_2 (15 mL). Compound **26c**, obtained by a reprecipitation procedure using hexane (~ 20 mL), was then collected and dried in vacuo; yield 0.19 g, 40%.*

Compound **26c** obtained from either method (1) or (2) has the same ^{31}P and ^{195}Pt NMR solution spectra which prove the identity of the complex but satisfactory elemental analysis was not obtained. Anal. (optimum) calcd. for $C_{60}H_{48}N_{12}P_4Pt$: C 57.37, H 3.85, N 13.38; found: C 59.38, H 3.80, N 13.49. $^{31}P\{^1H\}$ NMR ($CDCl_3$, -40°C): δ_P = 30.1 (s†), $^1J_{PtP}$ = 3829 Hz. $^{195}Pt\{^1H\}$ NMR ($CDCl_3$, -40°C): δ_P = -538.3 (quintet), $^1J_{Pt\text{-}P}$ = 3840 Hz.

---

* An identical procedure but using no added PN_3 gave a smaller yield (18%) of **26c**.

† The $^{31}P\{^1H\}$ NMR pattern containing a major singlet, doublet or triplet, as well as the corresponding platinum satellites, is noted in this thesis simply as a singlet, a doublet or a triplet.

Use of ethanol, the solvent used in the original preparation of $Pt(PPh_3)_4$,[5] resulted in formation of orange solutions on reaction of $PtCl_4^{2-}$ with PN_3 or cis-$PtCl_2(PN_3)_2$ in the presence of N_2H_4; upon concentration, the solutions yielded only a red oil.

An oxygen complex of **26c**, tentatively formulated as "$Pt(PN_3)_3O_2$", was isolated as an orange solid by leaving crude **26c**, obtained from method (2) (~80 mg, 0.064 mmol), in CH_2Cl_2 (15 mL) and hexanes (15 mL) at 0°C under N_2 for four days (~30 mg, yield 38%). Anal. calcd. for $C_{45}H_{36}N_9O_2Pt$: C 52.83, H 3.55, N 12.32; found: C 52.23, H 3.51, N 11.85. $^{31}P\{^1H\}$ NMR ($CDCl_3$, r.t.): δ_P = 23.3 (d), 22.5 (t); J_{PtP} = 2700, 4050 Hz; J_{PP} = 14 Hz. IR data are given in Fig. 5.5.

2.8.2. Tris[2-(diphenylphosphino)pyridine]platinum(0), **27a**

The exact experimental procedure described for the synthesis of $Pt(PPh_3)_3$ was followed.[5] A saturated aqueous solution of K_2PtCl_4 (1.0 g, 2.4 mmol; in 10 mL) was added to a refluxing EtOH solution (20 mL) containing KOH (0.27g, 4.8 mmol) and 3.5 equivalents of PN_1 ligand (2.3 g, 8.5 mmol). The mixture was refluxed for 20 min, and the resulting yellowish-orange solution was cooled to r.t. and then concentrated to 15 mL. A yellow solid that formed was collected by filtration and then washed with cold EtOH (5 mL) thrice. This product was then redissolved in CH_2Cl_2 (12 mL), reprecipitated by the addition of hexane (20 mL), and then dried in vacuo; yield of $Pt(PN_1)_3$ 1.7 g (72%). Anal. calcd. for $C_{51}H_{42}N_3P_3Pt$: C 62.19, H 4.30, N 4.27; found: C 62.63, H 4.49, N 3.90. $^{31}P\{^1H\}$ NMR (toluene-d_8, -70°C): δ_P = 57.02 (s), $^1J_{PtP}$ = 4444 Hz. $^{195}Pt\{^1H\}$ NMR (toluene-d_8, -70°C): δ_{Pt} = -300.3 (quartet), $^1J_{PtP}$ = 4433 Hz.

2.8.3. Olefin derivatives from Pt(0) complexes of pyridylphosphines

2.8.3.1. Acrylonitrile, methacrylonitrile and crotonitrile complexes (**44a**, **44c**, **45a**, **46a**)

A solution of excess acrylonitrile (distilled, ~1ml) in Et_2O (5 mL) was degassed by the freeze-and-thaw method three times. This solution was added dropwise to a suspension of $Pt(PN_1)_3$ (93 mg, 0.094 mmol) in Et_2O (20 mL) until the yellow solid dissolved and the solution turned colourless. This reaction mixture was then left at -20°C overnight. A white solid which deposited on the side-wall of the flask was collected. The supernatant was then transferred to a beaker where a second crop of solid was obtained by scratching the side of the beaker. The product $Pt(PN_1)_2(\eta^2\text{-}CH_2CHCN)$, **44a**, is air-stable; yield 54 mg (air dried), ~75%. Pumping on the wet reaction product resulted in reformation of yellow $Pt(PN_1)_3$.

The complex $Pt(PN_3)_2(\eta^2\text{-}CH_2CHCN)$, **44c**, was formed *in situ* in an NMR tube when an excess of liquid acrylonitrile was added to a yellow $CDCl_3$ solution of $Pt(PN_3)_4$ at r.t. The colour of the resulting solution became pale yellow.

The exact procedure outlined for isolation of the acrylonitrile complex **44a** was also used for synthesis of the methacrylonitrile and crotonitrile species. The complexes $Pt(PN_1)_2(\eta^2\text{-}CH_2C(CH_3)CN)$, **45a**, and $Pt(PN_1)_2(\eta^2\text{-}CH_3CHCHCN)$, **46a**, are also white solids. Because a mixture of cis and trans crotonitrile is used, two isomers of **46a** which differ in the geometry of the olefin are obtained (Sect. 5.2.1). Yields of **45a**, **46a** are ~60%.

Unfortunately, because of the loss of coordinated olefin on pumping, these olefin complexes (**44a**, **45a**, **46a**) could not be dried properly and therefore did not analyze to a satisfactory standard for confirmation of their chemical formulation.

2.8.3.2. Maleic anhydride (MA) and diethyl maleate (DEMA) complexes (**47a**, **47c** **48a**)

A saturated solution of maleic anhydride, MA, in Et_2O (3 mL) was degassed by three freeze-and-thaw cycles and added slowly to a solution of $Pt(PN_1)_3$ (98 mg, 0.1 mmol) in benzene (20 mL). After the solution rapidly became pale yellow, n-hexane (20 mL) was added. The pale yellow precipitate that gradually formed upon cooling the solution to -20°C was filtered, washed with Et_2O, and dried in vacuo; yield of $Pt(PN_1)_2[\eta^2\text{-}(CHCO)_2O]$, **47a**, is 89% (72 mg). Anal. calcd. for $C_{38}H_{28}N_2O_3Pt$: C 55.68, H 3.69, N 3.42; found: C 55.61, H 4.00, N 3.19.

The $Pt(PN_3)_4$ complex also reacts with MA, under the same experimental conditions used for the synthesis of **47a**, to form a pale yellow compound $Pt(PN_3)_2[\eta^2\text{-}(CHCO)_2O]$, **47c**; yield 80%. Anal. calcd. for $C_{34}H_{26}N_6O_3Pt$: C 49.58, H 3.18, N 10.21; found: C 49.25, H 3.19, N 10.42.

The preparation of a mixture of $Pt(PN_1)_2$(DEMA), **48a.1**, and $Pt(PN_1)_2$(DEFM) (DEFM = diethyl fumarate), **48a.2**, was carried out in Et_2O using $Pt(PN_1)_3$ as described for the preparation of **47a**. The addition of DEMA in Et_2O was controlled very carefully in order to obtain a solid product, because excess DEMA resulted in the formation of a white, colloidal product. White microcrystals of **48a.1** and **48a.2** were obtained upon leaving the solution at -20°C for two days; yield 30%. Anal. calcd. for $C_{42}H_{40}N_2O_4Pt$: C 56.43, H 4.51, N 3.13; found: C 55.95, H 4.72, N 3.37.

The $^{31}P\{^1H\}$ NMR data of **47a**, **47c**, **48a.1** and **48a.2** are presented in Table 5.2.

2.8.4. Hydridochloro derivatives from Pt(0) complexes of pyridylphosphines

2.8.4.1. Trans-chlorohydridobis[(2-diphenylphosphino)pyridine]platinum(II), **50a**

The complex trans-$Pt(H)Cl(PN_1)_2$, **50a**, was obtained by reaction of a THF solution (40 mL) of $Pt(PN_1)_3$ **27a** (200 mg, 0.2 mmol), initially under N_2, with anhydrous HCl gas at 1 atm.

The solution was stirred vigorously for 20 min until the yellow colour dissipated. Excess HCl was pumped off completely and an N_2 atmosphere was re-established. Hexane (40 mL) was then laid on top of the colourless THF solution, the mixture then being left in a freezer at -20°C for 72 h. White crystals formed and these were collected by filtration and washed with hexanes/THF (v/v 1:1) and then THF alone; yield 67 mg (45%). The complex, **50a**, is air-sensitive and turns orange when exposed to air. Anal. calcd. for $C_{34}H_{29}N_2ClP_2Pt$: C 53.87, H 3.86, N 3.70; found: C 54.01, H 4.31, N 3.34. IR (Nujol): ν_{PtH} = 2212 cm^{-1}; ^1H NMR of the hydride (CD_2Cl_2, r.t.): δ = -16.32 (t), J_{PH} = 12.7 Hz, J_{PtH} = 1213 Hz; ^{31}P NMR (CD_2Cl_2, r.t.): δ = 30.00 (s), J_{PtP} = 3031 Hz.

Excess HCl in solution, after the reactant solution turned colourless, must be removed immediately because otherwise the reaction is more complex. A new, white solid was isolated under similar experimental conditions in the presence of excess HCl. The IR and ^1H and $^{31}P\{^1H\}$ NMR data of this unknown platinum hydride species are different from those of **50a**: IR ($CDCl_3$): ν_{PtH} = 2219 cm^{-1}; ^1H NMR of the hydride ($CDCl_3$, r.t.): δ = -15.5 (br. s), J_{PtH} = 1173 Hz; $^{31}P\{^1H\}$ NMR ($CDCl_3$, r.t.): δ = 35.2 (s), J_{PtP} = 3136 Hz.

2.8.4.2. Attempted preparation of hydridochlorobis[tri(2-pyridyl)phosphine]platinum(II)

The following procedures were used for the preparation of the title complex:

(1) Tetrakis[tris(2-pyridyl)phosphine]platinum(0), **26c**, (31.4 mg, 0.024 mmol) was dissolved in CH_2Cl_2 (10 mL). Anhydrous HCl (g) was bubbled through deoxygenated CH_2Cl_2 for about 5 min, and this HCl-saturated solution (0.2 mL) was added slowly, using a syringe, to the CH_2Cl_2 solution of **26c**, the colour of the reaction mixture turning from bright yellow to greyish yellow. The solid that gradually deposited (30 min) was filtered, washed three times with CH_2Cl_2/hexanes (5 mL, v/v 1:1) and dried in vacuo.

(2) Compound **26c** (15.4 mg, 0.012 mmol) was suspended in benzene (10 mL) under a positive pressure of N_2 in a septum-capped Schlenk tube. The HCl (g) (5 mL at 1 atm) was

injected slowly, and the suspension was then stirred for about 10 min until the yellow solid dissolved. A canary yellow solid formed after 30 min, and was collected by filtration, washed twice with benzene (5 mL), and dried under vacuum.

(3) Some **26c** (10.2 mg, 0.008 mmol) was suspended in THF (10 mL) at r.t.; and 0.5 mL THF solution of DMA·HCl* (0.016M, 0.008 mmol; 1.0 equiv) was then added dropwise. The colour of the suspension turned from bright yellow to pale yellow upon stirring (~10 min), and the suspension was allowed to settle at 0°C. No further colour change was observed. The resulting canary yellow solid was collected and washed with THF (3x5 mL) to remove DMA.

2.8.5. Iodo(methyl) derivatives from Pt(0) complexes of pyridylphosphines, trans-$PtI(Me)(PN_1)_2$, **52a**,* and trans-$PtI(Me)(PN_3)_2$, **52c**

Some $Pt(PN_1)_3$ (100 mg, 0.10 mmol) was dissolved in benzene (20 mL) and four equivalents of MeI (0.035 mL, 0.40 mmol) were added. The reaction mixture was refluxed at 80°C for 20 min and then cooled to ~5°C. A pale yellow precipitate formed when the solution was concentrated by evacuation to 5 mL at this temperature. The solid was collected by filtration, redissolved in water (5 mL), and extracted with CH_2Cl_2 (20 mL). The colourless CH_2Cl_2 portion was then transferred via a cannula tube to another Schlenk flask where the solution was concentrated to 5 mL. The white solid of trans-$PtI(Me)(PN_1)_2$, **52a**, was precipitated by addition of hexanes (10 mL); yield 58 mg (67%). Anal. calcd. for $C_{35}H_{31}IN_2P_2Pt$: C 48.68 , H 3.62 , N 3.24; found: C 47.71, H 3.61, N 2.92. $^{31}P\{^1H\}$ NMR ($CDCl_3$, r.t.): δ_P = 26.82 (s), $^1J_{PtP}$ = 3078 Hz; ^1H NMR ($CDCl_3$, r.t.): δ_{Me} = 0.05 (t) $^3J_{PH}$ = 5.7, $^2J_{PtH}$ = 75 Hz. ($[MePN_1]I$ was made *in situ* in the present study by adding excess MeI to the $CDCl_3$ solution of PN_1 at r.t.: δ_P = 17.5 (s): δ_{Me} = 3.21 (d), $^2J_{PH}$ = 12.1 Hz).

---

* DMA·HCl: N,N-dimethylacetamide hydrogen chloride was provided by A. Joshi, its synthesis is described in ref. 21.

* A recent paper (Jain, V.K. et al. *J. Organomet. Chem.*, **1990**, *389*, 417.) has noted the synthesis of trans-$PtI(Me)(PN_1)_2$ from the reaction of $PtI(Me)(COD)$ with 2 equivalents of PN_1 in benzene; the reported spectral properties are essentially the same as those presented here.

Trans-PtI(Me)$(PN_3)_2$, **52c**, was obtained in the same manner. The final product was isolated as a pale yellow solid; yield 57%. Anal. calcd. for $C_{31}H_{27}IN_6P_2Pt$: C 42.92, H 3.14, N 9.69; found: C 43.45, H 3.37, N 9.51. $^{31}P\{^1H\}$ NMR ($CDCl_3$, r.t.): δ_P = 25.64 (s), $^1J_{PtP}$ = 3133 Hz. ($[MePN_3]I$ was made *in situ* in the same manner as described for $[MePN_1]I$: δ_P = 12.46 (s)).

2.9. Preparation of bis(maleato) and bis(malato) chromium (III) species

Preparations of $K[Cr(maleato)_2(H_2O)_2]$, **53**, and $K[Cr(malato)_2(H_2O)_2]$, **54**, complexes have not been reported in the literature. The procedure adopted here follows the reported synthesis for the cis-$K[Cr(malonato)_2(H_2O)_2]$ complex.[22]

2.9.1. Cis-potassium diaquobis(maleato)chromate(III) trihydrate, 53

Solutions of $K_2Cr_2O_7$ (2.95 g, 0.01 mol; 6 mL) and maleic acid (5.80 g, 0.05 mol; 6 mL) in boiling water were mixed, and allowed to react until no more carbon dioxide evolved. About 45 mL water was then added to the mixture. After being cooled, the solution was added very slowly with vigorous stirring to 100 mL of 95% ethanol; the product thus precipitated was collected by filtration, washed with 95% ethanol and ether, and dried in air; yield of the greyish blue solid was 5.4 g (78%). Anal. Calcd. for $C_8H_{14}O_{13}CrK$: C 23.47, H 3.45; found: C 23.59, H 3.75. Visible spectral data in H_2O (λ_{max} nm, ε $M^{-1}cm^{-1}$): 420 (72.9), 572 (74.4).

2.9.2. Cis-potassium diaquobis(malato)chromate(III) monohydrate, 54

The procedure described for the preparation of the maleato complex was adopted, except that 3.42 g R, S-malic acid and 1.5 g $K_2Cr_2O_7$ were used instead; yield 4.1 g (90%). Anal. Calcd. for $C_8H_{14}O_{13}CrK$: C 23.47, H 3.45; found: C 23.46, H 3.35. Visible spectral data in H_2O (λ_{max} nm, ε $M^{-1}cm^{-1}$): 420 (76.4), 572 (77.0)

References

1. Conard, C.R.; Dolliver, M.A.; *Organic Synthesis;* Blatt, A.H., Ed.; John Wiley & Sons: New York, 1943; Coll. Vol.2, p.167.

2. Brevard, C.; Granger, P. *Handbook of High Resolution Multinuclear NMR;* Wiley: New York, 1981; p.200.

3. Georgii, I.; Mann, B.E.; Taylor, B.F. *Inorg. Chim. Acta* , **1984**, *86*, L81.

4. Kerrison, S.T.S.; Sadler, P.J. *J. Mag. Res.*, **1978**, *31*, 321.

5. Hartley, F.R. *Organometallic Rev. A.*, **1976**, *6*, 119.

6. McDermott, J.X.; White, J.F.; Whitesides, G.M. *J. Am. Chem. Soc.*, **1976**, *98*, 652.

7. Ukai, T.; Kawazura, H.; Ishii, Y.; Bonnett, J.J.; Ibers, J.A. *J. Organomet. Chem.*, **1974**, *65*, 253.

8. Moseley, K.; Maitlis, P.M. *J. Chem. Soc. Dalton Trans.*, **1974**, 169 .

9. Shriver, D.F.; Drezdon, M.A. *The Manipulation of Air-Sensitive Compounds,* 2nd ed.; Wiley: New York, 1986.

10. Maisonnat, A.; Farr, J.P.; Olmstead, M.M.; Hunt, C.T.; Balch, A.L. *Inorg. Chem.*, **1982**, *21*, 3961.

11. Bianco, V.P.; Boronzo, S. *Inorg. Synth*, **1976**, *16*, 161.

12. Mann, F.G.; Watson, J. *J. Org. Chem.*, **1948**, *13*, 502.

13. Kurtev, K.; Ribola, D.; Jones, R.A.; Cole-Hamilton, D.J.; Wilkinson, G. *J. Chem. Soc. Dalton* , **1980**, 55.

14. Keene, F.R.; Snow, M.R.; Stephenson, P.J.; Tiekink, E.R.T. *Inorg. Chem.*, **1987**, *27*, 2040.

15. Boggess, R.K.; Zatko, D.A. *J. Coord. Chem.*, **1975**, *4*, 217.

16. Farr, J.P.; Wood, F.E.; Balch, A.L. *Inorg. Chem.*, **1983**, *22*, 3387.

17. Farr, J.P.; Olmstead, M.M.; Balch, A.L. *Inorg. Chem.*, **1983**, *22*, 1229.

18. Newkome, G.R.; Evans, D.W.; Fronczek, F.R. *Inorg. Chem.* **1987**, *26*, 3500.

19. Lee, C-L.; James, B.R. unpublished results.

20. Maisonnat, A.; Farr, J.P; Balch, A.L. *Inorg. Chim. Acta,* **1981**, *53*, L217.

21. Thorburn, I.S. *Ph.D Dissertation*, University of British Columbia, 1985; Ch.2.

22. Chong, J.C. *Inorg. Synth.*, **1976**, *16*, 81.

Chapter 3

Structures of M(II) and M(I) Pyridylphosphine Complexes and Their Solution Chemistry

3.1. Introduction

The oxidation state M(II) is the most common for both palladium and platinum. Due largely to the crystal field splitting effects (Fig. 3.1),[1] these d^8 metal ions prefer square-planar geometry because the greatest stabilization energy is achieved compared to any other coordination number and geometry.[2] All the M(II) bisphosphine complexes are of square-planar geometry and are generally formulated as MX_2P_2, and consequently, two possible geometric isomers — cis and trans* — exist (see below). Because of the potential catalytic properties of these divalent complexes, isomerization of one geometric form to another has been a research topic for several decades and studies in this area still remain active.[3 - 9] These mononuclear complexes of Pt^{II} have also been used as models for catalytic intermediates in mechanistic investigations.[10 - 12]

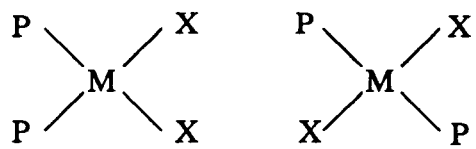

cis trans

M = Pd, Pt; P = tertiary phosphines;

X = halides, or other monoanions

Another now well established oxidation state for Pt and Pd is +1, which was previously considered to be rare.[13] However, this oxidation state is readily found among binuclear complexes, both homonuclear and heteronuclear, that contain a formal single metal-metal bond.[14, 15] The metal-metal bond formed by the overlap of single electrons on each metal stabilizes the binuclear framework against the disproportionation reaction ($M_2^I \longrightarrow M^{II} + M^0$) — the reverse of the M_2^I synthesis, the conproportionation reaction. Two metal centres, acting cooperatively, offer unique reactivity patterns which differ from the well-established reactivity of

* The term cis and trans are used throughout with reference to the position of two phosphine ligands in a complex.

the mononuclear metal complexes: examples include the insertion of small molecules such as H_2S,[16] CO,[14, 17 - 19] and SO_2[17, 18] into the metal-metal bond. In the field of catalysis particularly, the binuclear complexes have been used as simplified models for understanding the mechanisms of catalysis taking place on metal surfaces, because the bridging coordination mode available with binuclear systems may resemble a chemisorption mode of small molecules on such surfaces.[10]

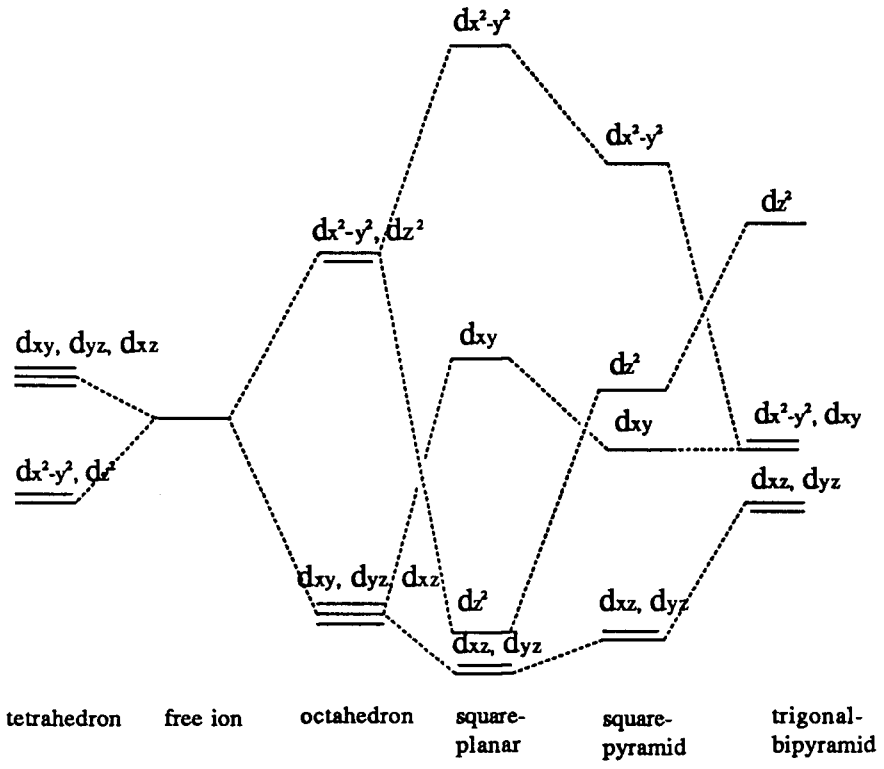

Fig. 3.1. Relative energy levels of d-orbitals in different geometries.

The M(I) binuclear complexes (M = Pt, Pd) to be described here are made from a conproportionation reaction of M(0) and M(II) (see below).[21, 22] The pyridylphosphine ligands in these binuclear complexes adopt a P-N bridging mode, forming a five-member ring with the two metal atoms. The Pt(I) or Pd(I) centres in the molecule resemble Pt(II) or Pd(II) centres, and adopt a four-coordinated, square-planar configuration. Stereoisomerism thus arises from two different orientations of the bridging pyridyl ligand, that is, the head-to-head (HH) and head-to-tail (HT) configurations. The complexes prepared in the present work are shown below:

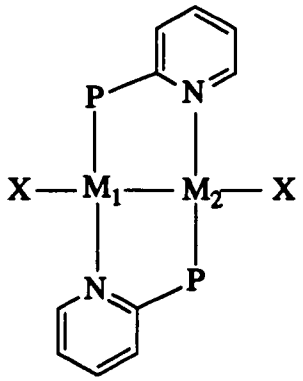

Head-to-Tail, HT
$M_1 = M_2 = Pd, Pt$
$M_1 = Pd, M_2 = Pt$
X = Cl, Br, I
P = Ph_2P, PhPpy, Ppy_2

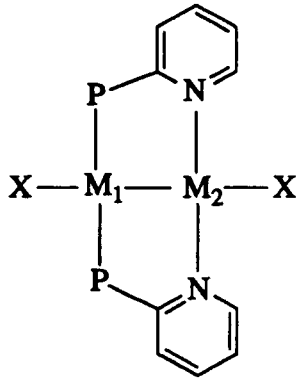

Head-to-Head, HH
$M_1 = M_2 = Pt$
X = I
P= Ph_2P, PhPpy, Ppy_2

The compound $Pd_2Cl_2(\mu\text{-}PN_1)_2$, **11a**, was prepared in 1981 by Maisonnat et al.[21] Two years later, the syntheses of $Pt_2X_2(\mu\text{-}PN_1)_2$(HT) (X = Cl (**7a**), I (**9a**)) and $Pt_2I_2(\mu\text{-}PN_1)_2$(HH) (**10a**) were reported by Farr et al.[22] Independently, the tris(2-pyridyl)phosphine palladium binuclear complex, $Pd_2Cl_2(\mu\text{-}PN_3)_2$ (**11c**), was made in our group.[20] The $Pd_2Cl_2(\mu\text{-}PN_1)_2$ complex was reported not to give the insertion product with CO;[21] also $Pd_2Cl_2(\mu\text{-}PN_3)_2$ was shown in the present work not to react with 1 atm CO in CH_2Cl_2 at room temperature. The reactivity of the M-M bond toward insertion of small molecules is common for the systems with the bridging diphosphine ligand bis(diphenylphosphino)methane, dppm, which was being used for gas separation study in our group originally.[17] The lack of flexibility of the bridging pyridylphosphines was thought responsible for the loss of reactivity.[21] However, the bridging pyridylphosphines are perhaps not as rigid as suggested because Lee and Yang in our group discovered that the reaction of dimethylacetylenedicarboxylate, DMAD, with $Pd_2Cl_2(\mu\text{-}PN_3)_2$ led to the formation of the bridged acetylene compound, $Pd_2Cl_2(\mu\text{-}DMAD)(\mu\text{-}PN_3)_2$.[20] The interest in this thesis work was then directed more toward activation of unsaturated hydrocarbons, such as olefins and acetylenes. This study was also extended here to the platinum system. Use of bis- and tris(2-pyridyl)phosphine increases gradually the hydrophilicity of the complexes, which was considered to be an asset for hydration catalysis. The aqueous solution chemistry of the tris(2-

pyridyl)phosphine complexes $Pd_2Cl_2(\mu\text{-}PN_3)_2(HT)$ and $PdCl_2(PN_3)_2$ will be considered in Sect. 3.4. The incidental phosphine chirality induced by the bridging of one pyridyl group within the PN_2 systems leads to many interesting features in the $^{31}P\{^1H\}$ NMR spectroscopic data, which will be dealt with later on.

The present study was originally directed to the potential catalytic hydration of activated olefins by the pyridylphosphine complexes. However, preliminary results showed that none of the M(I) and M(II) complexes made activated olefins (acrylonitrile and maleic acid) either in organic solvents or in water; although, acetylenes (dimethylacetylenedicarboxylate, DMAD, and methylpropiolate, MPP) inserted into M_2^I metal-metal bond, forming olefinic complexes (Sect. 2.7), further chemistry on the bridging molecules was not observed. In this Chapter, the structural characterizations of M(II) mononuclear and M(I) binuclear complexes of pyridylphosphines by spectroscopic methods are presented.

3.2. Structural characterization of pyridylphosphine complexes

3.2.1. Pt(II) pyridylphosphine complexes

The complexes synthesized are shown below:

$PtX_2(PN_1)_2$	$PtX_2(PN_2)_2$	$PtX_2(PN_3)_2$
X = Cl, **1a**	X = Cl, **1b**	X = Cl, **1c**
X = I, **3a**	X = I, **3b**	X = Br, **2c**
		X = I, **3c**

The synthetic route to dichlorobisphosphineplatinum(II) complexes is basically via reaction of phosphine with potassium tetrachloroplatinate(II) in ethanol solution, or phosphine reaction with a platinum(II) precursor containing a readily displaceable ligand such as cyclooctadiene and benzonitrile. The latter was chosen in the present study, and $PtCl_2(PhCN)_2$ and $PtCl_2(COD)$ were used as precursor complexes. Dichlorobis(2-pyridylphosphine) derivatives of platinum(II) were obtained by simple replacement of PhCN or COD with the appropriate phosphine ligand. The corresponding bromo and iodo complexes were readily

obtained by metathesis of $PtCl_2(PhCN)_2$ with appropriate sodium halides. All these isolated mononuclear compounds show satisfactory elemental analysis (see Table 2.1). The $PtX_2(PN_1)_2$ (X = Cl, I) species have been made previously.[22]

The geometry of the dihalobis(2-pyridylphosphine)platinum(II) species **1-3** in solution can be easily identified by means of $^{31}P\{^1H\}$ NMR spectroscopy. The magnitude of the ^{195}Pt-^{31}P coupling constant diagnoses the geometry of the complex. It was first revealed by Pidcock and coworkers in 1962 that the cis $^1J_{Pt-P}$ value was significantly larger than the corresponding trans one in $PtX_2(PR_3)_2$ systems.[23] This observation was later supported by Grim et al. using a different series of Pt(II) bisphosphine complexes.[24] Since these studies, the one bond $^1J_{Pt-P}$ coupling constants have been well documented.[25 - 29] The ratio of $^1J_{Pt-P}$ cis to trans is normally about 1.5.[24] The assignments for all the $PtX_2(PN_n)_2$ listed in Table 3.1 are made according to the above coupling constant criteria. A typical $^{31}P\{^1H\}$ NMR spectrum of a cis-$PtX_2(PN_n)_2$ species is shown in Fig. 3.2.

Table 3.1. $^{31}P\{^1H\}$ NMR Parameters for $PtX_2(PN_n)_2$ Complexes

Complexes	Solvent	δ(ppm)	$^1J_{PtP}$(Hz)	Ref.[a]
cis-$PtCl_2(PN_1)_2$, **1a**	CD_2Cl_2	11.6(s)	3676	tw
cis-$PtI_2(PN_1)_2$, **3a**	CD_2Cl_2	6.7(s)	3514	tw
trans-$PtI_2(PN_1)_2$	$CDCl_3$	9.8(s)	2503	22
cis-$PtCl_2(PN_2)_2$, **1b**	CD_2Cl_2	13.3(s)	3765	tw
cis-$PtI_2(PN_2)_2$, **3b**[b]	CD_2Cl_2	7.4(s)	3630	tw
trans-$PtI_2(PN_2)_2$[b]	$CDCl_3$	10.4(s)	2500	tw
cis-$PtCl_2(PN_3)_2$, **1c**[c]	CD_2Cl_2	20.0(s)	3910	tw
cis-$PtBr_2(PN_3)_2$, **2c**[c]	CD_2Cl_2	17.3(s)	3833	tw
cis-$Pt_2I_2(PN_3)$, **3c**[c]	CD_2Cl_2	11.24(s)	3660	tw

(a) tw = this work; (b) Recorded at -50°C; (c) Recorded at -70°C.

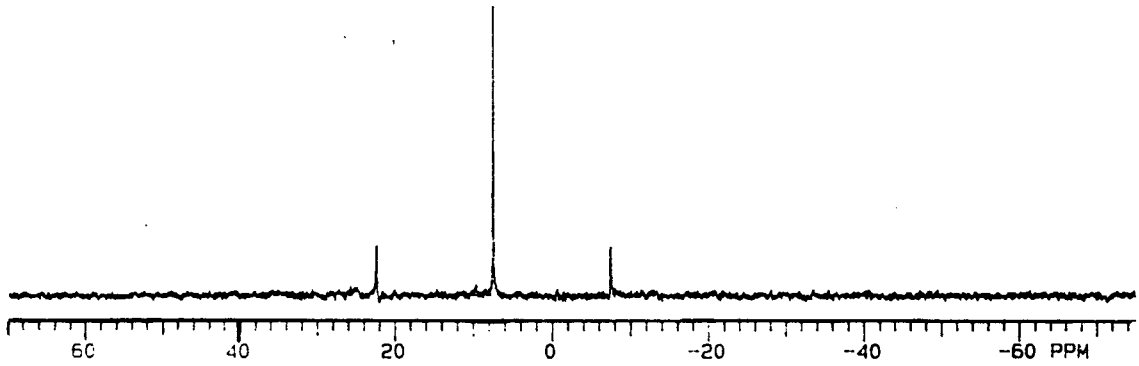

Fig. 3.2. 121.4 MHz $^{31}P\{^1H\}$ NMR spectrum of cis-$PtI_2(PN_2)_2$, **3b**, in CD_2Cl_2 at -50°C.

Based on the assignments in Table 3.1, general trends in the ^{31}P NMR chemical shifts and coupling constants of these pyridylphosphine Pt^{II} complexes become obvious. A shift to lower resonance frequency is seen on going from **1a** (11.6), through **1b** (13.3), to **1c** (20.0 ppm), when PN_1 is replaced by PN_2 and then PN_3 for the chloro complexes; and an upfield shift of the phosphorus resonance is observed on going, for example, from **1c** (20.0), through **2c** (17.3), to **3c** (11.2 ppm), when chlorine is replaced by bromine and then iodine for the complexes of the same phosphine. The coupling constant J_{PtP} of the complex increases, for example, on going from **1a** (3676), through **1b** (3765), to **1c** (3910 Hz), and decreases on going from **1c** (3910), through **2c** (3833), to **3c** (3660 Hz).

The downfield shift in the phosphorus resonance signals of the series compared to those of the free ligands, and the trend within **1a** to **1c**, can be understood in a simplified manner in terms of the ligand basicity and the metal deshielding ability. The $^{31}P\{^1H\}$ NMR chemical shifts of the free ligands move downfield from -3.28 for PN_1 through -1.7 for PN_2 to -0.05 ppm for PN_3, indicating that the phosphorus nucleus in PN_1 is more shielded than that in PN_3 by the lone pair electron density and implying that as a free phosphine, PN_1 is more basic than PN_3. Upon coordination, the phosphorus nucleus is deshielded by the metal. The M-P bond is formed by the σ donation of the phosphine lone pair of electrons to the empty dsp^2 hybrid orbital and π back donation from the filled d_{xz}, d_{yz} of the metal to the 3d orbital of the phosphorus. A reduction of

electron density on the phosphorus nucleus occurs, and the phosphorus resonance on coordination is expected to shift downfield with respect to the free ligand resonance. The difference between the chemical shift of phosphorus in a coordination compound and in the free ligand is referred to as the coordination shift. The larger the coordination shift is , the greater the degree of electron transfer from the ligand to the metal. Apparently, PN_3 with a coordination shift of 20.05 ppm in **1c** perhaps forms a stronger interaction with Pt(II) than PN_1 which shows a coordination shift of 14.9 ppm in **1a**. This interaction between metal and ligand is also reflected in another NMR parameter, the J_{PtP} coupling constant, where the trend is $J_{PtP(1c)} > J_{PtP(1b)} > J_{PtP(1a)}$, consistent with the conclusion made based on the coordination shifts. For a particular phosphine ligand, the observed upfield chemical shift trend $\delta_{Cl} > \delta_{Br} > \delta_{I}$, as the halogen changes from chlorine through bromine to iodine, possibly reflects the successive weakening of the platinum-phosphorus σ-bond which is consistent with the decrease in the directly bonded spin-spin coupling constant $^1J_{PtP}$, $J_{PtP(Cl)} > J_{PtP(Br)} > J_{PtP(I)}$, as observed previously.[29a]

3.2.2. Pd(II) pyridylphosphine complexes

The complexes synthesized in this category are shown below:

$PdX_2(PN_1)_2$	$PdX_2(PN_2)_2$	$PdX_2(PN_3)_2$
X = Cl, **4a**	X = Cl, **4b**	X = Cl, **4c**
X = I, **6a**	X = I, **6b**	X = Br, **5c**
		X = I, **6c**

As described in Chapter 2 (Sect. 2.5.2), $PdCl_2(PN_n)_2$ complexes were synthesized by the reaction of $PdCl_2(PhCN)_2$ with PN_n ligand in dichloromethane solvent. The bromo and iodo complexes were again obtained from the metathesis reaction of the PN_n dichloro species with sodium halides. In contrast to the Pt(II) phosphine complexes, the corresponding Pd(II) complexes presented problems in assignment of cis or trans geometry. The $^{31}P\{^1H\}$ NMR spectroscopy reveals no information regarding metal-phosphorus (J_{MP}) coupling — palladium is

NMR inactive. The $^{31}P\{^1H\}$ NMR data of these palladium complexes (Table 3.2) do not serve independently as a structural probe. Apart from the NMR spectroscopy including $^{31}P\{^1H\}$, ^1H and $^{13}C\{^1H\}$ which will be discussed later on in more detail, two other techniques — dipole moment measurement and infrared spectroscopy — used for identification of cis and trans isomers of PdX_2P_2 type compounds in the solution and in the solid state fail to provide a concrete assignment for these complexes. The basic principles and limitations of these techniques are discussed in the following paragraphs.

Table 3.2. $^{31}P\{^1H\}$ NMR Parameters of $PdX_2(PN_n)_2$ Complexes[a]

Complexes	δ Chemical Shifts (ppm) cis	trans	Ref.[b]
$PdCl_2(PN_1)_2$, **4a**	29.5(s)	23.4(s)	21 & tw
$PdBr_2(PN_1)_2$, **5a**[c]	26.5(s)	20.5(s)	tw
$PdI_2(PN_1)_2$, **6a**[c]	—	9.6(s)	tw
$PdCl_2(PN_2)_2$, **4b**	30.9(s)[d]	17.7(s)[d]	30 & tw
$PdBr_2(PN_2)_2$, **5b**[c]	27.9(s)	—	tw
$PdI_2(PN_2)_2$, **6b**[c]	—	8.9(s)	tw
$Pd_2Cl_2(PN_3)_2$, **4c**	34.6(s)	—	tw
$PdBr_2(PN_3)_2$, **5c**[c]	32.1(s)	—	tw
$PdI_2(PN_3)_2$, **6c**[c]	—	7.0(s)	tw

(a) Recorded in CD_2Cl_2 at r.t. unless otherwise noted; (b) tw = this work; (c) Recorded at -70°C; (d) Cis and trans were made separately in ref. 30.

Dipole moment measurement: The geometric isomers of the square-planar type complexes MX_2L_2 are distinguishable by their dipole moments.[31, 32] In principle, trans-PdX_2P_2 with D_{2h} symmetry has zero dipole moment, as opposed to the cis-complex having a non-zero dipole moment, and measurement of the dielectric constant of a non-polar solvent containing either a cis or a trans isomer of PdX_2P_2 relates to the dipole moment of the solute. A zero dipole moment indicates that the solute is of trans structure; however, a non-zero dipole moment does not

exclude the presence of trans isomer. To distinguish whether the solute is pure cis or a mixture of cis and trans, a standard cis-compound of similar composition with known dipole moment is required. It is important for the test compound to have good solubility in a non-polar solvent. Unfortunately, the pyridylphosphine Pd(II) series do not dissolve in benzene or carbon tetrachloride (two common solvents used for measurement of dielectric constant) and are only slightly soluble in dichloromethane; the low solubilities made the measurement impractical.

Infrared spectroscopy (IR): The position and band shape of palladium halogen (ν_{Pd-X}) and palladium phosphorus (ν_{Pd-P}) stretches are often cited in the literature in reporting the geometry of PdX_2P_2 compounds. In principle, for the cis-isomer with C_{2v} symmetry, Pd-X and Pd-P stretches appear as two bands; for the trans isomer with D_{2h} symmetry, the symmetric stretch is IR inactive, therefore the Pd-X and Pd-P stretches appear as single bands.[26, 33] The palladium-halogen stretching frequencies in cis isomers are lower than those in trans isomers [$\nu_{Pd-Cl(cis)}$ = 280 - 310 cm^{-1}, $\nu_{Pd-Cl(trans)}$ = 350 - 357 cm^{-1}],[34 - 40] because the trans influence of phosphine in a cis isomer weakens the palladium halogen bond.[37b] On the other hand, the palladium-phosphorus stretching frequencies in cis isomers are higher than those in trans ones [$\nu_{Pd-P(cis)}$ = 400 - 450 cm^{-1}, $\nu_{Pd-P(trans)}$ = 340 - 400 cm^{-1}],[34 -36, 37a] because the greater trans influence of the second trans phosphine reduces the palladium phosphorus bond strength more efficiently than does the halogen. As the halogen changes from chlorine through bromine to iodine, the reduced mass μ [$\mu = m_1m_2/(m_1 + m_2)$] increases, which leads to the lowering of vibration frequency according to the following equation:

$$\bar{\nu} = \frac{1}{2\pi c}\sqrt{\frac{k}{\mu}}$$

The stretching frequencies of Pd-X bands (X = Br, I) should apparently be below 280 cm^{-1}. Unfortunately, the free pyridylphosphines absorb strongly in the stretching frequency range of the palladium-halogen and palladium-phosphorus atoms; the absorption bands of the coordinated pyridylphosphines also cover up the bands of interest and make the identification of the Pd-X and Pd-P vibration modes and geometry assignment impossible (Figs. 3.3 and 3.4).

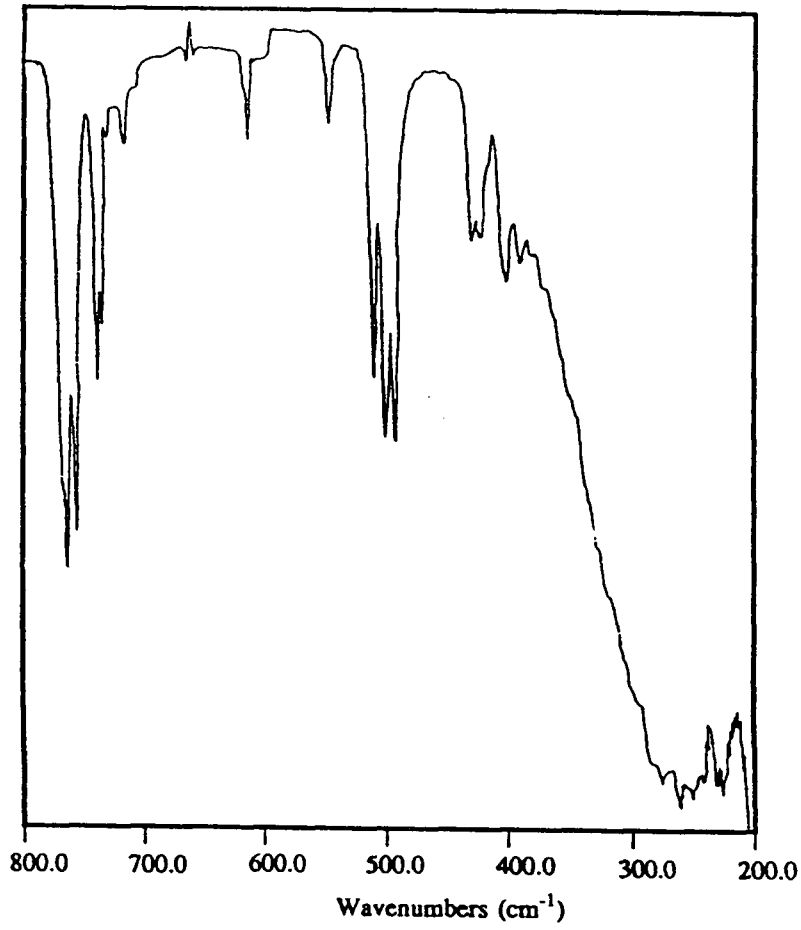

Fig. 3.3. Infrared spectrum of the phosphine ligand PN_3 in Nujol on KBr plate.

Nuclear magnetic resonance: Apart from the one bond metal-phosphorus coupling constant criterion which has been used very successfully in PtX_2P_2 systems, the magnitude of a two bond phosphorus-phosphorus coupling constant is also known to be dependent on whether the atoms are mutually cis or trans, and is thereby characteristic of the geometry of the complex.[25, 41, 42] This is particularly important for the palladium systems where the one bond metal-phosphorus coupling does not exist. It is well established that, in bis(phosphine) complexes of palladium(II), phosphorus-phosphorus coupling in trans geometry is much greater than in cis; for example, the values of $^2J_{PP}$ in cis and trans $PdCl_2(PMe_3)_2$ are -8.0 and +610 Hz respectively.[42] Direct observation of a ^{31}P NMR spectrum does not show this $^2J_{PP}$ because the two phosphorus atoms are always chemically and magnetically equivalent. Indirect observation

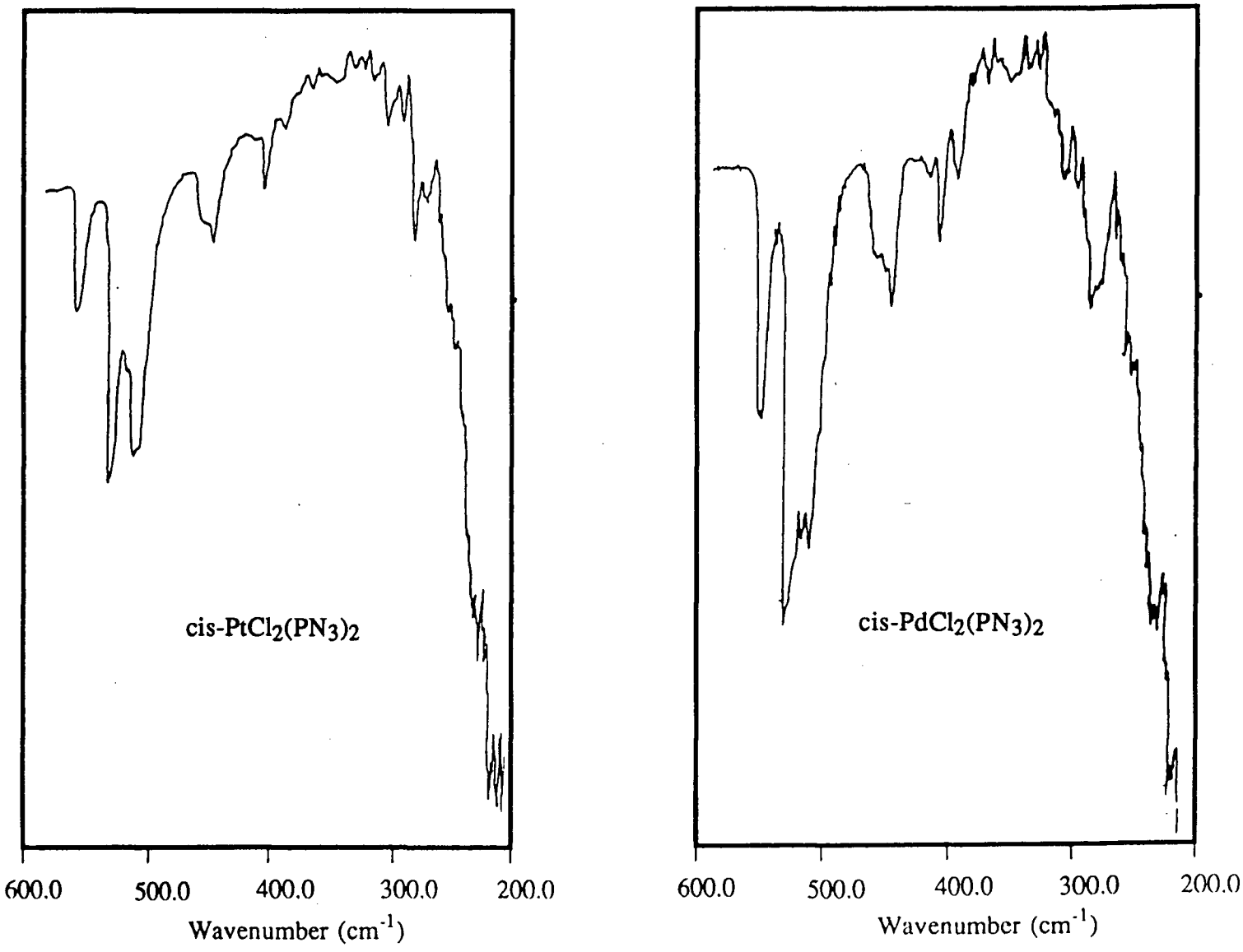

Fig. 3.4. Infrared spectra of the complexes cis-$PtCl_2(PN_3)_2$, **1c**, and cis-$PdCl_2(PN_3)_2$, **4c**, in Nujol on KRS-5 plate (42% TlBr + 58% TlI).

of $^2J_{PP}$ is possible, however, by ^1H or $^{13}C\{^1H\}$ NMR spectroscopies in which the magnetic inequivalence of the phosphorus nuclei gives rise to a complicated second order spectrum.[26, 42 - 46] These techniques work particularly well for determining the gross geometry of bis(phosphine) palladium(II) complexes with phosphines containing α-methyl or methylene groups, as the phosphines when trans are virtually coupled. The spin systems for these complexes are $A_nXX'A_n'$ (n = 3 or 2) for the ^1H and AXX' for the $^{13}C\{^1H\}$ NMR spectra, respectively, of the phosphine methyl and methylene groups (A = the measured nucleus, ^1H, or ^{13}C; X = ^{31}P). Mann et al. extended this method to an aromatic ^{13}C atom and obtained similar results.[44] The multiplicity of the ^1H or ^{13}C signals in the ^1H or $^{13}C\{^1H\}$ NMR spectra is largely dependent on the magnitude of $^2J_{PP}$. Unfortunately, the limited resolving power of the NMR spectrometer in many cases only allows for an estimate of $^2J_{PP}$ after lengthy mathematical calculations and spectrum simulation. In practice, the splitting pattern — a doublet or triplet — is found to be characteristic of the geometry. This is possible because in trans complexes the α-methyls or -methylenes are virtually coupled, and $^2J_{PP}$ is usually large (approximately 400 Hz) such that the phosphine ^1H and $^{13}C\{^1H\}$ resonances appear as a 1:2:1 triplet.[26] When the phosphines are mutually cis, these resonances normally appear as a 1:1 doublet since $^2J_{PP}$ is usually small. A ^1H NMR 1:2:1 triplet for the methyl or methylene protons will be observed when $|J_{PH} - J_{P'H}|^2 < 2J_{PP'}\Delta\nu_{1/2}$, where $\Delta\nu_{1/2}$ is the resolving power of the spectrometer; and a 1:1 doublet will be observed when $|J_{PH} - J_{P'H}|^2 > 4J_{PP'}\Delta\nu_{1/2}$. The condition for the occurrence of a 1:2:1 triplet in the $^{13}C\{^1H\}$ NMR spectrum is that $|J_{PC} - J_{P'C}|^2 < 8J_{PP'}\Delta\nu_{1/2}$. The intensity ratio of 1:2:1 is essential in judging the authenticity of trans geometry because cis complexes sometimes give a pseudo triplet with variable intensity ratio, the so-called "filled-in" doublet. This pseudo triplet can be misleading, especially when the signal-to-noise ratio is low.[4c, 25, 45]

As mentioned above, the $^{31}P\{^1H\}$ NMR spectrum of either a cis or a trans PdX_2P_2 species in solution shows as a singlet because in both circumstances the phosphorus nuclei are chemically and magnetically equivalent. When only one isomer is present, the $^{31}P\{^1H\}$ NMR spectroscopy does not tell whether that species is cis or trans. If both isomers are present, the

resonance at lower field is often assigned to the cis-PdX_2P_2 species,[30, 40, 46] despite the opposite order being seen for the platinum analogues.[24, 30] The $^{31}P\{^1H\}$ NMR spectral data in Table 3.2 show that all except **4a** and **5a** of the $PdX_2(PN_n)_2$ complexes made give one $^{31}P\{^1H\}$ singlet in CD_2Cl_2, which presents difficulty in making assignments for these phosphine complexes. However, if the singlet at 29.5 ppm of **4a** is assigned to the cis isomer and the upfield singlet at 23.4 ppm to the trans one (the assignments to cis and trans were not made by the authors who first reported **4a**)[21] a downfield shift, $\delta_{4a(cis)} < \delta_{4b(cis)} < \delta_{4c(cis)}$, becomes evident. Newkome and coworkers[30] also found that the $^{31}P\{^1H\}$ NMR chemical shifts of cis-$PdCl_2(PPh_3)_2$, cis-$PdCl_2(PN_1)_2$, and the crystallographically characterized cis-$PdCl_2(PN_2)_2$, moved downfield with the sequential replacement of the phenyl groups by the pyridyl groups on the phosphorus. Apart from this, an upfield shift trend is established for the trans iodo complexes, $\delta_{6a(trans)} > \delta_{6b(trans)} > \delta_{6c(trans)}$. The halide substitution induced shifts within both series can be understood in terms of the trans influence order I > Br > Cl.

The ^1H NMR spectra of the above phosphine complexes showed overlapping multiplets in the pyridyl and phenyl resonance regions, and the lack of methyl or methylene protons makes a clear-cut judgement of the signal pattern impossible. Fortunately, the $^{13}C\{^1H\}$ NMR spectra of the complexes, whose $^{31}P\{^1H\}$ NMR spectra show one singlet at -40°C in $CDCl_3$, showed more definitive results. The basic patterns described previously — doublet for a cis isomer and triplet for a trans isomer — are observed. The complexes $PdI_2(PN_1)_2$, **6a**, and $PdI_2(PN_2)_2$, **6b**, showed 1:2:1 triplets for the ortho- and meta-carbons on both pyridyl and phenyl rings, indicative of a trans geometry; on the other hand, $PdCl_2(PN_3)_2$, **4c**, gave 1:1 doublets for the ortho- and meta-carbons on the pyridyl rings, indicative of a cis geometry (Fig. 3.5). These results are consistent with the previous assignments based on the ^{31}P NMR chemical shift trends. The positions of the ^{13}C signals of the selected compounds are listed in Table 3.3. Because the assignments are based on the solution $^{31}P\{^1H\}$ and $^{13}C\{^1H\}$ NMR data, the assigned structures are then the preferred geometries in solution under the conditions of study. Isomerization may have taken place when the solid complex dissolves in solution. An attempt was made using

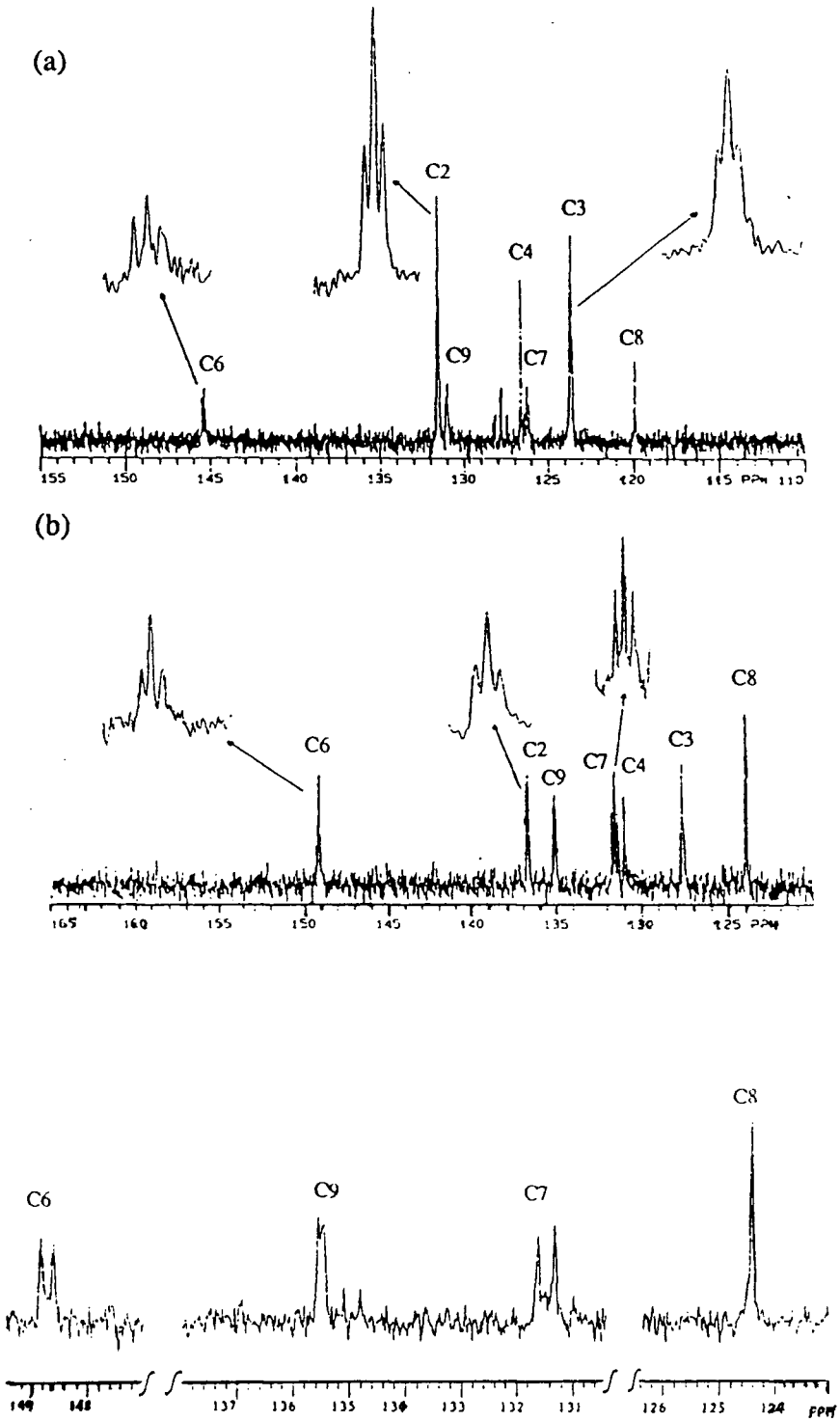

Fig. 3.5. $^{13}C\{^1H\}$ NMR spectra (75.4 MHz) of palladium pyridylphosphine complexes: (a) trans-$PdI_2(PN_1)_2$, **6a**, (b) trans-$PdI_2(PN_2)_2$, **6b** and (c) cis-$PdCl_2(PN_3)_2$, **4c**; in CD_2Cl_2 at -20°C (see Table 3.3 for C atom numbering system).

Table 3.3. $^{13}C\{^1H\}$ NMR Chemical Shifts of **4c**, **6a** and **6b**, in CD_2Cl_2 at -20°C[a]

	C(1)	C(2)	C(3)	C(4)	C(5)	C(6)	C(7)	C(8)	C(9)
PN_1	136.2(d,11.6)	134.2(d,20.0)	128.7(d,7.4)	129.1(s)	164.0	150.4(d,12.7)	127.9(d,15.2)	122.2(s)	135.8(d,2.1)
PN_2	—	135.1(d,20.6)	128.9(d,7.8)	129.7(s)	162.9(d)	150.5(d,11.9)	128.5(d,17.9)	122.6(s)	135.9(d,3.0)
PN_3	—	—	—	—	161.9(d)	150.5(d,11.5)	129.3(d,19.5)	122.9(s)	136.0(d,3.4)
6a	—	131.6(t,11.8)	123.6(t,10.2)	126.6(s)	—	145.4(t,15.2)	126.3(t,24.6)	119.9(s)	131.0(br.s)
6b	—	136.8(t,14.0)	127.6(t,12.2)	131.0(s)	—	149.1(t,17.0)	131.5(t,24.0)	124.0(s)	135.1(t,10.0)
4c	—	—	—	—	—	148.7(d,20.0)	131.5(d,21.7)	124.3(s)	135.5(d,17.4)

(a) The $^{13}C\{^1H\}$ NMR spectra of the free ligands were measured in $CDCl_3$ solvent at r.t. and those of the complexes were recorded in CD_2Cl_2 at -20°C; the chemical shifts are referenced to TMS in ppm, and the number in the brackets is the $|{}^{n}J_{PC} + {}^{n+2}J_{PC}|$ value in Hz; s, d and t indicate singlet, doublet and triplet, respectively. The carbon atoms C(1) to C(9) correspond to the individual carbon atoms on the phosphine ligand as depicted below.

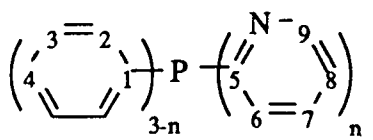

solid state $^{31}P\{^1H\}$ NMR (cross-polarization and magic angle spinning, CP/MAS) to correlate structures in solution with those in the solid state, but with little success (Table 3.4). The selected samples analyzed by CP/MAS $^{31}P\{^1H\}$ NMR show a pronounced chemical shift anisotropy for the phosphorus nuclei. The ^{31}P peaks are normally broad, up to 10 ppm; for instance, $PdCl_2(PN_1)_2$, **4a**, gives a singlet at 25.2 ppm with linewidth at half height of 8 ppm (Fig. 3.6). It is uncertain, therefore, whether one isomer or both are present in the solid state, knowing that the solution chemical shift of the cis is seen at 29.5 ppm and that of the trans at 23.4 ppm. Solid state site symmetry[47] also presents a problem in interpreting the spectra. For example, the $^{31}P\{^1H\}$ NMR spectrum of cis-$PtI_2(PN_3)_2$, **3c**, (Fig. 3.7a) shows two sets of signals with J_{PtP} values of 3599 and 3294 Hz. Both of these are assigned to cis isomers according to a literature report[48] in which a similar splitting pattern is seen for cis-$PtCl_2(PPh_3)_2$. The splitting is attributed to the site symmetry in the solid state. It is relatively easy to identify such splitting for Pt but is difficult for Pd. For example, even when two peaks appear at 46.4

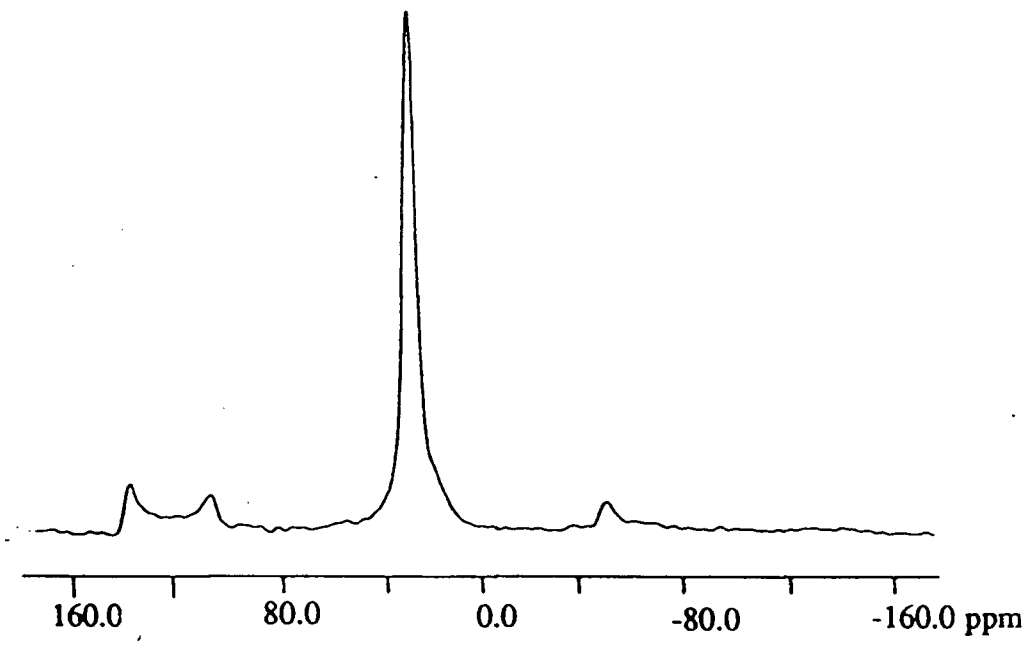

Fig. 3.6. Solid-state $^{31}P\{^1H\}$ NMR spectrum (40.4 MHz) of $PdCl_2(PN_1)_2$ obtained at r.t. using cross-polarization and magic angle spinning; $\delta = 25.5$ (s).

and 40.3 ppm in the case of $PdCl_2(PN_3)_2$ (Fig. 3.7b), it is still uncertain whether they are due to the resonances of cis and trans isomers or arise from the local site symmetry. In addition, chemical shifts measured in the solid state are somewhat different from those measured in solution. Nevertheless, for the iodo complexes **6a** - **6c**, the solid state $^{31}P\{^1H\}$ NMR data agree well with the solution spectra. The trans-$PdI_2(PN_n)_2$ species is confirmed to be the only isomer present both in solution and in the solid state. In the case of $PdBr_2(PN_3)_2$, **5c**, it seems reasonable to conclude that both cis and trans isomers are present in the solid state with their chemical shifts about 20 ppm apart. But it is impossible to correlate the observed solution singlet at 31.0 ppm with either of the two singlets observed in the solid state (Fig. 3.7c). The phosphorus resonances at 42.1 and 23.8 ppm are assigned to the cis and trans isomers, respectively.

Table 3.4. Solid State $^{31}P\{^1H\}$ NMR Data of $PdX_2(PN_n)_2$ Complexes at Ambient Temperature

Complexes	δ Chemical Shifts (ppm)
$PdCl_2PN_1)_2$, **4a**	25.2
$PdI_2(PN_1)_2$, **6a**	8.0
$PdCl_2(PN_3)_2$, **4c**	46.4 (50%), 40.3 (50%)
$PdBr_2(PN_3)_2$, **5c**	42.1 (50%), 23.8 (50%)
$PdI_2(PN_3)_2$, **6c**	-2.5

Thus despite the problems with the mononuclear Pd pyridylphosphine complexes, assignments are made. We also notice that the chloro and bromo complexes prefer cis geometry in solution at low temperature. A weak π interaction of the pyridyl group on one phosphine with the pyridyl group on the adjacent phosphine in the $PdCl_2(PN_2)_2$ crystal structure was noticed by Newkome et al.;[30] this weak interaction might provide extra stabilization energy for the cis geometry, especially at low temperature when molecular motion is restricted.

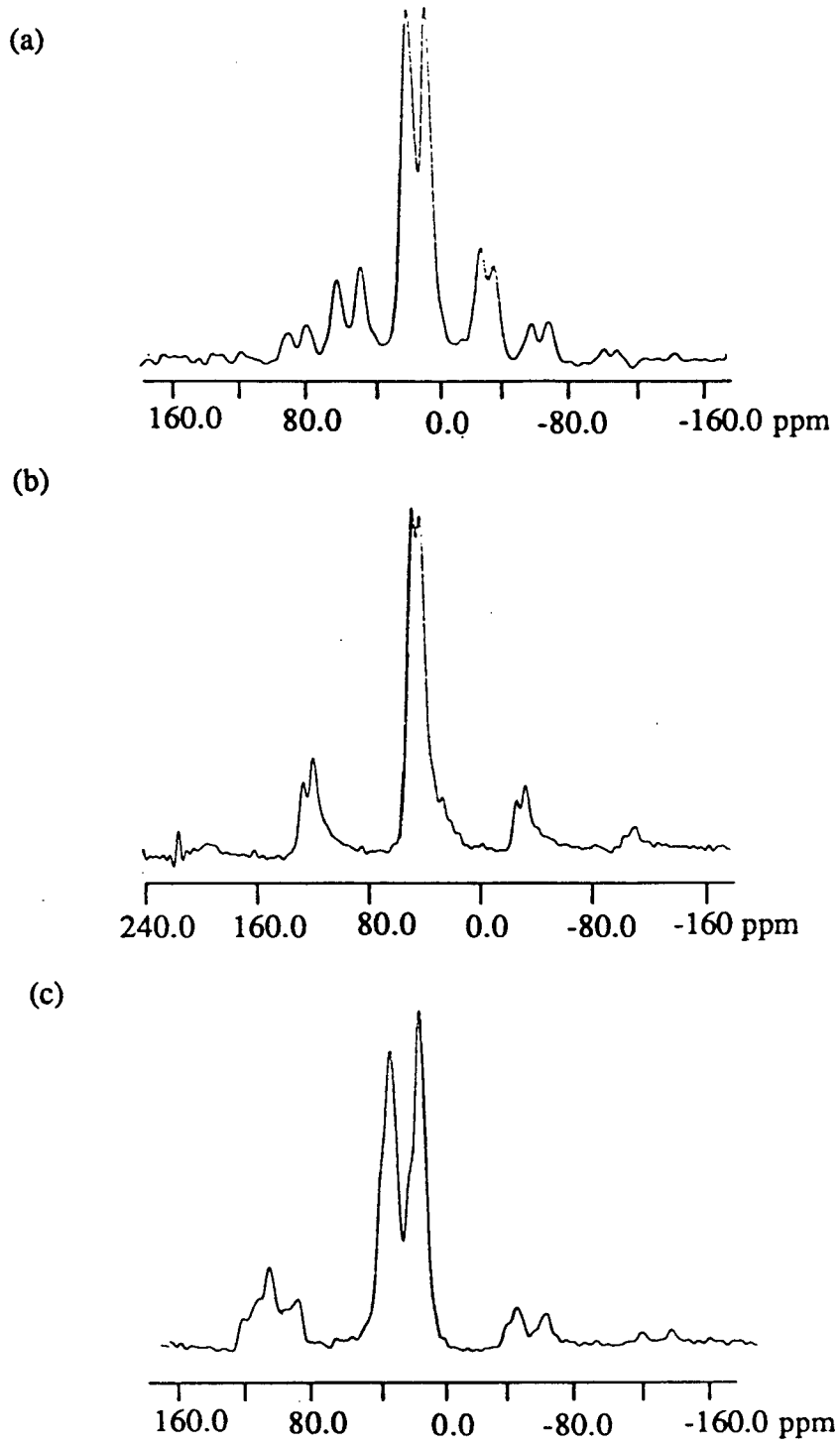

Fig. 3.7. Solid-state $^{31}P\{^{1}H\}$ NMR spectrum (40.4 MHz) of (a) **3c**, (δ = 13.1 (s) and 1.9 (s), $^{1}J_{PtP}$ = 3599 and 3294 Hz, respectively), (b) **4c**, and (c) **5c**, obtained at r.t. using cross-polarization and magic angle spinning.

3.2.3. Pt(I) binuclear pyridylphosphine complexes

The Pt^I binuclear bridging complexes discussed here were synthesized via the conproportionation reaction of Pt(0) and Pt(II) precursors (Sect. 2.6).[22] Two stereoisomers: head-to-head, HH, and head-to-tail, HT, are possible (see Sect. 3.1). However, the only isolable HH isomers were limited to the three iodo complexes $Pt_2I_2(\mu\text{-}PN_n)_2$. The head-to-tail isomers **7** - **9** discussed here are shown below:

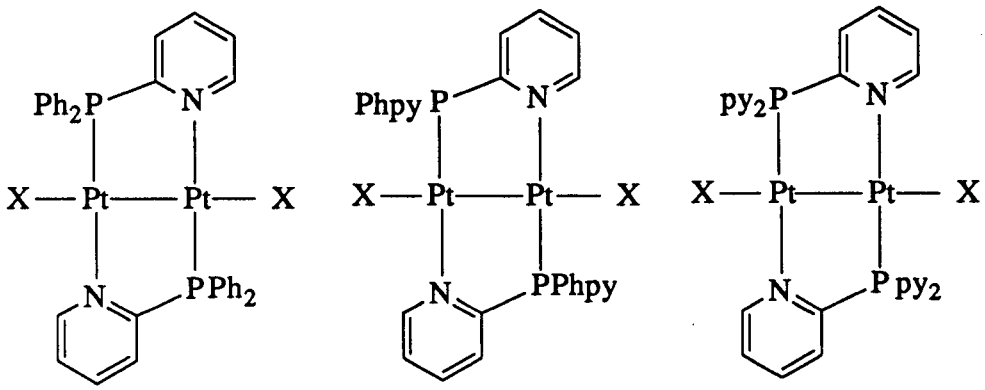

X = Cl, **7a**
X = I, **9a**

X = Cl, **7b**
X = I, **9b**

X = Cl, **7c**
X = Br, **8c**
X = I, **9c**

The $^{31}P\{^1H\}$ NMR spectroscopy was commonly used as the structural tool in assigning configurations. The isotopomers drawn below (Fig. 3.8) can be applied to any of the Pt-PN_n systems with an HT arrangement. The natural abundances indicated for each isotopomer arise from the presence of the ^{195}Pt spin labelled isotope.

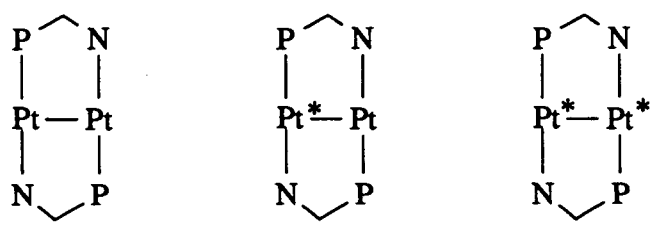

A	B	C
43.8%	44.8%	11.4%

Fig. 3.8. The isotopomers of a $Pt_2(\mu\text{-}PN_n)_2X_2$ (HT) type compound, n = 1, 2, 3, X = Cl, Br, I; Pt* = ^{195}Pt, natural abundance of ^{195}Pt = 33.8%, I = 1/2; P = PPh_2, PPhpy or Ppy_2; N = pyridyl moiety; halides are not shown.

The $^{31}P\{^1H\}$ NMR spectrum shown in Fig. 3.9 is that of $Pt_2I_2(\mu\text{-}PN_3)_2(HT)$, **9c**, which is typical of an HT-isomer. The major central peak A in Fig. 3.9 arises from the unlabelled isotopomer A, because in the absence of ^{195}Pt, the two phosphorus atoms are chemically as well as magnetically equivalent. The doublet of doublets labelled B comes from the singly labelled isotopomer B, in which the two phosphorus atoms are chemically equivalent but magnetically inequivalent, this giving rise to the fine satellite splitting centred at the A position. This is an AA'X spin system with J_{AX}-$J_{A'X}$ ($^1J_{PtP}$ -$^2J_{PtP}$) being >> J_{PP}, and hence the spectrum is pseudo-first-order with the outermost doublets given by the phosphorus directly bonded to ^{195}Pt centre and the innermost doublets arising from the phosphorus bonded to the non-spin labelled Pt. The signal labelled C arises from isotopomer C, but such signals are not always observable due to the low intensity.

The only situation where the $^{31}P\{^1H\}$ NMR spectrum is ambiguous for an HT/HH assignment is when the $^3J_{PP}$ coupling constant becomes very small or unresolvable (see Ch. 4, Sect. 4.3.1). When the ambiguity arises, $^{195}Pt\{^1H\}$ NMR can be used to distinguish the two possible phosphine orientations. The typical $^{195}Pt\{^1H\}$ spectrum of an HT isomer, e.g. **9c**, is shown in Fig. 3.9(b) as a "doublet of doublets" arising from the overlap of the signals due to the isotopomer B and C. The $^1J_{PtP}$ and $^2J_{PtP}$ can be obtained by spectrum simulation with good agreement with the $^{31}P\{^1H\}$ data.

The basic spectral pattern does not change as the number of pyridyl substituents on the phosphorus atom changes. A downfield δ_P chemical shift is seen on going from **7a** through **7b** to **7c** (Table 3.5). Fig. 3.10 shows the $^{31}P\{^1H\}$ NMR spectrum of **7b** as two distinct sets of the basic spectral pattern discussed above, and can be understood in terms of stereoisomers drawn in Fig. 3.10.

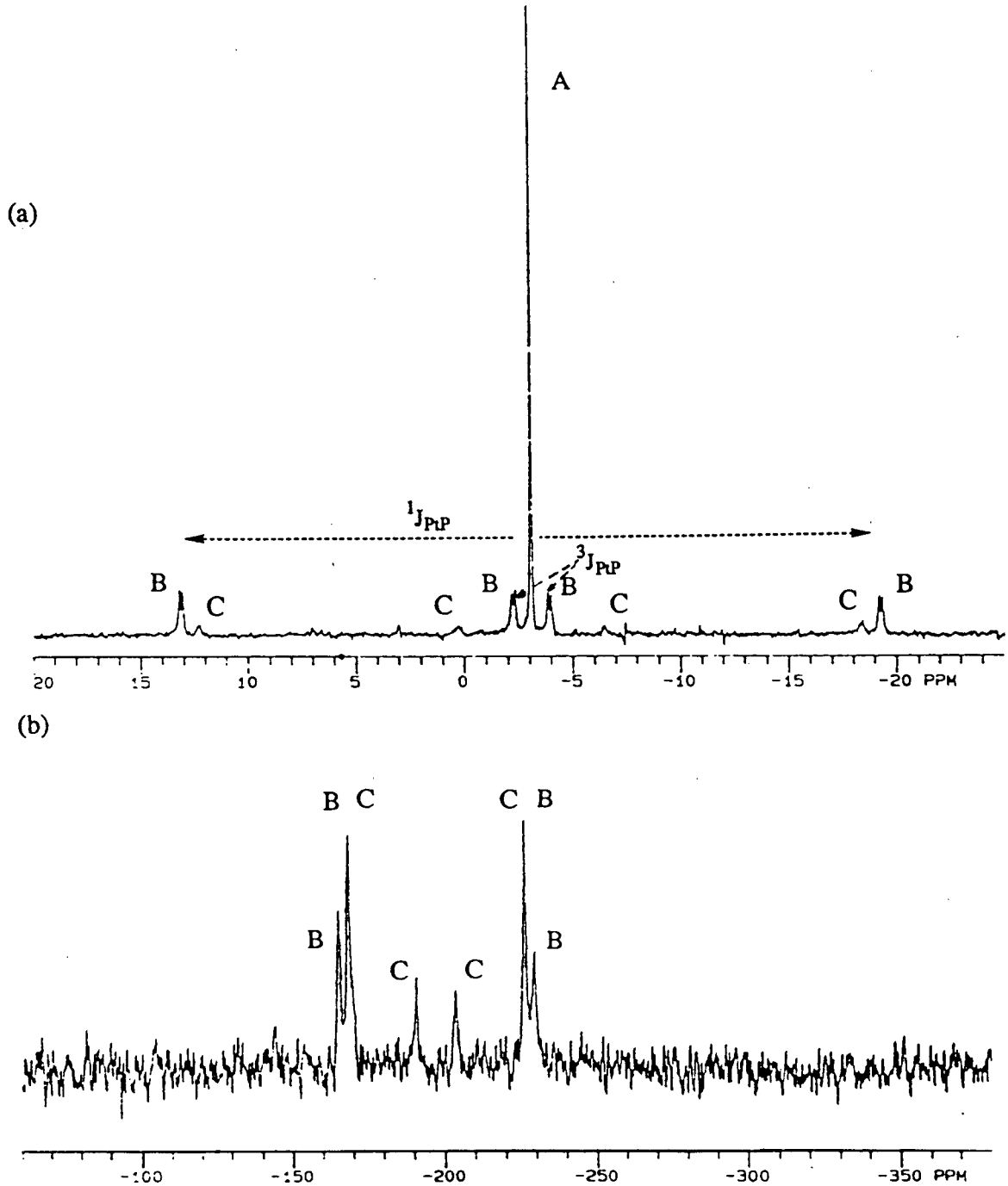

Fig. 3.9. $^{31}P\{^1H\}$ and $^{195}Pt\{^1H\}$ NMR spectra of $Pt_2I_2(\mu\text{-}PN_3)_2$ (HT), **9c**, in $CDCl_3$ at r.t.; (a) $^{31}P\{^1H\}$ NMR (121.4 MHz) and (b) $^{195}Pt\{^1H\}$ NMR (64.2 MHz) (data given in Table 3.5).

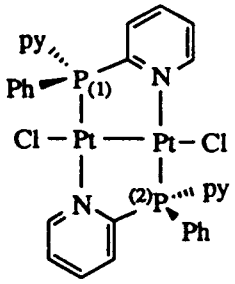

(1S, 2S)*

7b.1

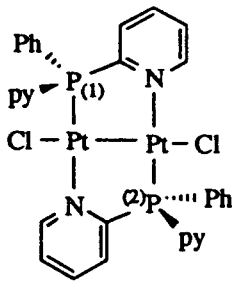

(1R, 2R)

7b.2

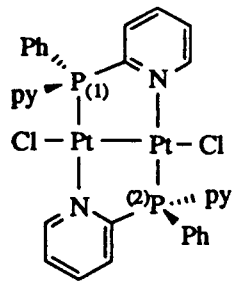

(1R, 2S)

7b.3

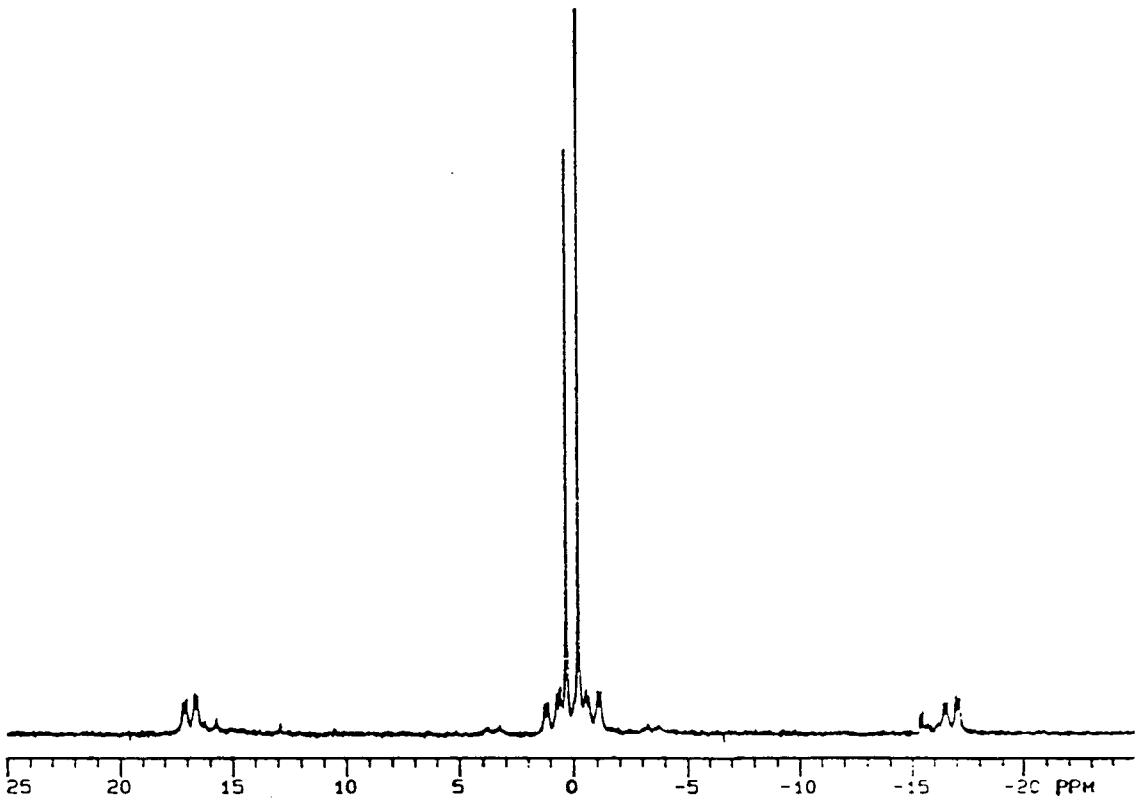

Fig. 3.10. $^{31}P\{^{1}H\}$ NMR spectrum of the diastereomers of **7b** in $CDCl_3$ at r.t. (data given in Table 3.5). Peaks are not assigned to specific diastereomers.

* Only the chiral phosphorus atoms are numbered; regardless of the configuration of the molecule drawn, in the paper plane, the P atom above Pt is labelled P(1), and the P atom below is labelled P(2).

Table 3.5. $^{31}P\{^1H\}$ and $^{195}Pt\{^1H\}$ NMR Data of $Pt_2X_2(\mu\text{-}PN_n)_2$ (HT)[a]

Complexes	Solvent	δ_P	δ_{Pt}	$^1J_{Pt\text{-}P}$	$^2J_{Pt\text{-}P}$	$^3J_{PP}$	Ref.[b]
$Pt_2Cl_2(\mu\text{-}PN_1)_2$ (HT), **7a**	$CDCl_3$	-1.5		4124	215	17.8	22
$Pt_2I_2(\mu\text{-}PN_1)_2$ (HT), **9a**	$CDCl_3$	5.7		3905	198	17.8	22
$Pt_2Cl_2(\mu\text{-}PN_2)_2$ (HT), **7b**	$CDCl_3$	0.3		4090	215	20.0	tw
		-0.2		4090	215	20.0	tw
$Pt_2I_2(\mu\text{-}PN_2)_2$ (HT), **9b**	CD_2Cl_2	-4.67		3945	196	~16[c]	tw
		-5.04		3945	196	~16[c]	tw
$Pt_2Cl_2(\mu\text{-}PN_3)_2$ (HT), **7c**	$CDCl_3$	0.66		4074	214	18.2	tw
$Pt_2Br_2(\mu\text{-}PN_3)_2$ (HT), **8c**	$CDCl_3$	-0.27		4006	214	17.6	tw
$Pt_2I_2(\mu\text{-}PN_3)_2$ (HT), **9c**	$CDCl_3$	-3.09		3936	205	18.9	tw
			-197.3	3901	207	—	tw

(a) Recorded at r.t.; δ_P and δ_{Pt} measured in ppm, coupling constants in Hz. (b) tw = this work. (c) Satellites difficult to resolve.

When one of the two pyridyl groups attached to a phosphorus atom forms a bridging bond across Pt-Pt, that phosphorus atom becomes asymmetric. Assuming no or slow exchange between the bridging and non-bridging pyridyl groups, three compounds, **7b.1**, **7b.2** and **7b.3**, are expected. The stereochemical relationships between these isomers are described by symmetry operations. **7b.1** and **7b.2**, related by a mirror plane, are enantiomeric; **7b.3** is not related by any symmetry to **7b.1/7b.2** and therefore, is a diastereomer of these.[49, 50] In an achiral solvent, diastereomers are chemically different, but enantiomers are indistinguishable.[49] Consequently, **7b.1** and **7b.2** give one set of signals and **7b.3** gives another set (Fig. 3.10).

The well-resolved resonances in the $^{31}P\{^1H\}$ NMR spectrum of $Pt_2Cl_2(\mu\text{-}PN_2)_2$ (HT) at room temperature imply that either no exchange of the bridging pyridyl with nonbridging pyridyl takes place or the exchange is too slow relative to the NMR time scale.

The crystal structure of **7b.1**, $Pt_2Cl_2(\mu\text{-}PN_2)_2$(HT) (1S, 2S) was done by S.J. Rettig in this department (Fig. 3.11). In the solid state, this molecule is, in fact, not coplanar as drawn above. The dihedral angle between two coordination square planes of platinum is 36.19°. The Pt, P, and N atoms are arranged rather like a boat conformation. There is a C_2 axis through the centre of the Pt_1-Pt_2 bond for the main frame, and the noncoordinated phenyl and pyridyl groups are severely twisted (the dihedral angles between two phenyl rings and two pyridyl rings are 44.10 and 41.25°, respectively). On the whole, the C_2 symmetry of **7b.1**, present in solution, no longer exists; the phosphorus atoms become diastereotopic in the crystal lattice.

The other P-N phosphine arrangement is the head-to-head, as described in Sect. 3.1. The iodo complexes of HH configuration discussed here are shown as follows:

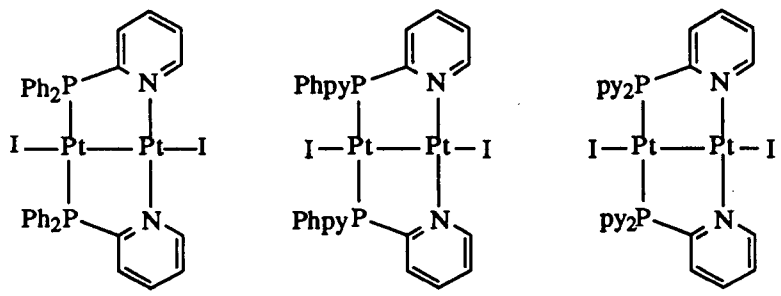

10a **10b** **10c**

The change of ligand orientation from HT to HH brings about significant changes in the appearance of the $^{31}P\{^1H\}$ spectrum. In general, four isotopomers with appropriate abundances need to be considered (see Fig. 3.12). The representative $^{31}P\{^1H\}$ spectrum of $Pt_2I_2(\mu\text{-}PN_3)_2$ (HH), **10c**, is shown in Fig. 3.13. The major singlet D is due to the unlabelled isotopomer D. The outermost satellites labelled E arise from isotopomer E, where the splitting, $^1J_{Pt\text{-}P}$, is determined by the 3260 Hz difference between the two lines, which correspond to the one bond Pt-P coupling. This value is significantly smaller than that of the HT isomer, 3936 Hz, due to the trans effect of the phosphine ligands. The inner satellites labelled F are considerably broader and are due to the isotopomer F. The broadening is accounted for by the fast relaxation

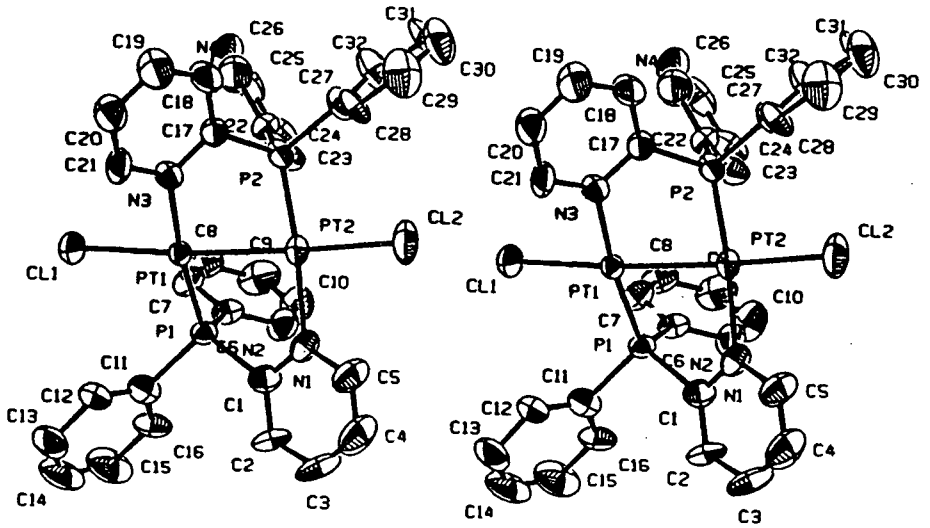

Fig. 3.11. 3D structure of $Pt_2Cl_2(\mu\text{-}PN_2)_2$ (HT), **7b.1**; the ORTEP drawing and atomic numbering scheme.

Representative bond lengths and angles, in Å and °, respectively:

Pt(1)-Pt(2) = 2.574 (1)	N(3)-Pt(1)-Pt(2) = 91.4
Pt(1)-P(1) = 2.169 (3)	N(3)-Pt(1)-Cl(1) = 88.0
Pt(1)-N(3) = 2.10 (1)	P(1)-Pt(1)-Cl(2) = 99.1
Pt(2)-P(2) = 2.169 (1)	P(1)-Pt(1)-Pt(2) = 81.5
Pt(2)-N(1) = 2.08 (1)	Cl(1)-Pt(1)-Pt(2) = 173.5
	Cl(2)-Pt(2)-Pt(1) = 176.6

transmitted from the quadrupolar nitrogen atoms through ^{195}Pt to P. Isotopomer G is supposed to give a doublet of doublets, but the signal-to-noise ratio is insufficient to allow identification of the peaks.

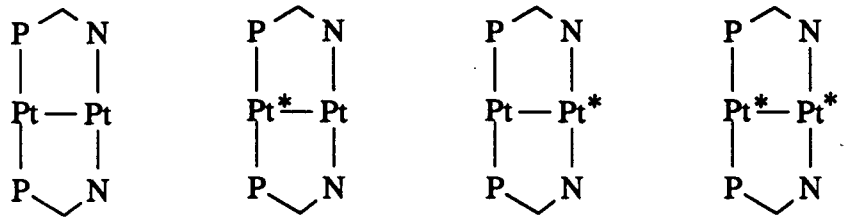

D 43.8% E 22.4% F 22.4% G 11.4%

Fig. 3.12. The isotopomers of a $Pt_2I_2(\mu\text{-}PN_n)_2$ (HH), n = 1, 2, 3; natural abundance of ^{195}Pt = 33.8%, I = 1/2. Pt* = ^{195}Pt; N = pyridyl moiety; P = PPh_2, PhPpy, or Ppy_2; halides are not shown.

In all the isotopomers shown, the phosphorus nuclei within each isotopomer are always equivalent. The splitting of satellites seen in the HT isomers is no longer visible in the HH system. The differences in the ^{31}P NMR spectral appearance, as well as the magnitude of $^1J_{PtP}$ coupling constant, provide a good probe for elucidating the structure of these bridging Pt complexes. The typical $^{195}Pt\{^1H\}$ NMR spectrum of an HH isomer, for example **10c**, is shown in Fig. 3.13(b) as an authentic triplet arising from the isotopomer E. The $^{31}P\{^1H\}$ and $^{195}Pt\{^1H\}$ NMR data for the $Pt_2I_2(\mu\text{-}PN_n)_2$(HH) complexes are listed in Table 3.6.

Examining the stereochemical relationship between the stereoisomers of $Pt_2I_2(\mu\text{-}PN_2)_2$ (HH), **10b**, generated *in situ*, one expects for planar structures two similar sets of signals for **10b.1** and **10b.2/10b.3** because **10b.2** and **10b.3** are enantiomers and both of them are diastereomers of **10b.1** by external comparison.[42, 43] The two phosphorus nuclei in **10b.1**, related by a mirror plane perpendicular to the P-Pt-P axis, are enantiotopic and, therefore, a ^{31}P

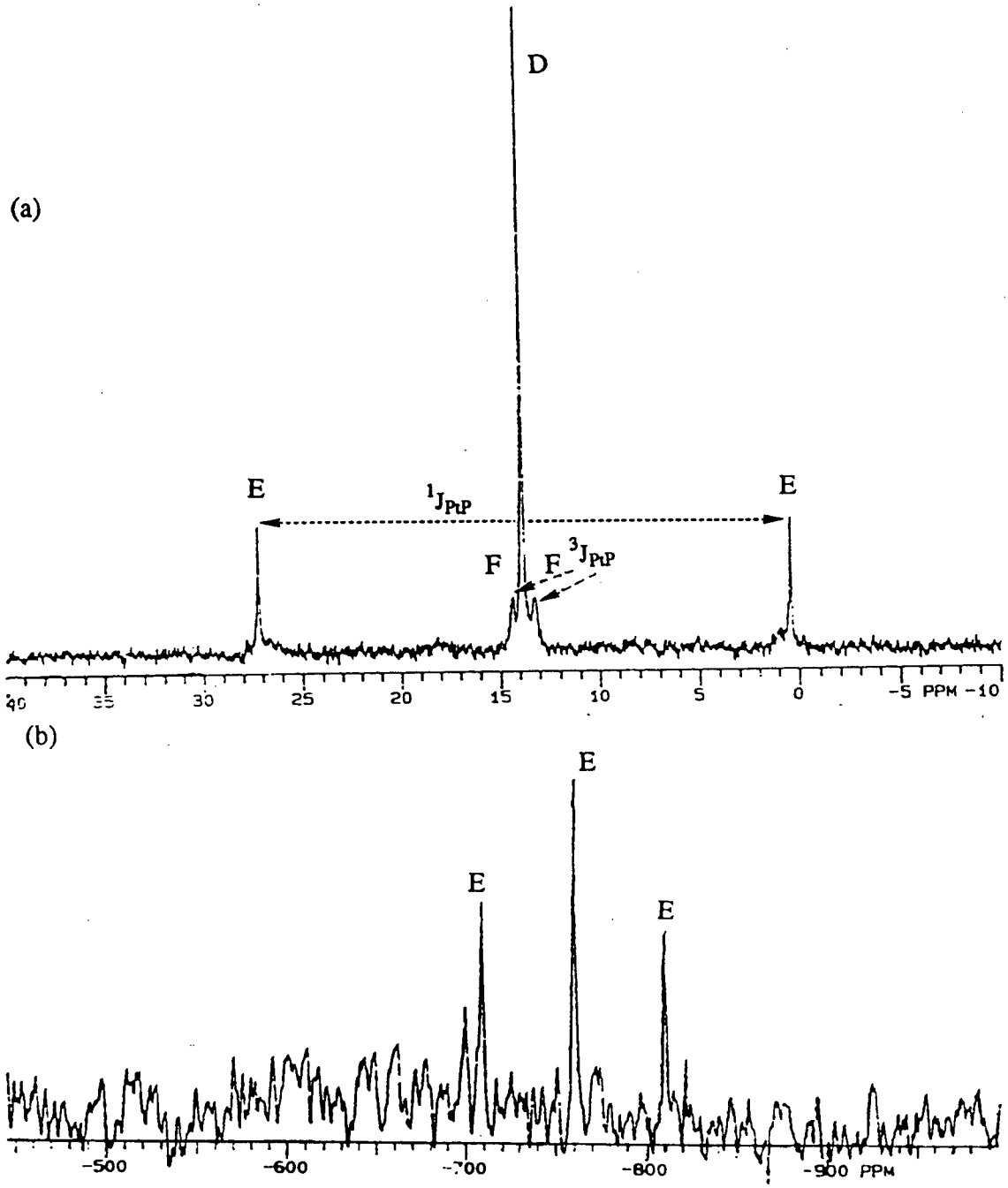

Fig. 3.13. $^{31}P\{^1H\}$ and $^{195}Pt\{^1H\}$ NMR spectra of $Pt_2I_2(\mu\text{-}PN_3)_2$ (HH), **10c**, in $CDCl_3$ at r.t.; (a) $^{31}P\{^1H\}$ NMR (121.4 MHz) and (b) $^{195}Pt\{^1H\}$ NMR (64.2 MHz) (data given in Table 3.6).

Table 3.6. $^{31}P\{^1H\}$ and $^{195}Pt\{^1H\}$ NMR Data of $Pt_2(\mu\text{-}PN_n)_2I_2$ (HH)[a]

Complexes	Solvent	δ_P	δ_{Pt}	$^1J_{PtP}$	$^2J_{PtP}$	$^3J_{PP}$	Ref.[b]
$Pt_2I_2(\mu\text{-}PN_1)_2$, **10a**	$CDCl_3$	9.6		3260	153	—	22 & tw
$Pt_2I_2(\mu\text{-}PN_2)_2$, **10b.1**[c]	CD_2Cl_2	12.55		3276	122	441	tw
		11.0		3276	122	441	tw
			-739.4(t)	3261	—	—	tw
10b.2/10b.3[c]	CD_2Cl_2	11.30		3249	182	—	tw
$Pt_2I_2(\mu\text{-}PN_3)_2$, **10c**	$CDCl_3$	14.11		3260	136	—	tw
			-759.5(t)	3259	—	—	tw

(a) Recorded at r.t.; chemical shifts δ_P and δ_{Pt} measured in ppm, coupling constants in Hz. (b) tw = this work. (c) Recorded at -20°C.

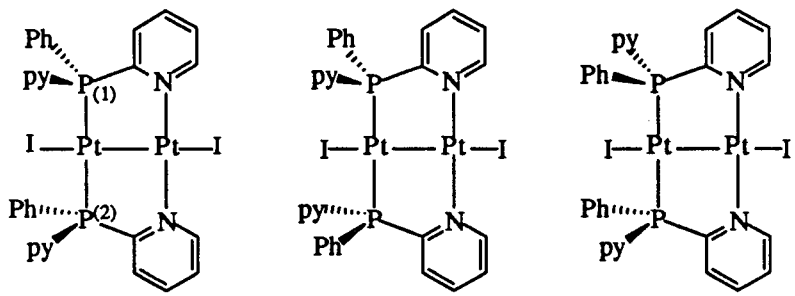

(1S, 2R) **10b.1** (1S, 2S) **10b.2** (1R, 2R) **10b.3**

singlet with Pt satellites is expected. The two phosphorus atoms in **10b.2/10b.3**, related by the C_2 axis in the molecular plane perpendicular to the P-Pt-P axis, are equivalent and should give rise to a singlet and Pt satellites. However, the actual experimental spectrum of the diastereomeric mixture of **10b** (Fig. 3.14) is different from that expected for planar structures. It appears to be composed of a singlet and an AB quartet with their respective Pt satellites. This was ascertained by measuring the ^{31}P NMR spectrum of both the separated diastereomer **10b.1** and the **10b.2/10b.3** mixture — enantiomers are not separable by TLC (see Sect. 2.6.2 for detailed separation procedure) (Fig. 3.15). The tight AB quartet reflects inequivalent P atoms in the molecule. The coupling constants of this compound were resolved by spectrum simulation:

J_{PP}, $^1J_{PtP}$ and $^2J_{PtP}$ were found to be 441, 3276 and 122 Hz, respectively. The magnitude of the P-P coupling confirms that the two P atoms are trans to each other, and this is reinforced by the value of $^1J_{PtP}$ (3276 Hz). The inequivalence of the P atoms can only arise from lack of symmetry element in the molecule: the P atoms are no longer enantiotopic as in **10b.1**, or equivalent as in **10b.2/10b.3**, and must be diastereotopic.

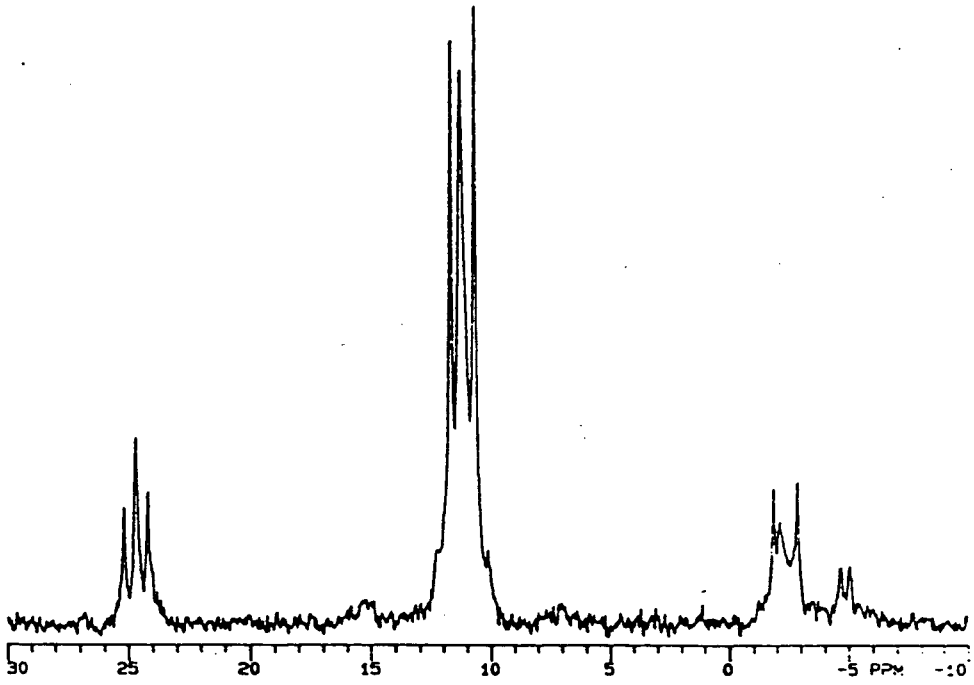

Fig. 3.14. 121.4 MHz $^{31}P\{^1H\}$ NMR spectrum of the mixture of diastereomers of **10b** in CD_2Cl_2 at r.t.

The correlation between the diastereomeric structures depicted above and the $^{31}P\{^1H\}$ NMR spectra in Fig. 3.15 was not obvious. Some single crystals of **10b.1** obtained were highly disordered, and species **10b.2/10b.3** grew as twin crystals in three occasions (Sect. 2.6.2). The problem in assigning the structures was finally solved later by the $^{31}P\{^1H\}$ NMR spectral analyses of the DMAD derivatives of **10b.1** and **10b.2/10b.3** which will be discussed in full detail in Chapter 4, Sect. 4.3.4. Species **10b.1**, the second fraction obtained from a TLC plate, turns out to be the one giving the "abnormal" ^{31}P spectrum shown in Fig. 3.15(b). The **10b.2/10b.3** mixture, the first fraction from the TLC, gives the typical ^{31}P NMR spectrum as in Fig. 3.15(d) expected for coplanar geometry. The inequivalence of phosphorus atoms in **10b.1** arises because the mirror plane relating these atoms must be disrupted. However, the C_2

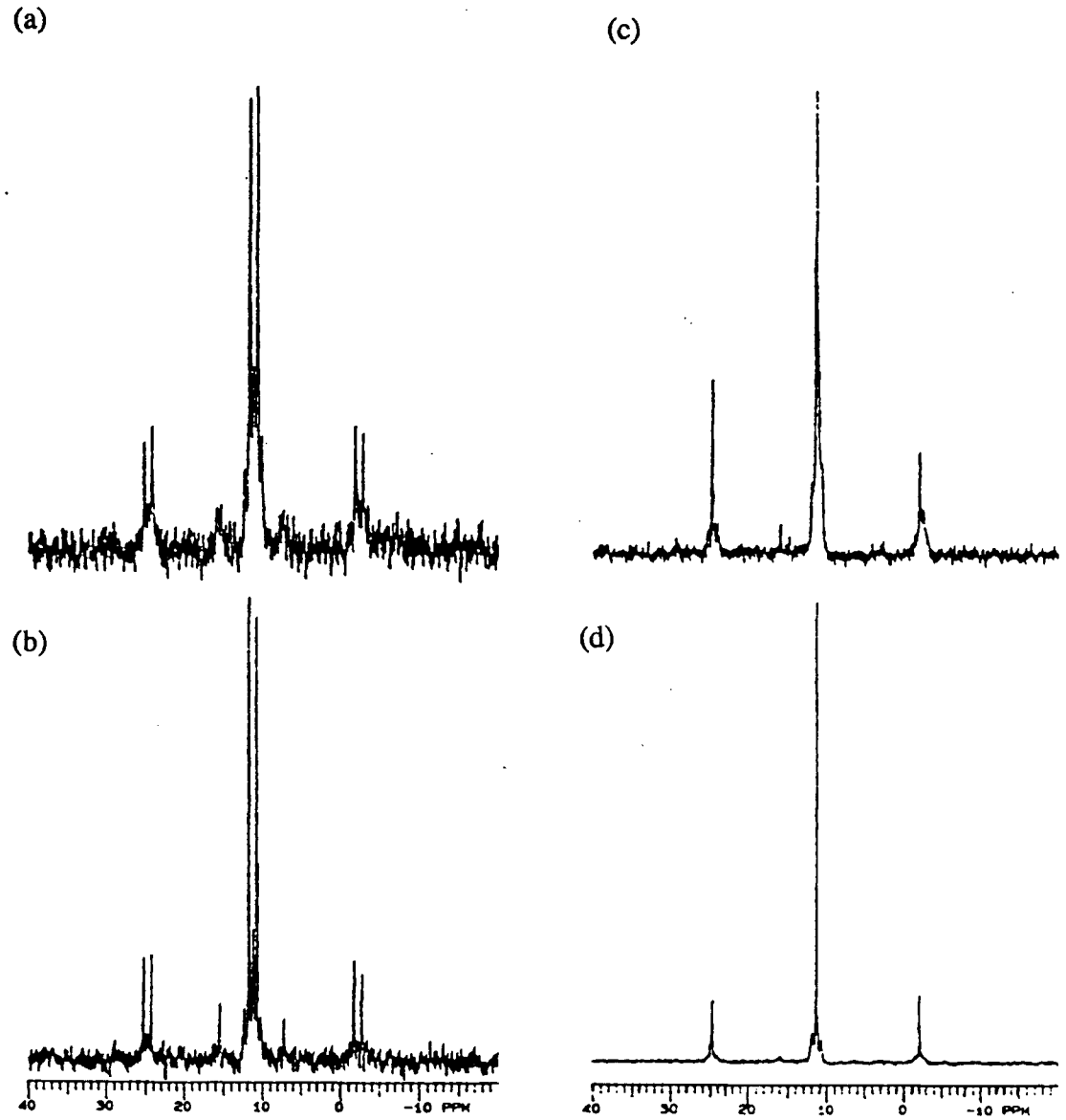

Fig. 3.15. $^{31}P\{^{1}H\}$ NMR spectra (121.4 MHz) of the separated diastereomers of **10b** in CD_2Cl_2; (a) **10b.1** at r.t., (b) **10b.1** at -10°C, (c) **10b.2/10b.3** at r.t., and (d) **10b.2/10b.3** at -20°C (data given in Table 3.6).

symmetry of the molecule does not seem to be affacted. Recall that in the X-ray structure of the HT isomer **7b.1** (Fig. 3.11), the noncoordinated pyridyl and phenyl groups on one phosphorus atom are twisted with respect to those on the another, despite these groups being relatively far away from one another spacewise. In the HH isomer, two phosphorus atoms are situated on one platinum, the interaction between the groups on the phosphorus atoms being so severe that, even in solution, the expected mirror plane for **10b.1** molecules symmetry cannot be maintained.

3.2.4. Pd(I) pyridylphosphine complexes

Dichlorobis[2-(diphenylphosphino)pyridine]dipalladium(I), $Pd_2Cl_2(\mu\text{-}PN_1)_2$, was reported by Maisonnat et al.[21] and was assigned the head-to-tail structure based on analogous structures for heterodinuclear complexes of the same phosphine ligand, for example, with Pd^IPt^I [22, 51] and Pd^IRh^{II}.[51, 52] In these cases, the P-N phosphine arrangement on the metal centre can be easily distinguished by the spectroscopic analysis. The Pd^IPt^I/PN_3 heterodinuclear complexes made in the present work, **14c-16c**, were shown to have exclusively the HT configuration by their ^{31}P NMR spectra (Table 3.7, Fig. 3.16). The doublet must arise from the chemical inequivalence of the two P atoms attached to two different metal centres. The P atom attached to Pt is split by ^{195}Pt and gives rise to the larger satellite (3900 Hz), while the P atom attached to Pd is split (by ^{195}Pt) by only about 100 Hz (Table 3.7). The splitting between the two phosphorus atoms, 14.3 - 16.8 Hz, is characteristic of an HT disposed phosphine (see the corresponding Pt_2 analog, Sect. 3.2.3). No HH-isomer with both P atoms on palladium has ever been found.

Table 3.7. $^{31}P\{^1H\}$ NMR Data for $PtPdX_2(\mu\text{-}PN_3)_2$(HT) Complexes[a]

Complexes	$\delta_{P(Pt)}$	$\delta_{P(Pd)}$	$^1J_{PtP}$	$^2J_{PtP}$	$^3J_{PP}$
$PtPdCl_2(\mu\text{-}PN_3)_2$. **14c**	-3.92 (d)	9.4 (d)	3988	110.5	14.3
$PtPdBr_2(\mu\text{-}PN_3)_2$. **15c**	-5.62 (d)	7.78 (d)	3951	100.0	15.6
$PtPdI_2(\mu\text{-}PN_3)_2$. **16c**	-8.36 (d)	4.46 (d)	3863	75.4	16.8

(a) The spectra were recorded at r.t. in $CDCl_3$; δ_P's are measured in ppm and the coupling constants are in Hz.

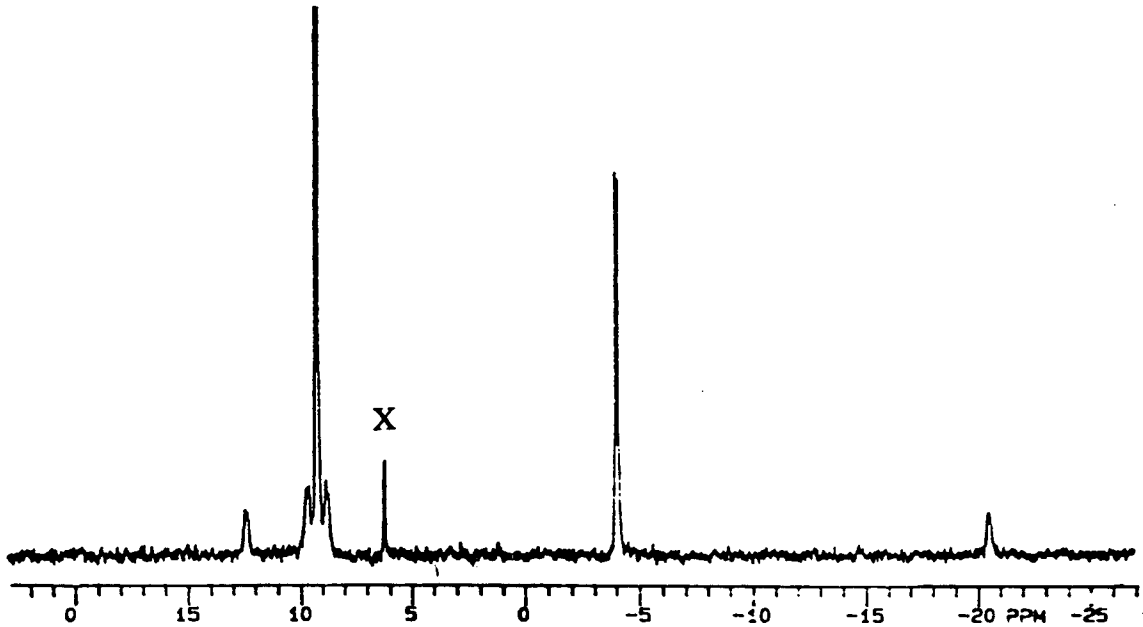

Fig. 3.16. $^{31}P\{^1H\}$ NMR spectrum of **14c** in $CDCl_3$ at r.t., see Table 3.7. The singlet at 6.3 labelled X is the $Pd_2Cl_2(\mu\text{-}PN_3)_2$ impurity.

The molecular structure of $Pd_2I_2(\mu\text{-}PN_1)_2$ was determined crystallographically,[20] where the HT orientation was shown explicitly. The downfield shift of ^{31}P NMR resonances through the series **13a**, **13b** and **13c** (Table 3.8) is normal, as is the downfield shift induced by the halogen substitution from **11a**, **12a**, to **13a** (Sect. 3.2.2). In the case of $Pd_2Cl_2(\mu\text{-}PN_3)_2$, support for the HT configuration comes indirectly from the HT configuration determined for the DMAD insertion adduct, assuming no rearrangement occurs during the course of reaction (see X-ray structure in Fig. 4.1). Hence, the HT configuration is assigned to all the dipalladium complexes, based on the relationships between their $^{31}P\{^1H\}$ NMR data (Table 3.8). The structures of the HT $Pd_2X_2(\mu\text{-}PN_n)_2$ species discussed here are shown below:

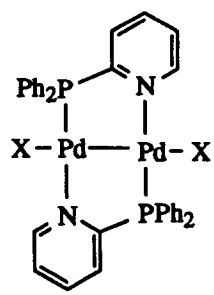

X = Cl, 11a
X = Br, 12a
X = I, 13a

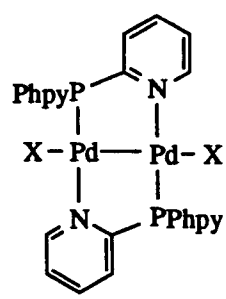

X = Cl, 11b
X = Br, 12b
X = I, 13b

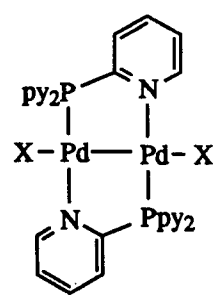

X = Cl, 11c
X = Br, 12c
X = I, 13c

Table 3.8. $^{31}P\{^1H\}$ Chemical Shifts for $Pd_2X_2(\mu\text{-}PN_n)_2$ (HT) Complexes[a]

Complexes	Solvent	δ_P (ppm)	Ref.[b]
$Pd_2Cl_2(\mu\text{-}PN_1)_2$, **11a**	CD_2Cl_2	4.4	21 & tw
$Pd_2Br_2(\mu\text{-}PN_1)_2$, **12a**	$CDCl_3$	2.92	tw
$Pd_2I_2(\mu\text{-}PN_1)_2$, **13a**	$CDCl_3$	-0.44	tw
$Pd_2Cl_2(\mu\text{-}PN_2)_2$, **11b**	CD_2Cl_2	5.2	tw
$Pd_2Br_2(\mu\text{-}PN_2)_2$, **12b**	CD_2Cl_2	3.28	tw
$Pd_2I_2(\mu\text{-}PN_2)_2$, **13b**	CD_2Cl_2	-0.16	tw
$Pd_2Cl_2(\mu\text{-}PN_3)_2$, **11c**	$CDCl_3$	6.3	tw
$Pd_2Br_2(\mu\text{-}PN_3)_2$, **12c**	$CDCl_3$	4.35	tw
$Pd_2(\mu\text{-}PN_3)_2I_2$, **13c**	$CDCl_3$	0.55	tw

(a) All these chemical shifts are measured at r.t. (b) tw = this work.

A sharp ^{31}P NMR singlet signal is seen for **11a** and **11c**, while a broad singlet is obtained for **11b** where the diastereomeric mixture is present as **11b.1**, **11b.2** and **11b.3**, as depicted below:

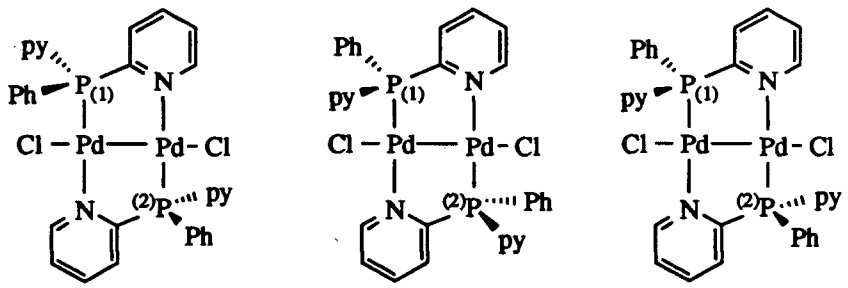

11b.1 **11b.2** **11b.3**

The P nuclei in **11b.1**/**11b.2** are equivalent and should give one singlet. The P atoms in **11b.3**, related by a centre of inversion located in the centre of the Pd-Pd bond, are enantiotopic and should also give rise to a singlet. Therefore, two singlets reflecting the presence of two sets of diastereomers are anticipated. The broad singlet in experimental spectrum in CD_2Cl_2 at room temperature indicates the presence of an exchange process responsible for an

averaging of the two singlets. Two sharp singlets do appear at -20°C and remain unchanged down to -85°C (Fig. 3.17). This broadening phenomenon is not seen in the Pt_2 case (see **7b**, Sect. 3.2.3). It is well-known that Pd systems are substitutionally more labile than Pt systems,[53, 54] therefore, it is not surprising that **11b.1**, **11b.2** and **11b.3** are interconvertible. Direct inversion of the phosphorus centre is not feasible.[55, 56] Dissociation of the pyridyl moiety from the Pd seems to be involved: subsequent rotation of the Pd-P bond would allow for the two pyridyl groups to be indistinguishable in reforming the bridging binuclear compound. The inversion of absolute configuration of the P atom is realized via the dissociation-rotation-recoordination. This cycle is prevented when the sample is subjected to sufficiently low temperature. This mechanism also explains the resolution of the diastereomers at low temperature.

The iodo complex **13b** exhibits much more complex ^{31}P NMR behaviour in a variable temperature experiment (Fig. 3.18). These spectra are reproducible in the temperature range from room temperature down to -85°C, and are unaffected by addition of an acetone solution of sodium iodide. The broad peak seen at room temperature separates into two broad peaks at -20°C; however, further cooling allows the downfield signal to coalesce at -40°C and to reappear at -60°C as a doublets of doublets (or an AB quartet) centred at the original position. The upfield singlet stays at the same position with enhanced intensity. We have no definite explanation at this stage for the observed ^{31}P NMR spectra; perhaps, a non-planar structure (cf. **7b** and **10b.1**) is responsible for the inequivalence of the two phosphorus atoms, especially when the molecular motion is restricted at low temperature.

3.3. Solution equilibrium of the cis-$PtI_2(PN_2)_2$ complex in $CDCl_3$

In previous discussion, the geometry of the $PtX_2(PN_n)_2$ compounds was assumed to be cis, according to the magnitude of their J_{PtP} coupling constants in the ^{31}P NMR spectra (Sect. 3.2.1). No signals of any other species are detected from room temperature down to -70°C from 100 to -200 ppm in CD_2Cl_2 solvent for such species. However, the ^{31}P NMR spectrum of **3b**

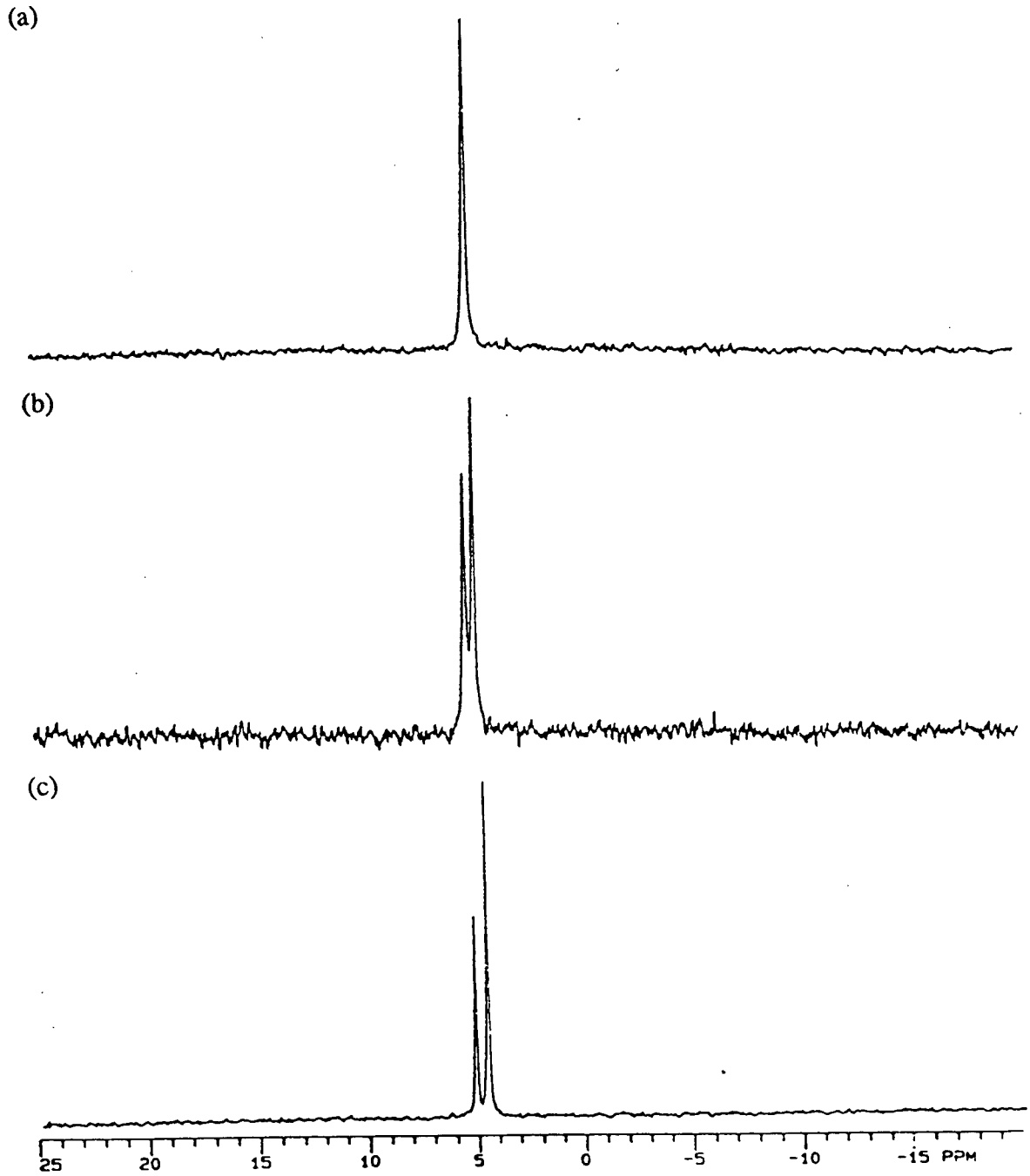

Fig. 3.17. Variable temperature $^{31}P\{^{1}H\}$ NMR spectra (121.4 MHz) of **11b** in CD_2Cl_2: (a) at r.t., (b) at -20° and (c) -85°C. Peaks are not assigned.

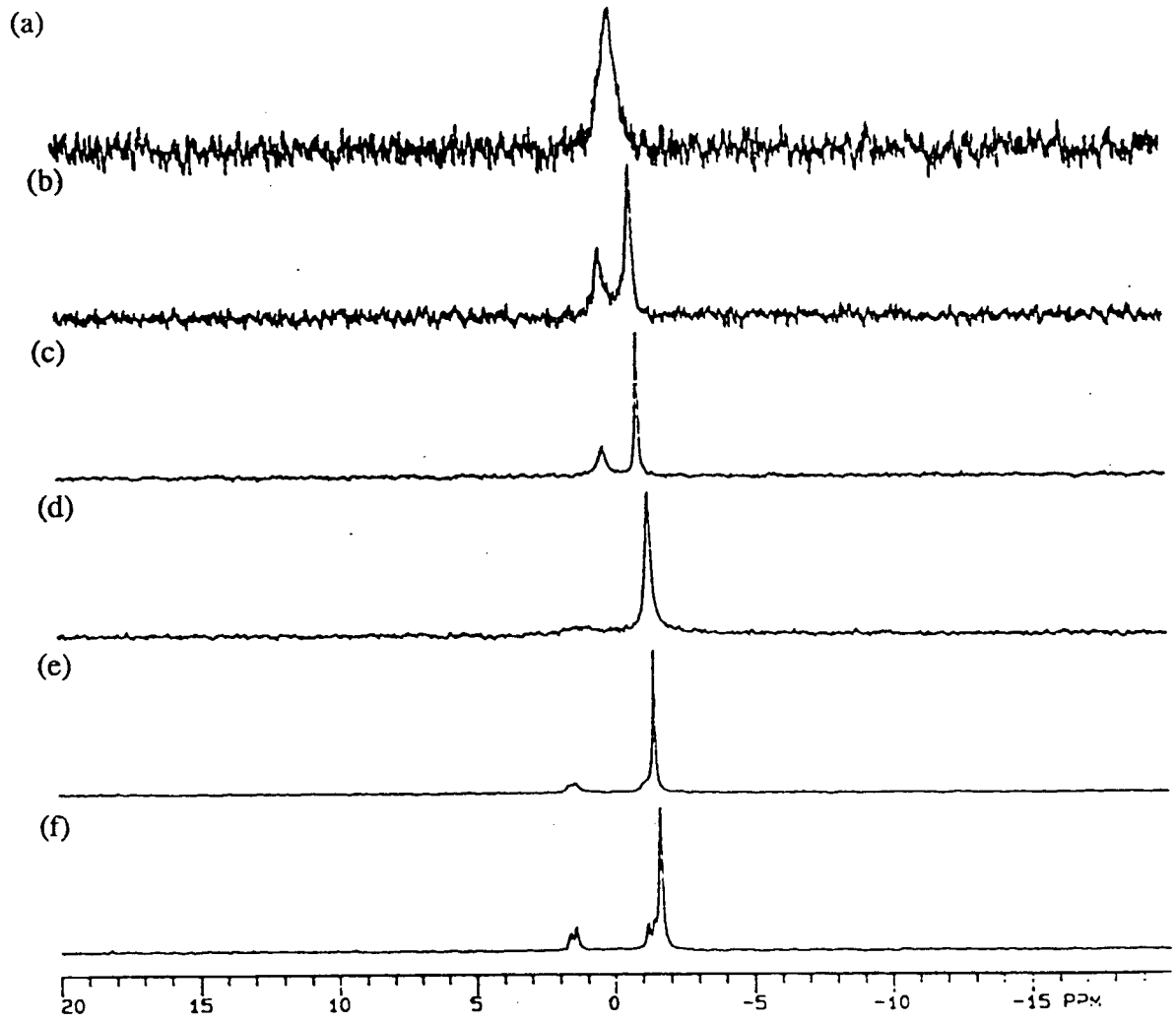

Fig. 3.18. Variable temperature $^{31}P\{^{1}H\}$ NMR spectra (121.4 MHz) of **13b** in CD_2Cl_2: (a) at r.t., (b) 0°, (c) -20°, (d) -45°, (e) -60° and (f) -85°C. Peaks are not assigned.

in $CDCl_3$ at -55°C exhibits a complex pattern (Fig. 3.19); the analysis is based on the presence of three species, cis and trans isomers, and another unknown compound which is believed to be responsible for the broad peaks at 24.0 and -70.3 ppm. The relative intensities of all these signals vary with temperature. As the solution is warmed from -55°C to -30°C, the intensity of the unknown species grows in and the resonance of the cis isomer broadens (δ = 7.4 ppm, based on the data in CD_2Cl_2). This unusual behaviour of cis-$PtI_2(PN_2)_2$ resembles that of the

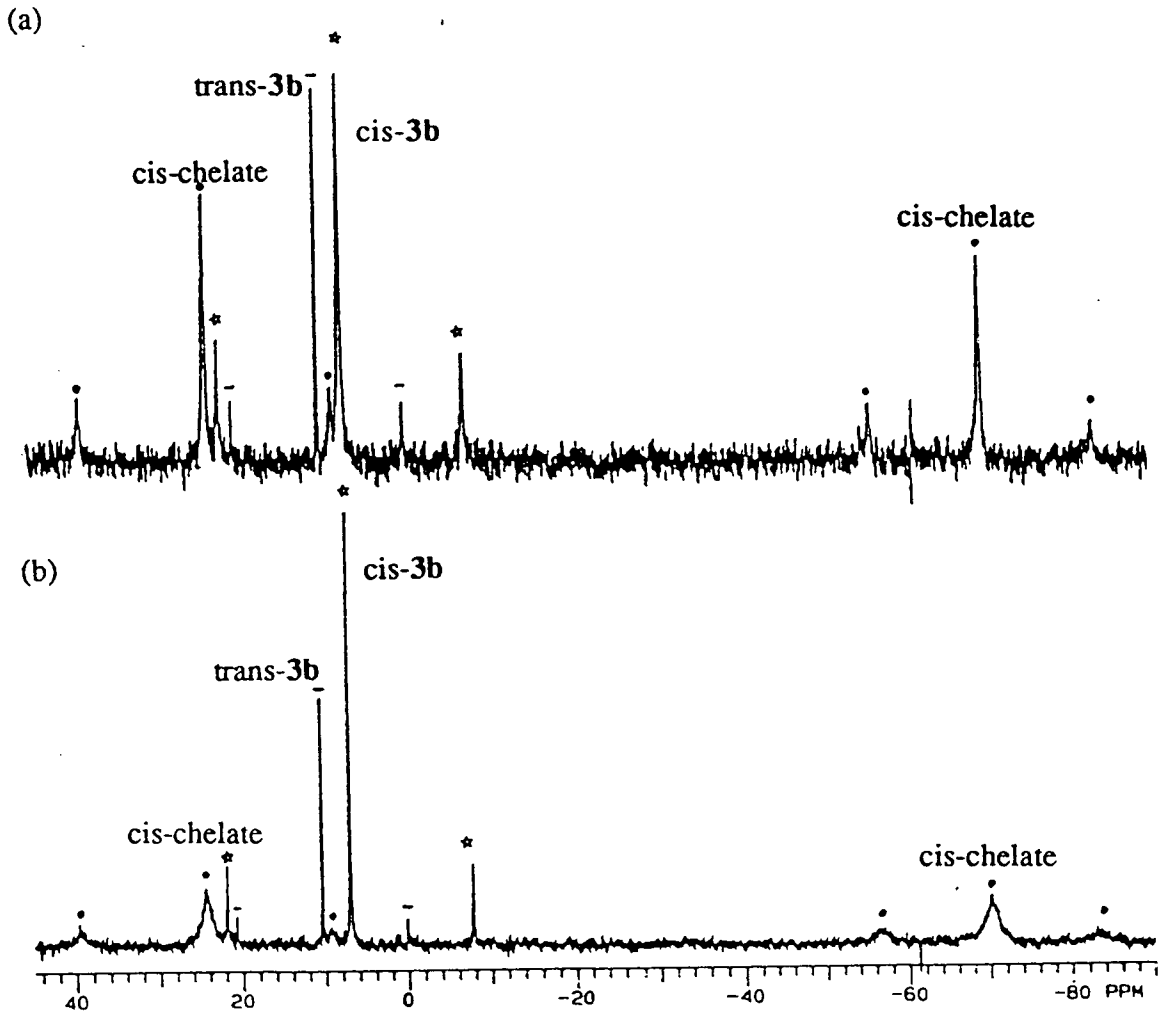

Fig. 3.19. Low temperature $^{31}P\{^{1}H\}$ NMR (121.4 MHz) spectra of cis-$PtI_2(PN_2)_2$, **3b**, in $CDCl_3$; (a) at -30°C and (b) at -55°C. The singlet at 7.4 with Pt-satellites are the signals of cis-**3b**, and the singlet at 10.4 with corresponding satellites are the resonances of trans-isomer of **3b**; the broad singlets at 24.0 and -70.3 with Pt-satellites are assigned to the signals of the cis-chelate.

analogous cis-$PtI_2(PN_1)_2$ system in $CDCl_3$ reported in the literature.[22] The peaks at 24.0 and -70.3 ppm in Fig. 3.19 are assigned to a cis-chelated ionic compound (Scheme 3.1). This assignment is supported by the reported ^{31}P NMR data of the corresponding isolated ionic compound cis-$[PtI(PN_1)_2]PF_6$,[22] and those of cis-$Pt(PN_3)_2(S)^+$ (S= solvent) generated *in situ* in the present work by reacting cis-$Pt(PN_3)_2Cl_2$ with two equivalents of $AgPF_6$ in CH_3CN (Fig. 3.20 and Table 3.9). The colourless solution of cis-$Pt(PN_3)_2(S)^+$ gradually changes on standing to a bright yellow, a colour characteristic of a trans-isomer.[57] The following scheme outlines the solution equilibria, which account for the three species observed; that the trans-chelated ionic species is not seen implies instability of this intermediate with respect to the trans neutral isomer.

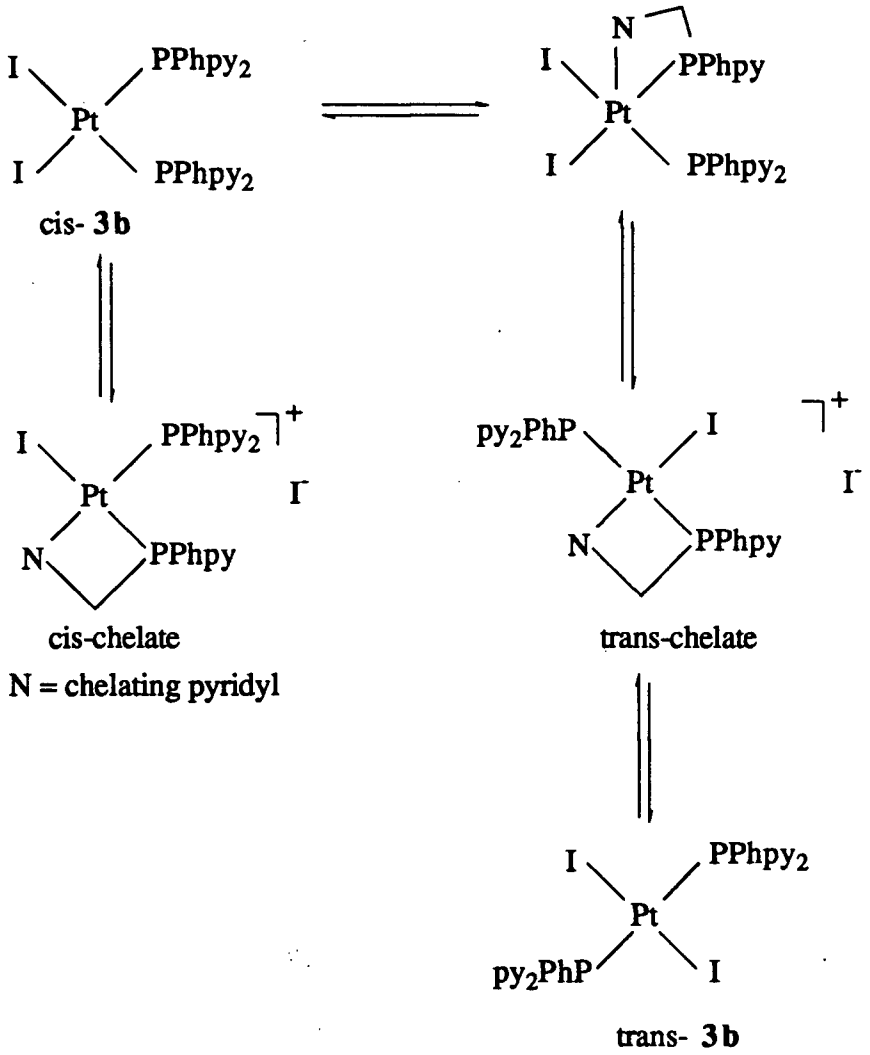

Scheme 3.1. The equilibria between the species possibly present in $CDCl_3$ solvent for cis-$PtI_2(PN_2)_2$, **3b**.

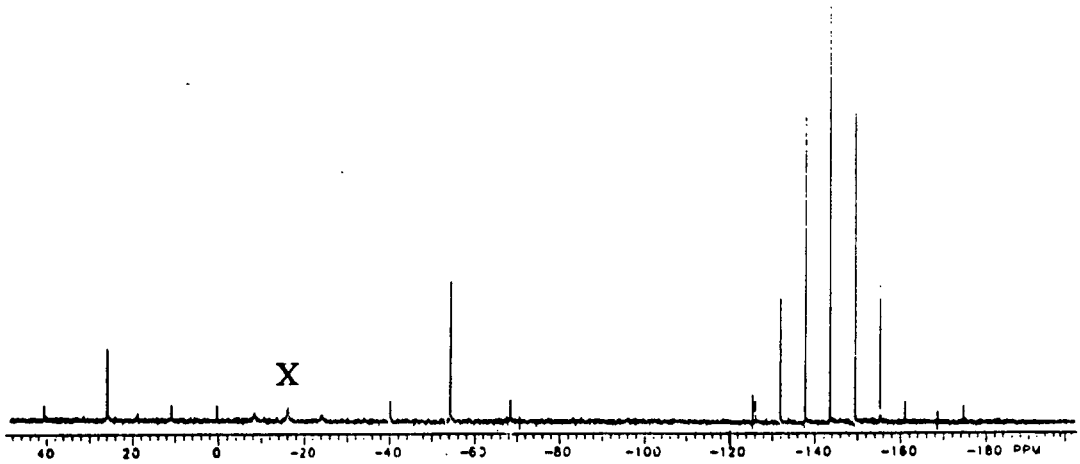

Fig. 3.20. $^{31}P\{^{1}H\}$ NMR spectrum (121.4 MHz) of the reaction product $Pt(PN_3)_2(S)^{2+}$, formed *in situ* from cis-$PtCl_2(PN_3)_2$ and $AgNO_3$ in CH_3CN; the heptet centred at -143.6 is the resonance of PF_6^-; X = $PF_2O_2^-$ impurity from PF_6^- hydrolysis (ref.58).

Despite the solution behaviour observed in $CDCl_3$, only the cis-$PtX_2(PN_n)_2$ species are observed in CD_2Cl_2. The solvent dependent nature of the equilibria cannot be rationalized in terms of solvent polarity as CD_2Cl_2 (dielectric constant $\varepsilon = 9.0$) is more polar than $CDCl_3$ ($\varepsilon = 6.0$). The ionic dissociation was originally thought to be caused by H_2O impurity present in $CDCl_3$; however, this is ruled out by a ^{31}P experiment using **3b** in CD_2Cl_2 with added D_2O — the cis-isomer is still the only one present. This ionic dissociation phenomenon was observed by ^{31}P NMR for several cis-$PtX_2(PN_n)_2$ complexes in $CDCl_3$ (Table 3.9).

3.4. Aqueous solution studies

The water solubility of the neutral $PdX_2(PN_n)_2$ and $Pd_2X_2(\mu\text{-}PN_n)_2$ complexes increases with n (the number of pyridyl groups on phosphorus) and decreases in the order of Cl > Br > I. The cis-$PdCl_2(PN_3)_2$ complex is the most water soluble species, 100 mg in 40 mL at ambient conditions (Conc. = 3.7×10^{-3} M). The chemistry of $Pd_2Cl_2(\mu\text{-}PN_3)_2$ (HT), **11c**, and cis-$PdCl_2(PN_3)_2$, **4c**, in aqueous solution is discussed in the following sections.

Table 3.9. $^{31}P\{^1H\}$ NMR Data for Cis-$PtX_2(PN_n)_2$ Species in $CDCl_3$[a]

Complex	δ_P	δ_{P_c}	$^1J_{PtP}$	$^1J_{PtP_c}$	$^2J_{PP_c}$	Ref.[b]
1a	18.5	-51.5	3695	3443	c	22
3a	19.2	-61.0	3645	3240	c	22
1b	22.4	-60.9	c	c	c	tw
3b	24.0	-70.3	3654	3280	c	tw
3c	24.4	-73.7	3693	3457	16.5	tw
$[PtI(PN_1)_2]PF_6$	19.3	-61.2	3637	3241	c	22
$Pt(PN_3)_2(S)^{2+}$	26.34	-53.74	3642	3478	12.0	tw

(a) Only the data for the cis-chelated species are included in this Table; all the spectra except that of the $Pt(PN_3)_2(S)^{2+}$ done in the present work were taken at -55°C. The chemical shifts are recorded in ppm and the coupling constants are in Hz. P represents the P atom of the non-chelated phosphine and the P_c represents the P atom of the chelated phosphine. (b) tw = this work. (c) The Pt-satellites are buried in the background noise, or the coupling constants are not resolved.

3.4.1. Dichlorobis[tris-(2-pyridyl)phosphine]dipalladium(I) $Pd_2Cl_2(\mu\text{-}PN_3)_2(HT)$, **11c**

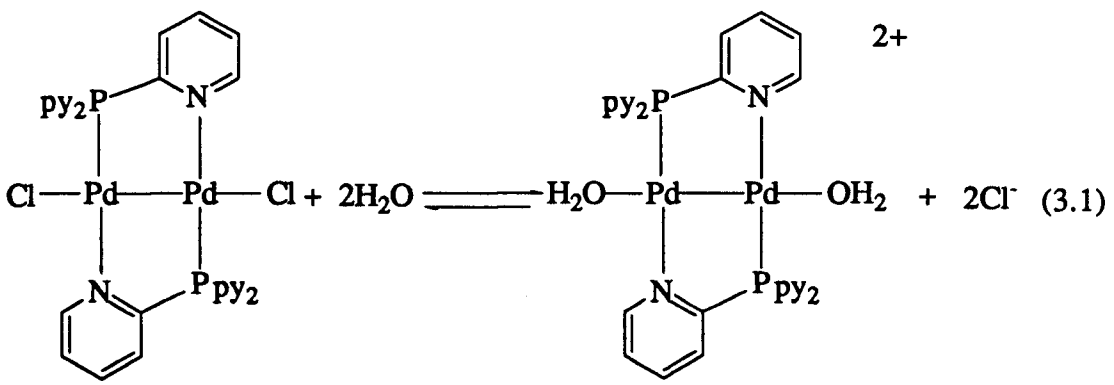

Dissolution of **11c** in water occurs according to equation (3.1); the liberation of chlorides and the formation of bisaquo dipalladium species are demonstrated by the isolation of bisaquo dipalladium salts using $NaBF_4$, KPF_6 and $NaBPh_4$. These green products can be redissolved in

acetone and acetonitrile for further purification by reprecipitation using diethyl ether, and do not dissolve in dichloromethane or chloroform. The elemental chemical analyses for these salts agree well with the proposed formulation $[Pd_2(\mu\text{-}PN_3)_2(OH_2)_2]X_2$ (X = BF_4, PF_6 or BPh_4) (Table 3.10). In addition, the conductivity data listed in Table 3.11 also support that the green products are 1:2 electrolytes (for the ideal 1:2 electrolyte, $\Lambda = 210 - 240\ \Omega^{-1}mol^{-1}cm^2$),[59] although the molar conductivity of $[Pd_2(\mu\text{-}PN_3)_2(OH_2)_2](BPh_4)_2$ is somewhat low. The ^{31}P NMR spectra show a singlet at much higher field than that of the corresponding dichloro complex **11c** ($\Delta\delta \cong 30$ ppm); a blue shift of 460 nm band of **11c** is observed in the visible spectra (Table 3.12). The infrared spectra of the BF_4^- and PF_6^- salts show a band assignable to the coordinated water and reveal no band assignable to a palladium-hydroxide stretch. The IR band of coordinated water in the BPh_4^- salt is obscured by stretching bands of the phenyl groups (Table 3.11). Although the configuration (HT or HH) of the ionic green species is not obvious from the above data, the reversibility of reaction (3.1) implies that the head-to-tail configuration is perhaps preserved: when a 10-fold excess of lithium chloride is introduced into the green aqueous solution, an orange solid, the original dichloro dipalladium complex, is precipitated.

Table 3.10. Chemical Analyses of $[Pd_2(\mu\text{-}PN_3)_2(OH_2)_2]X_2$ Species

X	C		H		N	
	calcd.	found	calcd.	found	calcd.	found
BF_4	37.81	37.37	2.96	2.90	8.82	8.47
PF_6	33.70	33.71	2.64	2.55	7.86	7.72
BPh_4	66.08	66.45	4.83	4.78	5.93	5.92

Table 3.11. IR, $^{31}P\{^1H\}$ NMR and Conductivity Data for Bis(aquo)dipalladium Salts

X	IR [a] $\nu_{H_2O}(cm^{-1})$	$^{31}P\{^1H\}$ δ(ppm)	conductivity[b] $\Lambda(\Omega^{-1}mol^{-1}cm^2)$
BF_4	1627	-21.81(s, CH_3CN)	269
PF_6	1627	-22.19(s, CH_3CN)	256
BPh_4	c	-21.63(s, acetone)	188

(a) In Nujol mull. (b) Solvent = CH_3CN. (c) Obscured by the IR bands of BPh_4^-.

Table 3.12. Visible Spectral Data for $Pd_2Cl_2(\mu\text{-}PN_3)_2$ Complexes in Different Solvents[a]

Complex	Solvent	$\lambda_1(\varepsilon x10^{-3})$	$\lambda_2(\varepsilon x10^{-3})$	$\lambda_3(\varepsilon x10^{-3})$
$Pd_2Cl_2(\mu\text{-}PN_3)_2$, **11c**	CH_2Cl_2	335 (12)	460 (8.4)	—
	H_2O	—	409 (9.3)	600 (1.7)
$[Pd_2(\mu\text{-}PN_3)_2(H_2O)_2](BF_4)_2$	CH_3CN	—	420 (6.1)	610 (0.41)
$[Pd_2(\mu\text{-}PN_3)_2(H_2O)_2](PF_6)_2$	CH_3CN	—	420 (6.1)	610 (0.41)
$[Pd_2(\mu\text{-}PN_3)_2(H_2O)_2](BPh_4)_2$	CH_3CN	—	420 (5.7)	610 (0.41)

(a) λ is a wavelength maximum in nm; ε is the molar absorptivity in $M^{-1}cm^{-1}$.

The other reported cases of a neutral phosphine binuclear bridged complex being soluble in water is the dihalobis(dimethylphosphino)methane bridged dipalladium complex $Pd_2X_2(\mu\text{-dmpm})_2$ (X = Cl and Br), which liberates hydrochloric acid and forms a neutral dihydroxo derivative.[14] However, the coordinated H_2O on the ionic bisaquo PN_3 species is not as acidic. Attempts were made to measure the pK_a value of the coordinated water by standard pH-titration experiments[60] in aqueous solution under vigorous bubbling of N_2. No appreciable amount of proton is titrated up to pH 11.0 (Fig. 3.21), implying that dissociation of proton from coordinated H_2O is negligible. An increase in the initial pH of the solution containing the complex with respect to the initial pH of the dilute acid without complex is attributed to perhaps protonation of nitrogen atoms on the noncoordinated pyridine rings by the added acid at pH < 5.6. The difference between two curves above pH 5.6 is perhaps due to some residual CO_2 in solution.

Unfortunately, neither the ionic compounds in aqueous solution nor the salts in organic solvents (acetone, acetonitrile) react with olefins (acrylonitrile, maleic acid) or acetylenes (DMAD, methylpropiolate) at room temperature.

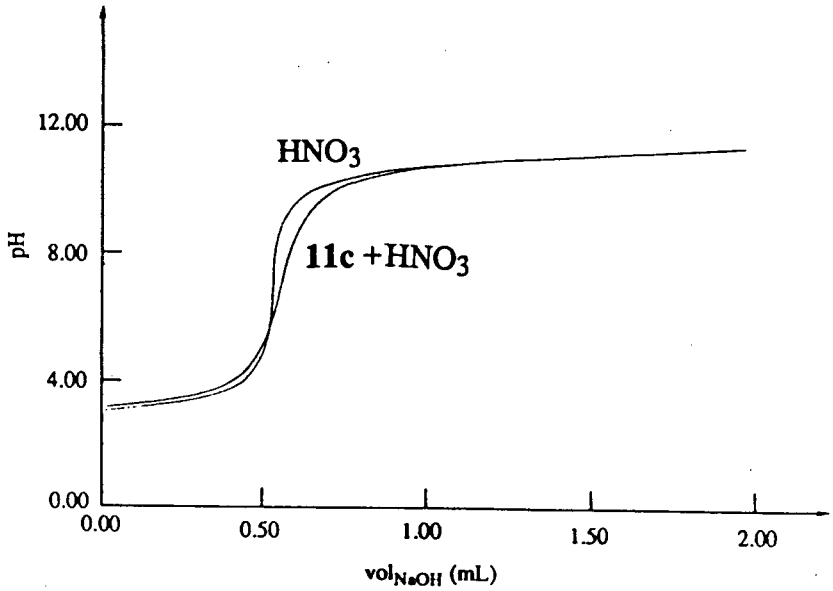

Fig. 3.21. The pH-titration curves of **11c** in 25.0 mL HNO_3 solution. $[HNO_3] = 9.8 \times 10^{-4}$ M, [**11c**] = 4.98×10^{-4} M, [NaOH] = 4.71×10^{-2} M; I = 0.3 M using $NaNO_3$, temp. = 22°C.

3.4.2. Cis-dichlorobis[tris(2-pyridyl)phosphine]palladium(II), cis-$PdCl_2(PN_3)_2$, **4c**

On dissolution in water, **4c** instantly gives a molar conductivity (267 $\Omega^{-1}mol^{-1}cm^2$ at 1.08×10^{-3} M) corresponding to a 1:2 electrolyte which results from loss of two chloride ligands as estimated by $AgNO_3$ titration. The relative high value infers the possible involvement of conduction by proton arising from the dissociation of coordinated water. In fact, one proton is titratable by NaOH (Fig. 3.22). The protonation/deprotonation equilibration between bisaquo and aquohydroxo is fast on the NMR time scale, as a result, only one singlet peak should be observed at the concentration-weighted average chemical shifts of bisaquo and aquohydroxo species.[62, 63] However, the $^{31}P\{^1H\}$ NMR specrum of **4c** in D_2O consists of two distinct singlets at 27.3 and 21.6 ppm with intensity ratio of approximately 2:1 (Fig. 3.23), and these peaks did not vary noticeably when the solution was titrated with NaOH. The observed ^{31}P NMR spectrum can be rationalized, based on a literature report that cis-palladium(II) bisaquo

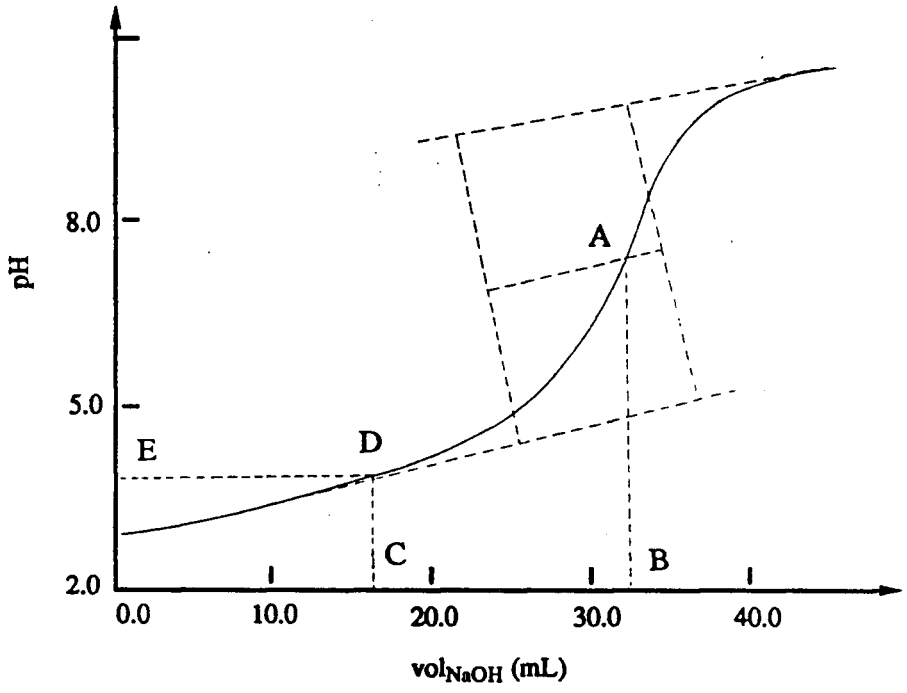

Fig. 3.22. The pH-titration curve of **4c** in 10 mL of H_2O in the absence of HNO_3. [**4c**] = 3.34×10^{-3} M, [NaOH] = 1.0×10^{-3} M; I = 0.3 M using $NaNO_3$, temp. = 25°C, under N_2. The method for graphical determination of pK_a is described in ref. 61. A: equivalence point, B: volume at equivalence point, C: volume at half equivalence point, D: half equivalence point, and E: pH at half equilvalence point.

species dimerize rapidly in aqueous solution, equation (3.2);[63] it is perhaps reasonable to assume that an analogous binuclear phosphine complex of this sort is formed in aqueous solution. Indeed, a purple solid, precipitated at the end of pH titration (pH = 11.0) as a BPh_4^-

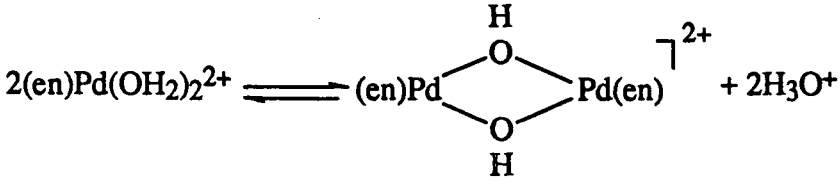

(3.2)

salt and recrystallized from CH_3CN and EtOH at -15°C as dark red crystals, analyzed well for $[Pd(\mu\text{-}OH)(PN_3)CH_3CN]_2(BPh_4)_2$ (calcd.: C 65.77, H 4.85, N 7.48, O 2.14; found: C 65.50, H. 4.64, N 7.34, O 2.24). The $^{31}P\{^1H\}$ NMR spectrum of this product consists of a singlet at 29.1 ppm in CD_3CN, indirectly suggesting that the phosphine is monocoordinated and that CH_3CN must occupy the fourth available coordination site. The presence of CH_3CN in this molecule is confirmed by a ^1H resonance at 2.35 ppm in the NMR spectrum in CD_3CN. The IR stretching band for OH is observed at 3680 cm^{-1} in CH_2Cl_2 after solvent subtraction, but no band is observed assignable to the coordinated CH_3CN.

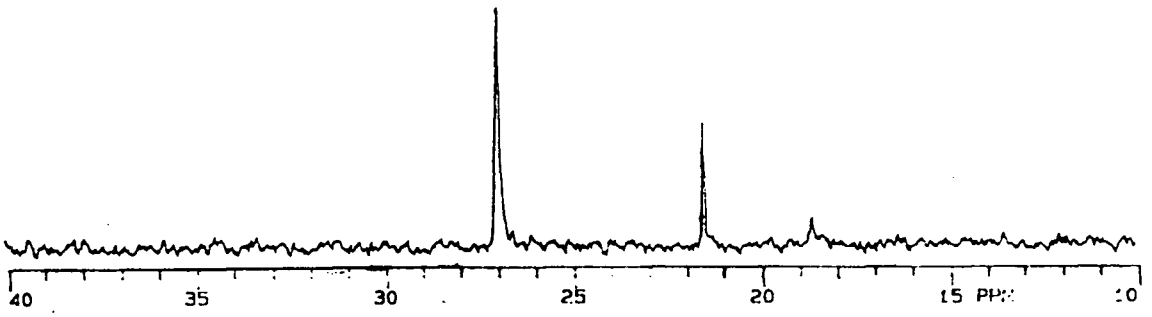

Fig. 3.23. 121.4 MHz $^{31}P\{^1H\}$ NMR spectrum of $PdCl_2(PN_3)_2$, **4c**, in D_2O at r.t.

Efforts were made to isolate the bisaquo species cis-$Pd(PN_3)_2(H_2O)_2^{2+}$ by adding methanol solutions of $NaBF_4$, KPF_6 or $NaBPh_4$ to the aqueous solution of $PdCl_2(PN_3)_2$. Because of the high solubility of the BF_4^- and PF_6^- product salts in water, isolation of these salts was more difficult; even when the solids were sometimes collected by filtration, further purification of the solids by a reprecipitation procedure proved to be difficult because of their poor solubilities in organic solvents (acetone or acetonitrile). Therefore, the attempted characterization is largely based on the BPh_4^- salt. An orange tetraphenylborate salt, obtained by reacting the aqueous solution of cis-$PdCl_2(PN_3)_2$ with a methanol solution of $NaBPh_4$, is readily dissolved in acetone and can be reprecipitated from the acetone solution by the addition of diethyl

ether. This isolated orange solid is believed to be the cis bisaquo exclusively, with a ^{31}P NMR singlet at 33.4 ppm in CD_3CN. Possibly because of the solubility difference between the mononuclear and binuclear species, only the mononuclear species appears to be precipitated. The equilibria are outlined in Scheme 3.2.

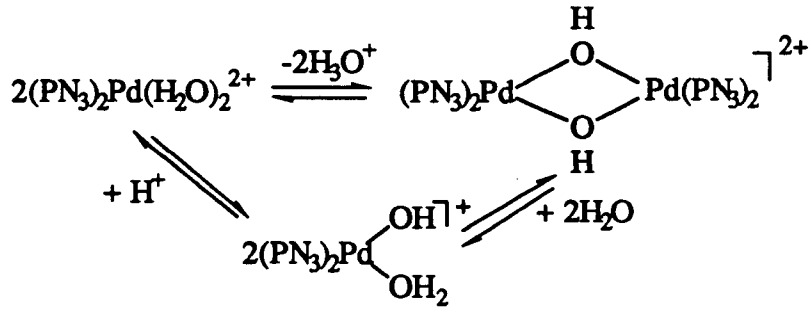

Scheme 3.2. Solution behaviour of the palladium(II) bisaquo species.

Any bisaquo and aquohydroxo species would equilibrate rapidly on the NMR time scale, as mentioned previously, perhaps giving the one singlet at 33.4 ppm in CH_3CN. This singlet may correlate with the 27.3 ppm singlet in D_2O, and thus the downfield singlet in the $^{31}P\{^1H\}$ NMR spectrum in D_2O is assigned to the bisaquo/aquohydroxo species, while the upfield one is assigned to the binuclear hydroxo bridged species. The elemental analysis required for $[Pd(PN_3)_2(H_2O)_2](BPh_4)_2$ (calcd: C 71.43, H 5.23, N 6.41; found: C 69.43, H 4.73, N 6.87), however, was low in carbon and hydrogen contents and somewhat high in nitrogen content. Further reprecipitation procedures gave species with gradually decreasing carbon and increasing nitrogen contents (for example, C 67.08, H 4.85, N 7.18). The molar conductivity of the 'best' salt sample in acetonitrile (Conc. = 8.4×10^{-4} M) was 170 $\Omega^{-1}mol^{-1}cm^2$ which is too high for a 1:1 electrolyte and somewhat low for a 1:2 electrolyte (for 1:1 electrolyte Λ_M = 110 - 120 $\Omega^{-1}mol^{-1}cm^2$, 1 : 2 electrolyte Λ_M = 210 - 240 $\Omega^{-1}mol^{-1}cm^2$).[58] The analytical and conductivity results are more sensible, however, when the above equilibria are taken into consideration (Scheme 3.2). In fact, the pH of an aqueous solution of **4c** at 3.7×10^{-3} M is 2.9, corresponding to 34% proton dissociation. The chemical analysis data, recalculated based on a 34% : 66% mixture of $[Pd(PN_3)_2(H_2O)(OH)](BPh_4)$ and $[Pd(PN_3)_2(H_2O)_2](BPh_4)_2$, assuming that this ratio is unaltered by precipitation (C 69.39, H 5.08, N 7.11), fit much better the experimental

result. This treatment is also applicable for the BF_4^- salt. The isolated solid, assumed to be a mixture of 66% $[Pd(PN_3)_2(H_2O)_2](BF_4)_2$ (calcd: C 42.56, H 3.33, N 9.93) and 34% $[Pd(PN_3)_2(H_2O)(OH)](BF_4)$ (calcd: C 47.48, H 3.59, N 11.08) gives experimentally found values for C, H and N of 43.84, 3.20 and 10.63, respectively, which match well the calculated values, 44.23, 3.42 and 10.32 .

The pK_a value of bisaquo species was estimated to be 3.8 ± 0.2 by a pH-titration shown in Fig. 3.22 and 4.8 ± 0.1 by the previously mentioned standard titration[60] (Fig. 3.24). These pK_a values are not true representations of the acid dissociation constants of a bisaquo species, but are mixed constants of proton dissociation and dimerization (Scheme 3.2). In the absence of acid, the measured constant reflects more of the dimerization; in the presence of acid, dimerization being inhibited, the measured constant reflects more proton dissociation. There are no comparable acid dissociation constant data available in the literature for this type of aquo/phosphine Pd^{2+} species; there are a few for the bisaquo/amino acid Pd^{2+} compounds $Pd(L)(H_2O)_2^{2+}$ (L = methionine, pK_a = 4.96; L = alanine, pK_a = 5.50; L = tyrosine, pK_a =4.77).[64] The reason for this is perhaps attributable to the complexity of reactions taking place in solution, dissociation of proton being usually accompanied by dimerization.[63, 65] The same problem was encountered for $Pd(en)(OH_2)_2^{2+}$, where only the endpoint of a titration, pH 7.5, was reported.[65] In contrast with the rapid dimer formation from $Pd(en)(H_2O)_2^{2+}$ (Eq. 3.2), the formation of the corresponding Pt^{2+} analog is slow with respect to the pK_a determination so that the pK_a's of $Pt(en)(H_2O)_2^{2+}$ were found to be 5.8 and 7.6.[65] This complexity in pK_a determination for bisaquo/phosphine Pd^{2+} species is best shown in the $\bar{n}$ vs pH plot (Fig. 3.24, inset) based on the data from the two titrations. A simple, one proton pH titration should give a smooth S-shaped curve. Despite the uncertainties, the pK_a values measured (3.8 and 4.8) seem to fall into the same range as the data for the bisaquo/amino acid species.

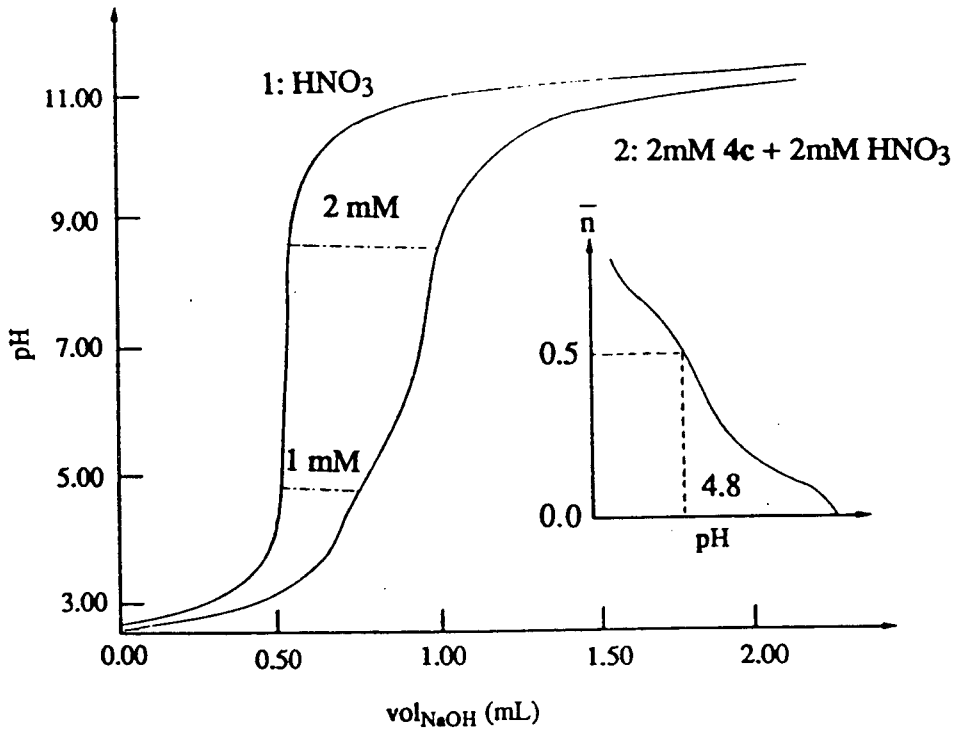

Fig. 3.24. The pH-titration curves of (1) HNO_3 and (2) **4c** in HNO_3. $[HNO_3] = 2.0 \times 10^{-3}$ M, $[\mathbf{4c}] = 2.0 \times 10^{-3}$ M, $[NaOH] = 9.42 \times 10^{-2}$ M; I = 0.3 using $NaNO_3$; temp. = 25.0 ± 0.2°C. Inset: $\bar{n}$ vs. pH plot, yielding $pK_a \approx 4.8$. $\bar{n}$ is defined as the molar fraction of the protonated species present, the value of which can be calculated from the volume difference between curves (2) and (1) divided by the volume used to titrate 2 mM HNO_3.

To avoid formation of a possible bisaquo and aquo-hydroxo mixture, the pH values of two aqueous **4c** solutions were adjusted to 1.5 by adding dilute HNO_3 and to 5.6 by adding solid $NaHCO_3$, respectively. The colour of the former solution (pH = 1.5) is orange-yellow and the latter (pH = 5.6) is brownish orange. A tetraphenylborate salt precipitates out from the acidified solution as a yellow powder with an improved chemical analysis result (found: C 70.12, H 5.10, N 6.60), and a CD_3CN solution of the sample still showed the same ^{31}P NMR shift, 33.4 ppm. The conductivity of this product in acetonitrile solution (Conc. = 7.5×10^{-4} M) is 217.6 $\Omega^{-1}mol^{-1}cm^2$. The orange solid precipitated from the pH 5.6 solution analyzes for $[Pd(PN_3)_2(H_2O)(OH)](BPh_4)$ with relatively satisfactory results except for nitrogen content

which is about 0.8% off (calcd: C 65.42, H 4.78, N 8.48; found: C 65.39, H 4.60, N 7.72); the conductivity is 183.6 $\Omega^{-1}mol^{-1}cm^2$ (Conc. = $6.3x10^{-4}$ M). The ν_{OH} and ν_{H_2O} stretches are detected in a sample assumed to be $[Pd(PN_3)_2(H_2O)(OH)](PF_6)$ (Fig. 3.26) but not in $[Pd(PN_3)_2(H_2O)(OH)](BPh_4)$.

On addition of lithium chloride to the aqueous solution of **4c**, the precursor **4c** complex is not precipitated; instead, an unknown pale yellow, water soluble species, possibly $PdCl_3(PN_3)_2^-$, is formed, giving a $^{31}P\{^1H\}$ resonance at 54.3 ppm in D_2O with no formation of an intermediate species between the assumed anionic species and the cationic species. Even if $PdCl_2(PN_3)_2$ is formed, it is only a transient species. The labile character of the Pd^{2+} centre would promote such product formation.

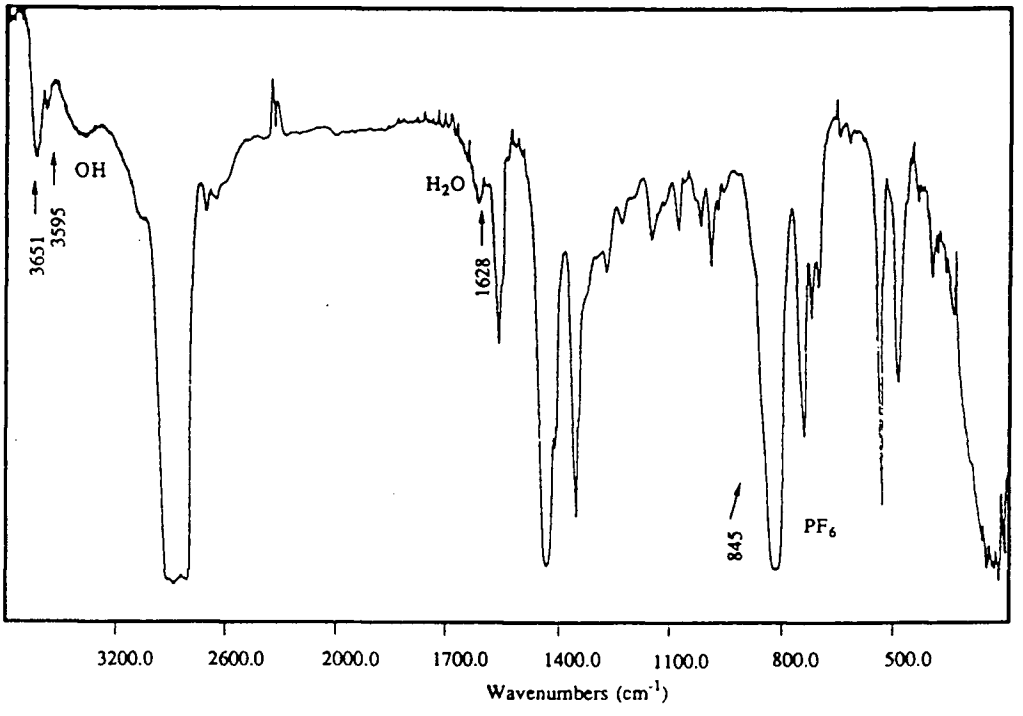

Fig. 3.25. Infrared spectrum of $[Pd(PN_3)_2(H_2O)(OH)](PF_6)$ in Nujol on KBr at r.t.

References

1. Basolo, F.; Pearson, R.G. *Mechanisms of Inorganic Reactions — A Study of Metal Complexes in Solution*, 2nd Ed.; John Wiley & Sons: New York, 1969; p.69.

2. Hartley, F.R. *The Chemistry of Platinum and Palladium;* John Wiley & Sons: New York, 1973; p.19.

3. Ref. 1, pp.423-427.

4. (a) Redfield, D.A.; Nelson, J.H. *Inorg. Chem.*, **1973**, *12*, 15. (b) Redfield, D.A.; Nelson, J.H.; Henry, R.A.; Moore, D.W.; Jonassen, H.B. *J. Am. Chem. Soc.*, **1974**, *96*, 6298. (c) Verstuyft, A.W.; Redfield, D.A.; Cary. L.W.; Nelson, J.H. *Inorg. Chem.*, **1976**, *15*, 1128

5. (a) MacDougall, J.J.; Mathey, F.; Nelson, J.H. *Inorg. Chem.*, **1980**, *19*, 1400 (b) MacDougall, J.J.; Nelson, J.H.; Mathey, F. *Inorg. Chem.*, **1982**, *21*, 2145.

6. (a) Haake, P.; Pfeiffer, R.M. *J. Chem. Soc. D* , **1969**, 1330. (b) Haake, P.; Pfeiffer, R.M. *J. Am. Chem. Soc.*, **1970**, *92*, 5243. (c) Haake, P.; Pfeiffer, R.M. *J. Am. Chem. Soc.*, **1970**, *92*, 4996.

7. (a) Cooper, D.G.; Powell, J. *Can. J. Chem.*, **1973**, *51*, 1634. (b) Cooper, D.G.; Powell, J. *J. Am. Chem. Soc.*, **1973**, *95*, 1102.

8. Romeo, R. *Inorg. Chem.*, **1978**, *17*, 2040 .

9. Favez, R.; Roulet, R.; Pinkerton, A.A.; Schwarzenbach, D. *Inorg. Chem.*, **1980**, *19*, 1356.

10. Brown, M.P.; Fisher, J.R.; Franklin, S.J.; Puddephatt, R.J.; Thomson, M.A. In *Catalytic Aspects of Metal Phosphine Complexes*, ACS Symposium Series 196; Alyea, E.C., Meek, D.W., Eds.; American Chemiccal Society: Washington, DC, 1982; p.231.

11. Collman, J.P.; Hegedus, L.S.; Norton, J.R.; Finke, R.G. *Principles and Applications of Organotransition Metal Chemistry*, 2nd ed.; University Science Books: Mill Valley, CA., 1987; pp.412-416.

12. Panunzi, A.; DeRenzi, A.; Paiaro, G. *J. Am. Chem. Soc.*, **1970**, *92*, 3488.

13. Ref. 2, pp.16-17.

14. (a) Kullberg, M.L.; Kubiak, C.P. *Organometallics*, **1984**, *3*, 632 and references therein. (b) Kullberg, M.L.; Lemke, F.R.; Powell, D.R.; Kubiak, C.P. *Inorg. Chem.*, **1985**, *24*, 3589. (c) Kullberg, M.L.; Kubiak, C.P. *C_1 Mol. Chem.*, **1984**, *1*, 171.

15. Mague, J.T.; Klein, C.L.; Majeste, R.J.; Stevens, E.D. *Organometallics*, **1984**, *3*, 1860.

16. (a) Barnabas, A.F. *M. Sc. thesis*, University of British Columbia, 1989. (b) James, B.R.; Lee, C-L.; Lilga, M.A.; Nelson, D.A. *U.S. Patent* 4,693,875, 1987; *C.A.* **1988**, *107*, 239618x. (c) Barnabas, A.F.; Sallin, D.; James, B.R. *Can. J. Chem.*, **1989**, *67*, 2009.

17. (a) Lee, C-L.; James, B.R.; Nelson, D.A.; Hallen, R.T. *Organometallics*, **1984**, *3*, 1360. (b) Lyke, S.F.; Lilga, M.A.; Nelson, D.A.; James, B.R.; Lee, C-L. *Ind. Eng. Chem. Prod. Res. Dev.*, **1986**, *25*, 517.

18. Balch, A.L.; Benner, L.S.; Olmstead, M.M. *Inorg. Chem.*, **1979**, *18*, 2996.

19. (a) Olmstead, M.M.; Hope, H.; Benner, L.S.; Balch, A.L. *J. Am. Chem. Soc.*, **1977**, *99*, 5502. (b)Holloway, R.G.; Penfold, B.R.; Colton, R.; McCormick, M.M. *J. Chem. Soc. Chem. Comm.*, **1976**, 485.

20. Lee, C-L.; Yang, Y-P.; James, B.R. to be submitted to Organometallics.

21. Maisonnat, A.; Farr, J.P.; Balch, A.L. *Inorg. Chim. Acta* , **1981**, *53*, L217.

22. Farr, J.P.; Wood, F.E.; Balch, A.L. *Inorg. Chem.*, **1983**, *22*, 3387.

23. Pidcock, A.; Richards, R.W.; Venanzi, L.M. *Proc. Chem. Soc.*, **1962**, 184.

24. Grim, S.O.; Keiter, R.L.; McFarlane, W. *Inorg. Chem.*, **1967**, *6*, 1133.

25. *Phosphorus-31 NMR Spectroscopy in Stereochemical Analysis;* Verkade, J. G., Quin, L. D., Eds.;VCH: Deerfield Beach, FL, 1987.

26. Verkade, J.G. *Coord. Chem. Rev.*, **1973**, *9*, 1.

27. (a) Goodfellow, R.J. *J. Chem. Soc. D*, **1968**, 114. (b) Goodfellow, R.J. *J. Chem. Soc. A*, **1967**, 1579.

28. Pregosin, P.S.; Kunz, R.W. *^{31}P and ^{13}C NMR of Transition Metal Phosphine Complexes;* Springer-Verlag: Berlin, 1979.

29. (a) Nixon, J.F.; Pidcock, A. *Ann. Rev. NMR Spectr.*, **1969**, *2*, 346. (b) Mather, G.G.; Rapsey, G.J.N.; Pidcock, A. *Inorg. Nucl. Chem. Letters*, **1973**, *9*, 567. (c) Sullen, F.H.; Pidcock, A.; Waterhouse, C.R. *J. Chem. Soc. A*, **1970**, 2087. (d) Allen, F.H.; Pidcock, A. *J. Chem. Soc. A*, **1968**, 2700.

30. Newkome, G.R.; Evans, D.W.; Fronczek, F.R. *Inorg. Chem.*, **1987**, *26*, 3500.

31. Jensen, K.A. *Z. Anorg. Chem.*, **1936**, *229*, 225.

32. (a) Chatt, J.; Wilkins, R.G. *J. Chem. Soc.,* **1952**, 273. (b) Chatt, J.; Wilkins, R.G. *Ibid.,* **1952**, 4300. (c) Chatt, J.; Wilkins, R.G. *Ibid.,* **1953**, 70. (d) Chatt, J.; Wilkins, R.G. *Ibid.,* **1956**, 525.

33. Nakamoto, K. *Infrared and Raman Spectra of Inorganic and Coordination Compounds,* 4th ed.; Wiley: New York, 1986; p.324, 339.

34. Coates, G.E.; Parkin, C. *J. Chem. Soc.,* **1963**, 421.

35. Park, P.J.D.; Hendra, P.J. *Spectrochimica Acta A,* **1969**, *25,* 227.

36. Rosevear, D.T.; Stone, F.G.A. *J. Chem. Soc.,* **1965**, 5275.

37. (a)Adams, D.M.; Chandler, P.J. *J. Chem. Soc. Chem. Commun.,* **1966**, 69. (b)Adams, D.M.; Chatt, J.; Gerratt, J.; Westland, A.D. *J. Chem. Soc.,* **1964**, 734.

38. Goggin, P.L.; Goodfellow, R.J. *J. Chem. Soc. A,* **1966**, 1402.

39. (a)Cheney, A.J.; Mann, B.E.; Shaw, B.L.; Slade, R.M. *J. Chem. Soc. A,* **1971**, 3833. (b)Cheney, A.L.; Shaw, B.L. *J. Chem. Soc. Dalton Trans.,* **1972**, 860.

40. Grim, S.O.; Keiter, R.L. *Inorg. Chim. Acta* , **1970**, *4,* 56.

41. Cheney, A.L.; Shaw, B.L. *J. Chem. Soc. Dalton Trans.,* **1972**, 754.

42. Goodfellow, R.J.; Taylor, B.F. *J. Chem. Soc. Dalton Trans.,* **1974**, 1676.

43. Jenkins, J.M.; Shaw, B.L. *J. Chem. Soc. A* , **1966**, 770.

44. Mann, B.E.; Shaw, B.L.; Stainbank, R.E. *J. Chem. Soc. Chem. Comm.,* **1972**, 151.

45. (a)Verstuyft, A.W.; Nelson, J.H.; Cary, L.W. *Inorg. Chem.,* **1976**, *15,* 732. (b) Redfield, D.A.; Cary, L.W.; Nelson, J.H. *Inorg. Chem.,* **1975**, *14,* 50.

46. Goggin, D.L.; Goodfellow, R.J.; Haddock, S.R.; Knight, J.R.; Reed, F.J.S.; Taylor, B.F. *J. Chem. Soc. Dalton Trans.,* **1974**, 523.

47. Fyfe, C.A. *Solid State NMR for Chemists;* C.F.C.Press: Guelph, Ontario, 1983; pp.363-365, 375-377.

48. Bermi, L.; Clark, H.C.; Davies, J.A.; Fyfe, C.A.; Wasylishen, R.E. *J. Am. Chem. Soc.,* **1982**, *104,* 438.

49. Mislow, K.; Raban, M. *Topics. Stereochem.,* **1974**, *1,* 1.

50. Mislow, K.; Bickart, P. *Isr. J. Chem.,* **1976/1977**, *15,* 1.

51. Maisonnat, A.; Farr, J.P.; Olmstead, M.M.; Hunt, C.T.; Balch, A.L. *Inorg. Chem.*, **1982**, *21*, 3961.

52. Farr, J.P.; Olmstead, M.M.; Balch, A.L. *Inorg. Chem.*, **1983**, *22*, 1229.

53. Ref. 11, p.214.

54. Ref. 1, pp. 414-417.

55. McEwen, W.E. In *Topics in Phosphorus Chemistry*, Vol. 2; Grayson, M., Griffith, E.L., Eds.; Interscience: New York, 1965; pp.17-19.

56. Gallagher, M.L.; Jenkins, I.D. In *Topics in Stereochemistry*, Vol. 3; Eliel, E.L., Alliger, N.L., Eds.; Interscience: New York, 1968; p.11.

57. Hartley, F.R. *Organomet. Chem. Rev. A* , **1970**, *6*, 119.

58. Sue, C-Y. *Ph.D. dissertation* , University of British Columbia, 1989; p.189.

59. (a) Dodd, R.E.; Robinson, P.L. *Experimental Inorganic Chemistry — A Guide to Laboratory Practice*, Elsevier: Amsterdam, 1954; p.378. (b) Geary, W.J. *Coord. Chem. Rev.*, **1971**, *7*, 81.

60. James, B.R. *D. Phil. dissertation* , Oxford, 1960.

61. Reynolds, C.A. *Principles of Analytical Chemistry*, Allyn & Bacon: Boston, 1966; p.79.

62. Appleton, T.G.; Hall, J.R.; Ralph, S.F.; Thompson, C.S.M. *Inorg. Chem.*, **1989**, *28*, 1989.

63. Lippard, S.J. *Science*, (Washington, D.C.) **1982**, *218*, 1075.

64. Chernova, N.N.; Kurskii, I.G. *Zh. Neorg. Khim.*, **1978**, *23*, 1014 through *C.A.*, **1978**, *89*, 31695x.

65. Lim, M.C.; Martin, R.B. *J. Inorg. Nucl. Chem.*, **1976**, *38*, 1911.

Chapter 4

Reactivities of the Head-to-Head Isomers of $Pt_2I_2(\mu\text{-}PN_n)_2$ Complexes (n = 1, 2 or 3) toward Dimethylacetylenedicarboxylate and toward Phosphine

4.1. Introduction

Many metal acetylene complexes have been characterized since the mid 1970s in a search for hydrogenation and cyclotrimerization catalysts for acetylenes. There is no ambiguity in the bonding mode of mononuclear metal acetylene complexes in which the acetylene molecule acts as a σ donor and π acceptor. In binuclear complexes, two acetylene bonding modes are most commonly observed: the tetrahedral $\mu_2\text{-}\eta^2$ geometry (A) in which the acetylene sits perpendicular to the metal-metal axis,[1-9] and the cis-bimetallated olefinic geometry (B) in which the acetylene lies parallel to the metal-metal axis.[10-16] Most of type A complexes are carbonyl complexes of the first row transition metals, whereas the B type complexes usually involve the phosphine complexes of the second or third row transition metals.

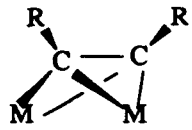

A

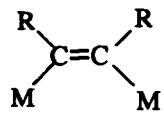

B

It is anticipated[13] that the binuclear acetylene complexes will show significantly enhanced activity over that of free acetylene because the 'coordinated' acetylenic bond is significantly lengthened with respect to that in free acetylene,[17] or even with respect to acetylene bound to one single metal.[18] One aspect of the present study was originally aimed at activation toward hydration of olefins and acetylenes via coordination to the previously described pyridylphosphine binuclear metal complexes.

As previously discussed, binuclear complexes containing the bridging PN_n ligands do not form A-frame insertion adducts with CO.[19] However, the dimethylacetylenedicarboxylate, DMAD, insertion complex with $Pd_2Cl_2(\mu\text{-}PN_3)_2$, **11c**, was prepared and crystallographically characterized by our group to have the cis-bimetallated olefinic structure (type B) (Fig. 4.1).[20] The reactivity seen in a chelating diphosphine to accommodate DMAD[13] is also observed in pyridylphosphine complexes, and the noted absence of a Pd-Pd bond is seen also in the similar insertion product $Pd_2Cl_2(\mu\text{-}CF_3C{\equiv}CCF_3)(dppm)_2$.[12] The head-to-tail, HT, configuration of the product allows us to suggest tentatively the HT configuration for the precursor **11c**, assuming no isomerization during the insertion reaction; the HT geometry is not demonstrated from other physical characterization data (Sect. 3.2.4). This study was extended in the present work to platinum complexes, and the insertion reaction seems to be a quite general one (Sect. 2.7).

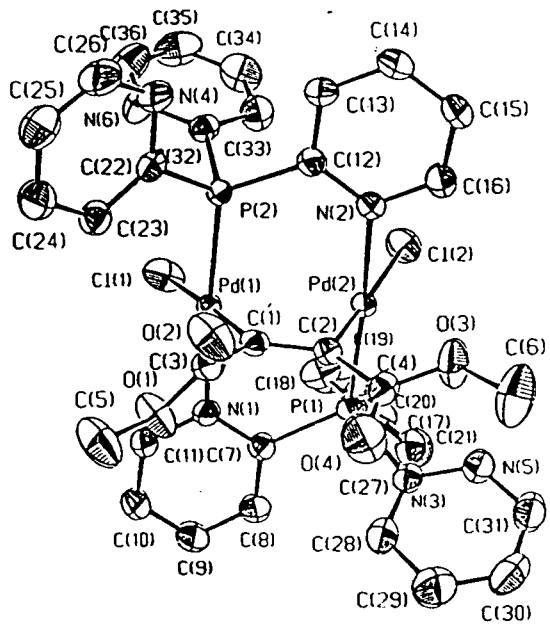

Fig. 4.1. ORTEP drawing of $Pd_2Cl_2(\mu\text{-}DMAD)(\mu\text{-}PN_3)_2$ and the atom numbering scheme.[20]

Some representative bond lengths (Å) and bond angles (°).

Pd(1)-C(1) = 2.010 (3)	Pd(1)-P(2) = 2.2434 (9)	Pd(1)-N(1) = 2.128 (3)
Pd(1)-Cl(1) = 2.3929(10)	Pd(2)-C(2) = 2.003 (3)	Pd(2)-P(1) = 2.2260 (9)
Pd(2)-N(2) = 2.127 (4)	Pd(2)-Cl(2) = 2.3841 (10)	C(1)-C(2) = 1.330 (5)
Pd(1)-C(1)-C(2) = 112.1 (3)	Pd(1)-C(1)-C(3) = 121.0 (2)	P(2)-Pd(1)-N(1) = 174.8 (8)
Cl(1)-Pd(1)-C(1) = 175.0 (1)	Cl(1)-Pd(1)-N(1) = 89.04 (8)	Cl(1)-Pd(1)-P(2) = 95.71 (4)

In this Chapter, general reactivities of the $Pt_2I_2(\mu\text{-}PN_n)_2$ head-to-tail (HT) and head-to-head (HH) species, **9** and **10**, toward DMAD will be described. The kinetic and spectroscopic studies are focused on the simple oxidative addition of DMAD to the HT isomer, and the same oxidative addition to the HH isomer followed by isomerization to the HT form (see below). To our knowledge, there has been no similar study reported in the literature on such isomerizations involving a binuclear metal framework. It was considered to be of interest from an organometallic chemistry point of view to investigate the detailed mechanism and the origin of such isomerization.

Also in this Chapter, a related isomerization reaction of $Pt_2I_2(\mu\text{-}PN_3)_2$ (HH), **10c**, in the presence of PN_3 to give $Pt_2I_2(\mu\text{-}PN_3)_2$ (HT), **9c**, will be discussed.

4.2. Experimental

Syntheses of the HH isomers of $Pt_2I_2(\mu\text{-}PN_n)_2$ (n = 1 - 3), **10a** - **10c**, and separation of the HH from the HT isomers have been described in Chapter 2, Sect. 2.6.1 - 2.6.2, and the structures of complexes $Pt_2I_2(\mu\text{-}PN_2)_2$, **10b**, were discussed in detail in Sect. 3.2.3. Reactions of **10a** - **10c** with DMAD have also been described in Chapter 2, Sect. 2.7. The isolated reaction products were characterized as 1:1 insertion complexes, and the configuration of adducts were determined unambiguously using ^{31}P and ^{195}Pt NMR spectroscopies. Table 4.1 lists the $^{31}P\{^1H\}$ parameters of the DMAD adducts made.

Kinetic experiments for reactions of the binuclear platinum complexes with DMAD were carried out using a thermostated (± 0.1°C) Perkin-Elmer 502 A UV/vis spectrophotometer. Pure DMAD liquid was added by a microsyringe so that the concentration of DMAD could be calculated from the known volume and density data, and was placed in the side-flask of the anaerobic optical cell (Fig. 2.1); a solution of the Pt complex of known concentration was transferred from a volumetric flask and placed in the cell (3 mL solution for 10 mm path length

Table 4.1. ^{31}P NMR Parameters of DMAD Insertion Adducts[a]

Compound	δ (ppm)	$^1J_{PtP}$	$^3J_{PtP}$
$Pt_2I_2(\mu\text{-DMAD})(\mu\text{-PN}_1)_2$ (HH), **17**	21.5 (s)	3496	242
$Pt_2I_2(\mu\text{-DMAD})(\mu\text{-PN}_2)_2$ (HT), **18**[b]	6.85 (s) (32%)	4480	268
	7.35 (s) & 8.47 (s)[c] (59%)	4517	257
	9.32 (s) (9%)	4540	272
$Pt_2I_2(\mu\text{-DMAD})(\mu\text{-PN}_3)_2$ (HT), **19**	8.37 (s)	4455	272
$Pt_2Cl_2(\mu\text{-DMAD})(\mu\text{-PN}_3)_2$ (HT), **20**	9.88 (s)	4605	272
$PtPdCl_2(\mu\text{-DMAD})(\mu\text{-PN}_3)_2$ (HT), **21**[d]	12.84 (d)	4486	478
	29.58 (d)		
$Pt_2I_2(\mu\text{-MPP})(\mu\text{-PN}_3)_2$ (HT), **22**[e]	12.24 (s)	4620	279
	10.12 (s)	4584	242
$Pd_2Cl_2(\mu\text{-DMAD})(\mu\text{-PN}_1)_2$ (HT), **23**	35.77 (s)		
$Pd_2Cl_2(\mu\text{-DMAD})(\mu\text{-PN}_2)_2$ (HT), **24**[b]	35.46 (s) (44%)		
	35.25 (s) & 33.83 (s)[c] (44%)		
	33.33 (s) (12%)		
$Pd_2I_2(\mu\text{-DMAD})(\mu\text{-PN}_2)_2$ (HT), **25**[b]	35.02 (s) (34%)		
	34.61 (s) & 33.46 (s)[c] (48%)		
	32.98 (s) (18%)		

(a) The spectra were recorded in $CDCl_3$ solvent at r.t. (b) Diastereomers of the DMAD adducts were detected, the relative intensities of the individual peaks being given as percentages in the brackets. (c) Diastereotopic P atoms give rise to two singlets with equal intensities. (d) $^4J_{PP}$ was resolved as 5.0 Hz. (e) This adduct was not isolated (Sect. 2.7).

quartz cell) shown in Fig. 2.1. No degassing procedure was required. Reaction times were recorded, following mixing of the reactants, on a Chron-Lab 1400 timer for faster reactions (10 - 20 seconds between readings), or recorded with the repetitive scanning spectra for the slower reactions (3 - 90 minutes between readings) by a built-in timer. For the binding of DMAD, a decrease of absorbance was monitored at one specific wavelength (e.g. 500 nm for **10c**, and 520 nm for **9c**, see Sect. 4.3.2) for most reactions, except for the reaction of **10a** and **10b** with DMAD in which the spectra from 400 to 600 nm were recorded (see Sect. 4.3.3); for the isomerization step (from **28.2** to **19**), a subsequent increase of absorbance was monitored from

450 to 600 nm (see below). The reactions were run under pseudo-first order conditions by using a 10 to 100-fold excess of DMAD. The concentrations of platinum complexes were usually in the range of 0.20 - 1.30×10^{-4} M. The absorbance data versus time, and the corresponding $-\ln(A_t-A_\infty)$ or $-\ln(A_\infty-A_t)$ vs. time data, are listed Tables AIII-AVIII in the Appendix.

The observed first-order rate constants were obtained from the slopes of the plots of $\ln(A_t-A_\infty)$ vs. t by a least-square analysis; the plots were generally linear with correlation coefficients higher than 0.996 (A_t is the absorbance at time t, and A_∞ normally is the absorbance at completion of the reaction for a one-step process). For consecutive DMAD binding and isomerization reactions, the lowest absorbances (see Fig. 4.5) were taken as A_∞ for the binding step. This method is justified by application of the Kezdy-Swinbourne treatment.[21, 22] The estimated A_∞ values from a K-S plots were usually very close (within two percent or less) to those obtained directly from the spectra. The Guggenheim treatment[23] was applied to confirm the accuracy of the rate constants in some cases. Detailed descriptions are given in Sect. 4.3.2. The activation enthalpies and entropies were obtained from Eyring plots of ln k/T vs. 1/T.

4.3. Results and discussion

4.3.1. Reactions of $Pt_2I_2(\mu\text{-}PN_3)_2$ (HT), **9c**, with acetylenes

Reaction of **9c** with DMAD yielded the A-frame product shown as **19** in Fig. 4.2, the expected analogue of the $Pd_2Cl_2(\mu\text{-DMAD})(\mu\text{-}PN_3)_2$ (HT) complex (Fig. 4.1). Initially surprising, however, was the $^{31}P\{^1H\}$ NMR spectrum (Fig. 4.2), which showed no splitting of the Pt satellites. The ^{31}P spectrum was expected to be similar to that of **9c** (Fig. 3.9) because of magnetic inequivalence of the P atoms in the ^{195}Pt spin labelled isotopomer. The apparent anomaly was clarified when **9c** was treated *in situ* in an NMR tube with methylpropiolate (MPP), and the ^{31}P NMR spectrum of the product $Pt_2I_2(\mu\text{-MPP})(\mu\text{-}PN_3)_2$ (HT), **22**, was measured (Fig. 4.3); the now chemically inequivalent P atoms are seen as two singlet (with Pt satellites) peaks, and there is no PP coupling (i.e. $J_{PP} \approx 0$ Hz or is unresolvable). Thus in **19**, the magnetic inequivalence of the two P atoms is not detected. The HT geometry is also supported by the

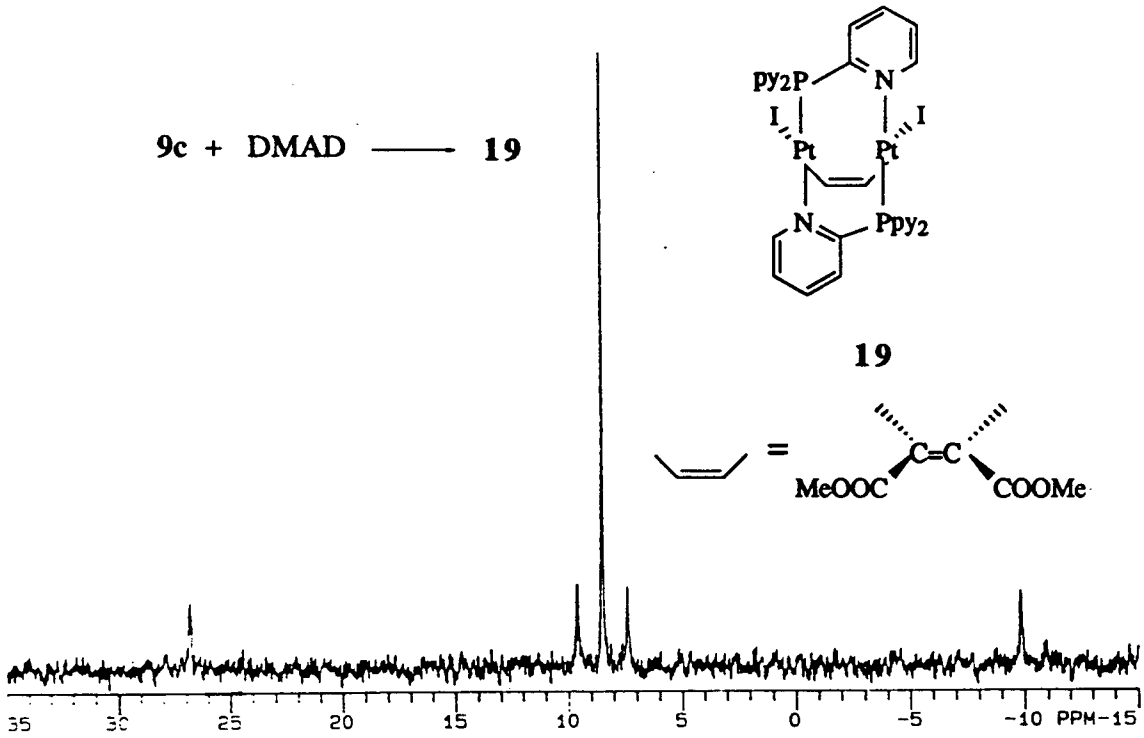

Fig. 4.2. $^{31}P\{^1H\}$ NMR spectrum (121.4 MHz) of **19** in $CDCl_3$ at r.t.: $\delta = 8.37$; $^1J_{PtP} = 4455$ Hz, $^3J_{PtP} = 272$ Hz.

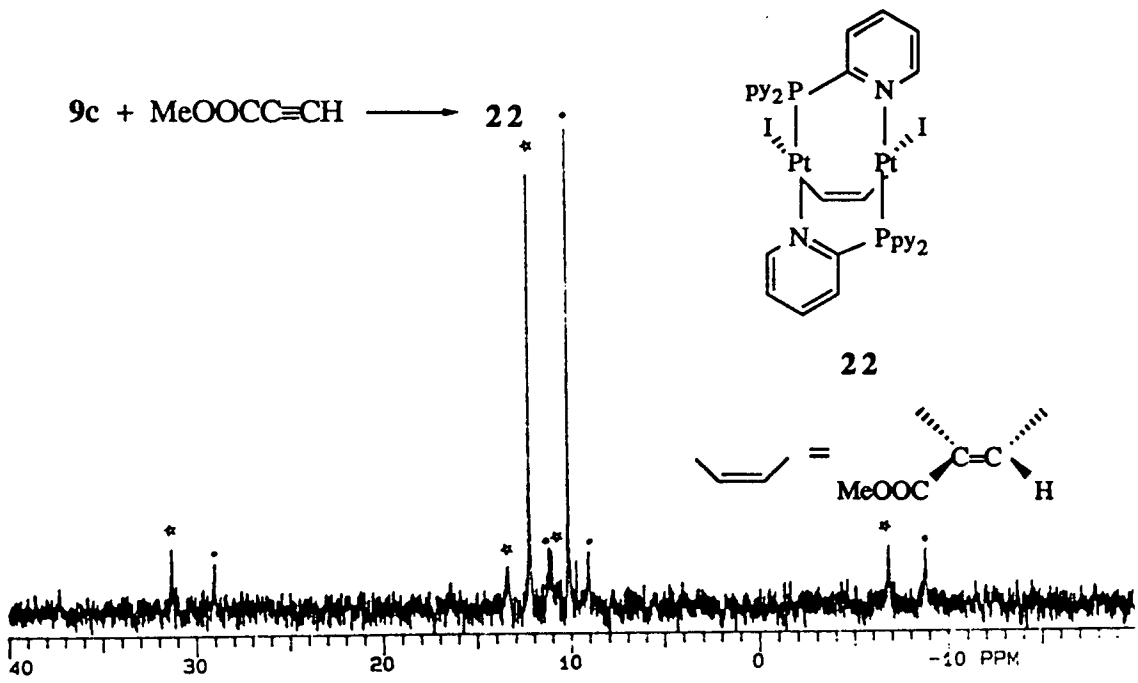

Fig. 4.3. $^{31}P\{^1H\}$ NMR spectrum (121.4 MHz) of **22** in $CDCl_3$ at r.t.: $\delta = 12.24$ (s), 10.12 (s); $^1J_{PtP} = 4620$, 4584 Hz; $^3J_{PtP} = 279$, 242 Hz, respectively. Peaks are not assigned to individual P atoms.

^{195}Pt NMR spectrum of **19** (δ = 293.2 (d), $^{1}J_{PtP}$ = 4453 Hz; in $CDCl_3$, r.t) which is similar to the pattern observed for **9c** in Fig. 3.9b and apparently dissimilar to that of **10c** in Fig. 3.13b.

4.3.2. Reaction of $Pt_2I_2(\mu\text{-}PN_3)_2$ (HH), **10c**, with DMAD

Extension of the concept of the acetylene reaction to reaction of **10c** with DMAD would lead to the expectation of a product with structure **28.1**. The ^{31}P NMR spectrum of **28.1** would basically look similar to that of **10c** (Fig. 3.13). However, the reaction of **10c** with DMAD finally yielded an orange compound which was clearly identical with **19**.

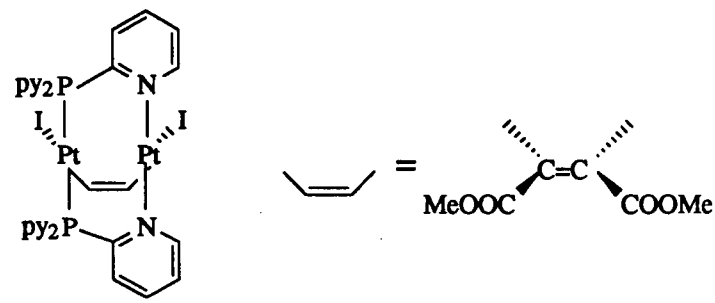

28.1

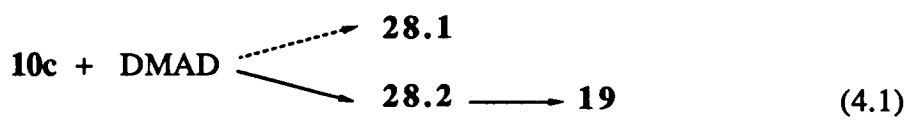

(4.1)

The difference in **28.1** and **19** lies only in the relative P-N orientation, one is being HH, and the other is HT. Obviously, an isomerization has taken place during the reaction. This reaction was monitored *in situ* by ^{31}P NMR spectroscopy and the results are shown in Fig. 4.4. In Fig. 4.4(a), the immediately formed species, **28.2**, has in fact a ^{31}P spectrum very different from either that of **19** (Fig. 4.2) or the expected pattern for **28.1** (cf. **10c** in Fig. 3.13a and **17** in Fig. 4.14). As indicated by the doublet of doublets, two phosphorus atoms in **28.2** are chemically inequivalent. The value of J_{PP}, 13 Hz, is typical of either a cis phosphorus, or diagonally oriented-HT, phosphorus coupling. The $^{195}Pt\{^{1}H\}$ NMR spectrum of intermediate **28.2**, shown in Fig. 4.4(b), consists of a pseudo-triplet which is in fact a doublet of doublets, ruling out the possibility of an HT configuration because of the apparent dissimilarity between (b)

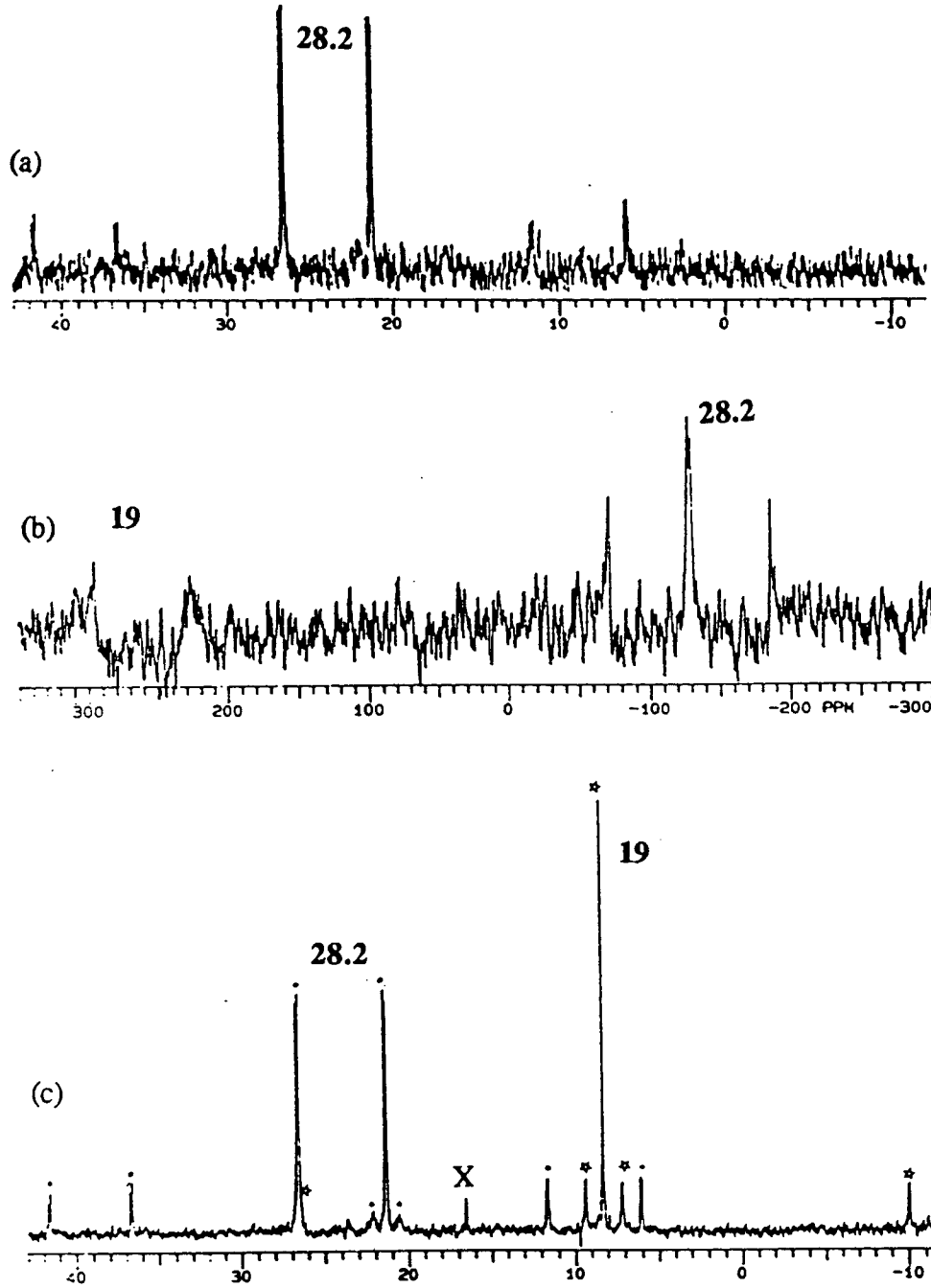

Fig. 4.4. (a) $^{31}P\{^1H\}$ NMR spectrum (121.4 MHz) of **28.2** the initially formed DMAD adduct of **10c**, in CD_2Cl_2 at r.t.: δ_{P_1} = 21.2 (d), δ_{P_2} = 26.5 (d); $^1J_{PtP_1}$ = 3719, $^1J_{PtP_2}$ = 3625 Hz; $^2J_{PP}$ = 13.5 Hz, respectively. (b) $^{195}Pt\{^1H\}$ NMR spectrum (64.2 MHz) of **28.2** obtained at -20°C in CD_2Cl_2: δ = -128.1(dd); $^1J_{PtP}$ = 3712, 3613 Hz. The broad peaks at 230.0 and 300.0 are assignable to the HT DMAD adduct, **19**. (c) $^{31}P\{^1H\}$ NMR spectrum (121.4 MHz) of the same sample taken 20 h after spectrum (b) was taken (sample was stored at -20°C); $^3J_{PtP_1}$ of **28.2** was resolved here as 190 Hz. X = impurity.

and the ^{195}Pt spectrum of **9c**, $Pt_2I_2(\mu\text{-}PN_3)_2$ (HT), (Fig. 3.9b). The basic "HH" configuration must therefore be maintained in **28.2** while distortion from 'perfect HH' must result in chemical inequivalence of the P nuclei. The $^1J_{PtP_1}$ and $^1J_{PtP_2}$ values measured in (b) are consistent with the values measured in (a). In Fig. 4.4(c), the upfield peaks, growing in with time, are the peaks due to the HT-A-frame adduct **19**, the result of a geometrical rearrangement.

Monitoring reaction 4.1 by visible spectroscopy consistently reveals that this overall reaction involves two consecutive steps; typical visible spectra recorded in kinetic experiments are displayed in Fig. 4.5.

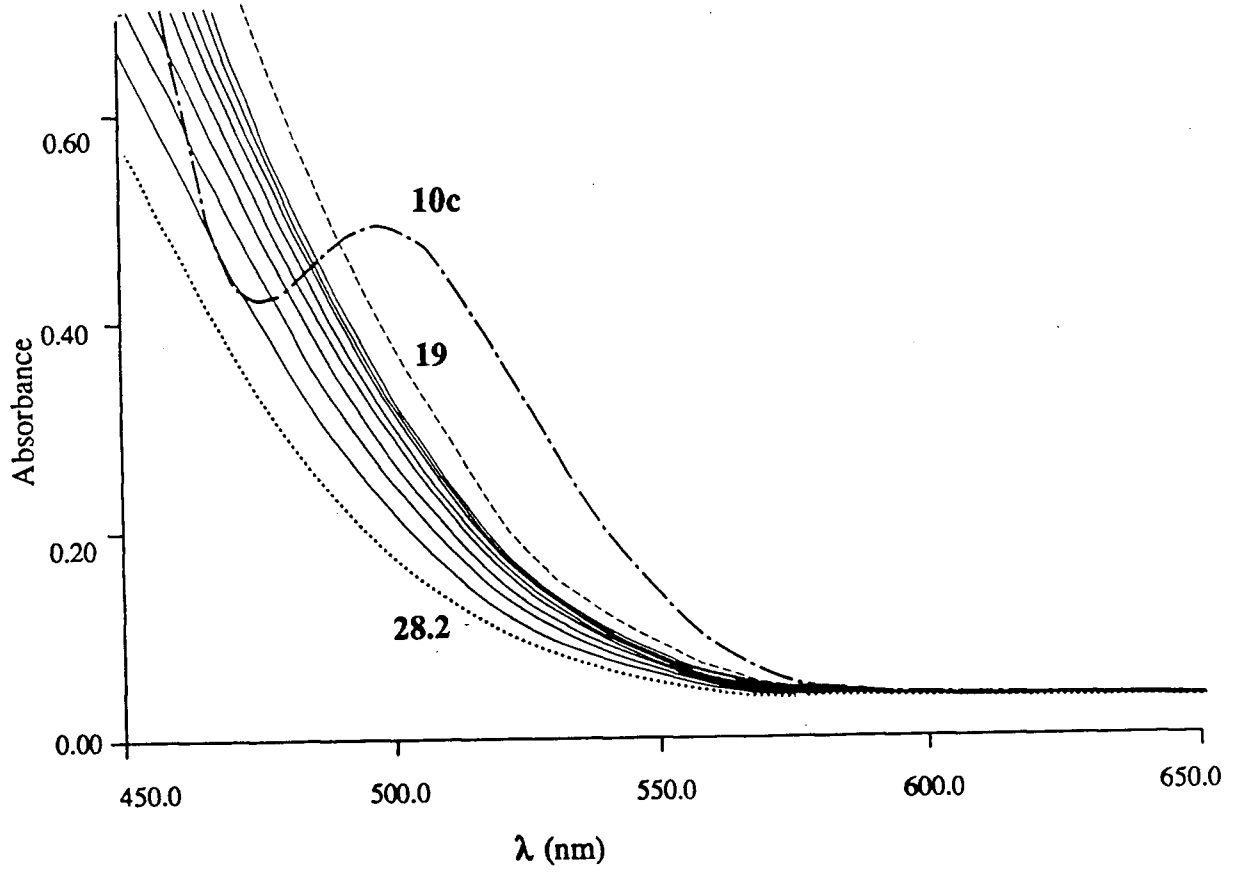

Fig. 4.5. The observed changes in visible spectra for reaction. 4.1 in CH_2Cl_2 at 25°C. — · — is the spectrum of the precursor **10c** (λ_{max} = 498 nm, ε = 456 $M^{-1}cm^{-1}$); ····· is the spectrum of the intermediate **28.2** (see Fig. 4.4a); ---- is the spectrum of the HT DMAD adduct **19**. The solid lines between **19** and **28.2** are the spectra recorded every 30 min for the formation of **19** from **28.2**; changes for the conversion of **10c** to **28.2** are not shown.

The first-order plot, $\ln(A_t-A_\infty)$ vs. t, for the spectral change from spectrum of **10c** to that of **28.2** in Fig. 4.5 is linear to about four half-lives ($t_{1/2}$ = 40.1 s) (Fig. 4.6). The direct reading of the lowest absorbance 0.170 at 500 nm was assumed to be A_∞, and the observed first-order rate constant obtained thereby is 1.73×10^{-2} s^{-1} (Appendix Tables AIV 1- 11). The problem of using $(A_\infty)_{exp}$ directly for the k_{obs} calculation is the degree of reliability of A_∞ because of the slow secondary reaction. Kezdy et al.[21] and Swinbourne[22] developed a method to estimate A_∞, based on the following equation, when the final instrument reading is unreliable or unavailable: $A_t = (A_{t+\tau})e^{k\tau} - A_\infty(e^{k\tau}-1)$, where τ is a suitably chosen time interval; and at the theoretical end point $A_t = A_{t+\tau} = A_\infty$. The intersection of the line (A_t vs. $A_{t+\tau}$) for the experimental data and the 45° line is the estimated A_∞. In this method, the τ value is chosen between $t_{1/2}$ and 1.5 $t_{1/2}$ to give the best accuracy. The absorbances were thus processed also according to the Kezdy-Swinbourne method, and the analysis is listed in Table 4.2. Fig. 4.7 shows the A_t vs. $A_{t+\tau}$ plot for the data, and the A_∞ thus found is 0.175. Several other experimental data analyzed in the same way show that the difference between the estimated A_∞ and the experimental value is less than two percent. The assumption that the lowest absorbance value is A_∞ is thus validated; hereafter, $(A_\infty)_{exp.}$ is used as the real A_∞, without further verification.

Table 4.2. Kezdy-Swinbourne Treatment of the Data in Table AIV 7 for Estimating A_∞

t (s)	A_t	$(t+\tau)^a$ (s)	$A_{t+\tau}$
0	0.488	40	0.325
30	0.352	70	0.263
40	0.325	80	0.250
50	0.299	90	0.237[b]
60	0.280	100	0.228
70	0.263	110	0.220[b]
80	0.250	120	0.212
90	0.237[b]	130	0.205[b]
100	0.228	140	0.200
110	0.220[b]	150	0.195[b]
120	0.212	160	0.191

(a) τ = 40 second was used based on the $t_{1/2}$ result from data in Table AIV 7. (b)These values are interpolated from the A_t vs. t plot.

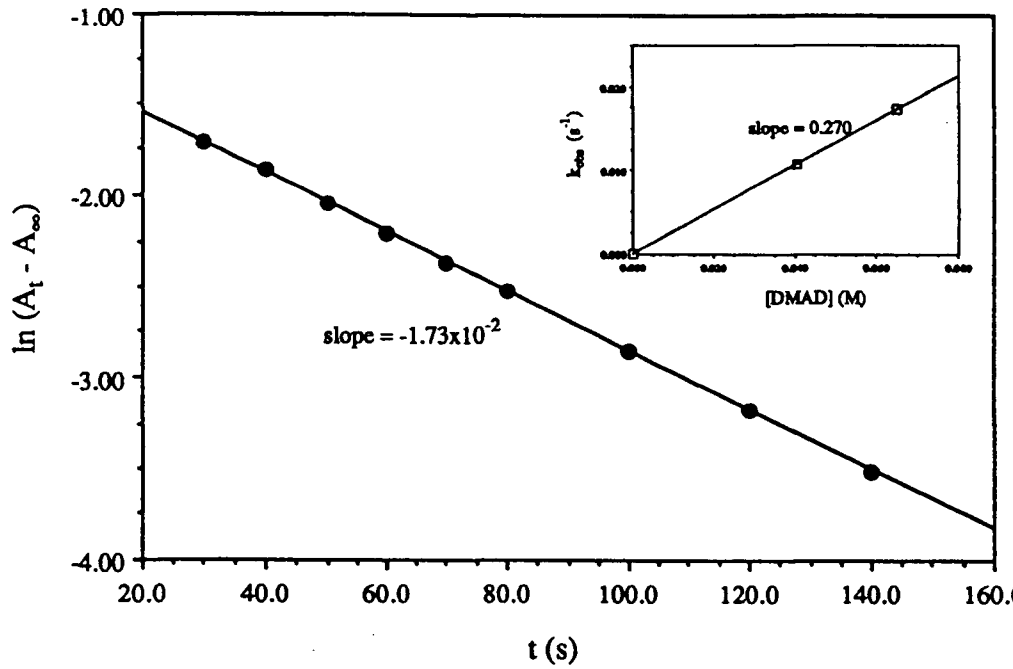

Fig. 4.6. Pseudo first-order rate plot, ln (A_t-A_∞) vs. t, for the DMAD binding step of reaction 4.1 (**10c** to **28.2**), at 25°C: [**10c**] = 1.10×10^{-3} M, [DMAD] = 6.50×10^{-2} M (Table AIV 7). Inset: the observed pseudo first-order rate constants vs. [DMAD] (see Table 4.4). At this particular temp., only two [DMAD] values were used; at 34°C, three [DMAD] values were used (Table AIV 1-3).

The Guggenheim treatment,[23] in which ln(A_t-$A_{t+\tau}$) is plotted against time, was also applied to avoid the complication of estimating A_∞ in order to obtain the k_{obs} value. The observed first-order rate constant is obtained from the slope without knowing the real A_∞; for the best accuracy, τ is chosen between two to three half-lives (Table 4.3, Fig. 4.8). The rate constant obtained in this way is 1.80×10^{-2} s^{-1}. Changing the DMAD concentration resulted in a change of the observed psuedo first-order rate constant, and a first-order dependence on [DMAD] was demonstrated by the linear relationship of the k_{obs} vs. [DMAD] plot including the origin (Fig. 4.6 inset). A summary of DMAD dependence data is given in Table 4.4. Direct involvement of DMAD in the conversion of **10c** to **28.2** is clearly indicated by the DMAD dependence result, and this step in later sections is called the DMAD binding step. The measured second-order rate constant k_1 at 25°C is 0.270 $M^{-1}s^{-1}$ (Fig. 4.6 inset).

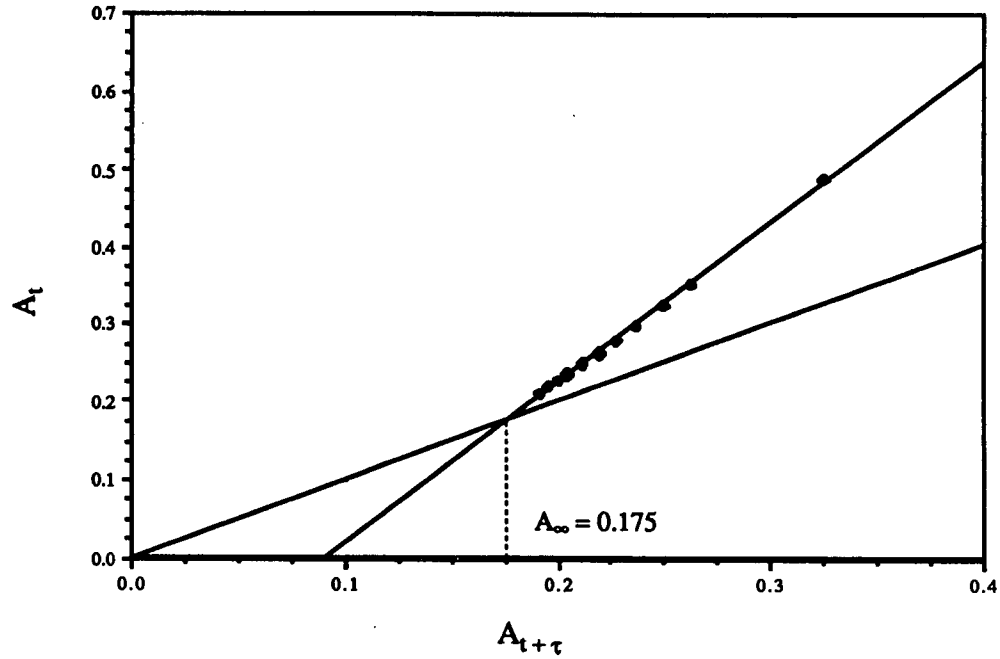

Fig. 4.7. Estimation of the A_∞ value by Kezdy-Swinbourne method; plot of A_t vs. $A_{t+\tau}$ (see Table 4.2; $\tau = 40.0$ s $\approx t_{1/2}$).

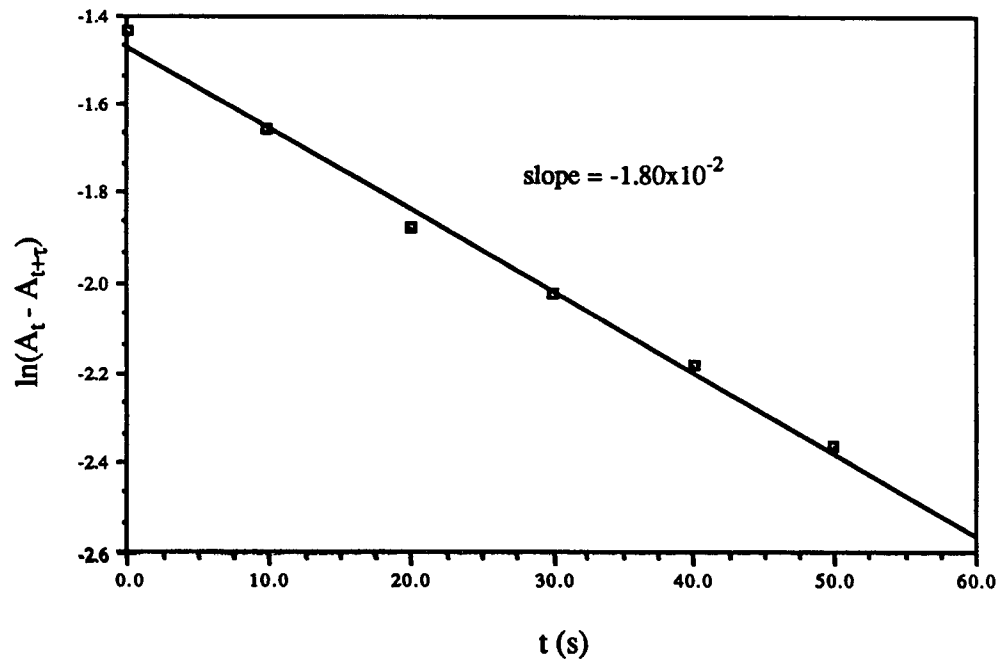

Fig. 4.8. The Guggenheim treatment to give k_{obs}; plot of $-\ln(A_t - A_{t+\tau})$ vs. t (see Table 4.3; $\tau = 80$ s $\approx 2t_{1/2}$).

The first-order plot for the subsequent step involving conversion of **28.2** to **19**, $\ln(A_\infty - A_t)$ vs. t (Fig. 4.9) is also essentially linear. The two observed rate constants, 4.77×10^{-5} and 4.70×10^{-5} s^{-1}, are essentially independent of [DMAD]. The zero-order kinetics with respect to DMAD are characteristic of an intramolecular rearrangement process; this step (**28.2** to **19**) is called the isomerization step.

Table 4.3. First-Order Analysis of the Data in Table AIV 7 by the Guggenheim Method

t (s)	A_t	$t + \tau$ (s)	$A_{t+\tau}$	$A_t - A_{t+\tau}$	$-\ln(A_t - A_{t+\tau})$
0	0.488	80	0.250	0.238	1.435
10	0.427	90	0.236	0.191	1.655
20	0.381	100	0.228	0.153	1.877
30	0.352	110	0.220	0.132	2.025
40	0.325	120	0.212	0.113	2.180
50	0.299	130	0.205	0.094	2.364

$k_{obs} = 1.80 \times 10^{-2}$ s^{-1}

Table 4.4. The Observed Pseudo First-Order Rate Constants at Different [DMAD], in CH_2Cl_2 at 25°C

[DMAD]x10^2 (M)	0.00	4.06	6.50
k_{obs} (s^{-1})	0.00	1.08	1.73

$k_1 = 0.270$ $M^{-1}s^{-1}$

The binding of DMAD to **10c** (4.1) is an oxidative addition reaction, as is the net DMAD insertion reaction into the metal-metal bond with **9c** (Sect. 4.3.1). However, the expected insertion product **28.1** (p. 106) is simply not observed throughout the reaction although, from the spectroscopic data, we know that the initially observed product **28.2** is structurally similar to **28.1**.

Based on the results from studies on reaction 4.1, a plausible reaction pathway is outlined as:

$$\mathbf{10c} + \text{DMAD} \xrightarrow{k_1} [\mathbf{28.2}] \xrightarrow{k_2} \mathbf{19}$$

$$(k_1 > k_2)$$

The second-order rate constants for the binding of DMAD (k_1), and the first-order rate constants for the isomerization (k_2) at various temperatures in CH_2Cl_2 are summarized in Table 4.5. The plot of $\ln k_1/T$ vs. $1/T$ (Fig. 4.10) yields the activation enthalpy, $\Delta H^{\neq} = 8.5 \pm 0.3$ kcal/mol, and the activation entropy, $\Delta S^{\neq} = -32.4 \pm 0.9$ e.u; and the plot of $-\ln k_2/T$ vs. $1/T$ gives $\Delta H^{\neq}$ (24.0 ± 1.0 kcal/mol) and $\Delta S^{\neq}$ (6 ± 4 e.u) for the isomerization reaction step.

Table 4.5. Temperature Dependence of Rate Constants k_1 and k_2 in CH_2Cl_2

T (K)	$1/T \times 10^3$	k_1 ($M^{-1}s^{-1}$)	$-\ln k_1/T$	$k_2 \times 10^5 (s^{-1})$	$-\ln k_2/T$
290.15	3.446	0.176	7.385	1.39	16.85
294.15	3.400	0.229	7.158	2.74	16.19
298.15	3.354	0.270	7.007	4.74	15.64
302.15	3.310	0.339	6.793	9.10	15.02
307.15	3.256	0.436	6.557	16.7	14.42
		$\Delta H^{\neq} = 8.5 \pm 0.3$ kcal/mol		$\Delta H^{\neq} = 24.0 \pm 1.0$ kcal/mol	
		$\Delta S^{\neq} = -32.4 \pm 0.9$ e.u.		$\Delta S^{\neq} = 6 \pm 4$ e.u.	

The activation parameters found for the oxidative addition step are typical of data for oxidative addition at a single metal centre, which has been reported upon extensively in the literature.[24] The parameters are also comparable to the data for oxidative addition of H_2S at $Pd_2Br_2(\mu\text{-dppm})_2$ ($\Delta H^{\neq} = 13$ kcal/mol, $\Delta S^{\neq} = -27$ e.u.),[25] and DMAD at $Pt_2I_2(\mu\text{-}PN_3)_2$ (HT), **9c**, ($\Delta H^{\neq} = 9.0 \pm 0.2$ kcal/mol, $\Delta S^{\neq} = -33.0 \pm 0.8$ e.u.) (see below), which are among the very few known for oxidative addition systems at binuclear metal centres.[26] The relatively high $\Delta H^{\neq}$ for the isomerization step is considered to result from a required Pt-P bond cleavage, while the $\Delta S^{\neq}$ value close to zero implies 'minimal' geometric changes in the process (see below for further discussion).

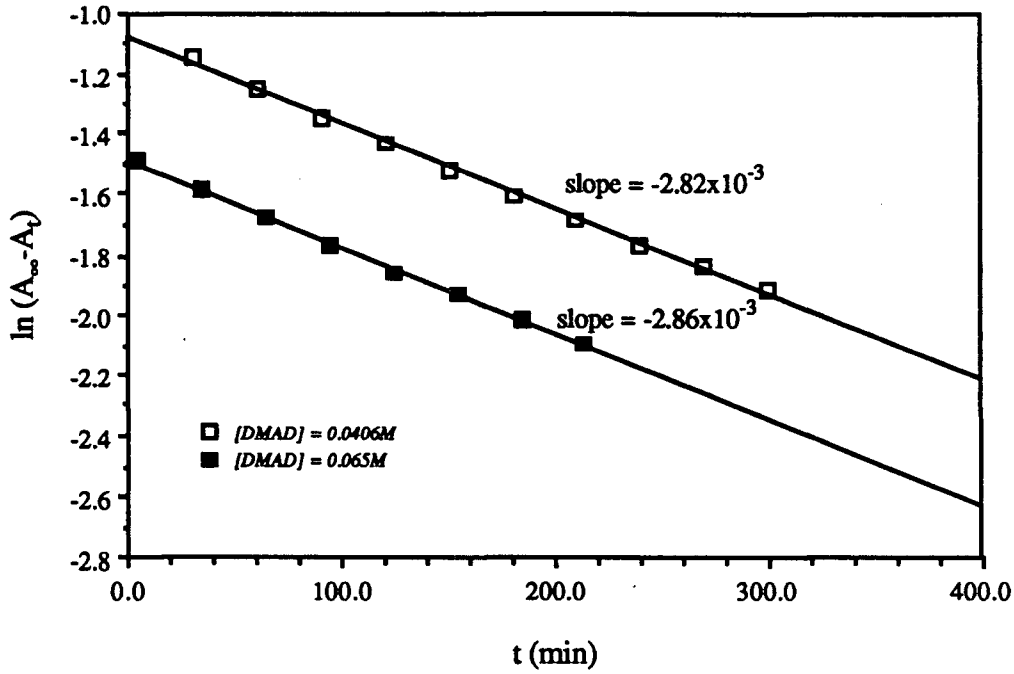

Fig. 4.9. Pseudo first-order rate plot, ln (A_t-A_∞) vs. t, for the isomerization step (**28.2** to **19**) in CH_2Cl_2 at 25°C; [**10c**] = 1.10x10^{-3} M (Table AV 6-7).

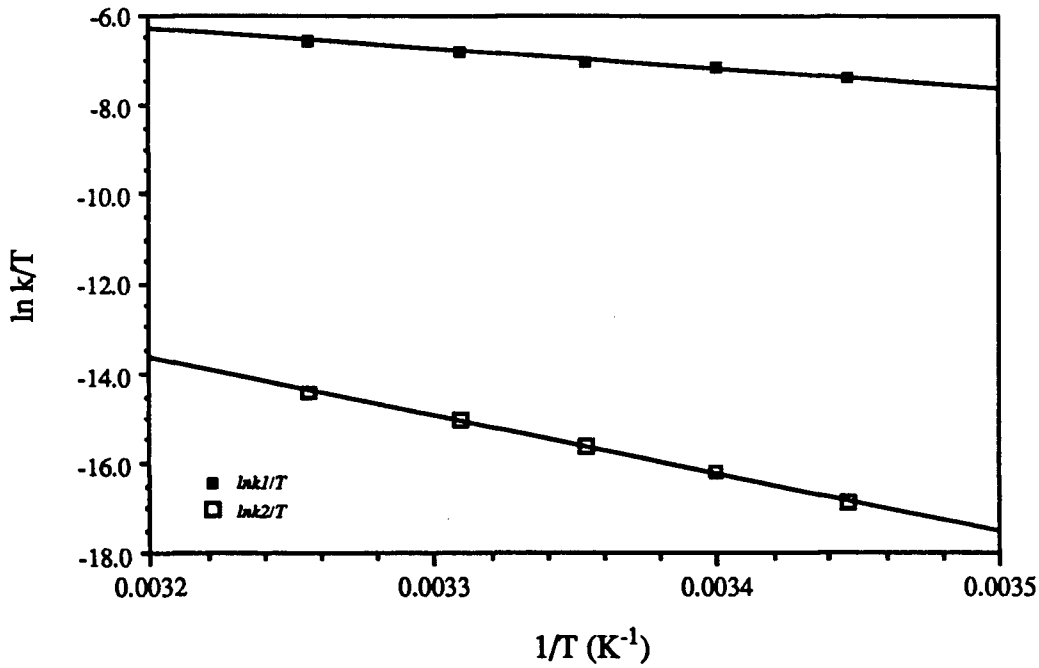

Fig. 4.10. The Eyring plots, ln k/T vs. 1/T, for the rate constants of step 1 (binding of DMAD) and step 2 (isomerization) (see Table 4.5).

By a similar approach, the rate of the reaction of $Pt_2I_2(\mu\text{-}PN_3)_2$, **9c**, with DMAD to give the expected HT insertion product **19** was investigated:

$$\mathbf{9c} + \text{DMAD} \longrightarrow \mathbf{19} \qquad (4.2)$$

The reaction was monitored by the absorbance decrease at the absorption maximum of **9c** at 520 nm or from spectral changes over 360 - 600 nm region (Fig. 4.11). The first-order plot, $\ln(A_t - A_\infty)$ vs. t, is linear with a correlation coefficient 0.999 (Fig. 4.12, Table AIII). The observed first-order rate constant is also DMAD dependent, and the straight line plot of k_{obs} vs. [DMAD] plot demonstrates the first-order relationship (Fig. 4.12, inset). The DMAD dependence data are summarized in Table 4.6. The temperature dependence of the second order rate constants for this reaction in CH_2Cl_2 (Table 4.7) is shown in Fig. 4.13 by the Eyring plot ln k/T against 1/T. $\Delta H^{\neq}$ and $\Delta S^{\neq}$ are found to be 9.0 ± 0.2 kcal/mol, and -33.0 ± 0.8 e.u. respectively.

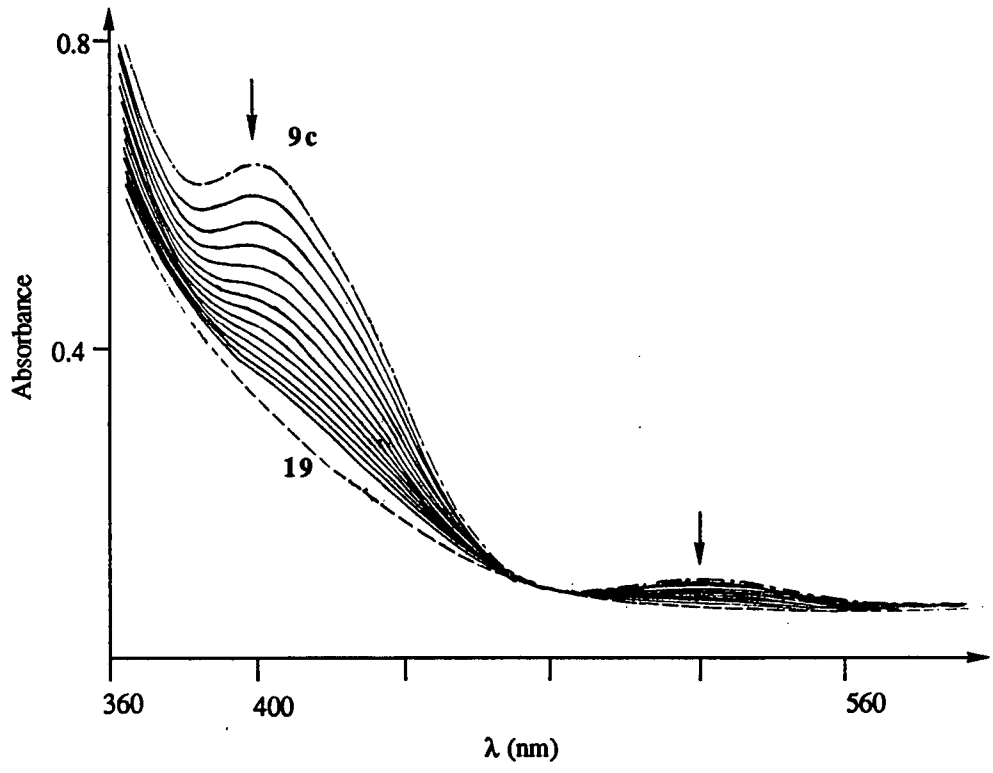

Fig. 4.11. The spectral changes for reaction 4.2 (**9c** to **19**) at 21°C in CH_2Cl_2: the spectrum labelled **9c** was taken before the mixing (λ_{max} = 320, 403 and 518 nm; $\varepsilon = 1.55\times10^4$, 5.04×10^3 and 725 $M^{-1}cm^{-1}$); the spectrum labelled **19** was taken at the experimental infinite time; the solid lines between **9c** and **19** were recorded every 3 min (an isosbestic point at 474 nm is seen). [**9c**] = 1.45×10^{-4} M, [DMAD] = 8.13×10^{-3} M (Table AIII 10).

Table 4.6. Dependence of k_{obs} on [DMAD] for Reaction **9c** with DMAD, at 18°C in CH_2Cl_2

[DMAD]x10^2 (M)	0.00	1.19	2.39	2.71	4.54
k_{obs} x10^3 (s^{-1})	0.00	0.764	1.49	2.00	2.75

$k = 6.2x10^{-2}\ M^{-1}s^{-1}$

Table 4.7. Rate Constants for Reaction of **9c** with DMAD, at Various Temperatures in CH_2Cl_2, and the Activation Parameters

T (K)	1/Tx10^3 (K^{-1})	kx10^2 ($M^{-1}s^{-1}$)	-lnk/T
286.15	3.495	4.54	8.749
291.15	3.435	6.19	8.456
294.15	3.400	8.11	8.196
298.15	3.354	9.00	8.106
302.15	3.310	11.7	7.840
307.15	3.256	14.4	7.645
$\Delta H^{\neq}$ = 9.0 ± 0.2 kcal/mol		$\Delta S^{\neq}$ = -33.0 ± 0.8 e.u.	

4.3.3. Reaction of $Pt_2I_2(\mu\text{-}PN_1)_2$ (HH), **10a**, with DMAD

In order to assist in identifying the structure of **28.2** in reaction (4.1), the structurally related compounds, **10a** and **10b** (the corresponding PN_2 complex), were reacted with DMAD. Reactions of the latter, as the various diastereomers **10b.1** and **10b.2/10b.3**, with DMAD will be dealt with in the next section.

When the title compound **10a** was reacted with DMAD, an orange solid, **17**, was isolated and characterized by ^{31}P and ^{195}Pt NMR spectroscopies (Fig. 4.14), as well as elemental analysis (Table 2.8). Both spectra strongly suggest the HH configuration. This particular product, **17**, is stable in solution for more than a week, and no isomerization process is apparent.

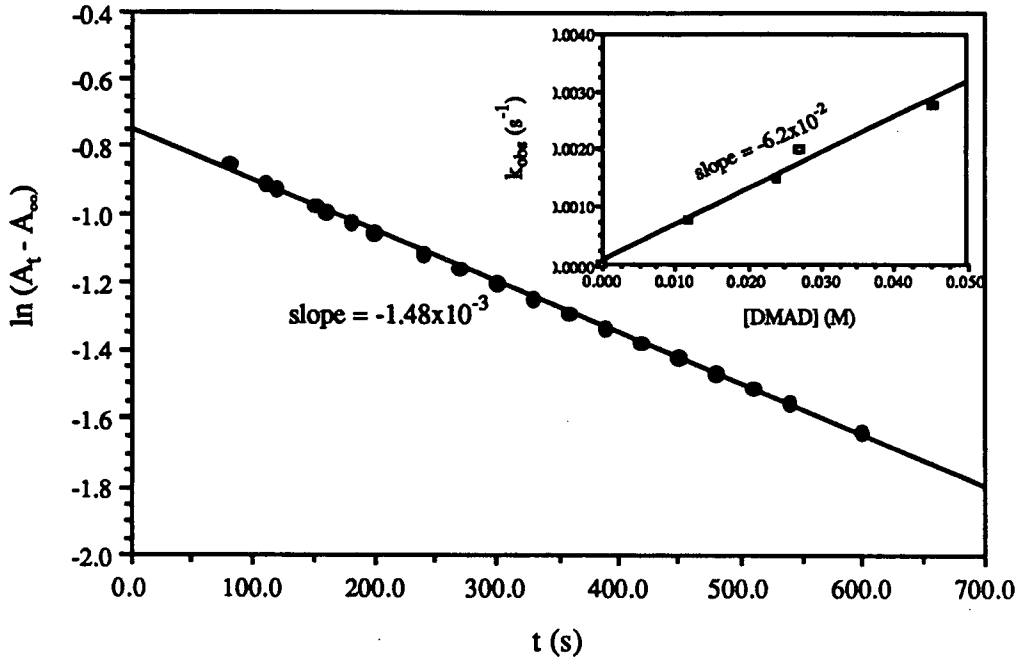

Fig. 4.12. Pseudo first-order rate plot, ln (A_t-A_∞) vs. t, for reaction 4.2 at 18°C in CH_2Cl_2: [**9c**] = 1.18x10^{-3} M, [DMAD] = 2.39x10^{-2} M (Table AIII 12). Inset: the observed first-order rate constants vs. [DMAD] (see Table 4.6).

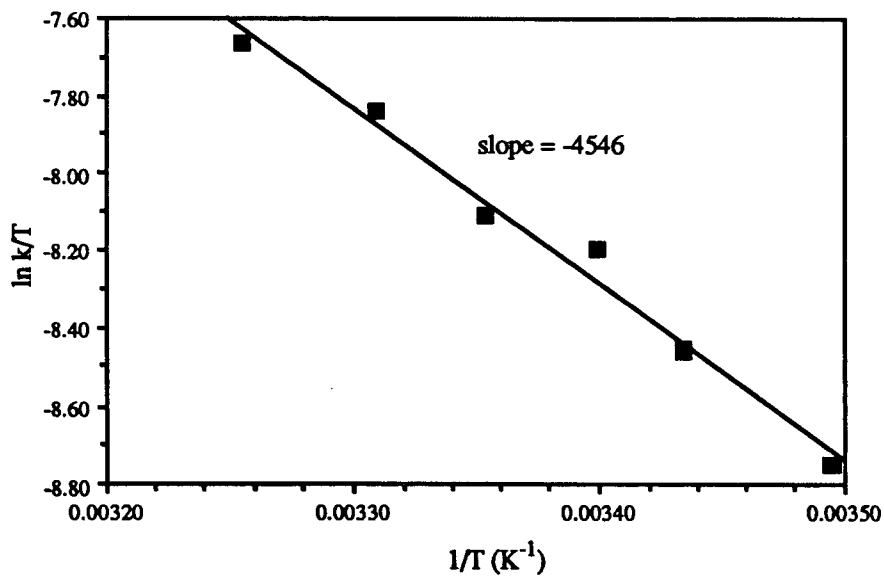

Fig. 4.13. The Eyring plot of ln k/T vs. 1/T for reaction 4.2 (Table 4.7).

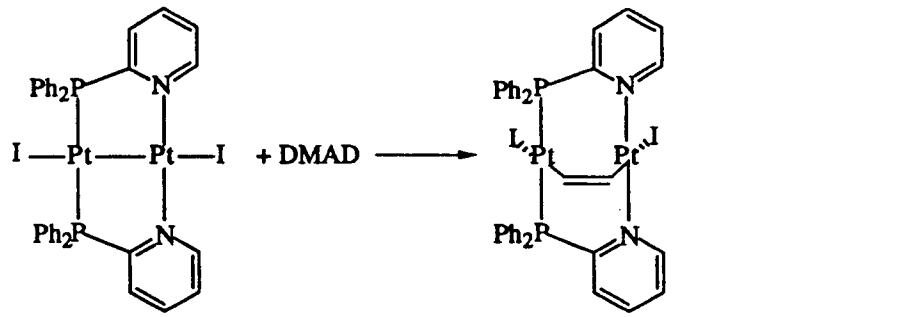

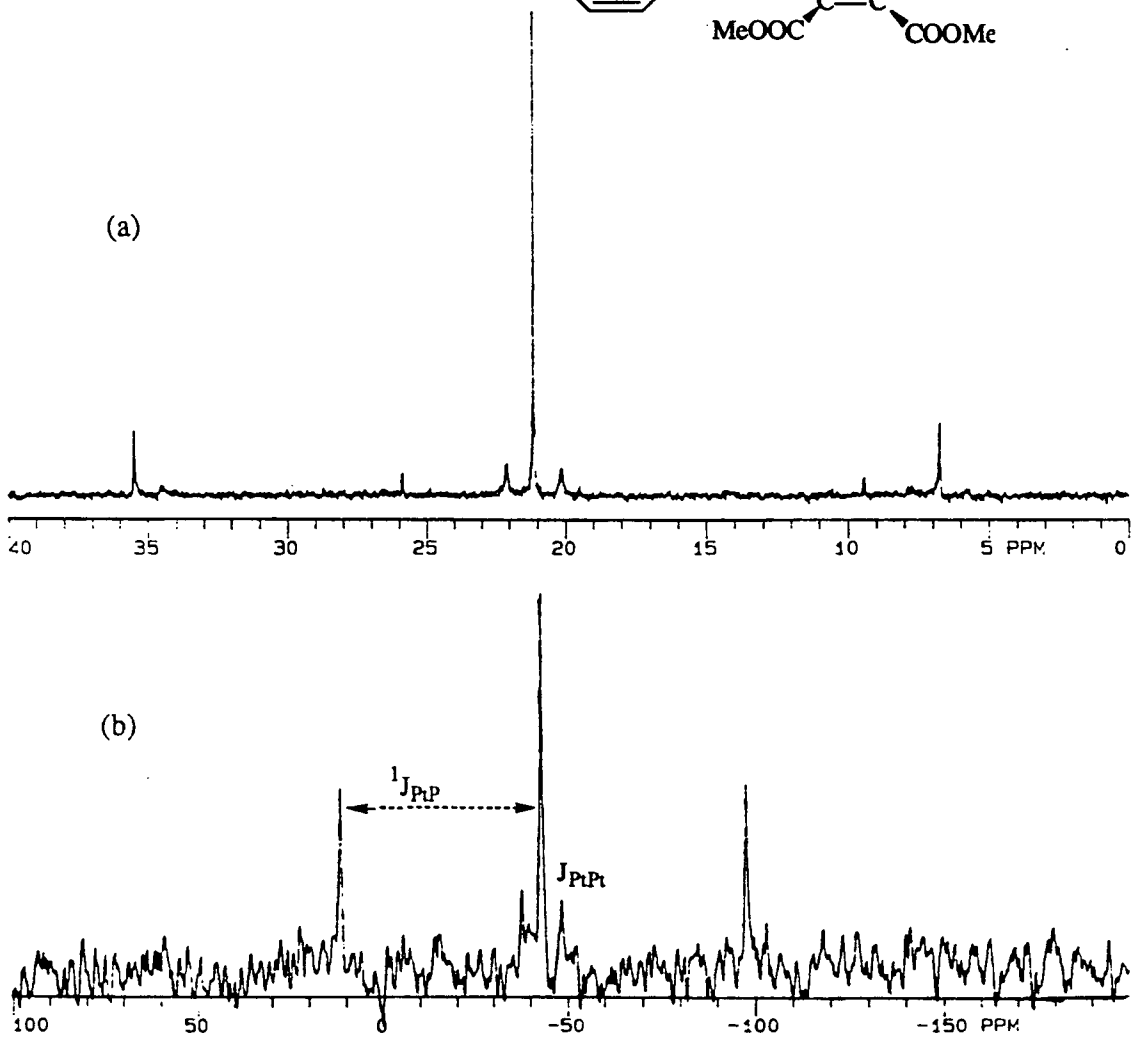

Fig. 4.14. (a) $^{31}P\{^1H\}$ NMR spectrum (121.4 MHz) of **17** in $CDCl_3$ at r.t.: $\delta = 21.2$ (s), $^1J_{PtP} = 3496$ Hz, $^3J_{PtP} = 242$ Hz. (b) $^{195}Pt\{^1H\}$ NMR spectrum (64.2 MHz) of **17** in $CDCl_3$ at r.t.: $\delta_{Pt} = -43.3$ (t), $^1J_{PtP} = 3496$ Hz, $J_{PtPt} = 670$ Hz.

The rate of reaction (4.3) was studied by monitoring absorbance decrease in the 400 to 600 nm region spectrophotometrically (the spectral changes are similar to those in Fig. 4.11, except only one absorbance maximum at 496 nm (405 $M^{-1}cm^{-1}$) is seen; an isosbestic point occurs at 476 nm). Analyzing data for the spectral changes at selected wavelengths (Tables AVI) gives a first-order dependence in $[Pt_2]$, i.e. the $\ln(A_t-A_\infty)$ vs. t plot is a straight line (Fig. 4.15). Doubling the concentration of DMAD doubles the pseudo first-order rate constant, implying a first-order dependence on [DMAD]. The simple first-order dependences in both metal and DMAD are the same as those found for the first steps of reaction 4.1.

The temperature dependence of the rate constants was also investigated, and the results are summarized in Table 4.8 and Fig. 4.16. The $\Delta H^{\neq}$ and $\Delta S^{\neq}$ values are again in the same range as for the oxidative addition reactions at binuclear metal centres described in the previous section.

Table 4.8. Rate Constants for Reaction 4.3 at Various Temperatures, and the Activation Parameters

T (K)	$1/T \times 10^3$ (K^{-1})	$k \times 10^2$ ($M^{-1}s^{-1}$)	$k/T \times 10^4$	-lnk/T
293.15	3.411	2.60	0.887	9.330
298.15	3.354	3.21	1.077	9.136
303.15	3.299	4.04	1.323	8.923
308.15	3.245	4.90	1.590	8.747
$\Delta H^{\neq} = 7.1 \pm 0.2$ kcal/mol			$\Delta S^{\neq} = -41.0 \pm 0.7$ e.u.	

The key point that the studies on this reaction demonstrate (in conjuction with findings on reaction 4.1) is that the instability of an HH DMAD adduct is not governed by simple steric factors: the phenyl group is little different in size to pyridine (cf. **17** vs. **28.1** (p.106)). The nonbridging pyridyl groups are clearly playing an important role in destabilizing the HH insertion product and in promoting isomerization to the HT product. The role of the nonbridging pyridyl group will be illustrated further in the following section.

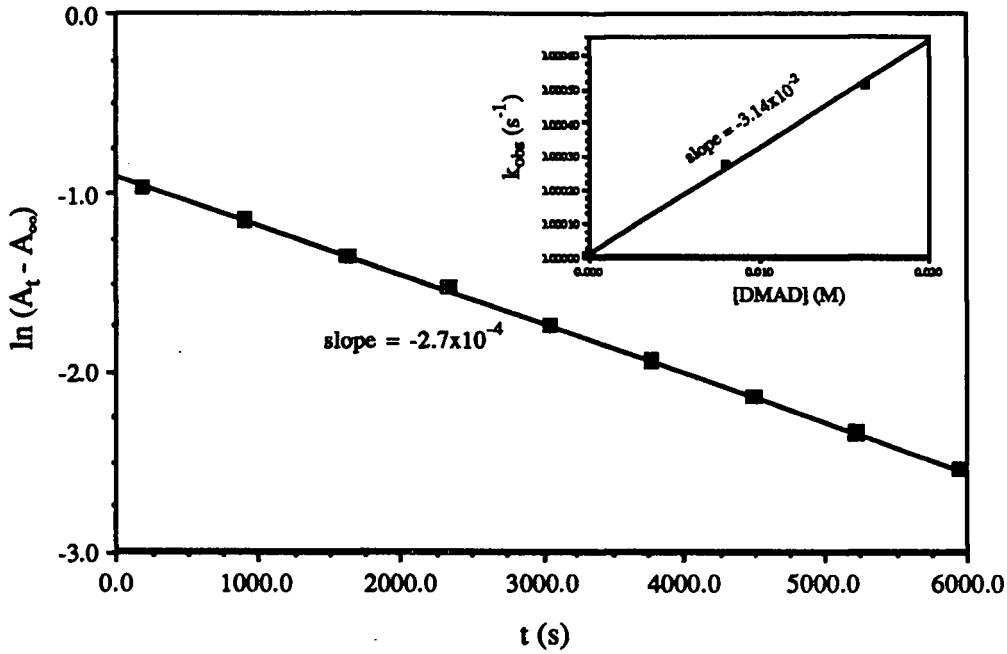

Fig. 4.15. Pseudo first-order rate plot, ln (A_t -A_∞) vs. t, for reaction 4.3 (**10a** to **17**) at 25°C in CH_2Cl_2: [**10a**] = 2.89x10^{-4} M; [DMAD] = 1.63x10^{-2} M. Inset: the observed rate constants at 25°C vs. [DMAD] (data in Table AVI 6).

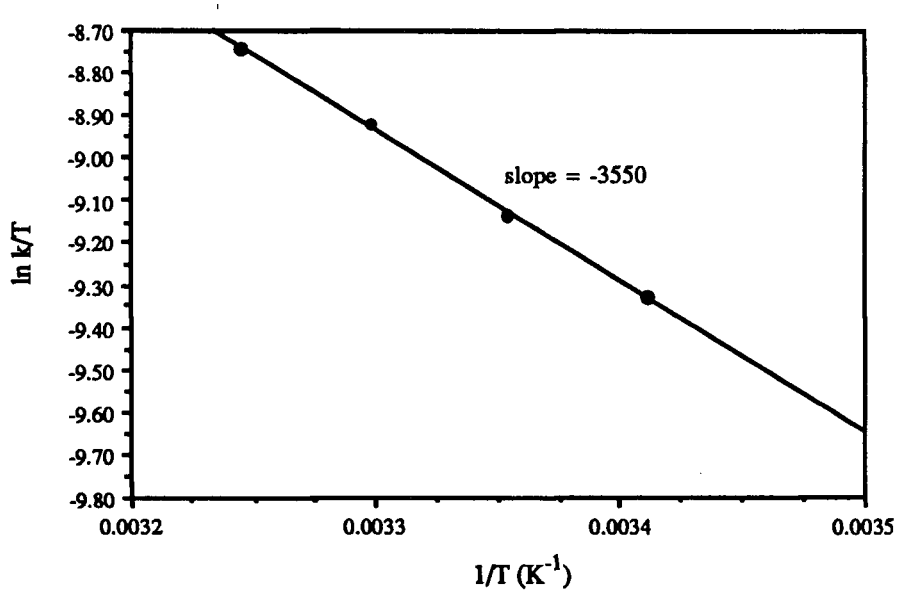

Fig. 4.16. The Eyring plot for the rate constants of reaction 4.3 (Table 4.8).

4.3.4. Reactions of $Pt_2I_2(\mu\text{-}PN_2)_2$ (HH), **10b**, with DMAD

Reactions of the diastereomers of **10b** with DMAD are shown to undergo initially the same oxidative addition with DMAD to form an A-frame insertion adduct; the diastereomers, in which the binuclear P-N bridging complex has one non-chelated pyridyl group and one phenyl group on the phosphorus atom, are found to combine reaction patterns of both **10a** and **10c**, leading to HH, HT or a mixture of HH and HT adducts (see below). Knowledge of the fates of the diastereomeric insertion adducts is essential in elucidating the origin of the isomerization. The use of the isolated diastereomers **10b.1** and **10b.2/10b.3** (Sect. 3.2.4) allows for a thorough understanding of the relationship between the structures of the starting complexes and the end-products. In this section, the results of $^{31}P\{^1H\}$ NMR and kinetic studies are presented.

4.3.4.1. Reaction of **10b.1** with DMAD

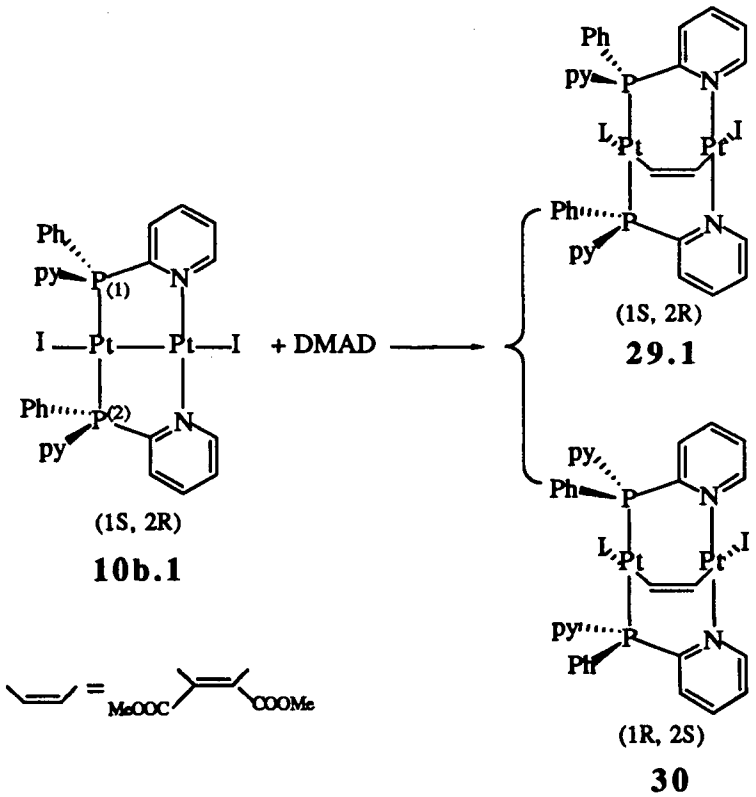

(4.4)

(4.5)

The reaction of **10b.1** with DMAD is expected to yield two diastereomers **29.1** and **30** (Eqs. 4.4 and 4.5). Each diastereomer is expected to give one set of ^{31}P NMR signals. The ^{31}P

NMR spectrum of the reaction mixture after 20 min is shown in Fig. 4.17(a), and consists of one upfield singlet and two downfield doublets with corresponding Pt satellites. The striking similarity in the spectral pattern of the downfield signals to that of **28.2** (Fig. 4.4a), and in the pattern of the upfield signals to that of **17** (Fig. 4.14a) suggests that **29.1** gives rise to the downfield doublet of doublets and **30** to the upfield singlet. More convincing evidence for these assignments is obtained from the ^{31}P NMR spectrum of the same sample taken after one week (Fig. 4.17b). Signals corresponding to **30** stay unchanged while those of **29.1** disappear completely. The upfield four singlets with different intensities are those of $Pt_2I_2(\mu\text{-DMAD})(\mu\text{-}PN_2)_2$ (HT), **18**, present as a diastereomeric mixture. In other words, adduct **30** mimics the reactivity of **17** as **30** and **17** are structurally similar; and adduct **29.1** mimics the reactivity of **28.2**. The stability of **30** against isomerization is thought to be due to steric reasons. Formation of the A-frame insertion product pushs the iodo group backwards in the same plane as the pyridyl groups; as a result, the pyridyl groups are blocked from possible contact with central Pt atom. On the other hand, the pyridyl groups in compound **29.1** are not blocked. The presence of properly positioned pyridyl group(s) is essential for the isomerization, which is thus predictable based on the structure of the initial A-frame adduct.

The equivalence of the phosphorus nuclei seen in compound **30** is due to the σ symmetry in the molecule. Obviously, the inequivalence of the P nuclei seen in **29.1** must result from an interaction similar to that observed in **28.2**; this is thought to be the chelating form of **29.1** is labelled as **29.2**.

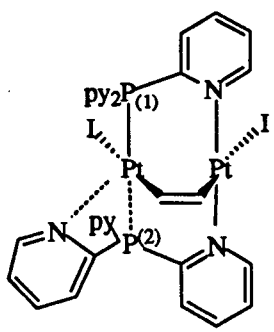

28.2

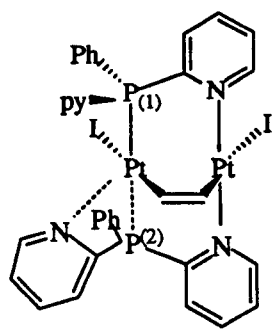

29.2

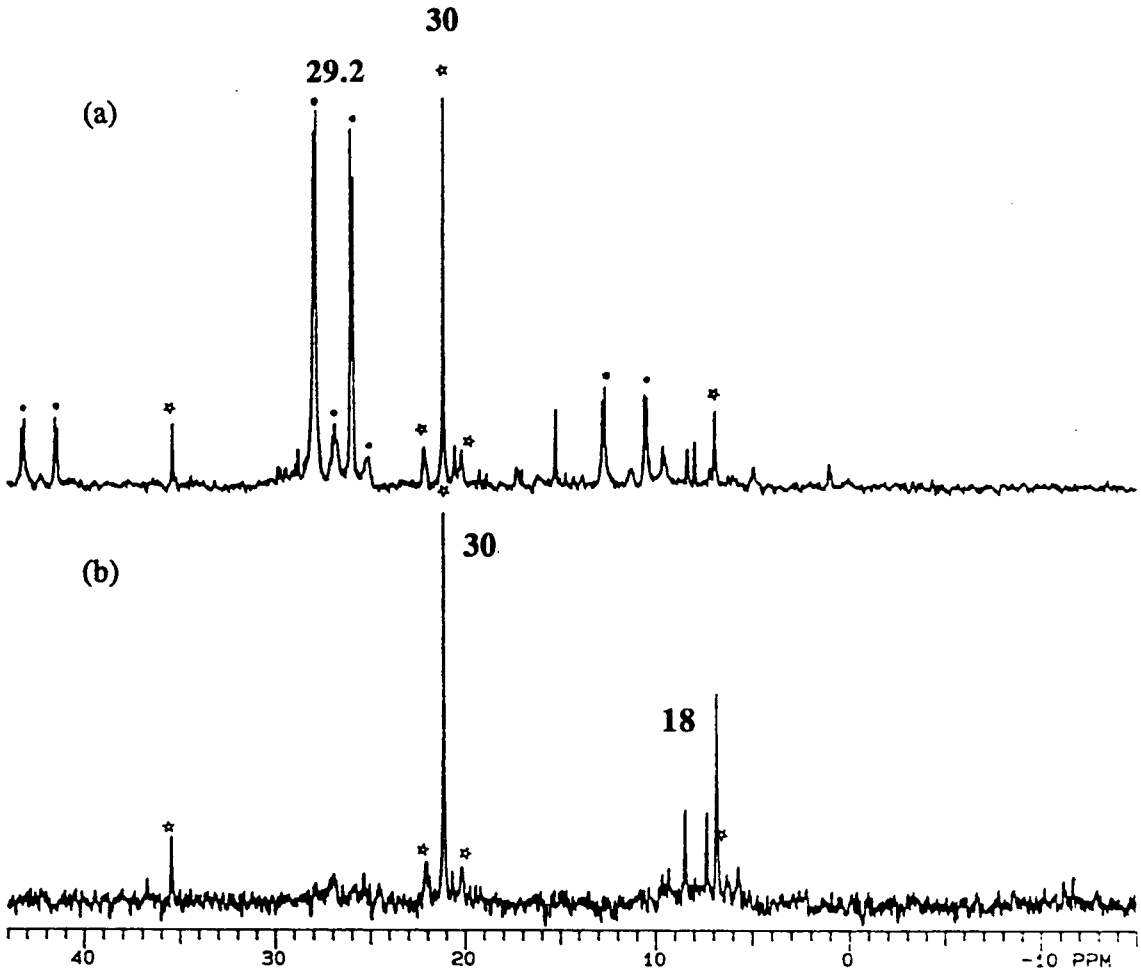

Fig. 4.17. $^{31}P\{^1H\}$ NMR spectra (121.4 MHz) for the products of reactions 4.4 and 4.5, in $CDCl_3$ at r.t.: (a) initially formed adducts **29.2** and **30** after 20 min, (b) products **18**, after isomerization (see also Fig. 4.18b), and **30** after one week; unlabelled peaks are unassigned. (**29.2**: δ = 28.3 (d), $^1J_{PtP}$ = 3705 Hz;δ = 26.4 (d), $^1J_{PtP}$ = 3763, $^3J_{PtP}$ = 215 Hz; $^2J_{PP}$ = 15.0 Hz. **30**: δ = 21.15 (s), $^1J_{PtP}$ = 3459, $^3J_{PtP}$ = 238 Hz).

The difference between a phenyl group and a pyridyl group is that the latter contains a nitrogen atom capable of chelation such that a five-coordinate square-pyramidal phosphorus-nitrogen chelatied intermediate can be formed. There are several examples in the literature of chelating pyridylphosphine complexes containing 4-membered rings.[27, 28] With this assumption, the splitting of the phosphorus signals in the $^{31}P\{^1H\}$ NMR spectra of **28.2** and **29.2** can be accounted for. This type of chemical inequivalence of the P nuclei has never been

observed for the HH precursors in the absence of DMAD. The isomerization of $Pt_2I_2(\mu\text{-}PN_3)_2$ (HH), **10c**, to the HT form, **9c**, does not proceed even at 60°C in $CHCl_3$ for 24 h, at least in the absence of PN_3 (see Sect. 4.4). The isomerization of **28.2** and **29.2** to their corresponding HT isomers is therefore promoted by the chelation which is itself promoted by the DMAD oxidative addition. Whether the chelation of the pyridyl group takes place simultaneously upon, or is preceded by, the oxidative addition of DMAD is clarified in the following section.

4.3.4.2. Reaction of the **10b.2/10b.3** mixture with DMAD

The reactions of the mixture of **10b.2/10b.3** with DMAD are assumed to proceed initially as follows:

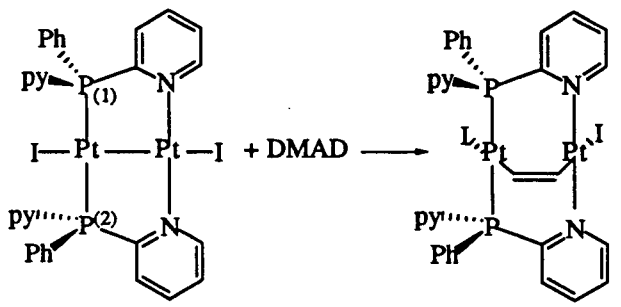

(1S, 2S) **10b.2** (1S, 2S) **31.1** (4.6)

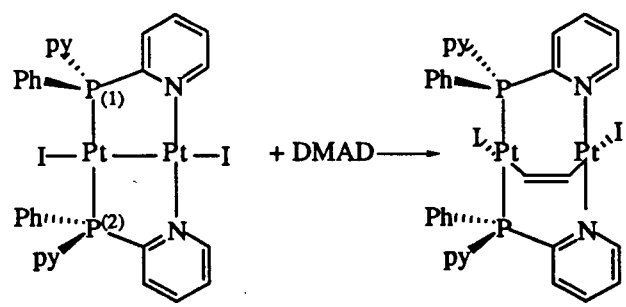

(1R, 2R) **10b.3** (1R, 2R) **32.1** (4.7)

Externally related by a mirror plane, **31.1** and **32.1** are enantiomers, as are the starting complexes **10b.2** and **10b.3**. Enantiomers are not distinguishable from each other in an achiral environment by NMR spectroscopy. The P atoms are diastereotopic within one enantiomer by internal comparison.[29] These inequivalent P atoms show strong mutual trans coupling, and

therefore a strongly coupled AB quartet with corresponding Pt satellites is expected in the ^{31}P NMR spectrum. The peaks labelled with stars in Fig. 4.18a are the expected signals for **31.1/32.1**. The inequivalence arising from the diastereotopic phosphorus nuclei is reflected in the J_{PP} value of these enantiomers, 454 Hz, which is comparable to the J_{PP} value in $Pt_2I_2(\mu\text{-}PN_2)_2$ (HH), **10b.1** (Fig. 3.15). The downfield closely spaced doublet of doublets is assigned to the subsequent chelating intermediate **31.2/32.2** (2 enantiomers) because of the similarity in spectral pattern to that of **28.2**. The prominent feature of this spectrum is that the direct insertion products in the HH forms, **31.1** and **32.1**, are detected; the corresponding products were never seen in reactions (4.1) and (4.4). There is no obvious explanation for the difference, except that statistically **31.1** and **32.1** have fifty percent less chance for chelation than the precursors (**28.1** and **29.1**) to **28.2** and **29.2** in which chelation is apparent. Also during the NMR experiment, the signals of **31.1/32.1** disappeared much faster than the other set. This evidence favours pathways involving initial oxidative addition of the acetylene, followed by chelation. With the availability of one pyridyl group for chelation, **31.1/32.1** have favourable geometry to isomerize. The ^{31}P NMR spectrum of the reaction products after one week is displayed in Fig. 4.18b. The final reaction mixture contains only the HT-insertion adduct **18**, the NMR signals being similar to the upfield signals in Fig. 4.17b. These experiments demonstrate again that if the Pt centre is accessible by the pyridyl group, the isomerization is inevitable.

4.3.4.3. Kinetic studies on the reaction of the diastereomers of **10b** with DMAD

The rate measurements for the reactions (4.4) and (4.5) were done by using the previously described methods, that is by monitoring the spectral changes from 400 to 600 nm, Fig. 4.19. Reaction of **10b.1** with DMAD produces the two diastereomers **29.2** and **30**, presumably by two, direct parallel reactions. The rate law, in terms of optical density data, is derived easily, assuming that **29.2** and **30** have the same absorptivities:

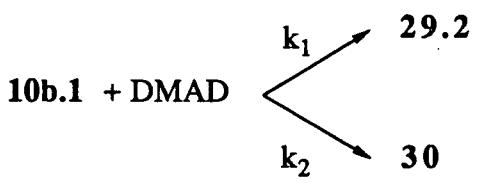

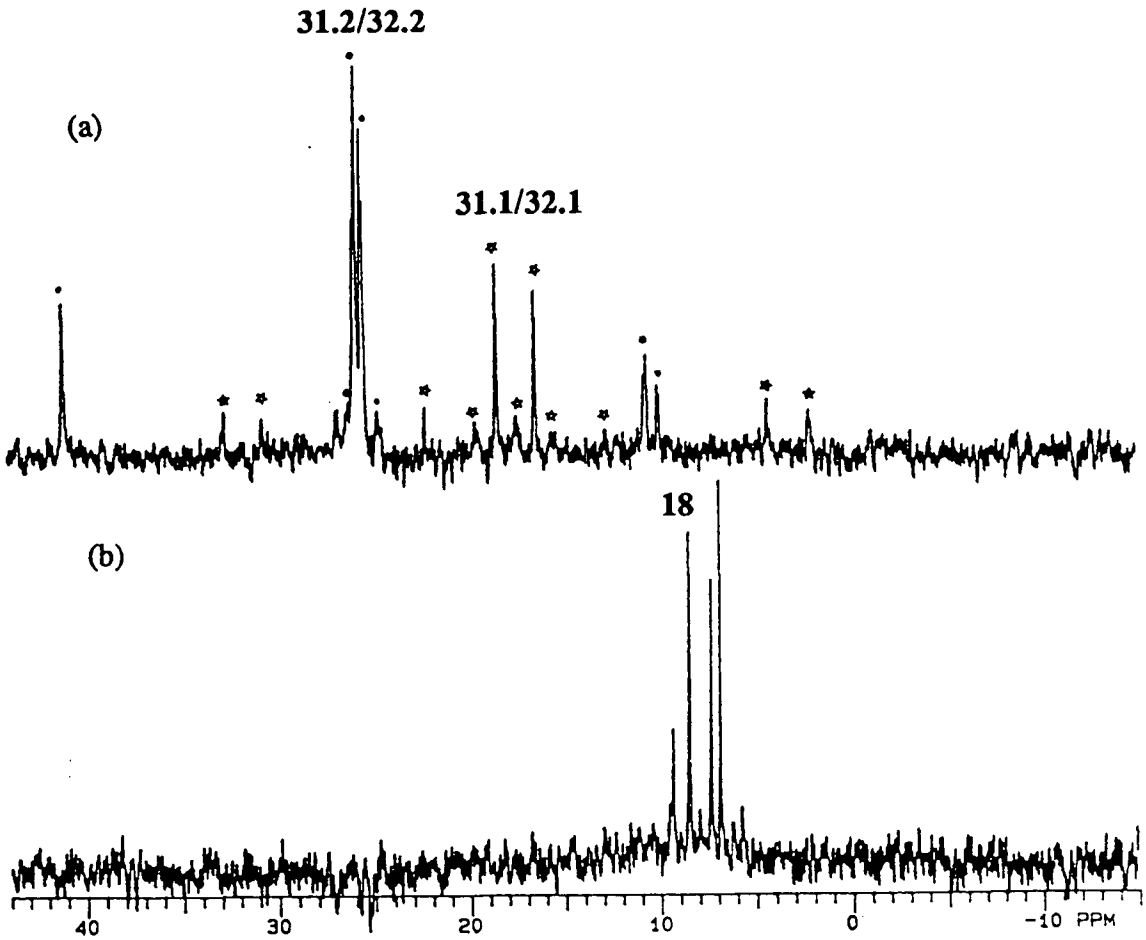

Fig. 4.18. $^{31}P\{^{1}H\}$ NMR spectra (121.4 MHz) for the products of reactions 4.6 and 4.7, in $CDCl_3$ at r.t.: (a) the initially formed (20 min) adducts **31.2/32.1** are labelled with stars, and the chelated intermediates **31.2/32.2** via which isomerization occurs, (b) the end products **18**, $Pt_2I_2(\mu\text{-DMAD})(\mu\text{-PN}_2)_2$ (HT), after one week (Pt satellites are not visible, see also Fig. 4.21b). (**31.1/32.1**: AB quartet centred at 18.5, $^{1}J_{PtP}$ = 3459, $^{3}J_{PtP}$ = 249, $^{2}J_{PP}$ = 454 Hz; **31.2/32.2**: δ = 25.5 (d), 25.9 (d); $^{1}J_{PtP}$ = 3763, 3654 Hz; $^{3}J_{PtP}$ = 169 Hz; $^{2}J_{PP}$= 14.7 Hz.

$$-d[\mathbf{10b.1}]/dt = k_1[\mathbf{10b.1}][DMAD] + k_2[\mathbf{10b.1}][DMAD]$$

$$=(k_1+k_2)[\mathbf{10b.1}][DMAD]$$

$$=k'_{obs}[\mathbf{10b.1}] \qquad \text{where } k'_{obs} = (k_1 + k_2)[DMAD]$$

By monitoring the decrease of **10b.1** concentration in conditions using excess DMAD, the observed pseudo first-order rate constant k'_{obs} is obtained from the slope of the ln $(A_t - A_\infty)$ vs. t plot. The true second-order rate constant for the loss of **10b.1** is the sum of rate constants for each of the parallel reactions. The difference in these latter rate constants is reflected by the difference in the final concentrations of **29.2** and **30**: that is, k_1/k_2 = [**29.2**]/[**30**]. The pseudo first-order plot, $\ln(A_t-A_\infty)$ vs. t, gives a very good straight line and the second-order rate constant, the sum of k_1 and k_2, obtained from the slope of k_{obs} vs. [DMAD] plot, is 8.10×10^{-3} $M^{-1}s^{-1}$ at 25°C (Fig. 4.20). The ratio of [**29.2**] to [**30**] was determined through the ^{31}P signal integration to be 3.5:1 (Fig. 4.17a); these data give $k_1 \approx 6.3\times10^{-3}$, and $k_2 \approx 1.8\times10^{-3}$ $M^{-1}s^{-1}$. The difference reflected in the rates must be attributed to the preferential binding of DMAD to the 'pyridyl face' over the 'phenyl face'. This preference seems to be applicable also in the reactions of the diastereomeric mixture within the $Pd_2X_2(\mu\text{-}PN_2)_2$ (HT) (X = Cl, I) and $Pt_2I_2(\mu\text{-}PN_2)_2$ (HT) complexes with DMAD (Fig. 4.21). The $\ln(A_t-A_\infty)$ vs. t data of reactions (4.4) and (4.5) are listed in Tables AVIII. Monitoring of the subsequent isomerization step (**29.2** to **18**) by visible spectroscopy was not possible because the acccompanying largest total absorbance change was too small (~0.03). However, a rough estimate of $t_{1/2}$ for this step at 25°C is 6 h (cf. for **10c**, $t_{1/2}$ = 4.1 h, Table 4.5).

The rate measurements for reactions (4.6) and (4.7) were also monitored by visible spectroscopy; spectral changes similar to those in Fig. 4.19 were observed. Compounds **10b.2** and **10b.3** are enantiomers, and so are the insertion adducts **31.1** and **32.1**, and the subsequently formed chelated species **31.2** and **32.2**. Reactions (4.6) and (4.7) are independent, occurring with the same rate constants,

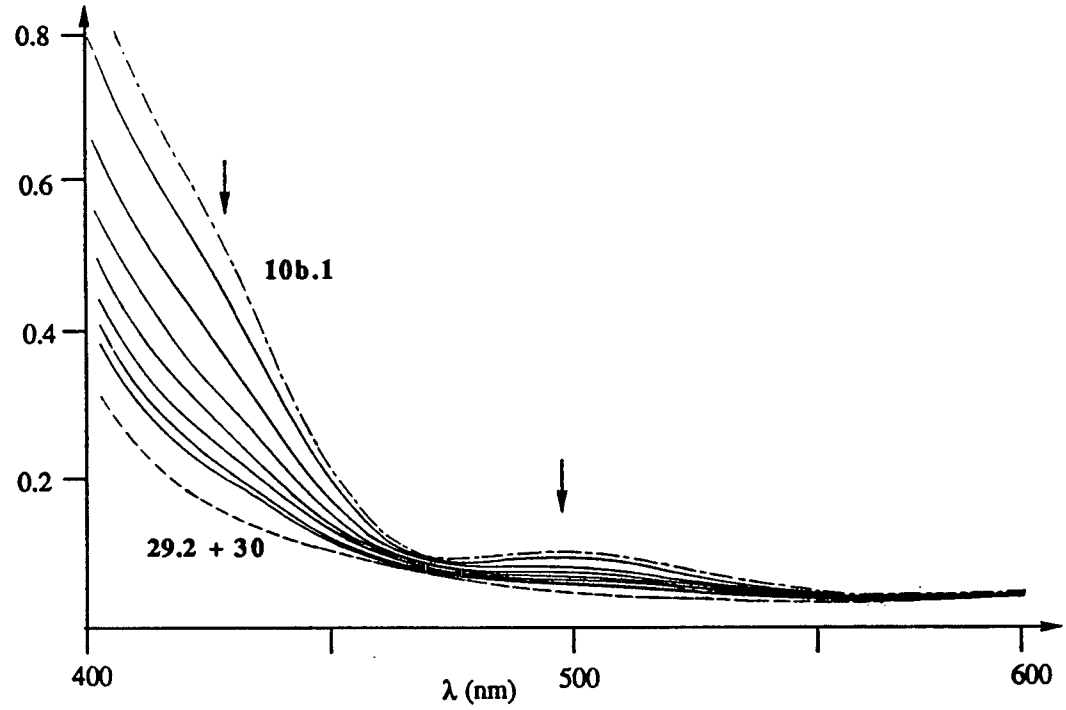

Fig. 4.19. The spectral changes for reactions 4.4 and 4.5 at 25°C in CH_2Cl_2: the spectrum labelled **10b.1** (— - —) was taken at t = 0 (λ_{max} = 496 nm, ε = 608 $M^{-1}cm^{-1}$); the spectrum labelled **29.2 + 30** (- - - -) gave the lowest absorption among the repetitive scan spectra; the solid lines in between were recorded every 5 min. [**10b.1**] = 1.99×10^{-4}, [DMAD] = 1.22×10^{-2} M (Table AVIII 4).

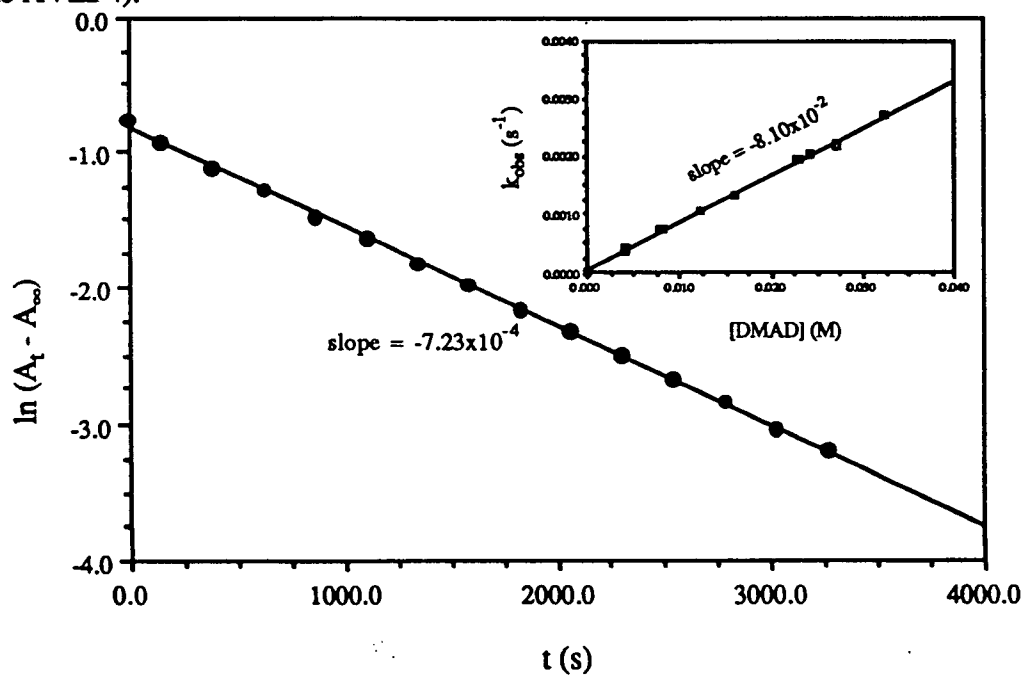

Fig. 4.20. Pseudo first-order plot, ln (A_t -A_∞) vs. t, for reactions 4.4 and 4.5, at 25°C in CH_2Cl_2: [**10b.1**] = 1.99×10^{-4} M, [DMAD] = 8.13×10^{-3} M. Inset: the observed rate constants (25°C) vs. [DMAD] (data in Tables AVIII).

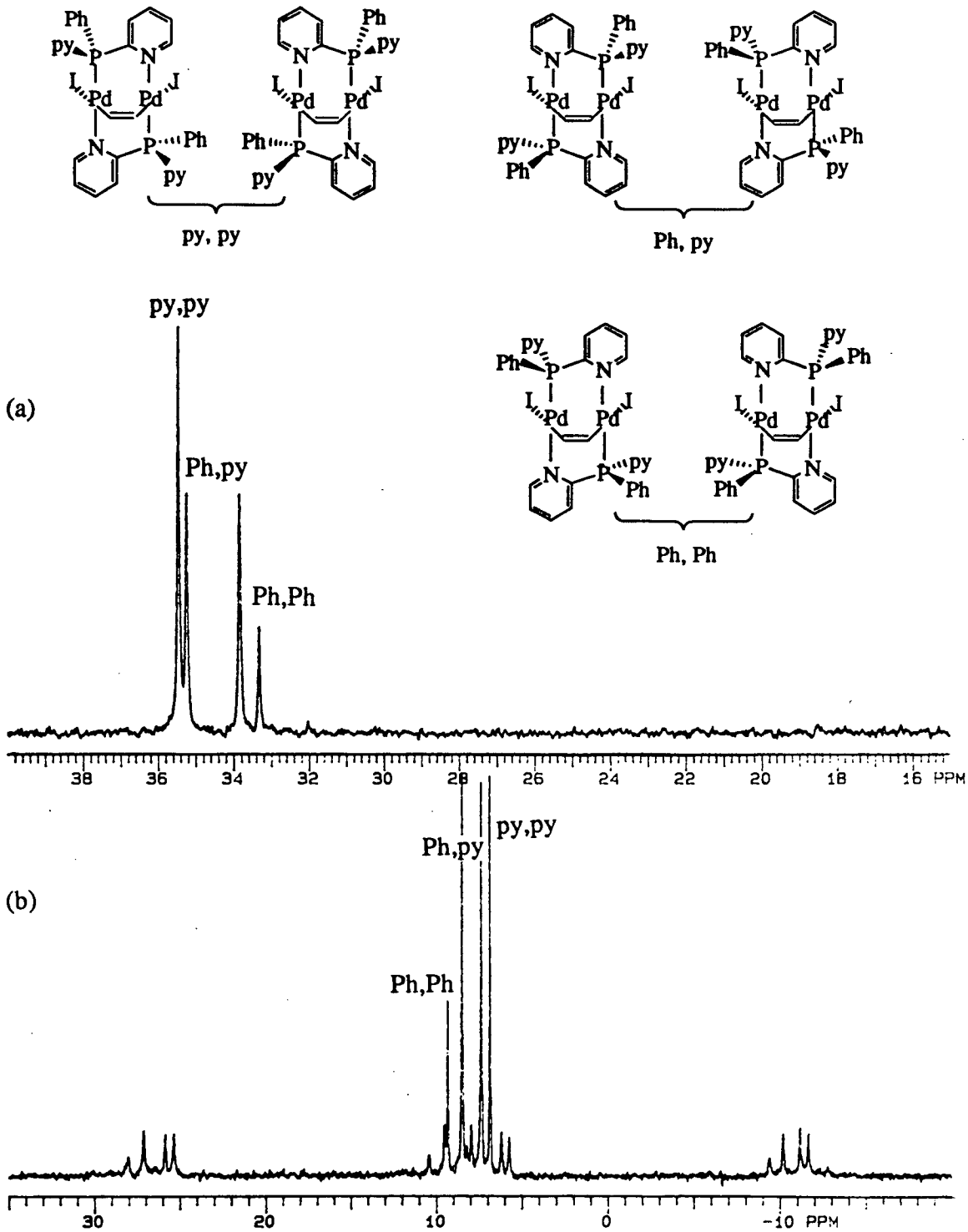

Fig. 4.21. ^{31}P NMR spectra (121.4 MHz) of the diastereomeric mixture of (a): $Pd_2I_2(\mu$-DMAD$)(\mu$-$PN_2)_2$ (HT), **25**, and (b): $Pt_2I_2(\mu$-DMAD$)(\mu$-$PN_2)_2$ (HT), **18**, in $CDCl_3$ at r.t. (data see Table 4.1); the structures of the diastereomeric mixture of **18** are identical to the Pd analogues except that the central metal atoms are Pt (Scheme 4.1).

$$\mathbf{10b.2} + \text{DMAD} \xrightarrow{k_3} \mathbf{31.1} \rightleftharpoons \mathbf{31.2}$$

$$k_3 = k_4 = k$$

$$\mathbf{10b.3} + \text{DMAD} \xrightarrow{k_4} \mathbf{32.1} \rightleftharpoons \mathbf{32.2}$$

The rate law is simply

$$-d\{[\mathbf{10b.2}]+[\mathbf{10b.3}]\}/dt = k[\text{DMAD}]\{[\mathbf{10b.2}]+[\mathbf{10b.3}]\} = k_{obs}\{[\mathbf{10b.2}]+[\mathbf{10b.3}]\}$$

Therefore, the rate of the individual reaction is first-order with respect to the concentration of the corresponding enantiomer, and the overall reaction rate is first-order with respect to the total $[Pt_2]$. With the assumption that the non-chelated and the chelated species are formed in a fixed ratio (by the fast equilibrium shown in Scheme 4.2), the plot of $\ln(A_t-A_\infty)$ vs. t should appear linear (see derivation in Appendix VII), and k_{obs} (= k[DMAD]) should be directly proportional to [DMAD]. Such analyses are obtained for this system (Fig. 4.22). At 20°C, the second-order rate constant is found to be $8.05\times10^{-3}\ M^{-1}s^{-1}$. The activation enthalpy and activation entropy are found to be 8.2 ± 0.5 Kcal/mol and -35.0 ± 0.8 e.u., respectively (Fig. 4.23) (the raw data are listed in Tables AVII). Accurate monitoring of the subsequent isomerization step was again very difficult because the largest total absorbance change was only about 0.06. A rough estimate of $t_{1/2}$ at 25°C is 5 h (cf. for **10c**, $t_{1/2}$ = 4.1 h, Table 4.5; for **10b.1**, $t_{1/2}$ = 6 h).

4.3.5. Mechanism of the reaction of $Pt_2I_2(\mu\text{-}PN_n)_2$ (HH) with DMAD

The ratios of relative intensities of the diastereomeric isomers of the final product $Pt_2I_2(\mu\text{-DMAD})(\mu\text{-}PN_2)_2$ (HT), **18**, in Fig. 4.17 and 4.18 are similar. This observation cannot be explained in terms of a concerted migration of a phosphorus atom from one Pt to the other, because this would lead to the stereospecific (HT) isomers, as shown in Scheme 4.1.

According to Scheme 4.1, compound **29.2** would undergo isomerization to give the enantiomers **33** and **34**. The expected ^{31}P NMR spectrum for **33** and **34** should contain only one singlet with the corresponding Pt-satellites, because the phosphorus atoms are chemically equivalent due to the presence of a C_2 axis. Compounds **31.2** and **32.2** would generate **35** and **36**, respectively, which are also enantiomers. The expected ^{31}P spectrum for **35** and **36** should

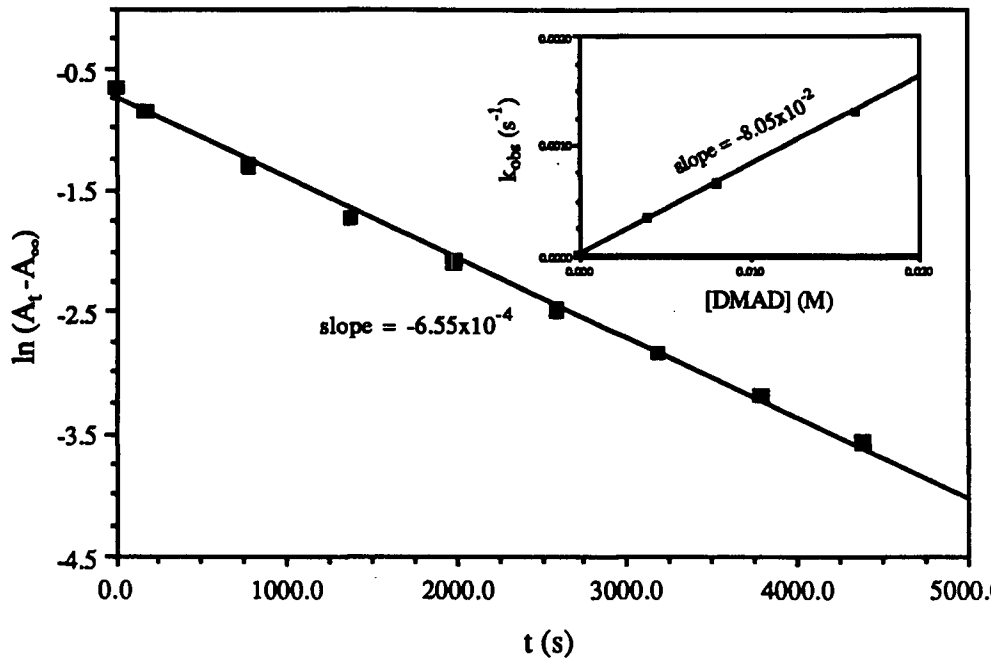

Fig. 4.22. Pseudo first-order plot, ln (A_t -A_∞) vs. t, for reactions 4.6 and 4.7, at 20°C in CH_2Cl_2: [**10b.2/10b.3**] = 2.18x10^{-4} M, [DMAD] = 8.13x10^{-3} M. Inset: the dependence of the pseudo first-order rate on [DMAD] (data in Tables AVII).

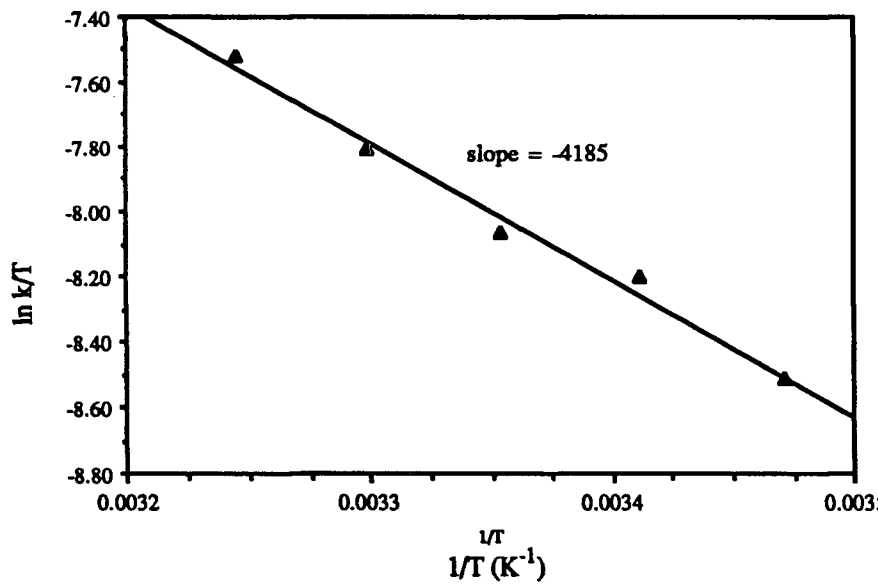

Fig. 4.23. The Eyring plot, ln k/T vs. 1/T, for the rate constants of reactions 4.6. and 4.7 (see Tables AVII 8).

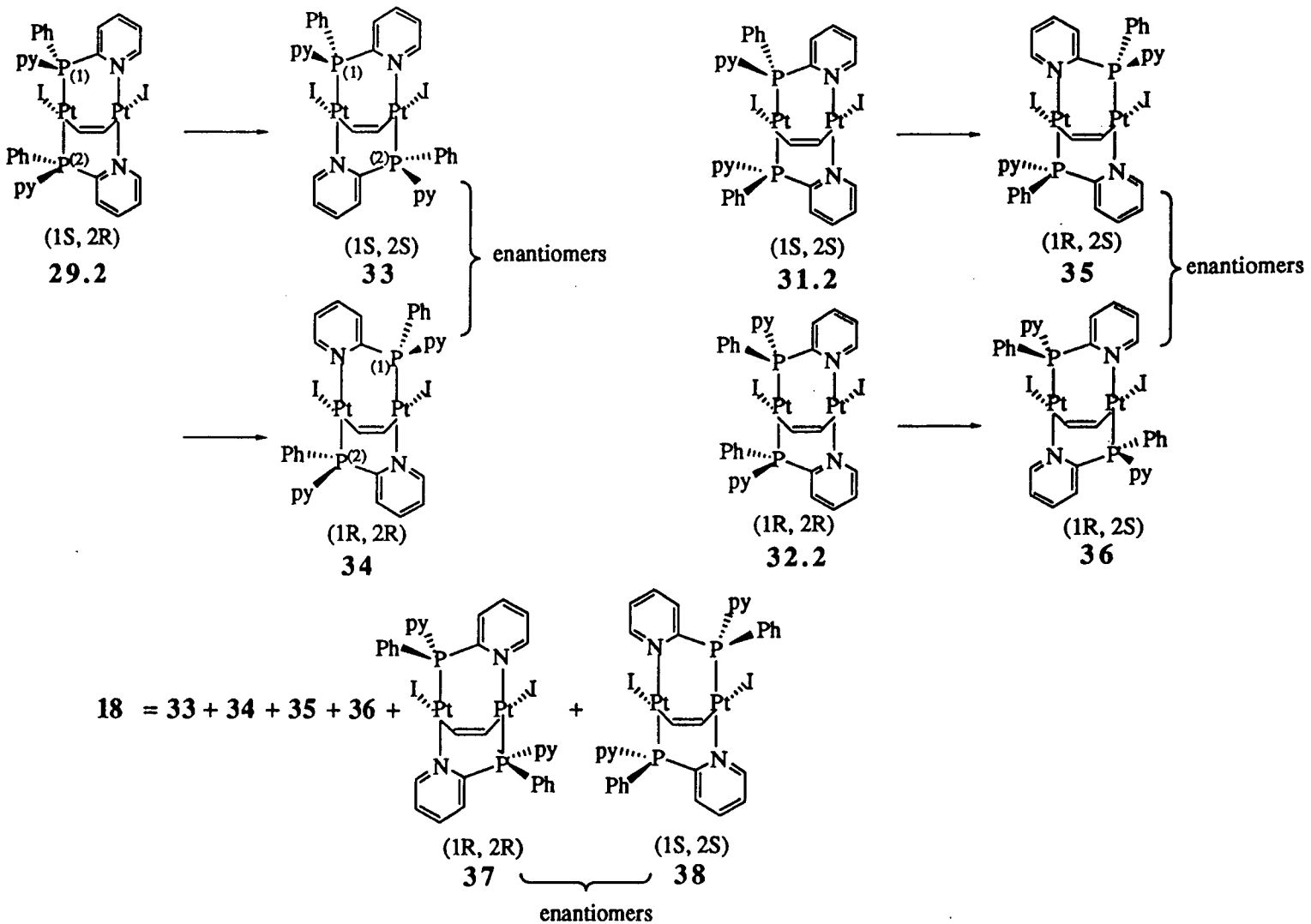

Scheme 4.1. The expected isomerization products, based on a concerted pathway involving phosphorus migration and nitrogen coordination, and the actual isomerization products observed.

contain two singlets with equal intensity due to the diastereotopic P atoms in the molecule (J_{PP} = 0, see Sect. 4.3.1). Instead, four singlets are seen (Figs. 4.17, 4.18). These are assigned to the three possible sets of enantiomers drawn above, and thus the concerted migration pathway of Scheme 4.1 does not account for the observed products. The mechanism is best explained as involving complete dissociation of a P atom from Pt, followed by recoordination to the other Pt, during which process the chiral identity of the P atom is lost. The activation enthalpy of 24 kcal/mol for reaction (4.1) seems consistent with the involvement of a P ligand dissociation in the isomerization step.[30]

Thus, the general reaction pathway for the reaction of DMAD with **10b** and **10c** (HH) species leading to the isomerized insertion adduct is presented in Scheme 4.2:

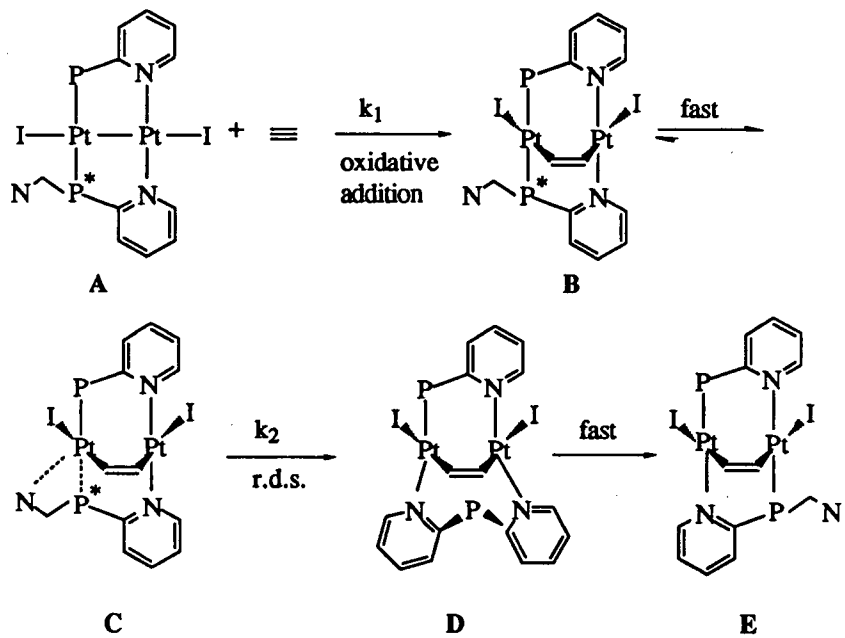

Scheme 4.2. The proposed mechanism for the oxidative addition of DMAD to $Pt_2I_2(\mu\text{-}PN_n)_2$ (HH) and the subsequent isomerization; ≡ and = represent the free and bridged acetylene, respectively; P* represents the chiral P atom; r.d.s = rate determining step.

In this scheme, the HH starting complexes A, comprising **10b.1**, **10b.2**/**10b.3** and **10c**, and the corresponding isomerized A-frame products, E (**18** and **19**), have been well

characterized. Among the three suggested intermediate species (B, C and D), only D has not been detected, and this is consistent with its subsequent rearrangement in a fast step to give the product E. Nevertheless formation of D is suggested by the relatively high activation enthalpy ($\Delta H^{\neq}$ = 24 kcal/mol) for the slow step in the isomerization (**28.2** to **19**) and also by the formation of the nonstereospecific HT products **18** from species **29.2**, **31.2** and **32.2** (Scheme 4.1). B is detected *in situ* by ^{31}P NMR spectroscopy in reaction (4.5) as **30**, and in reactions (4.6) and (4.7) as **31.1** and **32.1**. When the phosphine is PN_1, the HH-DMAD adduct was isolated as **17**. C, a key intermediate species, has been seen in every isomerization reaction as **28.2**, **29.2**, **31.2** and **32.2**. The suggested reaction pathway is fully supported by the ^{31}P and ^{195}Pt NMR spectral data and is consistent with the results of the kinetic experiments.

4.4. Reaction of $Pt_2I_2(\mu\text{-}PN_3)_2$ (HH), 10c, with PN_3 under air in organic solvents

The HH isomer $PtPdI_2(\mu\text{-}PN_1)_2$, with two P atoms on the Pt, has been shown to isomerize in solution under reflux in air to the HT isomer,[31] with the P coordinated to both Pd and Pt. This HT isomer was more stable thermodynamically, and the HH isomer was believed to be the kinetic product of the synthesis procedure used.[31] The $Pt_2I_2(\mu\text{-}PN_3)_2$ (HH) complex, **10c**, shows no tendency to isomerize in solution after refluxing in $CHCl_3$ or CH_2Cl_2 under air for 48 h. When tris(2-pyridyl)phosphine (PN_3) was introduced to the CH_2Cl_2 solution of **10c** at room temperature, the isomerization of **10c** and the oxidation of phosphine ligand were observed. If one equivalent of phosphine was added, the HT complex, **9c**, was produced; if two or more equivalents of phosphine were added, an ionic complex containing two HT bridging phosphines and two terminal phosphines could be isolated as the BPh_4^- salt (see below). Both of these reactions were investigated by ^{31}P NMR spectroscopy and the results are discussed here.

Reaction of **10c** with one equivalent of PN_3 in air, leading to the formation of **9c**, was followed by ^{31}P NMR spectroscopy; although a reaction of phosphine with the HH isomer is

observed almost instantaneously, as indicated by the colour change from orange to yellow, the isomerization proceeds relatively slowly. The ^{31}P NMR spectrum of the immediately formed yellow species **39** is shown in Fig. 4.24a; the splitting pattern and the coupling constants strongly suggest that compound **39** still contains an HH skeleton, while the third phosphine could be on either one of the Pt centres. Fig. 4.24b, taken one week after the mixing, suggests that the terminal phosphine coordinates to the Pt with two nitrogen atoms because the intermediate **40** has an HT isomerized skeleton. This conclusion is drawn based on the matching of the ^{31}P NMR spectrum of the reaction product from **9c** and PN_3 *in situ*, and the understanding of the spectral patterns; the ^{31}P NMR pattern of **40** indicates three inequivalent P atoms, these giving three sets of doublets of doublets. The only reasonable structure for **40** is the HT binuclear complex with an extra terminal phosphine on one of the Pt centres. As the isomerization proceeds via **39**, the terminal phosphine must become bridging while one of the bridged phosphines becomes non-bridging. The overall picture of the isomerization process is given in Scheme 4.3. The equilibrium between **10c** and **39** is established instantaneously and very much favours the formation of **39**, while the formation of **40** from **9c** is not as favourable, perhaps because of steric reasons. This infers that the incoming phosphine adds to the Pt with the two coordinated N atoms; the phosphine perhaps replaces the iodide so that the Pt still retains a square-planar geometry (**39**). The Scheme 4.3 illustrates the chemical processes which are monitored spectroscopically (Fig. 4.24). The formation of a cationic species from a Pt_2^I phosphine dihalide on reaction with phosphine is precedented in the literature.[32] In the final stage, the phosphine is oxidized to the phosphine oxide; this process does not occur normally in air in the absence of metal complex.

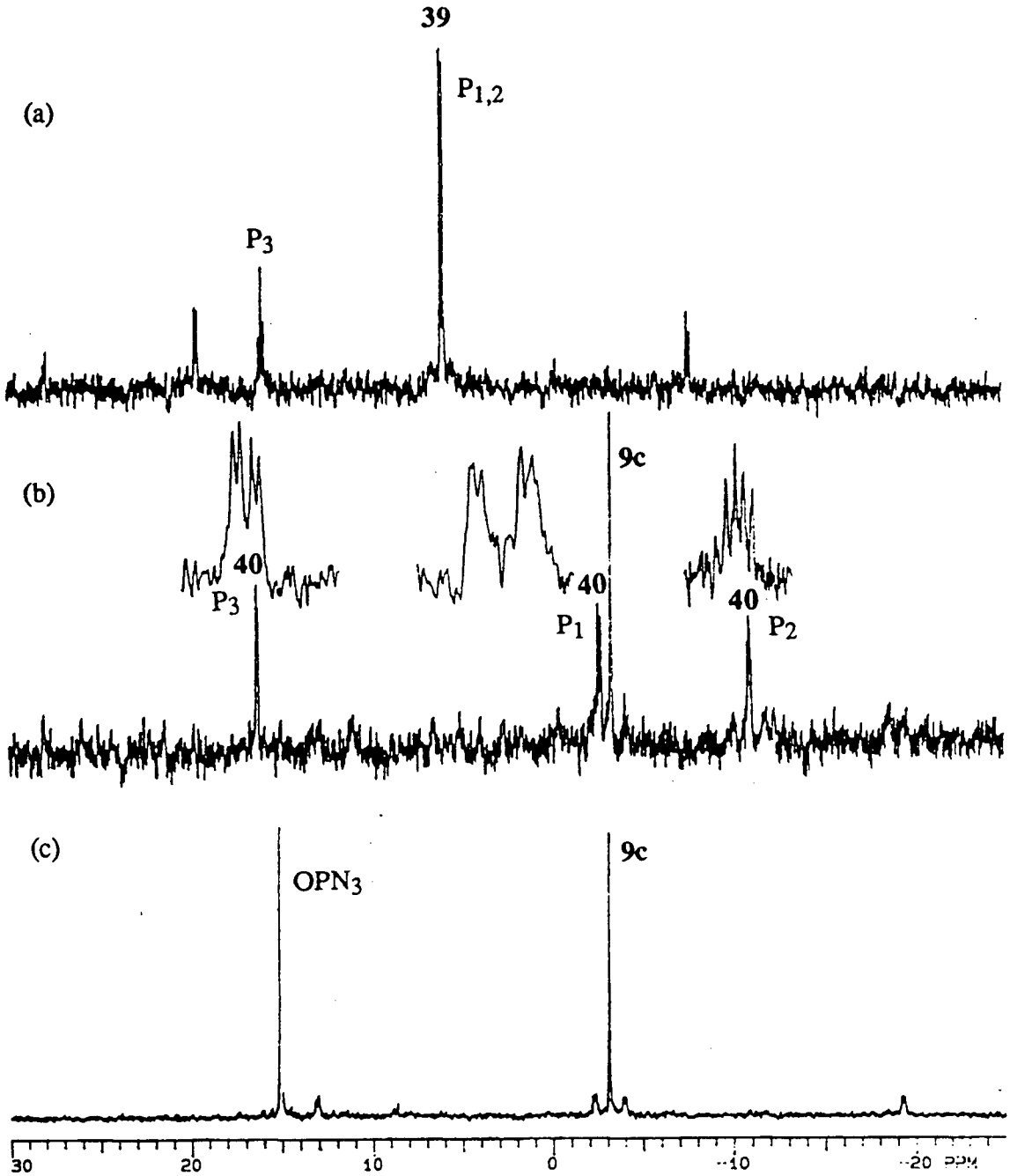

Fig. 4.24. Reaction of **10c** in air with one equivalent of PN_3, as followed by $^{31}P\{^1H\}$ NMR (121.4 MHz) spectroscopy at r.t. in $CDCl_3$. (a) immediately after addition of PN_3, (b) one week after addition of PN_3, (c) twenty days after. (**39**: $\delta_{P_{1,2}} = 6.0$ (d), $^1J_{PtP} = 3305$, $^2J_{PtP} = 126$ Hz; $\delta_{P_3} = 16.2$ (t), the Pt satellites of P_3 not being visible; $^2J_{PP} = 17.6$ Hz. **40**: see Fig. 4.26).

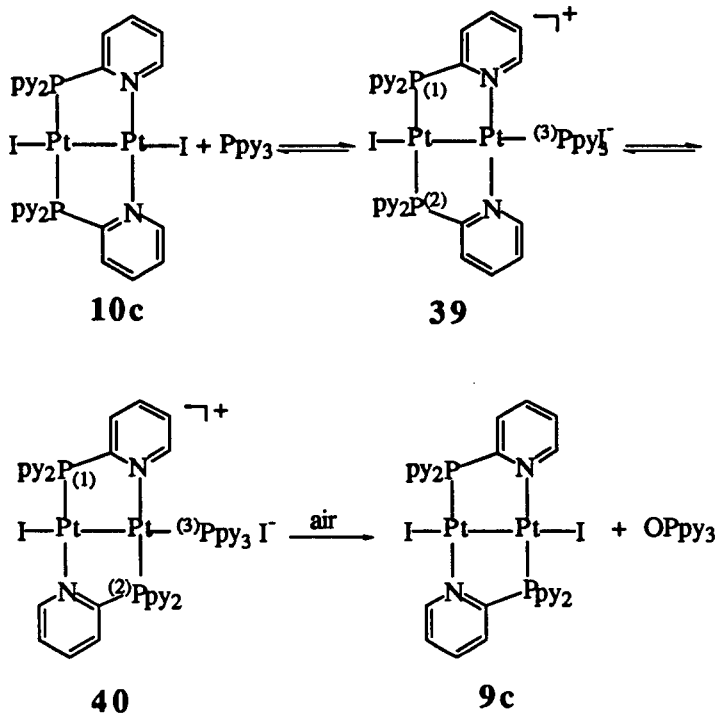

Scheme 4.3. Schematic presentation of the isomerization reaction promoted by one equivalent PN_3.

As the ratio of added phosphine to $[Pt_2]$ increases (≥ 2equiv.), the immediately formed species **41.1** has a ^{31}P NMR spectrum completely different to that of **39**; the spectrum of **41.1** in $CDCl_3$ consists of two parts — an upfield "singlet" with pseudo-first order Pt satellites and a downfield "singlet" with non-first-order Pt satellites — with equal integrals (Fig. 4.25). The upfield "singlet" is actually a triplet with some fine splitting of 5 Hz, and so is the downfield one. The upfield half of the spectrum indicates that **41.1** has at least two HT-arranged bridging phosphines, while the downfield half resembles the coupling pattern of the ^{31}P NMR spectrum of $Pt_2Cl_2(PPh_3)_2(CO)_2$ [33] ($^1J_{PtP}$ = 2189, $^2J_{PtP}$ = 475, $^3J_{PP}$ = 227 Hz) in which two phosphines are colinear with the binuclear Pt_2 core. Because of the magnetic inequivalence of four phosphorus nuclei and the quadruple broadening effect of two nitrogen nuclei, the fine splittings between cis-phosphorus atoms and between diagonally situated phosphorus atoms are not resolvable and the spectra are thus broadened. The broad peaks are not caused by fluxional behaviour of the molecule, as the low temperature ^{31}P NMR spectrum shows no improvement of

resolution. The ^{195}Pt NMR spectrum of **41.1** (Fig. 4.25b) indicates chemical equivalence of the Pt nuclei in the molecule. A tetrakisphosphine diplatinum complex is proposed with the structure shown in Scheme 4.4. The major coupling constants: $^{1}J_{PtP_1}$, $^{2}J_{PtP_2}$, $^{1}J_{PtP_3}$, $^{2}J_{PtP_4}$ and $^{3}J_{PP}$ are resolved by spectrum simulation to be 3936, 126, 2240, 750 and 220 Hz, respectively.

Compound **41.1** is not stable in CH_2Cl_2 or $CHCl_3$ in air, and gradually the phosphine is 'removed' as the oxide, and the HT complex, **9c**, is formed. The ^{31}P NMR spectrum of the species present in solution after one week consists of about 25% of **40**, while only the HT isomer **9c** is present after two weeks (Fig. 4.26). Scheme 4.4 shows a possible route for the formation of **41.1** and **9c** in solution.

The ionic nature of **41.1** is demonstrated by its large solubility in water. The tetraphenylborate salt of **41.1** was isolated and characterized as **41.2** (Sect. 2.6); the molecular conductivity measurement agrees with the presence of a 1:2 electrolyte (204.3 $\Omega^{-1}mol^{-1}cm^2$ at 1.9×10^{-3} M).[34] Complex **41.2** readily dissolves in acetone-d_6 and acetonitrile-d_3, giving a ^{31}P NMR spectrum which is the same as that of the **41.1** in $CDCl_3$; and this spectrum does not vary over a period of at least three weeks (Fig. 4.27). No decomposition was seen during an extensive purification procedure.*

Complexes **41.1** and **41.2** do not react with olefins, such as styrene, acrylonitrile and maleic acid, and no hydration of these olefins was found when **41.1** or **41.2** (~ 0.5 mM, in 1:1 acetone/H_2O mixture) was mixed with olefin substrate (~ 50 equivalents) under N_2 at 80°C for a period of 2 h.

* A recrystallization procedure from acetone generated yellow crystals of **41.2**, but unfortunately they were unsuitable for X-ray analysis.

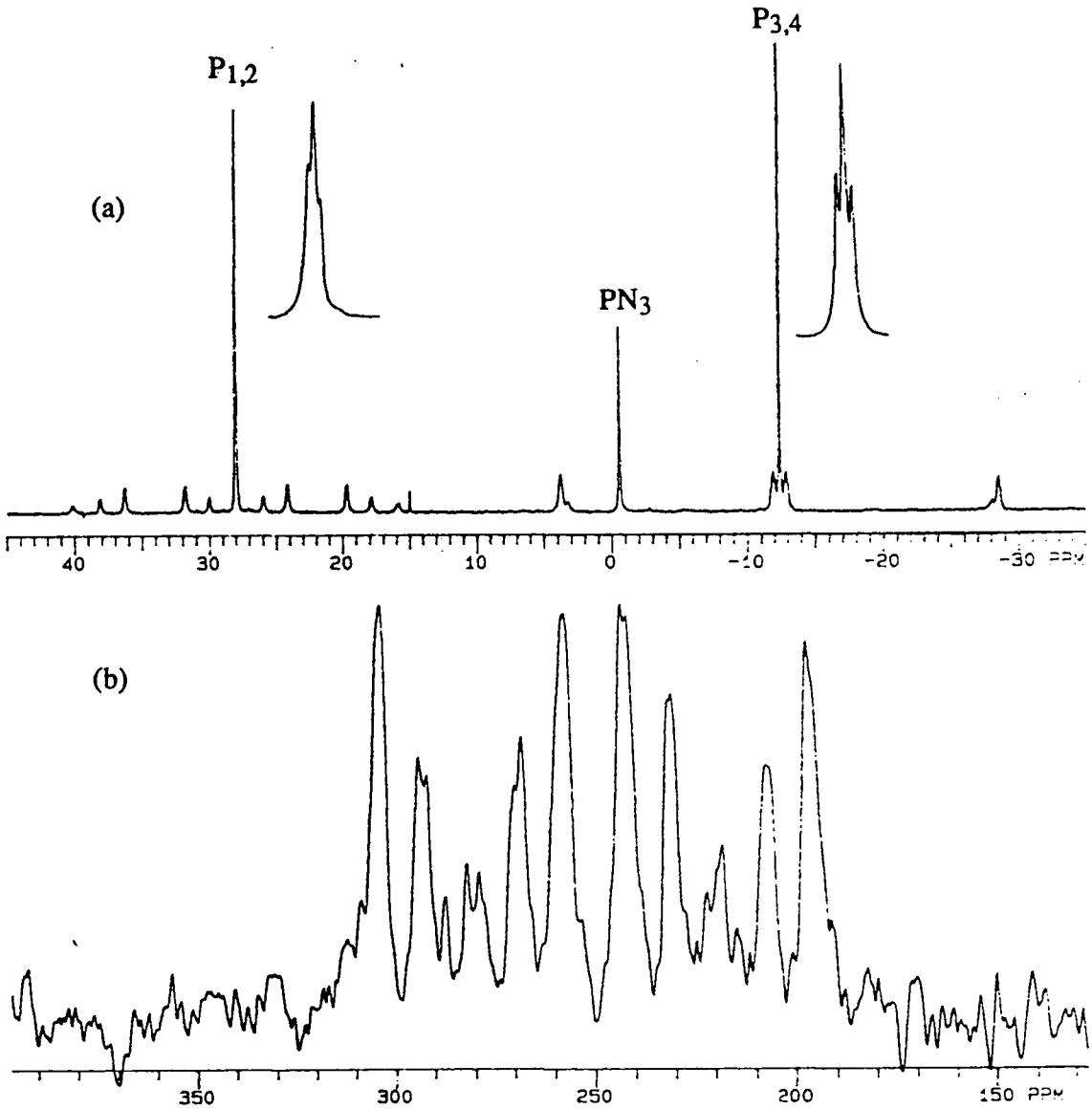

Fig. 4.25. (a) $^{31}P\{^1H\}$ NMR spectrum (121.4 MHz) of *in situ* formed $Pt_2I_2(\mu\text{-}PN_3)_2(PN_3)_2$, **41.1**, in $CDCl_3$ at r.t.: $\delta_{P_{1,2}}$ = -12.3 (t); $^1J_{PtP_1}$ = 3926, $^3J_{PtP_1}$ = 126 Hz; $\delta_{P_{3,4}}$= 27.9 (t), $^1J_{PtP_3}$ = 2240, $^2J_{PtP_3}$ = 750, $^3J_{P_3P_4}$ = 220 Hz; the two major peaks are split into a triplet with 5 Hz coupling. (b) $^{195}Pt\{^1H\}$ NMR spectrum (64.2 MHz) of **41.1** in $CDCl_3$ at r.t.: multiplets centred at 250.3, natural line width = 80 Hz.

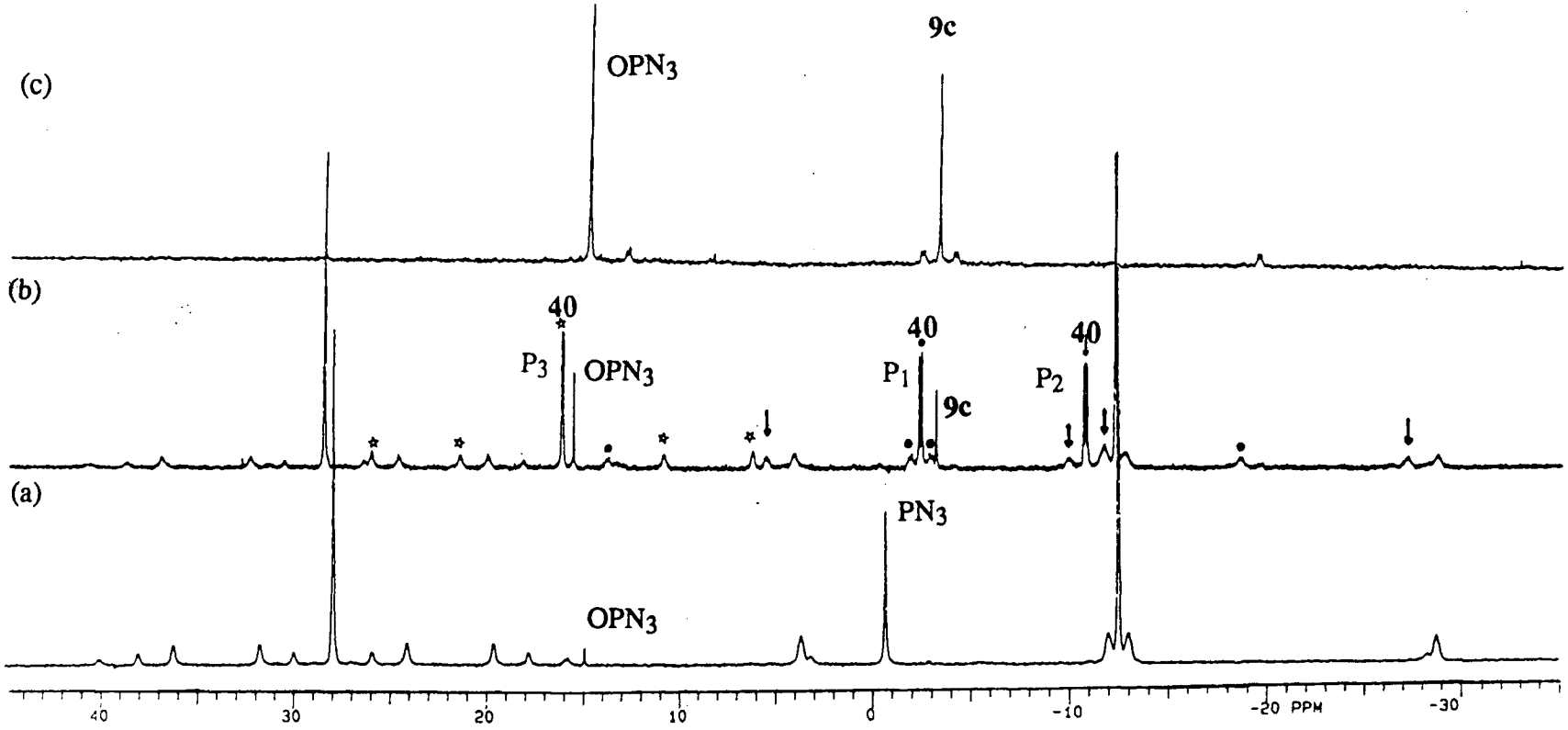

Fig. 4.26. The gradual dissociation and isomerization of **41.1** in $CDCl_3$ in air to the final product **9c**, as followed by $^{31}P\{^1H\}$ NMR spectroscopy (121.4 MHz) at r.t.: (a) immediately after addition of excess PN_3, (b) one week after addition, (c) three weeks after addition. (**40**: δ_{P_1} = -2.5 (dd), $^3J_{P_1P_2}$ = 18.3, $^3J_{P_1P_3}$= 3.6 ; $^1J_{PtP_1}$ = 3897, $^2J_{PtP_1}$ = 120 Hz; δ_{P_2} = -10.8 (dd), $^2J_{P_2P_3}$ = 9.7 ; $^1J_{PtP_2}$ = 3933, $^2J_{PtP_2}$ = 194 Hz; δ_{P_3} = 16.8 (dd), $^1J_{PtP_3}$ = 2430, $^2J_{PtP_3}$ = 550 Hz).

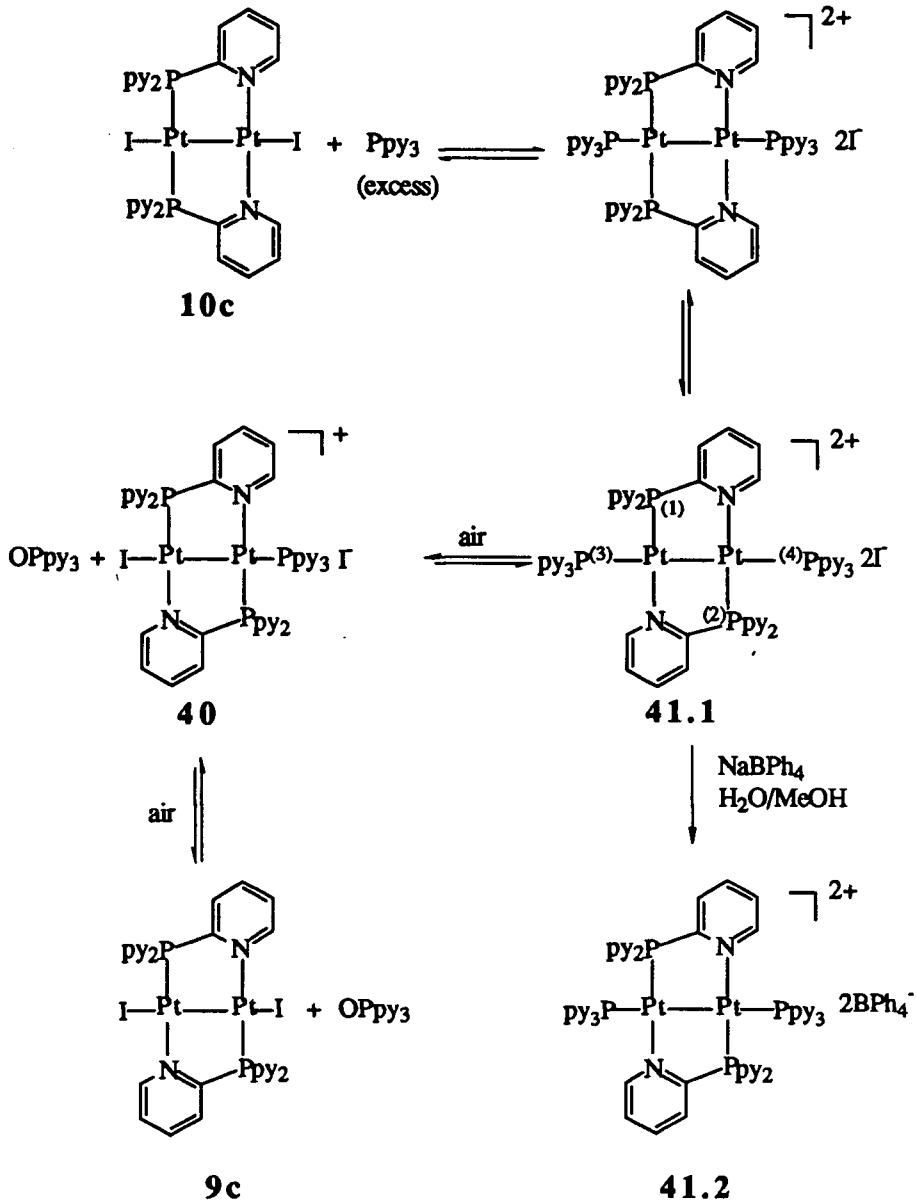

Scheme 4.4. Schematic diagram of possible reaction pathway with excess PN_3.

In conclusion, the HH configuration appears to be very stable toward frame rearrangement in the absence of added PN_3 or DMAD. The strong tendency to form the HT configuration in the presence of such reagents in air, however, suggests that the HH isomer is formed in a metastable state, and that a large kinetic barrier normally stops the isomerization in the absence of a nucleophile. Any factor which lowers this kinetic barrier will accelerate the isomerization. The fact that the HH configuration was not obtained in any Pd(I) binuclear

species is likely attributed to a low kinetic barrier under the experimental conditions for this metal which is a much more labile system. With Pd systems, even if an HH isomer is formed as an intermediate, it will soon isomerize to the HT form. On the other hand, the HT form plus PN_3 even in the Pt system, will never go to the HH configuration, because the process is thermodynamically unfavourable.

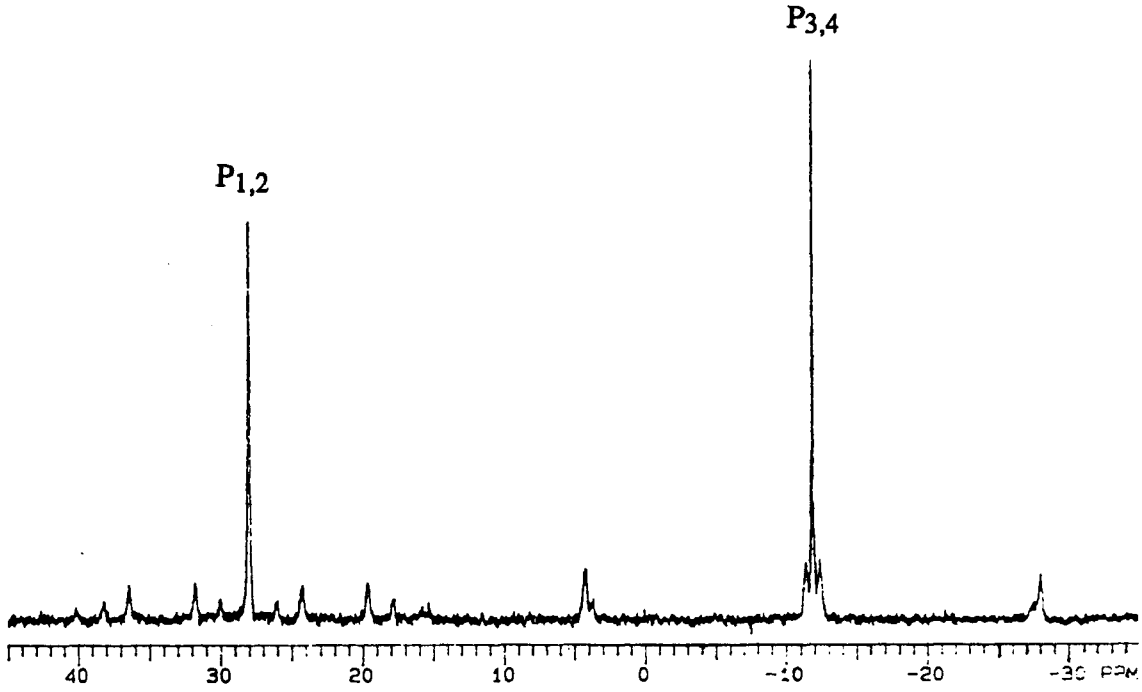

Fig. 4.27. $^{31}P\{^1H\}$ NMR spectrum of $[Pt_2(\mu\text{-}PN_3)_2(PN_3)_2](BPh_4)_2$, **41.2**, in acetone-$d_6$ at r.t. (see also Fig. 4.25).

References

1. Muetterties, E.L ; Pretzer, W.R.; Thomas, M.G.; Beier, B.F.; Thorn, D.L.; Day, V.W.; Anderson, A.B. *J. Am. Chem. Soc.*, **1978**, *100*, 2090.

2. Day, V.W.; Abdel-Meguid, S. S.; Dabestani, S.; Thomas, M.G.; Pretzer, W.R.; Muetterties, E.L. *J. Am. Chem. Soc.*, **1976**, *98*, 8289.

3. Bailey, W.I. Jr.; Cotton, F.A.; Jamerson, J.D.; Kolb. J.R. *J. Organomet. Chem.*, **1976**, *121*, C23.

4. Cotton, F.A.; Jamerson, J.D.; Stults, B.R. *J. Am. Chem. Soc.*, **1976**, *98*, 1774.

5. Sly, W.G. *J. Am. Chem. Soc.*, **1959**, *81*, 18.

6. Bennett, M.A.; Johnson, R.N.; Robertson, G.B.; Turney, T.W.; Whimp, P.O. *Inorg. Chem.*, **1976**, *15*, 97.

7. Wang, Y.; Coppens, P. *Inorg. Chem.*, **1976**, *15*, 1122 .

8. Millis, O.S.; Shaw, B.W. *J. Organomet. Chem.*, **1968**, *11*, 595.

9. Dickson, R.S.; Pain, G.N.; Mackay, M.F. *Acta Crystallogr. Sect B* , **1979**, *35*, 2321.

10. Davidson, J.L.; Harrison, W.; Sharp, D.W.A.; Sim, G.A. *J. Organomet. Chem.*, **1972**, *46*, C47.

11. Dickson, R.S.; Johnson, S.H.; Kirsch, H.P.; Lloyd, D.J. *Acta Crystallogr. Sect. B* , **1977**, *33*, 2057.

12. Balch, A.L.; Lee, C-L.; Lindsay, C.H.; Olmstead, M.M.; *J. Organomet. Chem.*, **1979**, *177*, C22.

13. Southern, T.G.; Cowie, M.A. *Inorg. Chem.*, **1982**, *21*, 246.

14. Mague, J.T. *Inorg. Chem.*, **1989**, *28*, 2215.

15. (a) Dickson, R.S.; Hames, B.W.; Cowie, M.A. *Organometallics* , **1984**, *3*, 1879. (b)*Idem.* **1985**, *4*, 852.

16. Koie, Y.; Shinoda, S.; Saito, Y.; Fitzgerald, B.; Pierpont, C.G. *Inorg. Chem.*, **1980**, *19*, 770.

17. *International Tables for X-ray Crystallography;* Ibers, J. A., Ed.; Kynoch Press: Birmingham, England, 1973 ; Vol.3, Table 4.2.2.

18. Ittel, S.D.; Ibers, J.A. *Adv. Organomet. Chem.*, **1976**, *14*, 33.

19. Maisonnat, A.; Farr, J.P.; Balch, A.L. *Inorg. Chim. Acta*, **1981**, *53*, L217, and Sect. 3.1. of this thesis.

20. Lee, C.-L.; Yang, Y-P.; James, B.R. unpublished results.

21. Kezdy, F.J.; Kaz, J.; Bruylants, A. *Bull. Soc. Chim. Belg.*, **1958**, *67*, 687.

22. (a)Swinbourne, E.S. *J. Chem. Soc.*, **1960**, 2371. (b)Manglesdorf, P.C. *J. Appl. Phys.*, **1958**, *30*, 443.

23. (a) Guggenheim, E.A. *Phil. Mag.*, **1926**, *2*, 538. (b) King, E.L. *J. Am. Chem. Soc.*, **1952**, *74*, 563.

24. Atwood, J.D. *Inorganic and Organometallic Reaction Mechanisms;* Brooks/Cole: New York, 1985; p.166.

25. Barnabas, A.F.; Sallin, D.; James, B.R. *Can. J. Chem.*, **1989**, *67*, 2009.

26. Brost, R.D.; Kimberly Freldsted, D.O.; Stobart, S.R. *Chem. Commun.*, **1989**, 488.

27. Farr, J.P.; Olmstead, M.M.; Wood, F.; Balch, A.L. *J. Am. Chem. Soc.*, **1983**, *105*, 792.

28. Farr, J.P.; Olmstead, M.M.; Balch, A.L. *Inorg. Chem.*, **1983**, *22*, 1229.

29. Mislow, K.; Roban, M. *Topics in Stereochemistry* **1977**, *1*, 1.

30. (a) Joshi, A.M.; James, B.R. *Organometallics*, **1990**, *9*, 199. (b) Krassowski, D.W.; Nelson, J.H.; Brower, K.R.; Nauenstein, D.; Jacobson, R.A. *Inorg. Chem.* **1988**, *27*, 4294.

31. Farr, J.P.; Wood, F.E.; Balch, A.L. *Inorg. Chem.*, **1983**, *22*, 3387.

32. Blau, R.J. *Energ Res. Abstr.*, **1985**, *10*, No.21297 through *C.A.* **1985**, *103*, 129835a.

33. Koie, Y.; Schinoda, S.; Saito, Y. *Inorg. Chem.*, **1976**, *20*, 4408.

34. (a) Dodd, R.E.; Robinson, P.L. *Experimental Inorganic Chemistry — A Guide to Laborotory Practice;* Elsevier: Amsterdam, 1954; p.378. (b) Geary, W.J. *Coord. Chem. Rev.*, **1971**, *7*, 81.

Chapter 5

Preparation and Reactivity of Pyridylphosphine Platinum(0) Complexes

The chemistry of the Pt(0) species, $Pt(PR_3)_m$ (m = 2, 3, 4), has been investigated in great detail since the synthesis of $Pt(PPh_3)_4$ was reported in 1958;[1] yet interest in this subject is not diminishing. Among the $Pt(PR_3)_m$ species (R = Et,[2] i-Pr,[3,4] aryl[5,6]), $Pt(PPh_3)_3$ and $Pt(PPh_3)_4$ are the most studied because they are easily handled and readily available. Even though the pyridylphosphine ligands were made forty years ago,[7] the chemistry of their platinum(0) compounds has not been investigated prior to this work. In this Chapter, the preparation of the platinum precursors $Pt(PN_3)_4$, **26c**, and $Pt(PN_1)_3$, **27a**, and their reactivities toward oxygen, olefin, HCl and methyl iodide will be discussed. By and large, the chemical behaviour of the $Pt(PN_n)_m$ species (n = 1, 3; m = 3, 4) resembles that of $Pt(PPh_3)_m$, but the differences in their reactivities with respect to this complex will be emphasized. The catalysis attempted using these platinum pyridylphosphine derivatives will be discussed at the end of this Chapter.

5.1. Platinum(0) complexes of pyridylphosphines

5.1.1. Tetrakis[tris(2-pyridyl)phosphine]platinum(0), 26c

The synthesis of $Pt(PN_3)_4$, **26c**, has been described previously in Chapter 2 (Sect. 2.8.1); **26c** is made by refluxing K_2PtCl_4 in aqueous solution with a THF solution of KOH in the presence of PN_3 ligand at temperatures higher than 60°C, or by reducing cis-$PtCl_2(PN_3)_2$, **1c**, with hydrazine in the presence of PN_3 in benzene solution. The yield in the former preparation varies from 18 to 43% with reaction time, and in the latter is about 40%. The solvents used in these reactions are critical, THF and benzene being found through trial-and-error to be the best solvents for the particular reactions, respectively. When ethanol, the solvent used for the successful preparation of $Pt(PPh_3)_4$ by either method,[8] is used in the present work, a deep red oil, which is not air-sensitive, results upon concentration and gives a complicated $^{31}P\{^1H\}$ NMR

spectrum. The role of ethanol played in these reduction reactions is unknown. The hydrazine reduction route was chosen for the larger scale preparation of **26c** because of its better reproducibility.

Sodium or potassium amalgam reduction of trans-$PtCl_2(PR_3)_2$ in THF is also known in the literature[4] for the preparation of bisphosphine and trisphosphine Pt(0) complexes. This method, however, does not yield any $Pt(PN_3)_m$ (m = 2, 3) species from a cis-$PtCl_2(PN_3)_2$ precursor. Preparation of trans-$PtCl_2(PN_3)_2$ for the starting material for the amalgam reduction (via Hg lamp photolysis of cis-$PtCl_2(PN_3)_2$ in benzene, as in the procedure for making trans-$PtCl_2(PPh_3)_2$[9]) leads to decomposition of the starting cis complex.

The $^{31}P\{^1H\}$ NMR spectrum of **26c** shows a singlet at δ 30.1 ppm, and two singlet satellites, at -20°C in CD_2Cl_2 (Fig. 5.1). The signals have relative intensities of 1:4:1, and the $^1J_{PtP}$ coupling constant is 3824 Hz, a typical value for $Pt(PR_3)_4$ tetrahedral complexes.[3] The $^{195}Pt\{^1H\}$ NMR spectrum of **26c** (Fig. 5.2) consists of a quintet centred at δ –538.3 ppm, having a $^1J_{PtP}$ coupling constant of 3839 Hz, close to the value measured from the $^{31}P\{^1H\}$ NMR spectrum. Complex **26c** certainly remains undissociated from -85° to -20°C in CD_2Cl_2, the signals beginning to broaden only around 0°C, behaviour unlike that of $Pt(PPh_3)_4$. The variable temperature $^{31}P\{^1H\}$ NMR experiment for $Pt(PPh_3)_4$, investigated by Sue in this group, shows that the 1:4:1 signal pattern of $Pt(PPh_3)_4$ can only be seen at -90°C, and the equilibrium constants for $Pt(PPh_3)_4$ dissociation into $Pt(PPh_3)_3$ and free phosphine in toluene-d_8 are 0.24 at 20°C and 0.013 M at -90°C, corresponding to 40 and 10% dissociation at 10^{-2} M, respectively.[10] Consequently, compound $Pt(PN_3)_3$, **27c**, tris[tri(2-pyridyl)phosphine]-platinum(0), cannot be made by refluxing **26c** in benzene, which is the corresponding method used for obtaining pure $Pt(PPh_3)_3$.[10] The unusual stability of **26c** was also noticed during the course of its synthesis via the hydrazine reduction method; **26c** was still the major product obtained even when the extra three equivalents of PN_3 were omitted (Sect. 2.8.1). Compound **27c** is only formed as a minor product (Fig. 5.3). The ^{31}P chemical shift, 52.9 ppm, and the

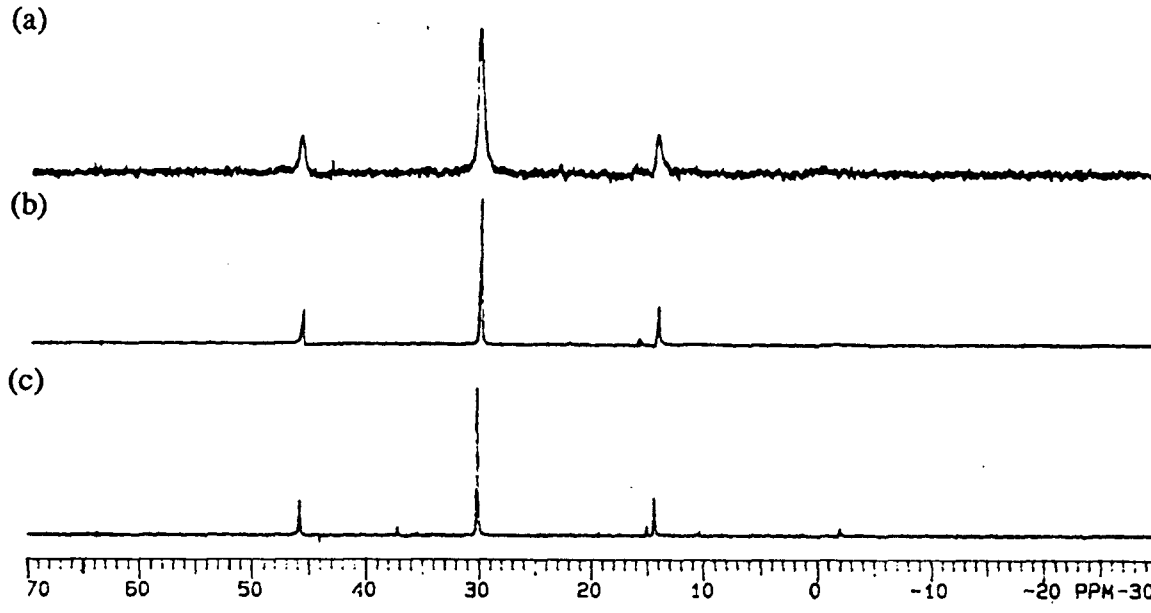

Fig. 5.1. $^{31}P\{^1H\}$ NMR spectra (121.4 MHz) of isolated $Pt(PN_3)_4$, **26c**, at $3.2x10^{-2}$ M in CD_2Cl_2 at various temperatures; (a) 0°C, (b) -20°C, (c) -85°C: δ = 30.1 (s), $^1J_{PtP}$ = 3824 Hz.

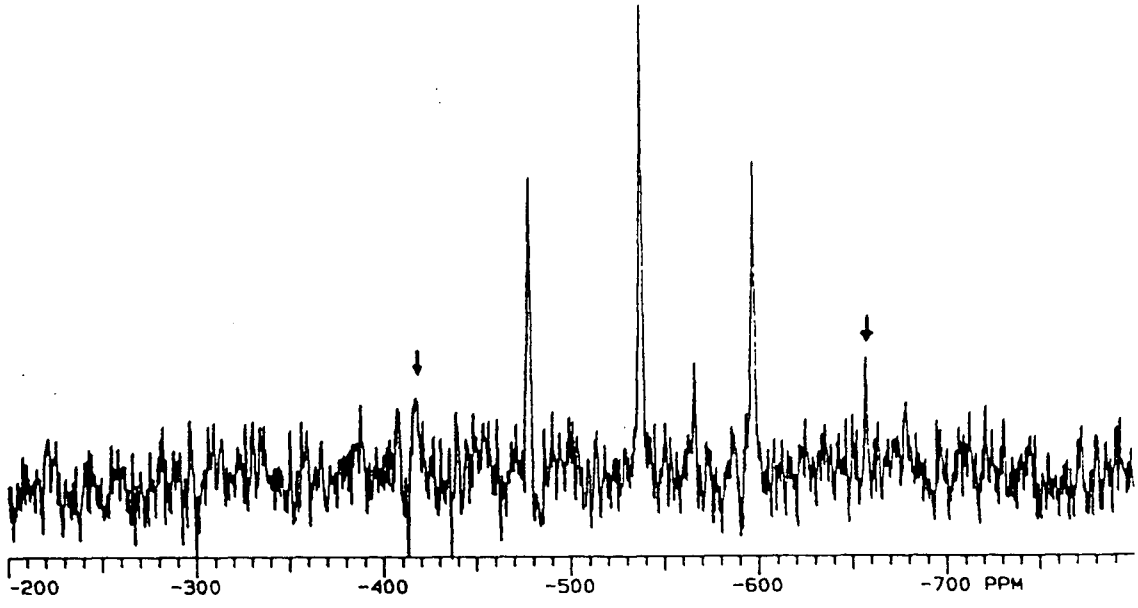

Fig. 5.2. $^{195}Pt\{^1H\}$ NMR spectrum (64.2 MHz) of **26c**, at $3.2x10^{-2}$ M in CD_2Cl_2 at -45°C: δ = -538.3 (quintet, the low intensity peaks being indicated by arrows), $^1J_{PtP}$ = 3839 Hz (the natural line width = 60 Hz).

coupling constant, 4435 Hz, for **27c** are comparable with those of $Pt(PPh_3)_3$ and $Pt(PN_1)_3$: ($Pt(PPh_3)_3$: 50.07 (s), 4449 Hz;[10] $Pt(PN_1)_3$: 52.0 (s), 4417 Hz, see below).

The $^{31}P\{^1H\}$ NMR spectra of **26c** mentioned above were recorded either immediately or within a few hours after sample preparation. Samples for $^{31}P\{^1H\}$ NMR studies were prepared under a vigorous flow of nitrogen using degassed deuterated solvents, and the sample tubes were capped with a rubber septum and then wrapped with parafilm. The original bright yellow sample solution gradually changes to finally deep red (after one week) on standing. The $^{31}P\{^1H\}$ NMR spectrum of a mixture of **26c** and **27c** after 48 h in $CDCl_3$ solution (still orange) displays a major doublet at δ_1 23.3 ppm and a major triplet at δ_2 22.5 ppm with an integration ratio of 2:1 (Fig. 5.4). The coupling constants ($^1J_{PtP_1}$, $^1J_{PtP_2}$ and $^2J_{PP}$) for the new complex are 2700, 4050 and 14 Hz, respectively. Another noticeable change in the $^{31}P\{^1H\}$ NMR spectrum is the significant enhancement of signal intensities of the free phosphine and the phosphine oxide. Tentative structures for the newly formed complex, **42**, are postulated to have a T-shaped phosphine arrangement, based on the coupling pattern and the magnitude of the coupling constants (see below for possible structures). There is no precedence in the literature for a Pt(0) (d^{10}) complex possessing a T-shaped phosphine geometry within a 3- or 4-coordinate complex. Logically, the oxidation state of compound **42** should be either I or II. The increase in the amount of phosphine oxide implies that oxygen coordination might be involved. A similar "doublet and triplet" $^{31}P\{^1H\}$ NMR pattern was reported in a spectroscopic investigation of phosphine oxidation catalyzed by Pt(0).[11] A five-coordinate, square pyramidal, trisphosphine peroxo intermediate (see (iii) below, where P = $PMePh_2$) was proposed based entirely on the $^{31}P\{^1H\}$ NMR parameters of this *in situ* formed compound, the data being indicative of a cis phosphine arrangement (δ = 13.2 (d), $^1J_{PtP_1}$ = 2740 Hz; δ = -12.7 (t), $^1J_{PtP_2}$ = 2930 Hz; $^2J_{PP}$ = 22 Hz). The oxidation of the phosphine in the presence of KOH was demonstrated by both kinetic and spectroscopic data to go via hydrogen peroxide formed *in situ*. The Pt-P coupling constants in **42** are very different from those in $Pt(PMePh_2)_3O_2$, and also no formation of such peroxo species is detected (see below).

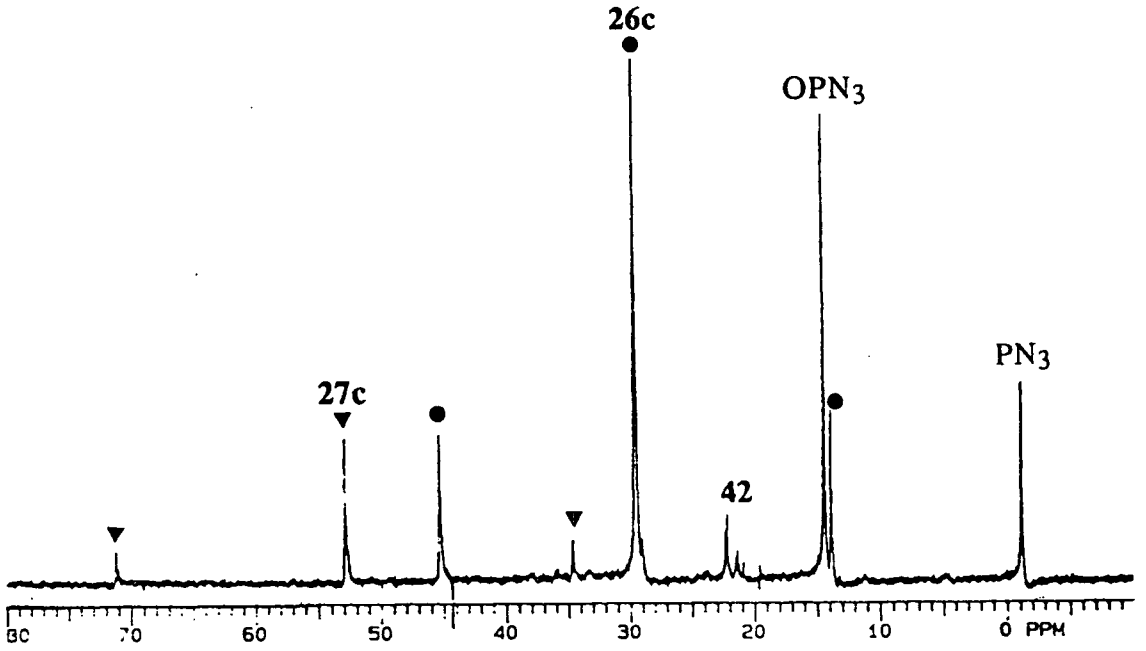

Fig. 5.3. $^{31}P\{^{1}H\}$ NMR spectrum (121.4 MHz), recorded in $CDCl_3$ at -45°C, of a freshly isolated but unpurified "$Pt(PN_3)_4$" sample formed by NH_2NH_2 reduction of cis-$PtCl_2(PN_3)_2$, **1c**, in the absence of extra PN_3 phosphine ligand: δ = 52.9 (s), $^{1}J_{PtP}$ = 4435 Hz for **27c**.

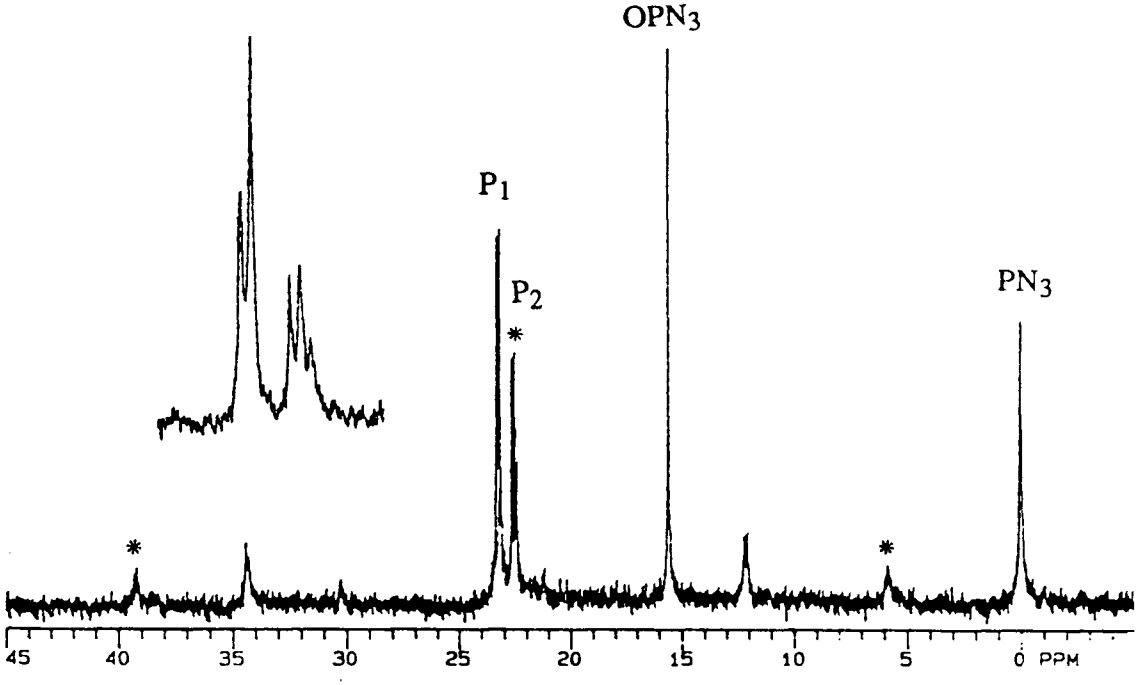

Fig. 5.4. $^{31}P\{^{1}H\}$ spectrum (121.4 MHz), recorded at -10°C, of the same sample of Fig. 5.3, after 48 h in $CDCl_3$ at -20°C; compounds $Pt(PN_3)_4$ and $Pt(PN_3)_3$ have disappeared completely. **42**: δ_{P_1} = 23.3 (d), δ_{P_2} = 22.5 (t); J_{PtP_1}, J_{PtP_2} and J_{PP} are 2700, 4050 and 14 Hz, respectively (see text).

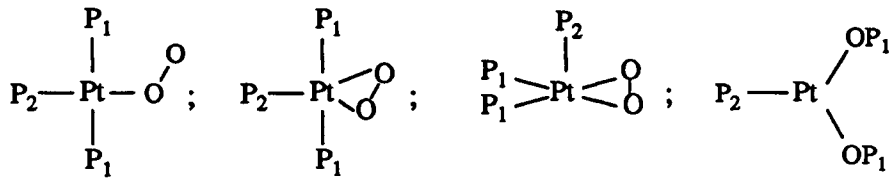

(i) (ii) (iii) (iv)

(possible structures for **42**)

Compound **42** was isolated as an orange solid from the reprecipitation of the product from hydrazine reduction of cis-**1c** (see Sect. 2.8.1). The $^{31}P\{^1H\}$ NMR spectrum of the isolated orange crystals in $CDCl_3$ shows only signals of **42** when taken immediately following sample preparation. When the solution of **42** in $CDCl_3$ was left for ten days, a dark red oil formed in the NMR tube; this sample showed only a singlet for OPN_3 in the $^{31}P\{^1H\}$ NMR spectrum. Similar chemical behaviour has been reported for triphenylphosphine platinum(0) species in the literature.[12, 13] An analogous red material was formed slowly in the presence of trace oxygen (impurity in commercial nitrogen gas[13]) and was characterized as the trinuclear $[Pt(PPh_3)_2]_3$ cluster.[12] The red oil in the present study is assumed to be a similar oligomeric platinum(0) phosphine species. The lack of a ^{31}P signal for this species is perhaps due to its low concentration because of the poor solubility of the oil. The source of oxygen in the *in situ* NMR experiment may be attributed to the slow permeation of air through the rubber septum, and in the preparatory scale, oxygen may come as the impurity in the nitrogen gas used.

Elemental analysis of the orange solid isolated fits the formulation of "$Pt(PN_3)_3O_2$" reasonably well (Sect. 2.8.1). The lack of a peroxo stretching band in the 740 - 930 cm^{-1} region[14] (Fig. 5.5) and the presence of new bands between 1093 - 1135 cm^{-1} suggest that complex **42** possibly contains a superoxo ligand((i) or (ii)). The classical superoxo metal complexes invariably bind the O_2 molecule in a "bent end-on" fashion, exhibiting an IR band between 1070 - 1200 cm^{-1}.[15] The only side-on, symmetrical bound superoxo species, characterized recently is $Tp'Co(O_2)$ (Tp' = hydridotris(3-tert-butyl-5-methylpyrazolyl)borate which has an IR band at 961 cm^{-1}.[16] Pt(0) is not a transition metal moiety favouring superoxo complex formation. Nonetheless, $Pt(PN_3)_3$ partially satisfies the general requirements: the metal must have one coordination site available and possibly a favourable one-electron oxidation

potential.[17] Compound **42** is unstable both in solution and in the solid state (a single crystal of the isolated material decomposed after a week in a grease-sealed capillary tube under N_2 atmosphere). In order to elucidate the likely role of oxygen in this reaction, a parallel reaction using pure oxygen gas (1 atm) with $Pt(PN_3)_4$ (~ 15 mg) in CH_2Cl_2 (8 mL) was performed at room temperature. There was no noticeable colour change during this reaction. The reaction was stopped after 15 min. The $^{31}P\{^1H\}$ NMR spectrum of the orange-yellow solid obtained by pumping off the solvent shows a major singlet at 18.2 ppm with the Pt-satellites (Fig. 5.6). The $^{31}P\{^1H\}$ data for this compound are comparable with those for the $Pt(PPh_3)_2O_2$ peroxo species (δ = 14.5 (s), $^1J_{PtP}$ = 4045 Hz;[10] δ = 16.4 (s), $^1J_{PtP}$ = 4059 Hz[11]). The typical IR band for peroxide is not obvious in $CDCl_3$, although a shoulder is evident at 812 cm^{-1} (Fig. 5.7); the corresponding band for the $Pt(PPh_3)_2O_2$ peroxo species is at 821 cm^{-1}. Based on these limited data, the formation of the $Pt(PN_3)_2O_2$ peroxide, **43c**, seems likely.

A superoxo structure (the more usual end-on[18, 19], or novel side-on arrangement[16]) for the unknown, supposed oxygen complex **42** is very speculative at this stage, confirmation by an X-ray crystal structure being critical. The possibility of **42** being a dinitrogen complex (a non air-sensitive, mononuclear dinitrogen complex of $Pt(AsPh_3)_3$ has been characterized recently[20]) is ruled out by the lack of a ν_{NN} stretching vibration around 2200 cm^{-1}, and also the elemental analysis which corresponds closely to that for a $Pt(PN_3)_3(O_2)$ formulation. The possibility of H_2O participation to give -OOH or -OH ligands is also ruled out by the lack of ν_{OOH} and ν_{OH} stretching vibrations around 3500-3600 cm^{-1}.

As the phosphine oxide OPN_3 is formed gradually in a relatively large quantity, the possibility of a phosphine oxide complex was examined. Balch's group has made a Pt(IV) phosphine oxide complex of OPN_1 ($PtBr_4(OPN_1)$, see below), this showing a ν_{PO} band at 1115 cm^{-1} (the band of the free phosphine oxide is seen at 1180 cm^{-1}).[21] The ^{31}P NMR spectrum of this Pt(IV) complex shows a singlet at 25.4 ppm with no Pt satellites being seen, this being attributed to the weak interaction between the Pt and P atoms separated by an O atom (the ^{31}P signal for the free OPN_1 is seen at 21.4 ppm).[21] The ^{31}P resonance of free OPN_3 is at 15.7 ppm, and the resonances at 23.3 and 22.5 ppm could be those of coordinated phosphine oxide,

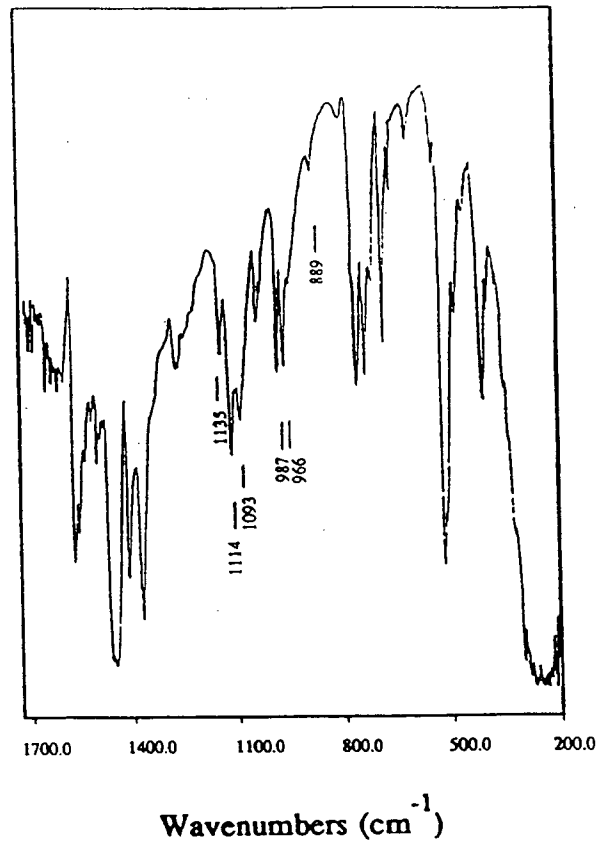

Fig. 5.5. Infrared spectrum of **42c** in Nujol.

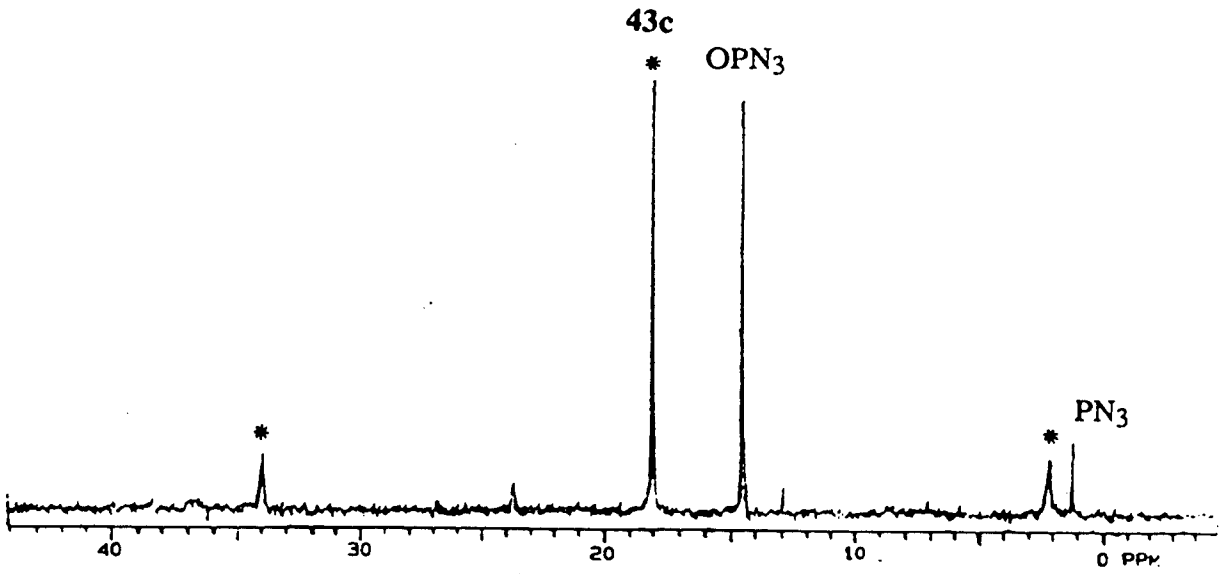

Fig. 5.6. $^{31}P\{^{1}H\}$ NMR spectrum (121.4 MHz) in $CDCl_3$ at r.t of an *in situ* reaction product formed from $Pt(PN_3)_4$ with pure oxygen gas: $\delta = 18.2$ (s), $^{1}J_{PtP} = 3848$ Hz for $Pt(PN_3)_2O_2$, **43c**.

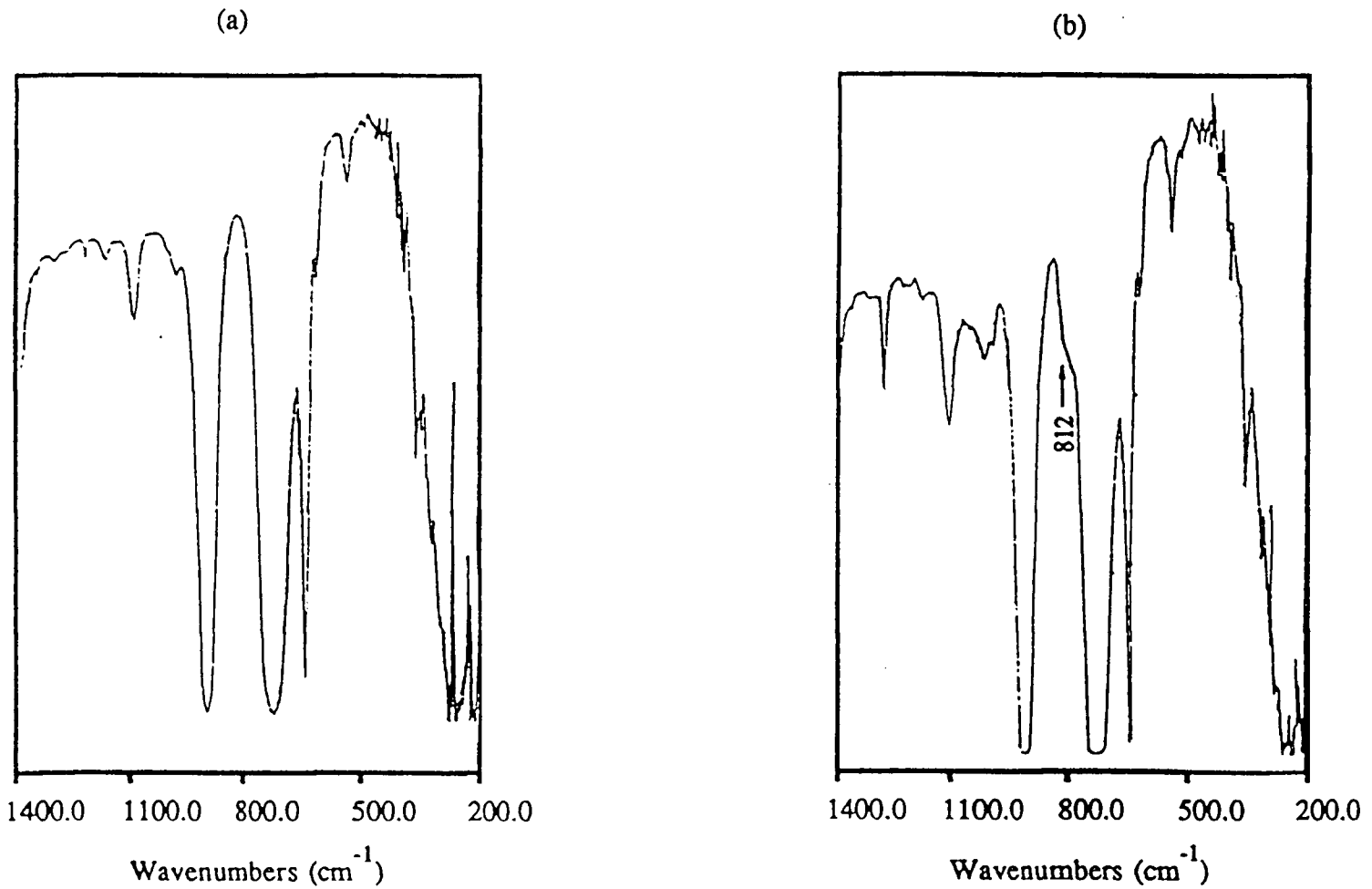

Fig. 5.7. (a) Infrared spectrum of solvent $CDCl_3$; (b) infrared spectrum of $Pt(PN_3)_2O_2$, **43c**, in $CDCl_3$ at r.t.

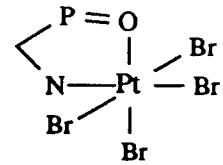

particularly in view of the IR band at 1114 cm^{-1} (Fig. 5.5). A possible structure of the Pt(0) phosphine oxide complex is depicted as (iv) (see above). The doublet in the $^{31}P\{^1H\}$ NMR spectrum could then be assigned to the two equivalent phosphorus atoms of coordinated OPN_3. The relatively small J_{PtP} value of 2700 Hz (compared to values of ~3800 Hz in $Pt(PN_3)_4$ and ~4400 Hz in $Pt(PN_3)_3$) would then be attributed to a two-bond Pt-P coupling, and the J_{PP} value of 14 Hz to a three-bond coupling. However, the evidence against this assignment is the value of the $^2J_{PtP}$ coupling, because the corresponding value in the $PtBr_4(OPN_1)$ species was reported to be too small to be resolved.[21] Further, the hard nature of the oxygen of the phosphine oxide ligand makes such oxygen coordination at a soft centre such as Pt(0) unlikely.

The different products formed from the oxygen reactions of **26c** may be caused by two different reaction pathways. Complex **26c** reacts quickly with oxygen molecules under O_2 atmosphere to form the peroxide **43c**. On the other hand, the formation of **42** occurs much more slowly, and is also solvent dependent, being promoted by chlorinated solvents, CH_2Cl_2 (or CD_2Cl_2), $CDCl_3$. Toluene-d_8 does not promote the formation of **42**, as demonstrated by the $^{31}P\{^1H\}$ NMR spectrum of **26c** taken one week after the sample preparation (Fig. 5.8).

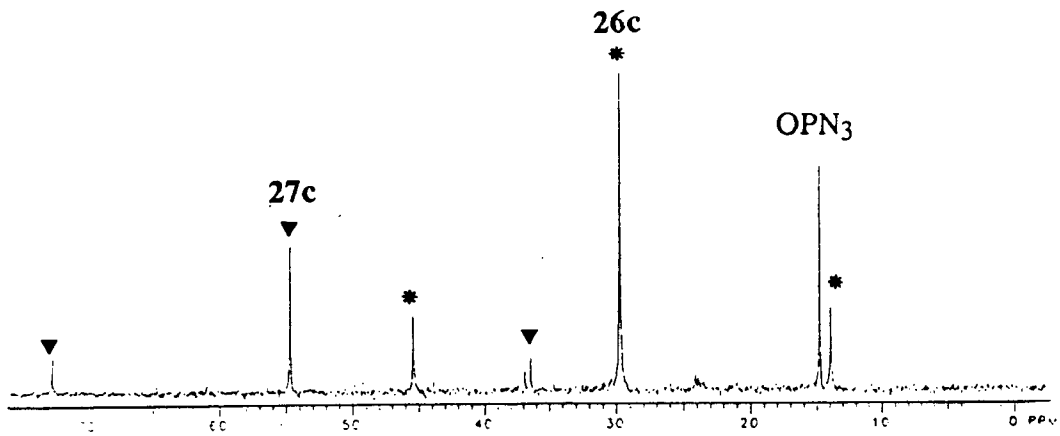

Fig. 5.8. $^{31}P\{^1H\}$ NMR spectrum (121.4 MHz), recorded at -50°C, of **26c** in toluene-d_8 after a week being stored in a freezer at -20°C.

5.1.2. Tris[2-(diphenylphosphino)pyridine]platinum(0), **27a**

The synthesis of $Pt(PN_1)_3$, **27a**, has been described in Sect. 2.8 2, the purity of the isolated product being dependent on the used phosphine concentration. A mixture of tetrakis- and tris-phosphine platinum(0) species resulted if the ratio of phosphine to platinum used was between 4 and 6.5.

The $^{31}P\{^1H\}$ NMR spectrum in CD_2Cl_2 at -50°C of **27a** contains a singlet at 52.0 ppm and two singlet satellites (Fig. 5.9); the coupling constant J_{PtP} is 4417 Hz which is typical of a $Pt(PR_3)_3$ trigonal planar complex.[3] The $^{195}Pt\{^1H\}$ NMR spectrum of **27a** reveals a quartet centred at δ -300.3 ppm at -45°C in $CDCl_3$ with a coupling constant $^1J_{PtP}$ of 4433 Hz (Fig. 5.10). An attempt was made to isolate the tetrakis PN_1 compound, $Pt(PN_1)_4$ **26a**, by adding five equivalents of PN_1 ligand (~ 60 mg, 0.23 mmol) of the tetrakis and tris species to a mixture at room temperature, with limited success: although in a solution of **27a** containing excess free ligand PN_1, **26a** is detected as a major singlet at 25.6 ppm ($^1J_{PtP}$ 3910 Hz) (Fig. 5.11), a precipitation procedure again produces the mixture of the tetrakis and tris Pt(0) species. The coupling constant and the chemical shift of **26a** are similar to those of $Pt(PN_3)_4$, **26c**. The reason for the unusually high coordination shifts for both tetrakis phosphine platinum(0) species, **26a** ($\Delta\delta$ = 28.1 ppm) and **26c** ($\Delta\delta$ = 29.8 ppm), compared to those of other four-coordinate complexes $Pt(PR_3)_4$, $\Delta\delta \approx$ 4.6 to 13.8 ppm,[3, 10, 22] is not understood.

The $^{31}P\{^1H\}$ NMR spectrum of **27a** after 48 h at -20°C indicates that more than two thirds of the $Pt(PN_1)_3$ complex is decomposed in $CDCl_3$ (Fig. 5.12). Three major, new, platinum containing complexes in addition to **27a** are seen: one has a singlet at 20.5 ppm with Pt satellites at 31.2 and 9.65 ppm ($^1J_{PtP}$ = 2616 Hz) and could be trans-$PtCl_2(PN_1)_2$ [cf. trans-$PtCl_2(PPh_3)_2$, 20.6 (s), $^1J_{PtP}$ = 2634 Hz[23]]; the second one has a singlet at 13.0 ppm with Pt satellites at 29.2 ppm and -3.1 ppm ($^1J_{PtP}$ = 3921 Hz) and is possibly a peroxo species, $Pt(PN_1)_2O_2$, **43a**, (cf. $Pt(PN_3)_2O_2$ **43c**: 18.2 (s), $^1J_{PtP}$ = 3848 Hz, Fig. 5.6; $Pt(PPh_3)_2O_2$, 14.5 (s), $^1J_{PtP}$ = 4045 Hz[10,11]); the third compound whose ^{31}P NMR signals are centred at 30.1

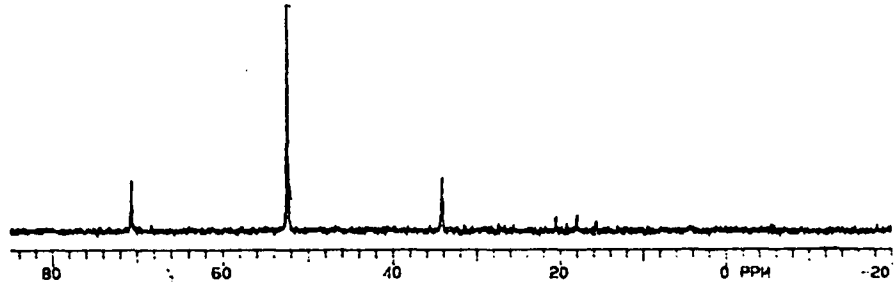

Fig. 5.9. $^{31}P\{^1H\}$ NMR spectrum (121.4 MHz) of $Pt(PN_1)_3$, **27a**, at $4.5x10^{-2}$ M in CD_2Cl_2 at -50°C: δ = 52.0 (s), $^1J_{PtP}$ = 4417 Hz.

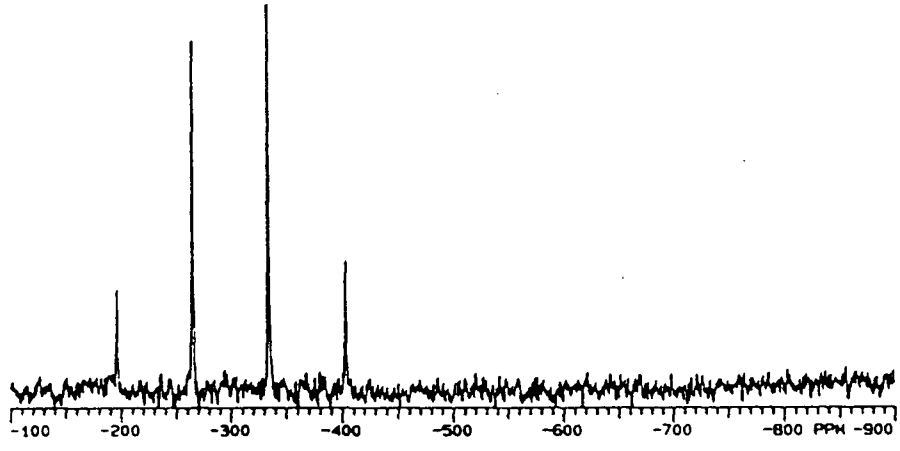

Fig. 5.10. 64.2 MHz $^{195}Pt\{^1H\}$ NMR spectrum of **27a** at $4.5x10^{-2}$ M in $CDCl_3$ at -45°C: δ = -300.3 (quartet), $^1J_{PtP}$ = 4433 Hz (the natural line width is 40 Hz).

26a

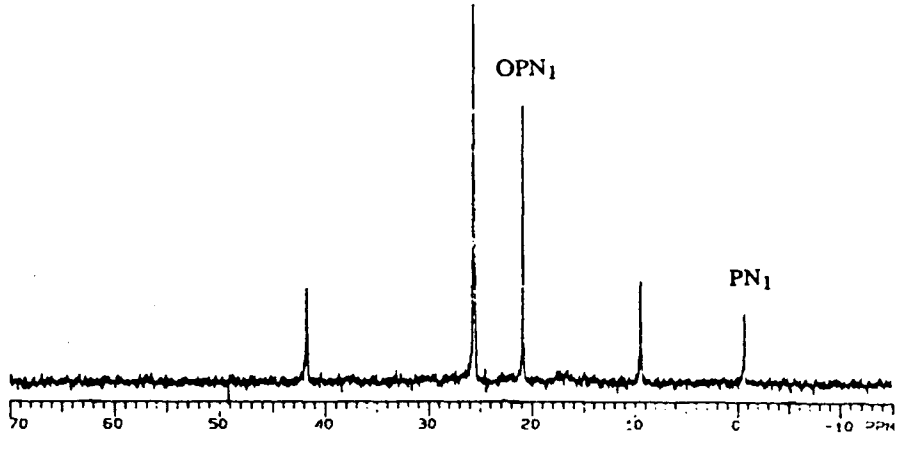

Fig. 5.11. $^{31}P\{^1H\}$ NMR spectrum (121.4 MHz) of the *in situ* formed $Pt(PN_1)_4$, **26a**, in $CDCl_3$ at -45°C: δ = 25.6 (s), $^1J_{PtP}$ = 3910 Hz.

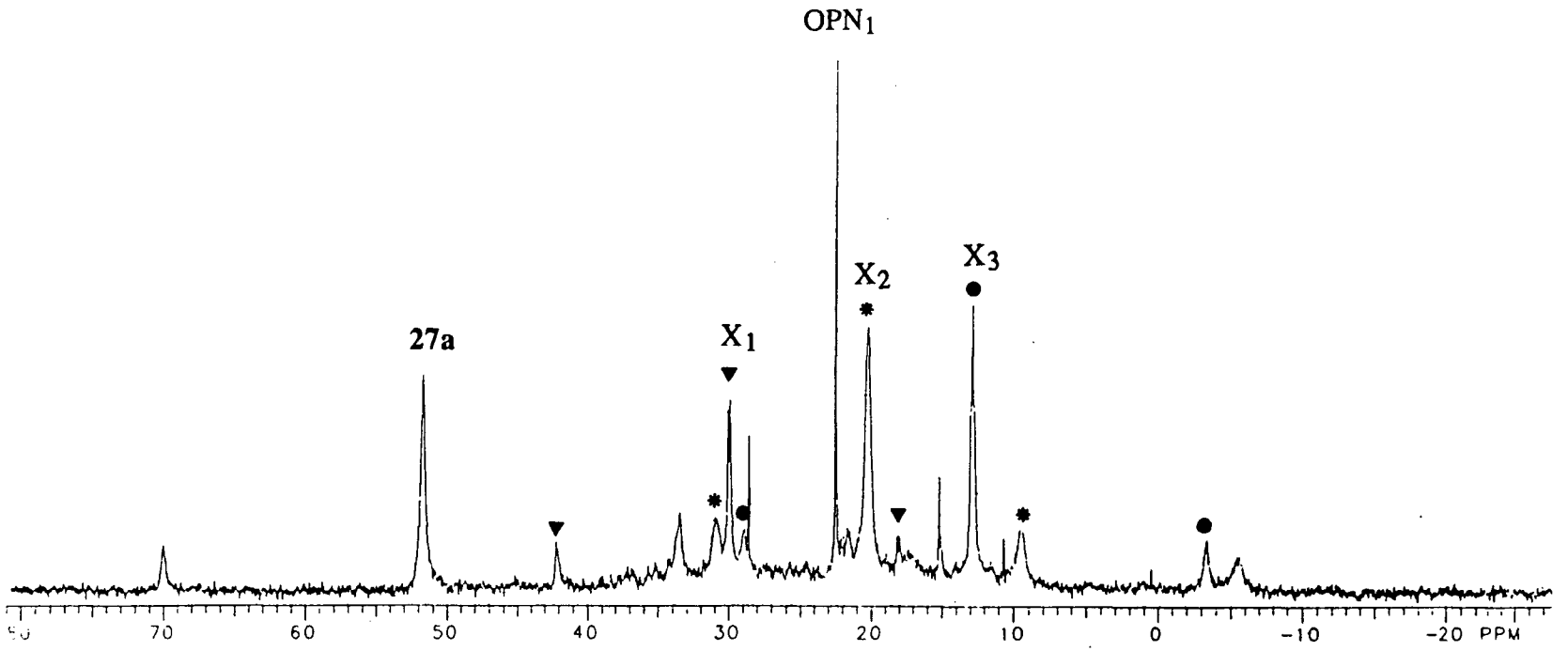

Fig. 5.12. Decomposition of $Pt(PN_1)_3$ in $CDCl_3$ after 48 h at -20°C shown by the $^{31}P\{^1H\}$ NMR spectrum ($CDCl_3$, -20°C). X_1: "$HPtCl(PN_1)_2$", see Fig. 5.20a; X_2: trans-$PtCl_2(PN_1)_2$, X_3: $Pt(PN_1)_2O_2$, **43a**: δ = 13.0 (s), $^1J_{PtP}$ = 3921 Hz.

ppm as a doublet with satellites at 42.2 and 18.0 pm (J_{PtP} = 2938 Hz) has parameters very similar to those of the trans-$Pt(H)Cl(PN_1)_2$ complex which will be discussed in Sect. 5.3.1 (30.2 (d), $^1J_{PtP}$ = 3023 Hz, Fig. 5.20a). The decomposition of $Pt(PN_1)_3$ is clearly complicated; no analog of $Pt(PN_3)_3O_2$, **42**, is detected. The formation of trans-$Pt(H)Cl(PN_1)_2$ and trans-$PtCl_2(PN_1)_2$ may be rationalized by the presence of HCl, Cl_2 and $COCl_2$ impurities produced by the light-promoted chloroform oxygen reaction.[24]

5.2. Characterization of olefin complexes of 2-(diphenylphosphino)-pyridine and tris(2-pyridyl)phosphine

5.2.1. Acrylonitrile, methacrylonitrile and crotonitrile complexes (**44a**, **44c**, **45a**, **46a**)

Syntheses of these olefin complexes have been described in detail in Chapter 2, Sect. 2.8.3.1. Although satisfactory chemical analyses were not obtained for complexes **44a** - **46a**, because of the loss of olefin in drying procedures, the ^1H and $^{31}P\{^1H\}$ NMR spectroscopic evidence (Table 5.1) unambiguously reveals that these complexes are essentially square-planar with a cis-phosphine arrangement (see below). For instance, the $^{31}P\{^1H\}$ NMR spectrum of $Pt(PN_1)_2(\eta^2\text{-}CH_2CHCN)$, **44a**, contains a major AB quartet and the corresponding Pt satellites with a phosphorus-to-phosphorus coupling of 34.7 Hz, typical of cis-phosphorus coupling (Fig. 5.13). Carbon C^1 probably has a stronger trans influence than does the C^2 carbon atom. Therefore, the downfield half of the AB quartet is assigned to P^2 which has the platinum-phosphorus coupling of 3969 Hz; the upfield half of the AB quartet is then due to the resonance of P^1 which has the smaller platinum-phosphorus coupling, 3445 Hz. The $^{31}P\{^1H\}$ NMR spectrum at 25°C shows that **44a** is non-fluxional, implying that the bonding between Pt and the hydrocarbon is more like the metallocyclic structure shown, than a π-bonded olefin structure which more readily allows for rotation of olefin around the Pt-olefin bond. Strong Pt d-π-back donation is also indicated by the multiplets at 2.0 and 3.8 ppm in the ^1H NMR spectrum of the coordinated acrylonitrile (free acrylonitrile appears as a multiplet between 5 - 6 ppm); strong olefin-to-metal σ-donation via the olefin π molecular orbital would result in a downfield shift of the olefinic protons to around 7 ppm.[25, 26]

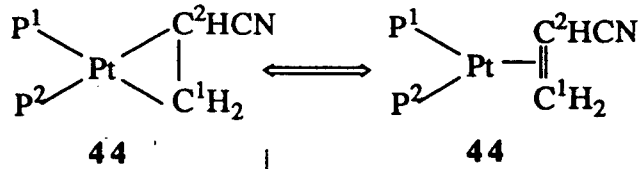

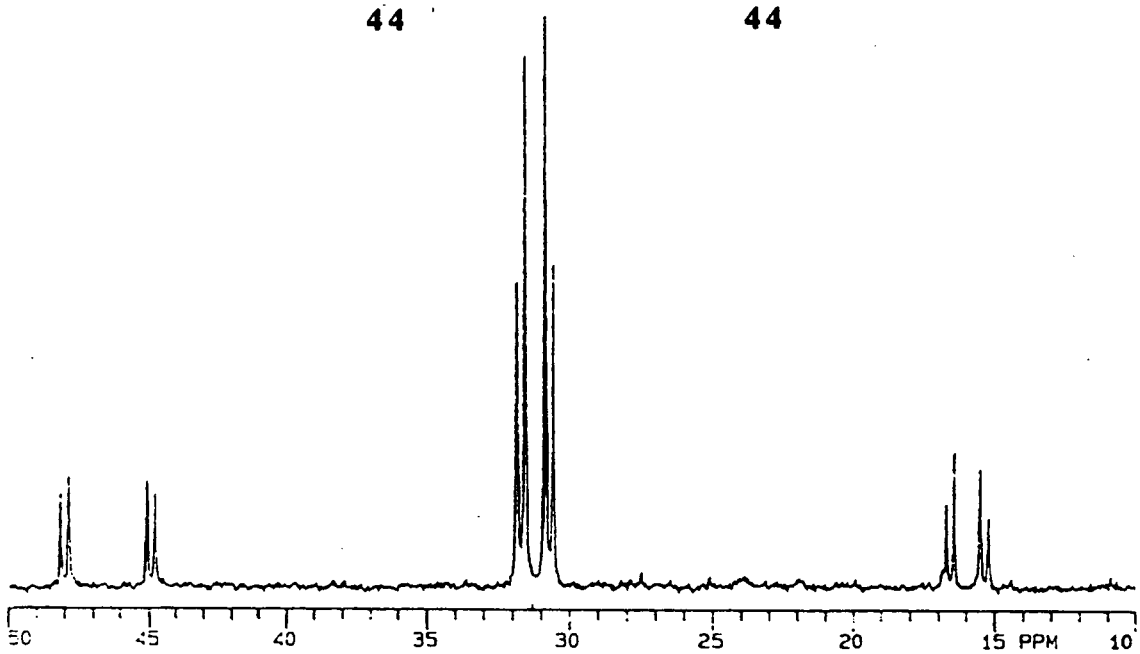

Fig. 5.13. $^{31}P\{^1H\}$ NMR spectrum (121.4 MHz) of $Pt(PN_1)_2(\eta^2\text{-}CH_2CHCN)$, **44a**, in $CDCl_3$ at 25°C (data are given in Table 5.1).

Table 5.1. $^{31}P\{^1H\}$ NMR Parameters of Compounds **44a** - **46a** in $CDCl_3$[a]

Complexes	Temp. (°C)	δ_{P1}	δ_{P2}	$^1J_{PtP1}$	$^1J_{PtP2}$	$^2J_{PP}$
$Pt(PN_1)_2(\eta^2\text{-}CH_2CHCN)$, **44a**	25	30.7	31.7	3445	3969	34.7
$Pt(PN_3)_2(\eta^2\text{-}CH_2CHCN)$, **44c**	-45	34.6	35.4	3406	3934	31.9
$Pt(PN_1)_2(\eta^2\text{-}CH_2C(CH_3)CN)$, **45a**	25	31.3	31.3	3538	3718	35.2
$Pt(PN_1)_2(\eta^2\text{-}CH(CH_3)CHCN)$, **46a.1**	25	31.8	32.6	3265	4095	38.5
$Pt(PN_1)_2(\eta^2\text{-}CH(CH_3)CHCN)$, **46a.2**	25	31.6	32.1	3240	4086	39.4

(a) The chemical shifts and coupling constants are in ppm and Hz, respectively.

The platinum(0) precursor $Pt(PN_3)_4$, **26c**, forms a complex with acrylonitrile, **44c**, whose $^{31}P\{^1H\}$ NMR spectrum (Table 5.1) contains also an AB quartet (with satellites) similar to that seen in Fig. 5.13, and the complex is considered to possess the same geometry as **44a**.

The Pt(0)-methacrylonitrile complex $Pt(PN_1)_2(\eta^2\text{-}CH_2C(CH_3)CN)$, **45a**, displays a distinct $^{31}P\{^1H\}$ NMR spectrum containing a very intense singlet at 31.3 ppm and symmetric AB quartets as Pt-satellites (Fig. 5.14a). The "accidental equivalence" of the two chemically different phosphines in **45a** is disrupted upon cooling the system to -20°C when the central singlet splits into a very close AB quartet (Fig. 5.14b). The P-P coupling constant in the AB quartet, arising from inequivalent phosphorus atoms, is 35.2 Hz which is similar to that of compound **44a**. The $^1J_{PtP_1}$ and $^1J_{PtP_2}$ values are found to be 3718 and 3538 Hz, respectively. The difference (180 Hz) is small compared to the difference in **44a** (524 Hz), this presumably reflecting the similar electron densities at the two olefinic carbon atoms: the electron density on the carbon with the electron withdrawing CN group and electron donating CH_3 group appears comparable with that on the methylene carbon, which consequently leads to similar trans influences imposed by the two carbon fragments. By inference, the difference in the two Pt-P coupling constants within the crotonitrile complexes **46a.1** or **46a.2** should be the largest among **44a**, **44c**, **45a** and **46a.1**/ **46a.2** (see below).

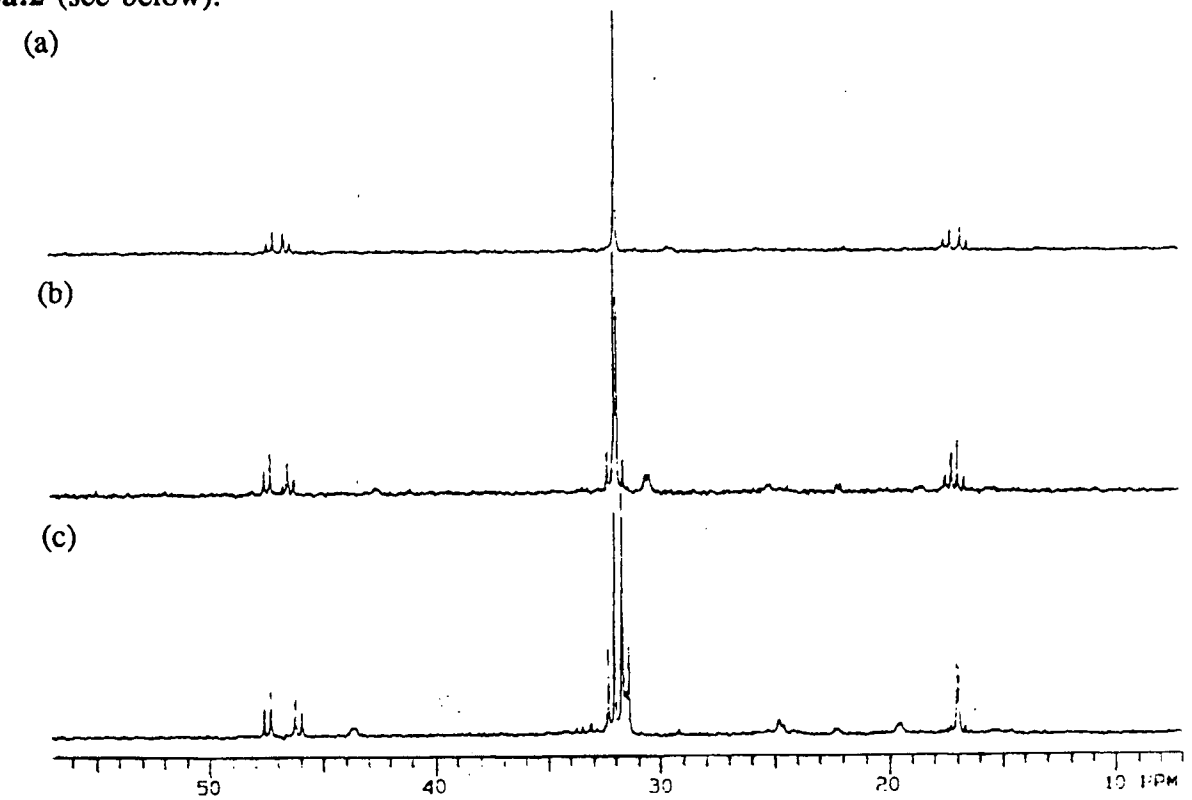

Fig. 5.14. $^{31}P\{^1H\}$ NMR spectra (121.4 MHz) of $Pt(PN_1)_2(\eta^2\text{-}CH_2C(CH_3)CN)$, **45a**, in $CDCl_3$ at various temperatures, (a) r.t., (b) -20°C, (c) -45°C; see Table 5.1.

When $Pt(PN_1)_3$, **27a**, is treated with a mixture of cis and trans crotonitrile, two product isomers are obtained (Sect. 2.8.3). The $^{31}P\{^1H\}$ NMR spectrum of this mixture basically consists of two sets of signals, each set composed of an AB quartet and the corresponding Pt satellites (Fig. 5.15). These two complexes **46a.1** and **46a.2** do not interconvert at room temperature. The peaks labelled with an asterisk (*) belong to one complex which has a major AB quartet centred at 32.2 ppm and the corresponding Pt-satellites ($^1J_{PtP_1}$, $^1J_{PtP_2}$ and $^2J_{PP}$ are 3265, 4095 and 38.5 Hz, respectively); the unlabelled resonances belong to a second complex with an AB quartet centred at 31.9 ppm and Pt-satellites ($^1J_{PtP_1}$, $^1J_{PtP_2}$ and $^2J_{PP}$ are 3240, 4086 and 39.4 Hz, respectively). The average difference of 840 Hz between $^1J_{PtP_1}$ and $^1J_{PtP_2}$, the largest among **44a** - **46a**, is attributed to the large difference in electron densities of the olefinic carbon atoms (see above) because one has the electron-withdrawing CN substituent and the other has the electron-donating methyl group. The $^{31}P\{^1H\}$ NMR spectra of Pt(0) complexes with prochiral olefins have not been reported before. The splitting pattern in the ^{31}P NMR signals in these complexes (**44a** - **46a**) strongly supports the assigned square-planar geometry.

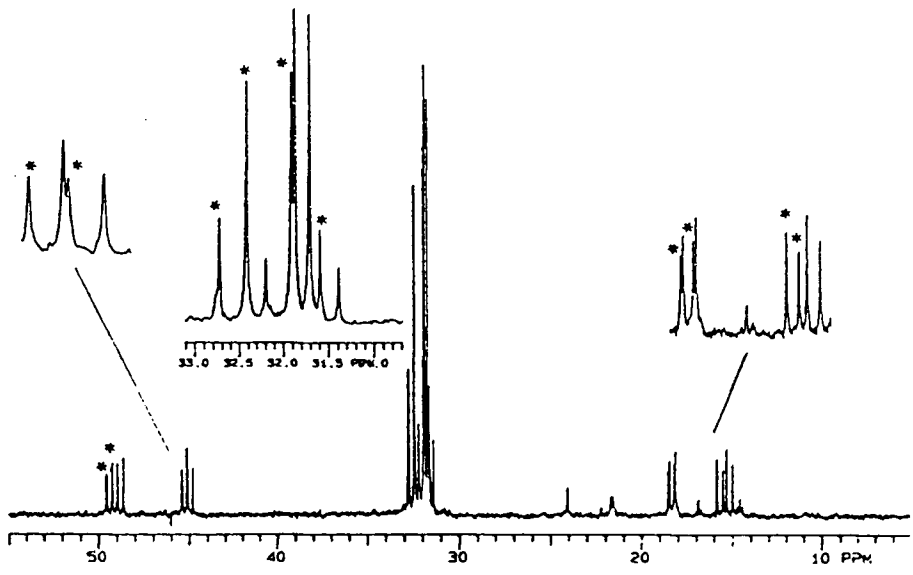

Fig. 5.15. $^{31}P\{^1H\}$ NMR spectrum (121.4 MHz) of $Pt(PN_1)_2(\eta^2\text{-}(CH_3)CHCHCN)$ in $CDCl_3$ at 25°C; peaks labelled with * belong to **46a.1**, unlabelled peaks belong to **46a.2**, see Table 5.1. No assignment regarding the geometry of the coordinated olefin for **46a.1** and **46a.2** is made.

5.2.2. Maleic anhydride (MA) and diethyl maleate (DEMA) complexes **47a**, **47c**, **48a**

Syntheses of $Pt(PN_1)_2(MA)$, **47a**, $Pt(PN_3)_2(MA)$, **47c**, and $Pt(PN_1)_2(DEMA)$, **48a**, have been described in Sect. 2.8.3.2. The reaction of diethyl maleate with $Pt(PN_1)_3$, **27a**, was carried out in diethyl ether; the addition of DEMA was done carefully to obtain a solid product, because excess DEMA results in the formation of a white, colloidal product. Reactions of MA or DEMA with the Pt(0) complexes were noticably more rapid than the nitrile reactions possibly because activation by the two carboxylate groups is greater than that by the one CN group. The geometries of these olefinic complexes are characterized using NMR techniques. The $^{31}P\{^1H\}$ NMR spectra of these complexes are not as informative as those of **44a** - **46a** because MA and DEMA are symmetric. For instance, the ^{31}P NMR spectrum of **47a**, shown in Fig. 5.16b, contains a major singlet at 27.0 ppm, indicating that the two P nuclei are equivalent. Although the coupling constant value of 3841 Hz implies a cis-phosphine geometry (cf. trans-$PtI_2(PN_2)_2$, $^1J_{PtP}$ = 2500 Hz, Table 3.1), whether the geometry of this molecule is square-planar or tetrahedral cannot be assertained from the ^{31}P data. Fig. 5.16a shows the ^1H NMR spectrum of **47a**: a pseudo triplet of doublets centred at 3.45 ppm is assigned to the olefinic protons of the coordinated maleic anhydride, which have shifted upfield by 3.65 ppm upon coordination.[18] The shift to high field is similar to that observed for complex **44a**. This infers that the olefin bonding in **47a** and **44a** is perhaps similar. This shift is caused by the increase of electron density on the carbon atom to which the olefinic protons are attached. These protons resonances, split by the adjacent ^{31}P into a doublet ($^3J_{PH}$ = 8.0 Hz) and by the ^{195}Pt into a larger doublet ($^2J_{PtP}$ = 60.0 Hz), are similar in position to those of the protons on saturated sp^3 carbon atoms, perhaps reflecting a lowering of the C-C bond order.

The maleic anhydride complex $Pt(PN_3)_2(MA)$, **47c**, formed from **26c** and MA (Sect. 2.8.3.3), is assumed to have a geometry similar to that of **47a**. The ^{31}P NMR data of **47c** are given in Table 5.2.

Table 5.2. $^{31}P\{^1H\}$ and ^1H NMR Parameters of **47a** - **48a**[a]

Complexes	δ_P	δ_H	J_{PtP}	J_{PtH}	J_{PH}
$Pt(PN_1)_2(MA)$, **47a**	27.0	3.45	3841	60.0	8.0
$Pt(PN_3)_2(MA)$, **47c**	32.3	—	3836	—	—
$Pt(PN_1)_2(DEMA)$, **48a.1**	30.0	—	3750	—	—
$Pt(PN_1)_2(DEFM)$, **48a.2**	28.1	—	3815	—	—

a) The spectra are recorded in $CDCl_3$ at r.t.; the chemical shifts are in ppm and the coupling constants are in Hz.

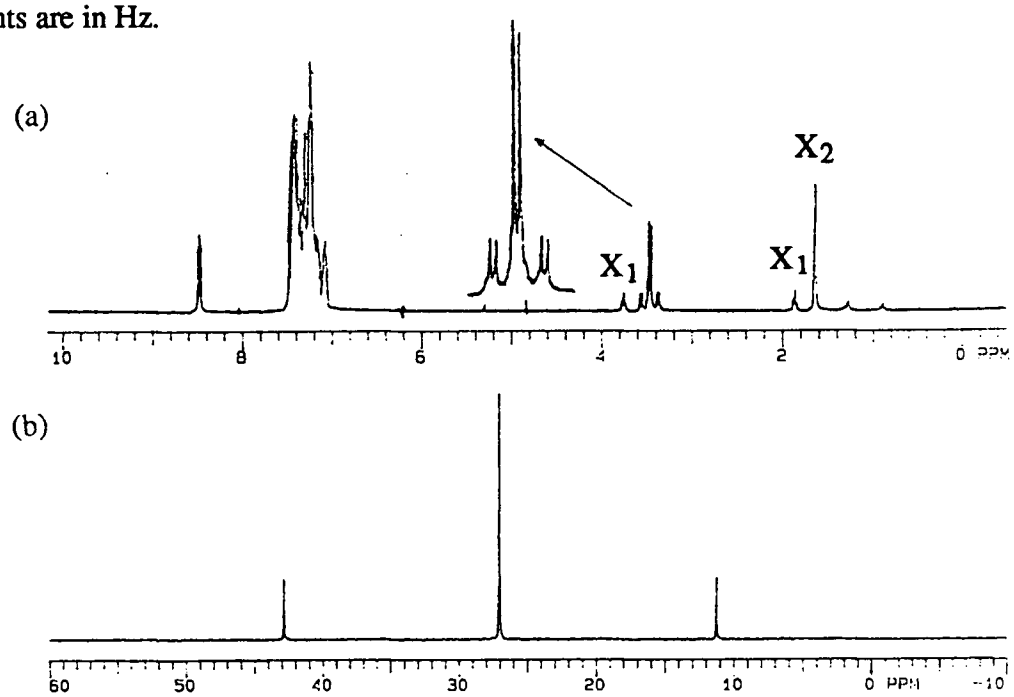

Fig. 5.16. ^1H (300 MHz) and $^{31}P\{^1H\}$ (121.4 MHz) NMR spectra of $Pt(PN_1)_2(MA)$, **47a**, in $CDCl_3$ at r.t. (a) ^1H NMR: $\delta = 3.45$ (d), $^2J_{PtP} = 60.0$, $^3J_{PH} = 8.0$ Hz; X_1 are signals due to Et_2O and X_2 is the H_2O peak in $CDCl_3$. (b) $^{31}P\{^1H\}$ NMR: $\delta = 27.0$ (s), $^1J_{PtP} = 3841$ Hz.

The $^{31}P\{^1H\}$ NMR spectrum of the isolated $Pt(PN_1)_2(DEMA)$ (DEMA = diethyl maleate), **48a.1**, at room temperature in $CDCl_3$ unexpectedly consists of two sets of signals with relative integration ratio 1:1.2 — the singlet at 30.0 ppm with coupling constant $^1J_{PtP}$ of about 3750 Hz and another singlet at 28.1 ppm with a $^1J_{PtP}$ of 3815 Hz (Fig. 5.17b). The mother solution, as indicated by the ^{31}P NMR spectrum, contains the same two compounds, but at remarkably different concentrations. The reaction of $Pt(PN_1)_3$ with DEMA initially (~ 20 min) gives one major compound (Fig. 5.17a), which on standing slowly converts to another species

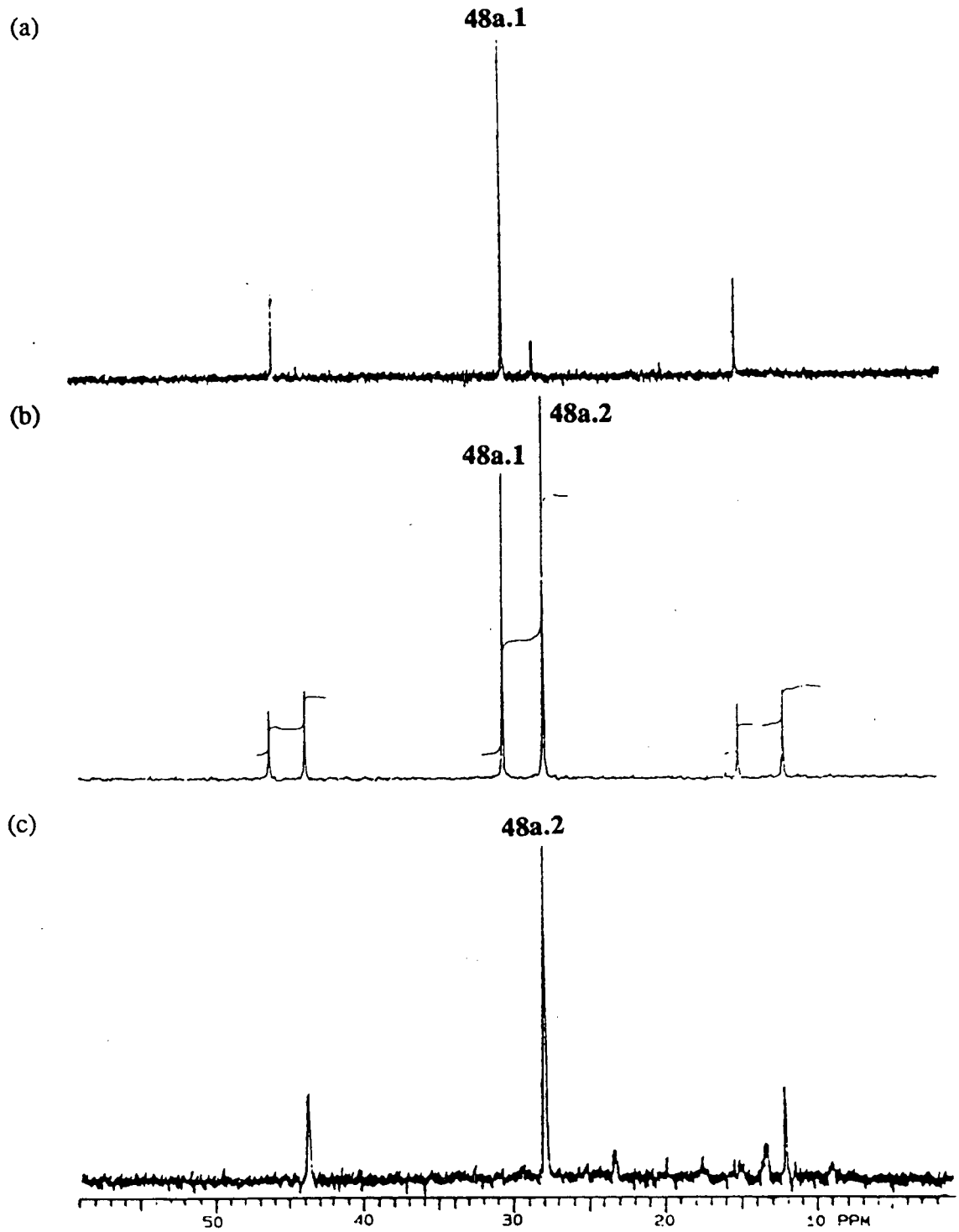

Fig. 5.17. $^{31}P\{^{1}H\}$ NMR spectra (121.4 MHz) of complexes **48a.1** and **48a.2** in $CDCl_3$. (a) the initial (20 min) *in situ* reaction product from $Pt(PN_1)_3$ **27a** + DEMA at -20°C. (b) the isolated white crystals of the $Pt(PN_1)_2$(DEMA) **48a.1** and $Pt(PN_1)_2$(DEFM) **48a.2** mixture at r.t. (c) the initial (10 min) *in situ* reaction product from **27a** + DEFM at -20°C. Data are given in Table 5.2.

whose ^{31}P signal is centred at 28.1 ppm. Isomerization of the coordinated olefin is involved. This is confirmed by the formation of $Pt(PN_1)_2(DEFM)$ (DEFM = diethyl fumarate), **48a.2**, *in situ* by reacting **27a** with DEFM: the single species formed immediately (~ 10 min) has the same ^{31}P NMR chemical shift and $^1J_{PtP}$ coupling constant as the isomerization product from **48a.1**; **48a.2** does not isomerize for 72 h in solution. A similar cis-trans isomerization of maleate to fumarate ester catalyzed by $Co_2(CO)_8$ complex has been reported recently by Ungváry.[27]

5.2.3. An ethylene complex **49a**

The ethylene complex, $Pt(PN_1)_2(\eta^2\text{-}CH_2CH_2)$, **49a**, was formed *in situ* by introducing via a syringe ethylene gas at 1 atm (2 mL) into a toluene-d_8 solution (1mL, ~7.0×10^{-3} M) of $Pt(PN_1)_3$, **27a**, in an NMR tube filled with N_2. The solution turned from yellow to colourless for reactions at room temperature. The $^{31}P\{^1H\}$ NMR spectrum of this colourless solution at -85°C (Fig. 5.18) showed the formation of new species whose ^{31}P parameters are very similar to those of $Pt(PPh_3)_2(\eta^2\text{-}CH_2CH_2)$ reported in the literature (δ = 32.5 (s), $^1J_{PtP}$ = 3694 Hz at -80°C in toluene-d_8).[22] On warming up to room temperature, the same sample gave a very broad peak centred at 26 ppm because species **27a** and **49a** exchange very rapidly according to (Eq. 5.1) in the presence of free PN_1 ligand. This exchange behaviour has also been observed in $Pt(PPh_3)_2(\eta^2\text{-}CH_2CH_2)$ system.

$$\underset{\textbf{27a}}{Pt(PN_1)_3} + CH_2{=}CH_2 \underset{\text{toluene-}d_8}{\rightleftharpoons} \underset{\textbf{49a}}{Pt(PN_1)_2(\eta^2\text{-}CH_2CH_2)} + PN_1 \qquad (5.1)$$

The $Pt(PN_3)_4$ species, **26c**, does not react with ethylene under the same conditions, as indicated by the $^{31}P\{^1H\}$ NMR spectrum of **26c** which remains unaltered after an attempted reaction .

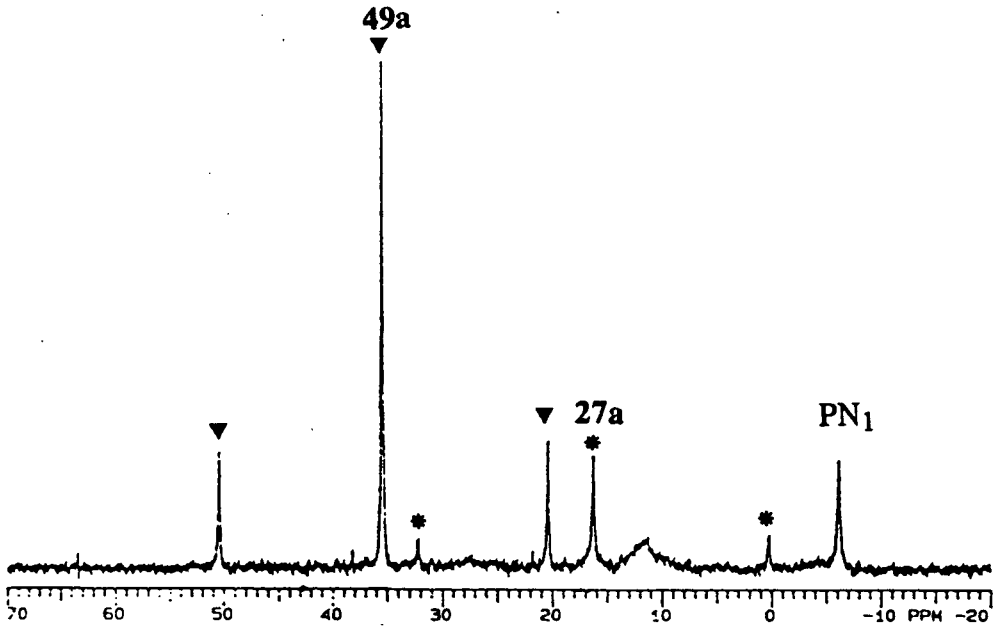

Fig. 5.18. $^{31}P\{^1H\}$ NMR spectrum (121.4 MHz) recorded at -85°C in toluene-d_8 of the Pt(0) ethylene adduct $Pt(PN_1)_2(\eta^2\text{-}CH_2CH_2)$, **49a**, formed *in situ* at r.t.: δ = 35.5 (s), $^1J_{PtP}$ = 3654 Hz.

In conclusion, $Pt(PN_3)_4$, **26c**, and $Pt(PN_1)_3$, **27a**, react with activated olefins in ways similar to the triphenylphosphine Pt(0) complexes $Pt(PPh_3)_2$ or $Pt(PPh_3)_3$; in the case of ethylene and DEMA, $Pt(PN_3)_4$ appears to be less reactive. The geometries of all the olefinic complexes made here are unambiguously square-planar, based on the $^{31}P\{^1H\}$ and ^1H NMR spectroscopic data. The square-planar geometry in these platinum olefin complexes infers that there is strong π-back-donation from the Pt to olefin which lessens the electron density on the platinum, of the formal oxidation state zero. As a result, the coordinated olefin is reduced to a nearly saturated state. This is consistent with the molecular orbital interpretation of the bonding between platinum and olefin in such complexes; that is, a negligible σ olefin to metal bond and a strong π metal to olefin bond.[28] The C-C distance in the tetracyanoethylene complex $Pt(PPh_3)_2[C_2(CN)_4]$ (1.52 Å[28a], 1.49Å[28b]) is stretched 0.21 or 0.18 Å compared to that in free TCNE, and is closer to a single C-C bond distance. By analogy, the C-C bond distances in the olefin complexes made here are likely to approximate those of a single bond.

5.3. Reactions of $Pt(PN_1)_3$ and $Pt(PN_3)_4$ with HCl

5.3.1. Reaction of $Pt(PN_1)_3$ with HCl

Oxidative addition of HCl to Pt(0) phosphine complexes generally yields trans-hydridochlorobisphosphineplatinum(II) species.[29, 30] A white crystal isolated using $Pt(PN_1)_3$ as reactant (Sect. 2.8.4.1) was analyzed to be trans-$Pt(H)Cl(PN_1)_2$, **50a**. The complication described in Sect. 2.8.4.1, regarding the necessity of removing excess HCl because of protonation of the pyridyl group, is not apparent in the triphenylphosphine system.[10, 30]

The hydride resonance in the ^1H NMR spectrum of **50a** appears at -16.32 ppm as a resolved pseudo triplet of triplets at room temperature, due to coupling to the ^{195}Pt nucleus and two equivalent ^{31}P nuclei (Fig. 5.19). The signals at 1.76 ppm and 3.73 ppm can be assigned to the presence of solvated THF in the crystal lattice, the integration of these signals corresponding to one half mole of THF per platinum complex. The microanalysis results for the hydrogen and nitrogen improve significantly based on the formula trans-$Pt(H)Cl(PN_1)_2 \cdot 1/2C_4H_8O$ (calcd. for $C_{36}H_{33}ClN_2O_{0.5}P_2Pt$: C 54.44, H 4.19, N 3.53; found: C 54.01, H 4.31, N 3.34). The Pt-H IR band at 2212 cm^{-1} (Nujol) is similar to those found for trans-$Pt(H)Cl(PPh_3)_2$ in the literature (2209, 2217 and 2210 cm^{-1} in refs. 10, 29 and 30, respectively). The original $^{31}P\{^1H\}$ NMR spectrum of **50a** showed a major doublet with corresponding doublet platinum satellites; the separation between the major doublet is ~12.0 Hz (Fig. 5.20a) which is indicative of phosphorus-hydride coupling (see Fig. 5.19). The appearance of the doublet in the $^{31}P\{^1H\}$ NMR spectrum was indeed due to the insufficient decoupling power applied to suppress the interference of the hydride; this coupling was suppressed by applying a stronger decoupling power (Fig. 5.20b).

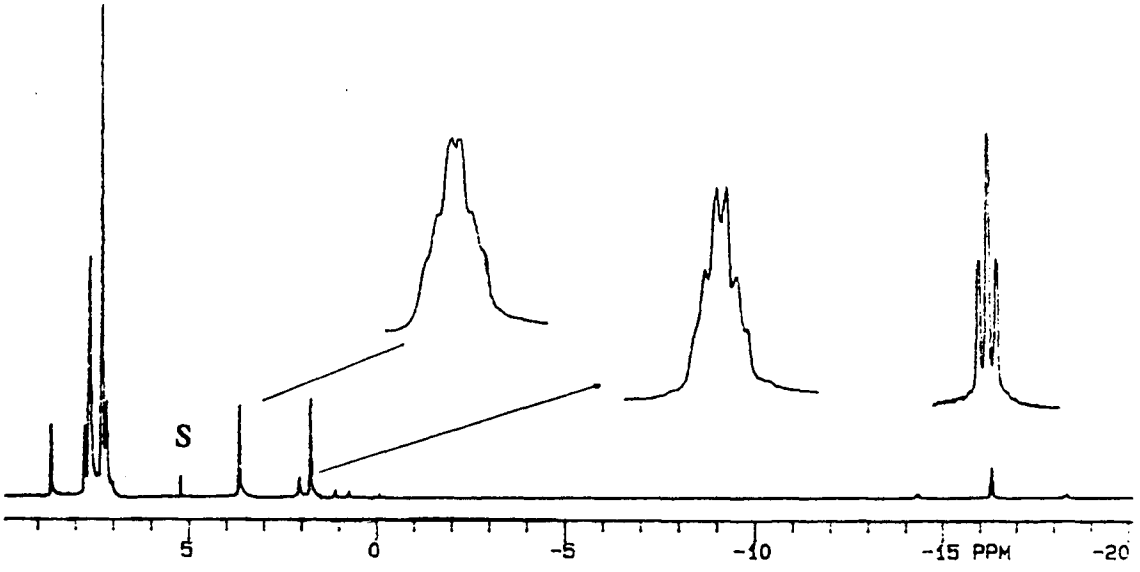

Fig. 5.19. ^1H NMR spectrum (300 MHz) of trans-Pt(H)Cl(PN_1)$_2$, **50a**, in CD_2Cl_2 at r.t.: δ(hydride) = -16.32 (t), $^2J_{PtH}$ = 1213, $^3J_{PH}$ = 12.7 Hz. Free THF is seen as multiplets at 1.76 and 3.73. S = solvent.

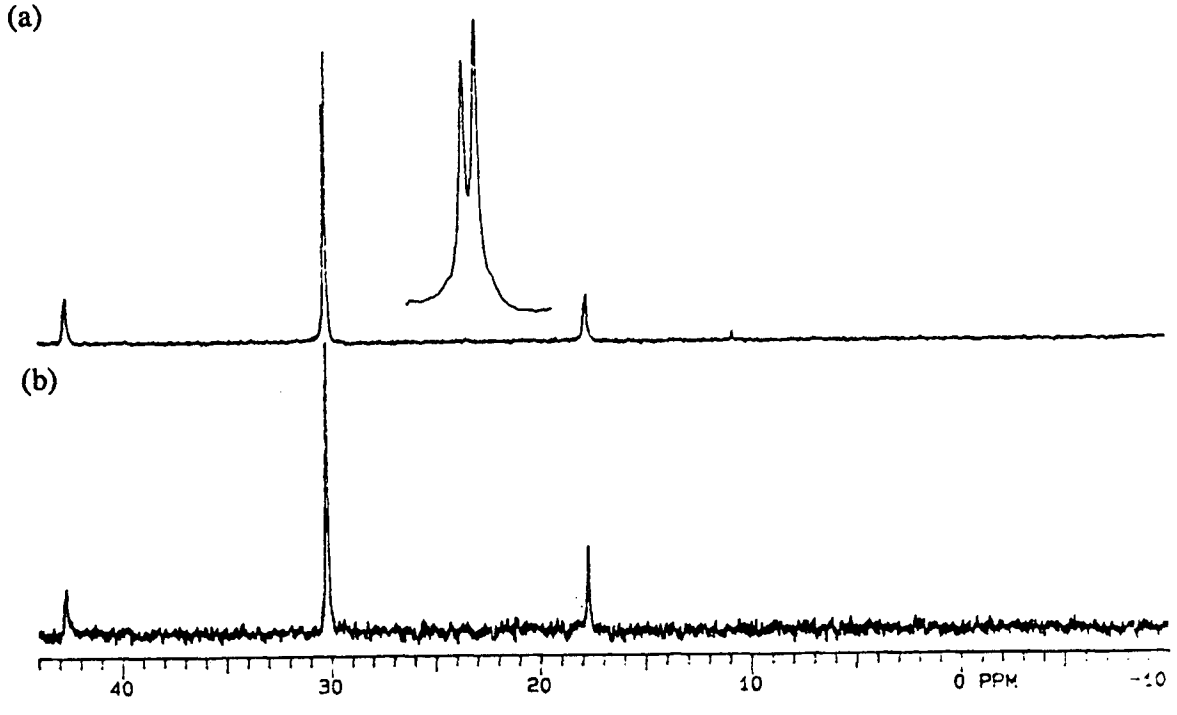

Fig. 5.20. $^{31}P\{^1H\}$ NMR spectra (121.4 MHz) of **50a** in CD_2Cl_2 at r.t.; (a) obtained with the decoupling power DLP = 6: δ = 30.2 (d), $^1J_{PtP}$ = 3023 Hz, $^2J_{PH}$ = 12.1 Hz. (b) obtained with the decoupling power increased by 2^6 (DLP = 0): δ = 30.2 (s), $^1J_{PtP}$ = 3026 Hz.

Transfer of a single hydrogen atom to an olefin is a common reaction for transition metal hydride complexes.[31] Compound **50a** reacts with acrylonitrile to form an alkyl complex, as indicated by the loss of intensity of the high field hydride signal and the appearance of multiplets in the methylene proton region in the ^1H NMR spectrum (Fig. 5.21). It is clear from the ^1H NMR data that the linear $-CH_2CH_2CN$ rather than the branched $-CH(CH_3)CN$ group is formed. Olefin insertion into an M-H bond in this anti-Markovnikov fashion is more commonly seen in the literature.[32] Accompanying this olefin insertion into the Pt-H bond is the isomerization of a trans phosphorus complex to a cis one (Eq. 5.2).

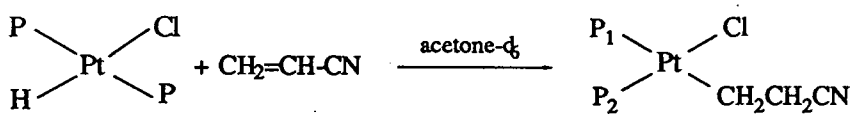

50a **51** (5.2)

The above reaction proceeds with no colour change, the solution remaining colourless. Fifty percent of the hydride is converted to the alkyl species in about an hour at room temperature. Compound **51** is not isolated. However, the $^{31}P\{^1H\}$ spectrum at -45°C in acetone-d_6 of *in situ,* fully formed **51** contains two doublets centred at 20.22 and 17.15 ppm with a J_{PP} coupling of 16.5 Hz, indicative of cis-phosphine geometry (Fig. 5.22b). The $^1J_{PtP}$ coupling for the phosphorus trans to the alkyl group is 1954 Hz, and that for the phosphorus trans to the chloride is 4254 Hz. The doublet assigned to the phosphorus trans to alkyl group collapses to a broad singlet when the sample is warmed to room temperature (Fig. 5.22a). The collapse of the phosphorus resonance at room temperature seemed not being caused by β-hydride elimination[33] of the cyanoethyl group because the ^1H NMR of the reaction mixture at room temperature showed no exchange between the methylene proton and the hydride resonances (Fig. 5.21). Interaction between the CN group and the central Pt atom in the following fashion seems likely.

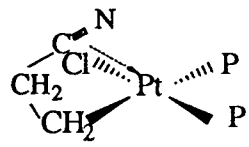

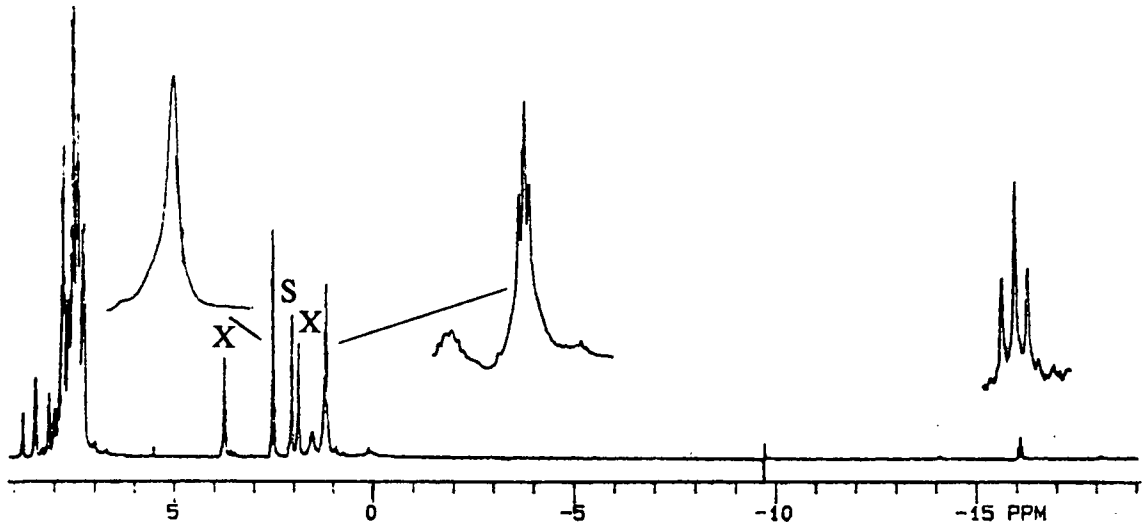

Fig. 5.21. ^{1}H NMR spectrum (300 MHz) of the *in situ* mixture of **50a** and **51** formed after 1 h reaction (Eq. 5.2) in acetone-d_6 at r.t. The signals at 2.53 and 1.19 (expanded) are the methylene resonances of **51**; the upfield triplet is the hydride resonance of **50a**; X = THF; S= solvent.

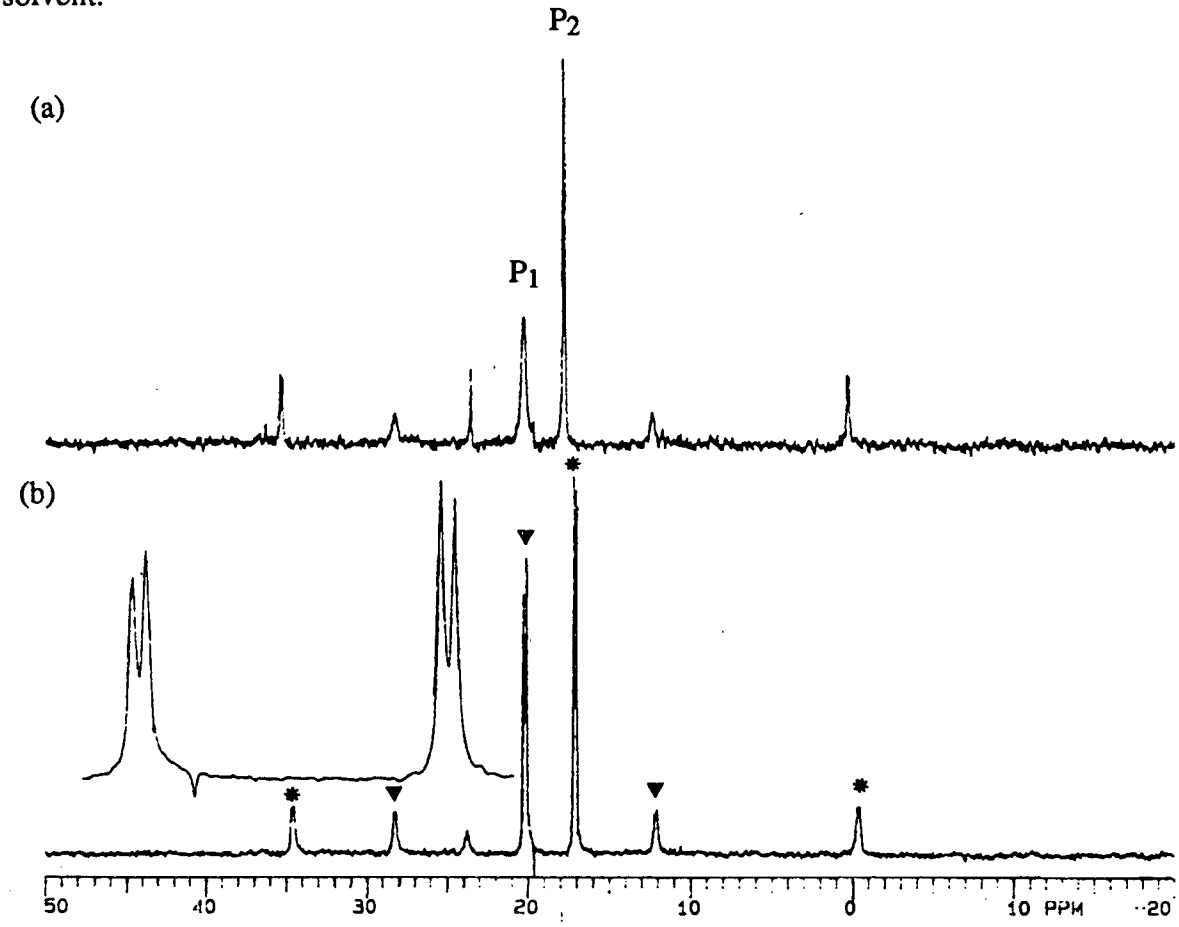

Fig. 5.22. $^{31}P\{^1H\}$ NMR spectra (121.4 MHz) of *in situ*, fully formed **51** in acetone-d_6: (a) at r.t., (b) at -45°C; δ_{P_1} = 20.22 (d), δ_{P_2} = 17.15 (d); $^1J_{PtP_1}$= 1954, $^1J_{PtP_2}$= 4254, J_{PP} = 16.5 Hz.

5.3.2. Reaction of $Pt(PN_3)_4$ with HCl

Attempted preparations of trans-$Pt(H)Cl(PN_3)_2$, **50c**, were unsuccessful using either HCl(g) or DMA·HCl (dimethylacetamide hydrogen chloride) as a source of HCl (Sect. 2.8.4.2). A canary yellow solid, isolated from the reaction of $Pt(PN_3)_4$ with HCl, is extremely air-sensitive in the solid state (turning to orange-red) and is sparsely soluble in chlorinated solvents, moderately soluble in acetone and in CH_3CN, and very soluble in EtOH and in H_2O giving deep red solutions under an inert atmosphere. Of interest, these red solutions appear to be less air-sensitive (see below for ^{31}P NMR data). The IR spectrum of this yellow solid displays three bands in the Pt-H region (2056, 1983 and 1947 cm^{-1}) and two bands in the N-H stretching region (3516, 3443 cm^{-1}) that presumably arise from protonation of the pyridine groups (Fig. 5.23). Samples for IR were prepared using degassed Nujol under a N_2 atmosphere in a glove-bag immediately before the measurement.

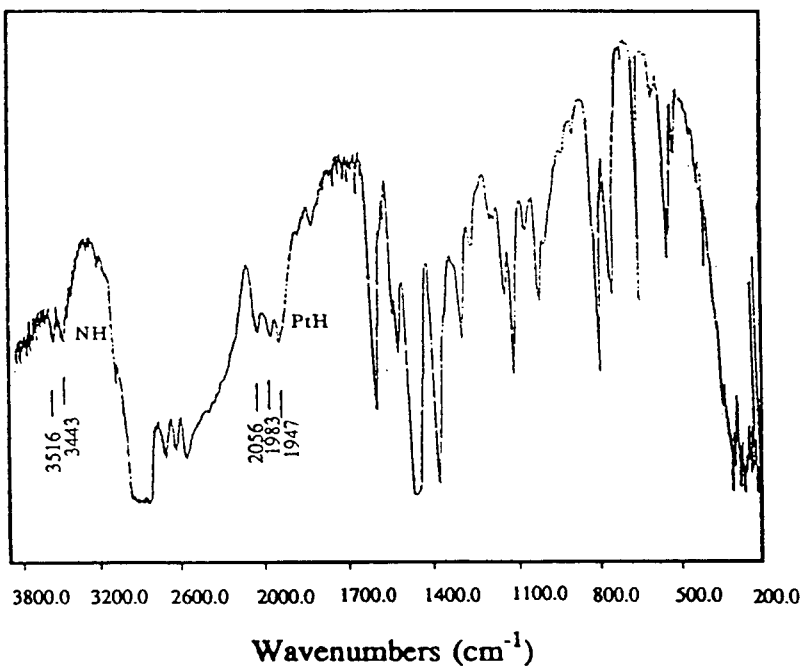

Fig. 5.23. Infrared spectrum of "$Pt(H)Cl(PN_3)_2$", **50c**, in Nujol at r.t. under N_2.

The yellow solid isolated from method 1 (Sect. 2.8.4.2) has a $^{31}P\{^1H\}$ NMR spectrum in CD_3CN containing a major singlet at 26.7 ppm and two singlet satellites ($^1J_{PtP}$ = 3869 Hz).

The ^1H NMR spectrum in CD_3CN showed a very weak multiplet around -5.5 ppm with no satellites; this signal was not seen when the spectrum was measured in D_2O. The $^{31}P\{^1H\}$ NMR spectrum of this unknown compound in either D_2O (δ = 27.1 (s), $^1J_{PtP}$ = 3875 Hz) or CD_3OD (δ = 26.8 (s), $^1J_{PtP}$ = 3879 Hz) showed no change under air.

The reason for the different reactivities of $Pt(PN_3)_4$, **26c**, and $Pt(PN_1)_3$, **27a**, toward HCl are not fully understood. One possible reason is the difference in the number of pyridyl groups on phosphine. The twelve pyridyl groups of **26c** appear to stabilize the tetrakis compound against dissociation (Sect. 5.1.1) and make bisphosphine Pt(0) species less readily available for reaction with HCl; furthermore, the pyridyl groups can compete with the Pt centre for HCl (see Fig. 5.23 for evidence of protonation of pyridine).

5.4. Reactions of $Pt(PN_1)_3$ and $Pt(PN_3)_4$ with methyl iodide

Both $Pt(PN_1)_3$ and $Pt(PN_3)_4$ react with MeI to give trans-$PtI(Me)(PN_n)_2$, in ways perhaps analogous to the triphenylphosphine Pt(0) systems.[34] The isolation of these complexes has been described in Sect. 2.8.5.

5.5. Attempted hydration of olefinic compounds using platinum and palladium pyridylphosphine complexes

5.5.1. Hydration of acrylonitrile

Compounds $Pt(PN_1)_3$, **27a**, $Pt(PN_3)_4$, **26c**, $Pt(PN_1)_2(\eta^2\text{-}CH_2CHCN)$, **44a**, and trans-$Pt(H)Cl(PN_1)_2$, **50a**, synthesized in the present work, were used as catalyst precursors in the hydration of acrylonitrile. The reaction mixture typically consisted of 0.5 mL of acrylonitrile, 0.5 mL of H_2O, 0.02 mmol of the complex and 0.02 mmol of NaOH. The reactant solutions were contained in ampules that were charged under N_2 and sealed under vacuum. After being loaded, the reaction vessels were placed in a flask containing refluxing benzene. At the end of the prescribed time (1 h), the vessels were opened and the metal complexes present were separated from organic products via vacuum distillation at ~40°C. The solid residues were extracted with Et_2O and the extracts combined with the organic distillates. The organic mixtures, in the

distillates and extracts were analyzed by gas chromatography (Sect. 2.9). An initial column pressure of 40 psi and an initial temperature of 150°C were used. After 14 min, the temperature was raised 15°C/min to 220°C. Table 5.3 summarizes the results obtained by GC. Sodium hydroxide was shown to be the likely catalyst in the hydration of acrylonitrile to the alcohol and the amide, because the platinum complexes were found to be inactive in the absence of NaOH. The turnover numbers of around 40 disagree with the number of 1.16 presented in reference 35. The acrylonitrile in the present study, distilled over CaH_2 (b.p. 54 - 56°C, 40 mmHg), has perhaps higher purity than that used in reference 35, because purification of acrylonitrile has been reported to increase the β-cyanoethanol production.[36] Another possible difference could result from the procedures used in separating organic compounds from the metal species prior to sample injection into the GC. Platinum metal, if contaminating the column, could be the active species performing the catalysis. It is interesting to point out that trans-$Pt(H)Cl(PN_1)_2$, cis-$PdCl_2(PN_3)_2$ and cis-$PtCl_2(PN_3)_2$ inhibit the base catalysis. In aqueous solution, the aquo complexes formed by substitution of chloride(s) show acidic behaviour (at least with **1c**, see Sect. 3.4.2); the added base likely generates M(OH) species that are inactive under these experimental conditions.

Table 5.3. Hydration of Acrylonitrile Catalyzed by Pt and Pd Complexes at 80°C

Catalyst[a]	Turnovers[b]	
	β-cyanoethanol	acrylamide
$Pt(PN_1)_3$, **27a**	40.2	—
$Pt(PN_3)_4$, **26c**	37.8	3.9
$Pt(PN_1)_2(\eta^2\text{-}CH_2CHCN)$, **44a**	42.5	—
trans-$Pt(H)Cl(PN_1)_2$, **50a**	—	—
cis-$PtCl_2(PN_3)_2$, **1c**	—	—
cis-$PdCl_2(PN_3)_2$, **4c**	—	—
NaOH	42.4	15.2

(a) Catalyst = 0.02 mmol complex + 0.02 mmol NaOH. (b) Turnover numbers = mole per mole of catalyst per hour; (—) implies non-detection.

5.5.2. Hydration of maleic acid

A strong acid, such as HCl (see below), and metal ions such as Cr^{3+} (Sect. 6.2.4), were found to catalyze the hydration of maleic acid at 100°C, a thermodynamically favourable but kinetically slow process. The water solubilities of the pyridylphosphine complexes cis-$PdCl_2(PN_3)_2$, **4c**, and $Pd_2Cl_2(\mu\text{-}PN_3)_2$, **11c** (Sect. 3.4), led to the investigation of these species as potential catalyst precursors for the hydration of maleic acid, during at the earlier stages of this thesis work. The reaction mixture typically consisted of a solution containing 2.0×10^{-4} to 1.0×10^{-3} M complex and 0.1 M maleic acid in 20 mL of H_2O (pH = 1.8). The pH of the solutions were adjusted by adding solid NaOH. Initially, the reaction mixtures at 80°, 100° or 120°C were contained in a 80 mL autoclave that was charged either under air or N_2, and later the autoclave was replaced by a regular Schlenk flask (see below). After being loaded, the autoclave or flask was placed in a thermostated oil-bath. At the end of 16 h, the autoclave was opened and the solution was concentrated to dryness. The solid obtained thereby was redissolved in acetone-d_6 for ^1H NMR analysis. A typical ^1H NMR spectrum that contains maleic acid, fumaric acid and malic acid is shown in Fig. 6.1 (Ch. 6). Initially, complex **4c** in the presence of NaOH (pH ≈ 7.0) showed positive results (3 - 40 turnovers in 16 h) but with poor reproducibility; Fe^{3+} impurity from the autoclave is almost certainly responsible for the catalysis (see also Sect. 6.2.4), because no catalysis was detected in a wide range of pH (3.0 - 12.5) when the autoclave was replaced by a glass flask and experiments were carried out at ~100°C. At pH > 10.0, **4c** started to decompose gradually to metal at 100°C under either an air or N_2 atmosphere. Because strong acid HCl (3.0 M) completely converted maleic acid (0.86 M) to fumaric acid (50%) and malic acid (50%) in 3 h at 100°C, the addition of acid was avoided in the catalysis experiments.

Complex **11c** is green in H_2O and the solution is stable for at least 5 h at 120°C; however, the solution decomposed to give metal after 3 h at 80°C when maleic acid was introduced. Neither malic acid nor fumaric acid was detected after the reaction.

The ionic complexes $[Pd(H_2O)(OH)(PN_3)_2](BPh_4)$, $[Pd_2(H_2O)_2(PN_3)_2](BPh_4)_2$, $[Pd_2(H_2O)_2(PN_3)_2](BF_4)_2$, and $[Pd_2(H_2O)_2(PN_3)_2](PF_6)_2$, derived from **4c** and **11c** (Sect. 3.4) are generally less water-soluble than **4c** and **11c**, and were shown in the present study to be inactive toward hydration of maleic acid.

The catalytic activity of the Pt(0) complex of maleic anhydride $Pt(PN_1)_2(MA)$, **47a**, was also tested; **47a** was reacted with NaOH (5-fold excess) in aqueous solution at 80°C for 1 h. No hydration product was found by ^1H NMR spectroscopy.

References

1. Malatesta, L.; Cariello, C. *J. Chem. Soc.,* **1958**, 2323.

2. Pearson, R.G.; Louw, W.; Rajaran, J. *Inorg. Chim. Acta* , **1974**, *9*, 251.

3. Mann, B.E.; Musco, A. *J Chem. Soc. Dalton Trans.*, **1980**, 776.

4. Otsuka, S.; Yoshida, T.; Matsumoto, M; Nakatsu, K. *J. Am. Chem. Soc.,* **1976**, *98,* 5850.

5. Tolman, C.A.; Seidel, W.C.; Gerlock, D.M. *J. Am. Chem. Soc.,* **1972**, *4,* 2669.

6. Halpern, J.; Weil, T.A. *J. Chem. Soc. Chem. Commun.*, **1976**, 631.

7. Mann, F.G.; Watson, J. *J. Org. Chem.,* **1948**, *13,* 502.

8. Hartley, F.R. *Organomet. Chem. Rev. A* , **1976**, *6,* 119.

9. Hartley, F.R. *The Chemistry of Platinum and Palladium;* John Wiley & Sons: New York, 1973; p.458.

10. Sue, C-Y. *Ph.D dessertation*, University of British Columbia , 1989; Chs. 2, 5.

11. Sweany, R.L.; Halpern, J. *J. Am. Chem. Soc.,* **1977**, *99,* 8337.

12. Gillard, R.D.; Ugo, R.; Cariati, F.; Cenini, S.; Bonati, F. *Chem. Commun.,* **1966**, 869.

13. Ugo, R.; La Monica, G.; Cariati, F.; Cenini, S.; Conti, F. *Inorg. Chim. Acta,* **1970**, *4*, 390.

14. Jones, R.D.; Summerville, D.A.; Basolo, F. *Chem. Rev.,* **1979**, *79*, 139.

15. Suzuki, M.; Ishiguro, T.; Kozuka, M.; Nakamoto, K. *Inorg. Chem.*, **1981**, *20*, 1993.

16. Egan, J.W. Jr.; Haggerty, B.S.; Rheingold, A.L.; Sendlinger, S.C.; Theopold, K.H. *J. Am. Chem. Soc.*, **1990**, *112*, 2445.

17. Collman, J.P.; Hegedus, L.S.; Norton, J.R.; Finke, R.G. *Principles and Applications of Organotransition Metal Chemistry,* 2nd ed.; University Science Books: Mill Valley, CA., 1987; p.400.

18. Neiderhoffer, E.C.; Timmons, J.H.; Martell, A.E. *Chem. Rev.*, **1984**, *84*, 137.

19. Ref. 17, pp.200-203.

20. Frem, R. Unpublished data, communicated to B.R. James.

21. Wood, F.E.; Olmstead, M.M.; Farr, J.P.; Balch, A.L. *Inorg. Chim. Acta,* **1985**, *97*, 77.

22. Sen, A. ; Halpern, J. *Inorg. Chem.,* **1976**, *19*, 1073.

23. Farr, J.P.; Wood, F.E.; Balch, A.L. *Inorg. Chem.*, **1983**, *22*, 3387.

24. Perrin, D.D.; Armarego, W.C.F.; Perrin, D.R. *Purification of Laboratory Chemicals,* 2nd ed.; Pergaman Press: Oxford, 1980; p.167.

25. (a)Cenini, S.; Ugo, R.; La Monica, G. *J. Chem. Soc. A,* **1971**, 409. (b)Cenini, S.; Ugo, R.; Bonati, F.; La Monica, G. *Inorg. Nucl. Chem. Letters* , **1976**, *3*, 191.

26. Maddox, M.L.; Stafford, S.L.; Kaesz, H.D. *Adv. Organometallic Chem.* **1965**, *3*, 1.

27. Ungváry, F. *Fifth IUPAC Symposium on Organometallic Chemistry Directed towards Organic Synthesis;* Florence, Italy, 1989; PSI-60.

28. (a) Panattoni, C.; Bombienri, G.; Belluco, U.; Baddley, W. H. *J. Am. Chem. Soc.,* **1968**, *90*, 798. (b) Bombieri, G.; Forsellini, E.; Parattoni, C.; Graziani, R.; Bandoli, G. *J. Chem. Soc. A,* **1970**, 1313.

29. Collamati, I.; Furlani, A.; Attioli, G. *J. Chem. Soc. A,* **1970**, 1694.

30. Carriati, F.; Ugo, R.; Bonati, F. *Inorg. Chem.*, **1966**, *5*, 1128.

31. Ref. 17, pp. 384, 698-700.

32. Docherty, N.M.; Bercaw, J.E. *J. Am. Chem. Soc.*, **1985**, *107*, 2670.

33. Clark, H.C.; Kurosawa, H. *Inorg. Chem.*, **1972**, *11*, 1275.

34. Hall, T.L.; Lappert, M.F.; Lednor, P.W. *J. Chem. Soc., Dalton Trans.,* **1980**, 1448.

35. Jensen, C.M.; Trogler, W.C. *J. Am. Chem. Soc.,* **1986**, *108*, 723.

36. Arnold, D.P.; Bennett, M.A. *J. Organomet. Chem.*, **1980**, *199*, 119.

Chapter 6

Catalytic Hydration of Maleic Acid by Chromium(III) Species

Olefins, such as maleic and fumaric acids, are activated toward nucleophilic attack by the presence of the electron-withdrawing carboxylic groups and, if coordinated to a metal via the C=C bond, the double bond is seen more susceptible to the nucleophilic attack (see Sect. 1.4.2). The hydration product of maleic or fumaric acid, malic acid, is a good synthetic substitute for citric acid used in food acidification.[1] Malic acid, containing a chiral carbon atom, is often obtained as a mixture of enantiomers. Asymmetric synthesis of S-malic acid is achieved using the biologically active enzyme, fumarase, via the hydration of fumaric acid under physiological conditions (Sect. 1.3). The salt $CrCl_3 \cdot 6H_2O$ has been reported to convert maleic acid in aqueous solution to malic and fumaric acid catalytically at 170°C.[2] In the absence of a strong acid or a metal ion, kinetic and thermodynamic data for the maleic acid hydration reaction shows that lowering the temperature favours the formation of malic acid.[1] The temperature employed in the Cr^{3+}/maleic acid system studied in the present work is 100°C, at which the catalysis operates at a measurable rate. Attempts to develop new catalysts and to extend the catalysis to other olefinic substrates were unsuccessful. In this chapter, preliminary kinetic results of this non-phosphine, transition metal complex catalyzed hydration of maleic acid are presented; preliminary data on coordination of the various carboxylic acids are also presented.

6.1. Kinetic experiments

The total chromium content of the catalyst precursor, $CrCl_3 \cdot 6H_2O$, was determined by the spectrophotometric measurement of the chromate (CrO_4^{2-}) concentration, formed quantitatively by oxidation of Cr(III) species by the action of peroxide in alkaline solution.[3] The characteristic absorption band at 371.9 nm of the formed yellow species (CrO_4^{2-}) has a molar extinction coefficient of 4.8×10^3 $M^{-1}cm^{-1}$. The average Cr^{III} content determined for standards prepared from $CrCl_3 \cdot 6H_2O$ was 1.5% higher than the calculated value.

The kinetic experiments were carried out in a series of reaction vessels for various periods of time, the reaction conditions being maintained as close as possible; each separate reaction yielded one kinetic data point. The typical initial [Cr^{3+}] in kinetic runs was 3.60×10^{-2} M, with the maleic acid present in a 50-fold excess. The reactions were carried out at 100 ± 1°C on a circulating steam-bath. The reaction mixture, 10 mL of an aqueous solution, whose pH was measured, was kept in a 50 mL Schlenk flask under air or N_2 which held more than 1 atm pressure when the quickfit stoppers and the stopcocks were tightened by rubber bands. The reaction was stopped immediately at any specified time by cooling the flask in an ice-water bath; no measurable product formation resulting from isomerization or hydration is detected at 40°C for 8 h. The volume of the resulting aqueous solution was then reduced to about 1 mL, and the organic compounds were extracted thoroughly by Et_2O (10 x10 mL portions) until the ethereal extract contained no more acids as shown by TLC. The blue, aqueous solution containing Cr^{3+} was discarded. The Et_2O solution was dried over anhydrous $MgSO_4$ for 5 h before evaporation to dryness on a rotary evaporator. The white solid obtained thereby was dried under vacuum overnight.

Analysis for product composition by gas chromatography was impractical because of the low vapour pressures and high boiling points of maleic, fumaric and malic acids. The molar composition of the reaction mixture was thus determined from the integration ratios of each component in the ^1H NMR spectrum; the isolated white solid product was dissolved in acetone-d_6 for the NMR analysis and, as noted above, each analysis provided one point for the rate plot. A typical ^1H NMR spectrum is shown in Fig. 6.1. Table 6.1 summarizes the results of ^1H NMR analysis of samples with known composition, which had been subjected to the same work-up procedure as described for the unknown samples from the kinetic runs. Some errors in the kinetic experiments are derived from the work-up procedure. The extraction recovery is about 98%, with some organic substrate possibly being lost in the coordination sphere of Cr^{3+}. Another error is from the measurement of the integrals in the ^1H NMR spectrum: the relative error is normally 1 - 2% for maleic acid, 2 - 5% for malic acid and 3 - 10% for fumaric acid.

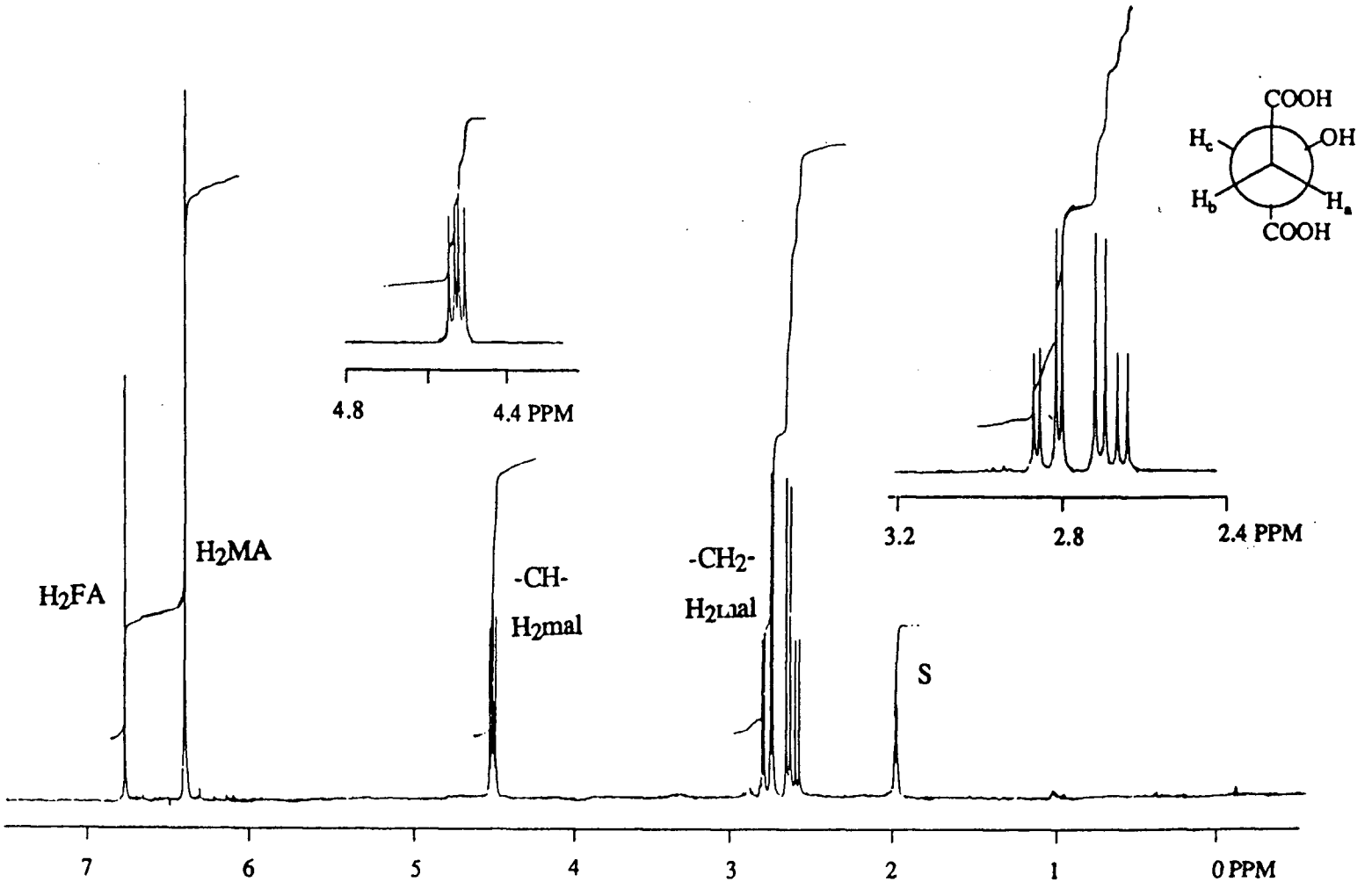

Fig.6.1. A typical ^1H NMR (300 MHz) spectrum of the hydration product mixture containing maleic, malic and fumaric acids in acetone-d_6 at r.t.; H_2MA: $\delta_{=CH-}$ = 6.4 (s); H_2FA: 6.8 (s); H_2mal: δ_{-CH-} = 4.52 , δ_{-CH_2-} = 2.75; $^2J_{H_aH_b}$ = 15.9, $^3J_{H_aH_c}$ = 4.5, $^3J_{H_bH_c}$ = 7.2 Hz. S = solvent peak.

Table 6.1. ^1H NMR Analysis of Control Samples[a]

Mixture I	H_2MA	H_2mal	H_2FA	Mixture II	H_2MA	H_2mal	H_2FA
calcd.(%)	49.5	42.2	8.3	calcd.(%)	47.2	43.6	9.2
found(%)	48.6	44.4	7.0	found(%)	50.0	42.4	7.6

(a) Maleic, malic and fumaric acids are abbreviated as H_2MA, H_2mal and H_2FA, respectively, throughout this Chapter.

6.2. Results and discussion

Hydration of maleic acid to R, S-malic acid (Eq. 6.1) at room temperature is, in fact, a thermodynamically favourable process with a ΔG^o value of -5.3 kcal/mol* (see Appendix AIX). However, in the present studies, the hydration was found not to proceed in the absence of a catalyst even at 100°C. Chromium(III), added as $CrCl_3 \cdot 6H_2O$, was found to be active in favour

$$\underset{\text{maleic acid}}{\text{cis-HOOCCH=CHCOOH}} + H_2O \longrightarrow \underset{\text{R, S-malic acid}}{HOOCCH_2CH(OH)COOH} \qquad (6.1)$$

of malic acid formation at 100°C, while Fe(III), added as $FeCl_3 \cdot 6H_2O$, gave a much higher percentage of the isomerization product fumaric acid, which was not hydrated at this temperature (see below).

6.2.1. Spectroscopic properties of Cr(III) and complexation with maleic and malic acids

Chromium(III) has a d^3 electronic configuration and is substitutionally inert.[5, 6] The weak electronic absorption of chromium(III) is the result of symmetry (Laporte) forbidden d-d transitions.[6] Two absorption maxima are often observed in the visible region, and their positions are influenced by the ligands coordinated according to the ligand field strength(s). When trans-$[CrCl_2(H_2O)_4]Cl \cdot 2H_2O$, the catalyst precursor (commercially available as $CrCl_3 \cdot 6H_2O$[7, 8]), dissolves in water, H_2O slowly replaces one chloride, resulting in a blue shift of both original absorption maxima. This process has a half life of 2.5 h at room temperature,[9] but the rate is

* A ΔG^o value of -7 kcal/mol in acidic solution was given in ref. 4.

greatly accelerated at 100°C. The chloropentaaquo species is relatively stable ($t_{1/2}$ = 70 h, r.t.).[10] The following table lists the room temperature visible spectral data of the hydration isomers, and these data serve as a guide for identification of the chemical species present in the catalytic reactions.

Table 6.2. Visible Spectral Data of Some Hydration Isomers of $CrCl_3 \cdot 6H_2O$[a]

complex	λ_1, ε_1	λ_2, ε_2	Ref.
trans-$[CrCl_2(H_2O)_4]^+$	650, 24.1	455, 22.0	8, 9
cis-$[CrCl_2(H_2O)_4]^+$	650.0, 18.0	455, 25.7	8, 9
$[CrCl(H_2O)_5]^{2+}$	609, 16.4	425, 20.8	10
$[Cr(H_2O)_6]^{3+}$	572, 13.4	409, 15.4	11, 12

(a) Wavelengths in nm and extinction coefficients in $M^{-1}cm^{-1}$.

The oligomerization of $Cr(H_2O)_6^{3+}$ at elevated temperature to form hydroxo bridged dimeric, trimeric and tetrameric species often becomes more important in basic, concentrated solutions.[13, 14] A study by Laswick and Plane[14] has shown that in the absence of the added base, some 70.4% of the Cr^{3+} species remained as hexaaquo species in a chromic perchlorate solution (0.05 - 0.10 M) after 24 h boiling, while only 38.8% remained as $Cr(H_2O)_6^{3+}$ after 3 h if NaOH (0.05 - 0.10 M) was added prior to reflux. The rest of the Cr(III) species were present as oligomerized hydroxo bridged forms. Oligomerization, however, could be controlled to a certain extent by lowering the pH of the solution. More detailed studies of chromic oligomers by Stunzi and Marty led these authors to state that the absorbance ratio of the shorter wavelength band over the longer one was 1.17 ± 0.01 for the monomer, 1.18 ± 0.01 for the dimer, 1.60 ± 0.01 for the trimer, 1.95 ± 0.04 for the tetramer, and 1.5 - 1.56 for the oligomers higher than four Cr units respectively.[15] A red shift of both maxima is also indicative of the oligomer formation.[15]

Table 6.3. Visible Spectral Parameters of Chromium(III) Oligomers[15]

	monomer	dimer	trimer	tetramer	hexamer
λ_1 (ε_1)	575 (13.2)	582 (17.4)	584 (19.2)	580 (15.6)	585 (18.6)
λ_2 (ε_2)	409 (15.5)	417 (20.4)	425 (30.5)	426 (30.3)	426 (29.0)
$\varepsilon_2/\varepsilon_1$[a]	1.17	1.17	1.59	1.94	1.56

(a) Calculated from data given in the ref. 15.

In the present study, both maleic and malic acid are found to form complexes with Cr^{3+} in solutions containing 0.20 M KNO_3 and 0.02 M HNO_3 at 100°C. These complexes are different from those formed by reduction of $K_2Cr_2O_7$ with the same acids (Sect. 2.9). The absorbances of $CrCl_3{\cdot}6H_2O$ solutions at different concentrations (in solutions containing 0.20 M KNO_3 and 0.02 M HNO_3 at pH = 2.0) which had been heated at 100°C for 30 min were recorded as 'blanks'; plots of ε at 410 and 572 nm against $[Cr^{3+}]$ is presented in Appendix (Fig. A.2) . The ratios of the two ε values are between 1.16 - 1.17 (Table AIX 1), indicating the formation of $Cr(H_2O)_6^{3+}$ under these conditions. The acid nitrate solutions containing $Cr(H_2O)_6^{3+}$ and the maleic (or malic) acid at various ratios were heated at 100°C for 30 min and the absorbances were recorded. Through Job's Continuous Variation method[16] (the data and treatment are shown in Appendix AIX 3), the composition of both complexes was determined to be 1:1, and the formation constants are 8.1×10^2 and 9.1×10^3 M^{-1} for the maleate and malate complexes, respectively. The *in situ* maleate complex **55**, considered to be $[Cr(HMA)(H_2O)_5]^{2+}$, has absorption band maxima at 418 and 572 nm (Fig. 6.2), while the corresponding malate complex (**56**) has maxima at 410 and 562 nm (Fig. 6.3). The positions of the absorption maxima indicate that these complexes are free of coordinated chloride ligands (cf. Table 6.2) because a carboxylate ligand is comparable to H_2O within the spectrochemical series. The malate complex formed under similar conditions from malic acid (0.25 M) and $CrCl_3{\cdot}6H_2O$ (0.25 M) was separated on a cation-exchange column, yielding largely a charge 2+ species with the same absorption maxima (410, 562 nm) as those of the *in situ* formed species.

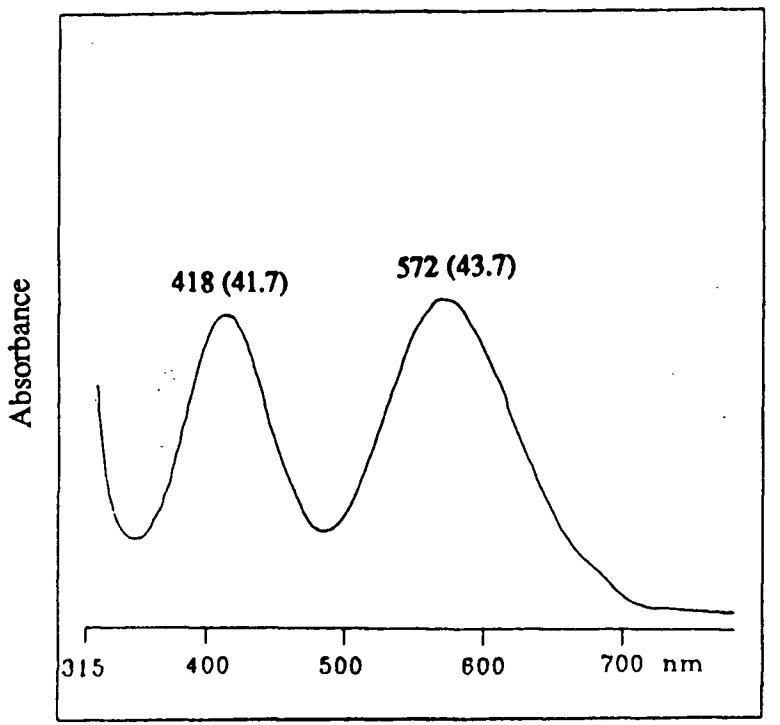

Fig. 6.2. The UV/vis absorption spectrum recorded at 25°C of $[Cr(HMA)(H_2O)_5]^{2+}$, **55**, in H_2O; $\lambda(\varepsilon, M^{-1}cm^{-1})$ data are noted. on the spectrum.

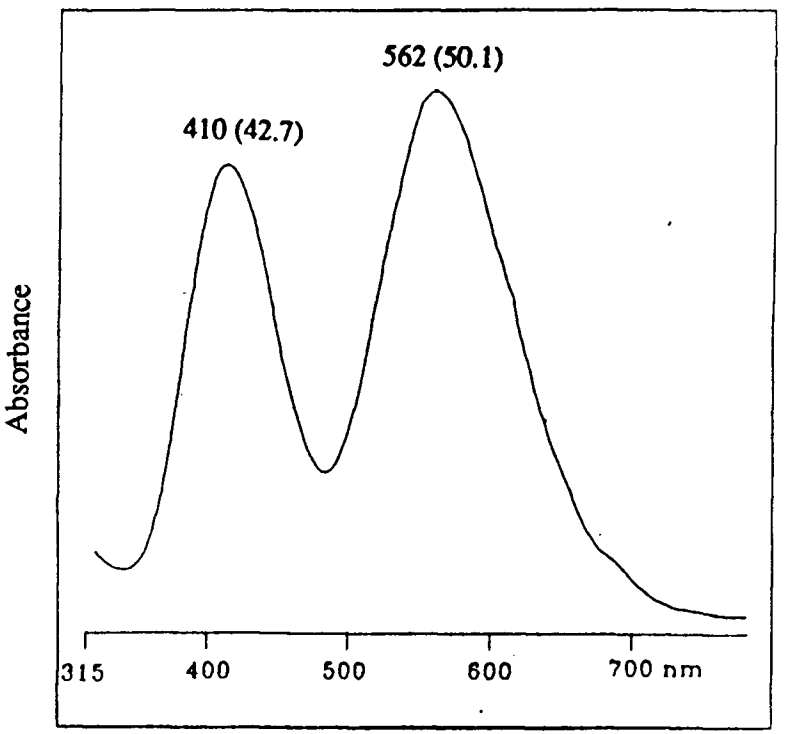

Fig. 6.3. The UV/vis absorption spectrum recorded at 25°C of $[Cr(Hmal)(H_2O)_5]^{2+}$, **56**, in H_2O; λ (ε, $M^{-1}cm^{-1}$) data are noted on the spectrum.

The maleate and malate complexes are thus written as containing the mono-protonated, monodentate, mono-anion. It was also shown in Olson and Taube's work that some 92% of the maleate Cr^{3+} complex was monodentate containing the HMA anion.[4] However, this monodentate and the chelate species $[Cr(MA)(H_2O)_4]^+$ containing the maleate dianion were found to be present in equilibrium with an equilibrium constant of 15.4 M^{-1} at 25°C, in favour of the formation of the monodentate form (Eq. 6.2).[17] Mixing fumaric acid and $CrCl_3 \cdot 6H_2O$ solutions under the same conditions gave green solutions whose absorbances varied with the concentration of the added chromic species, perhaps indicating no formation of a complex.

$$[Cr(MA)(H_2O)_4]^+ + H^+ \rightleftharpoons [Cr(HMA)(H_2O)_5]^{2+} \qquad (6.2)$$

6.2.2. Kinetic results

The experimental conditions of the kinetic runs have been described in the experimental section (Sect. 6.1). The reaction solution is homogeneous throughout. In this section, the maleic acid concentration dependence, the catalyst concentration dependence, and the pH dependence will be discussed. An observed competition between the malic acid formed *in situ* and the maleic acid for the $Cr(H_2O)_6^{3+}$ ion complicates the reaction kinetics. Another complication arises from a slow formation of fumaric acid from the coordinated maleato complex. Nevertheless, with certain simplifications and assumptions, the results of the kinetic study can be interpreted to some satisfaction.

6.2.2.1. Maleic acid dependence

Maleic acid dependence experiments were done through two different methods — measuring the initial rate of reaction at different starting maleic acid concentration, and monitoring the H_2MA concentration change with time. The initial rate measured at t = 2.0 h with <16% conversion gives a zero-order dependence on maleic acid concentration (Table 6.4), the slope of $\Delta[H_2MA]/\Delta t$ vs. $[H_2MA]$ plot being essentially zero (Fig. 6.4). The second method shows that

even up to first 8 h the rate is independent of maleic acid concentration (Fig. 6.5 inset), although after about 8 h a first-order dependence seemed apparent (Table 6.5, Fig. 6.5).

Table 6.4. Initial Rate of the Catalytic Hydration of Maleic Acid at Various $[H_2MA]^a$

$[H_2MA]_i$ (M)	0.344	0.688	1.03
$[Cr]x10^3$ (M)	3.6	3.6	3.6
$[H_2MA]_t$ (M)	0.289	0.638	0.972
$[H_2mal]_t$ (M)	0.039	0.020	0.025
$[H_2FA]_t$ (M)	0.015	0.029	0.033
$\Delta[H_2MA]/\Delta t$ (M/h)	0.0273	0.0248	0.0288

(a) Data measured after 2 h; subscripts i and t refer to initial and time of measurements, respectively. The pH levels of these reactions are between 1.6 to 1.8.

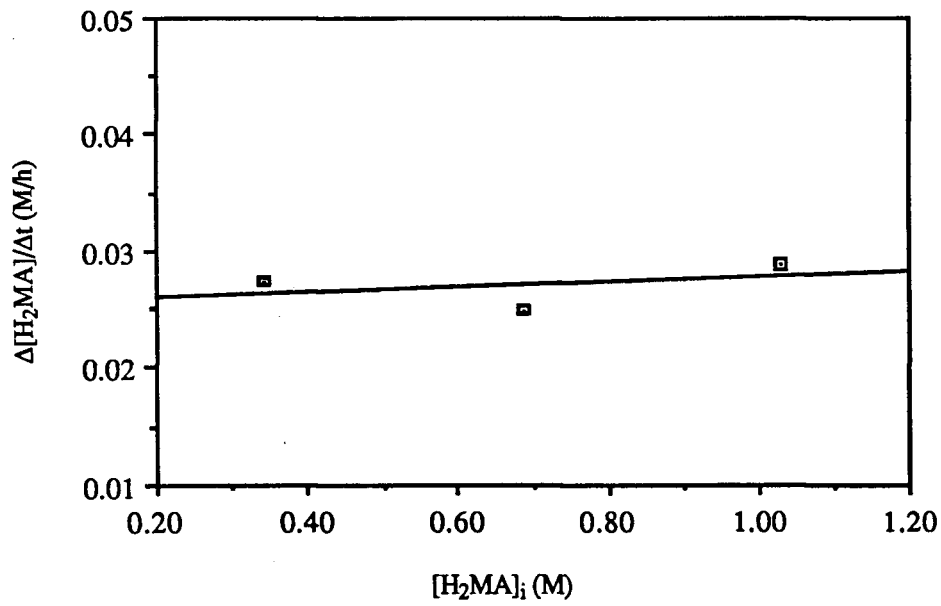

Fig. 6.4. Plot of $\Delta[H_2MA]/\Delta t$ vs. $[H_2MA]_i$ at the initial stage of the reaction; $[Cr] = 3.60x10^{-3}$ M, temp. = 100 ± 1°C, t = 2.0 h; pH = 1.6 - 1.8.

Table 6.5. Catalytic Conversion of Maleic Acid to Malic Acid and Fumaric Acid[a]

t (h)	H_2MA (%, M)	H_2mal (%, M)	H_2FA (%, M)
0.0	100.0, 1.72	0.0, 0.0	0.0, 0.0
0.5	94.5, 1.63	3.9, 0.067	1.5, 0.026
1.0	90.4, 1.55	7.3, 0.126	2.4, 0.041
1.0	90.0, 1.56	6.1, 0.105	3.0, 0.052
2.0	87.7, 1.51	7.8, 0.134	4.5, 0.077
2.0	86.1, 1.48	12.6, 0.217	1.4, 0.024
3.0	84.4, 1.45	11.2, 0.193	4.4, 0.076
4.0	78.6, 1.35	17.8, 0.306	3.7, 0.064
4.0	73.8, 1.27	23.7, 0.408	2.5, 0.043
5.0	80.8, 1.39	12.0, 0.206	7.1, 0.122
5.0	78.5, 1.35	15.9, 0.273	5.6, 0.096
6.0	68.6, 1.18	27.5, 0.473	4.0, 0.069
7.7	66.0, 1.14	30.4, 0.523	3.7, 0.064
8.0	66.2, 1.14	30.8, 0.530	3.1, 0.053
16.0	55.1, 0.948	37.9, 0.652	6.9, 0.119
20.0	47.2, 0.812	46.8, 0.805	6.0, 0.103
24.0	34.3, 0.590	53.8, 0.925	11.9, 0.205
24.0	31.9, 0.549	53.9, 0.927	14.2, 0.244
24.0	38.0, 0.654	52.6, 0.905	9.5, 0.163
32.0	27.4, 0.471	63.1, 1.09	9.4, 0.162
32.0	29.3, 0.504	62.6, 1.08	8.2, 0.141
32.0	29.9, 0.514	55.1, 0.948	15.6, 0.268
40.0	23.6, 0.406	67.7, 1.15	7.9, 0.136
40.0	23.4, 0.402	62.8, 1.08	12.4, 0.213

(Table 6.5 continued)

40.0	20.9, 0.359	69.3, 1.19	9.8, 0.169
48.0	14.4, 0.248	71.5, 1.23	14.1, 0.243
48.0	17.4, 0.299	72.8, 1.25	9.8, 0.169

(a) $[H_2MA]_i$ = 1.72 M, $[Cr^{3+}]$ = 3.6x10^{-2} M; temp. = 100 ± 1°C; pH = 1.3.

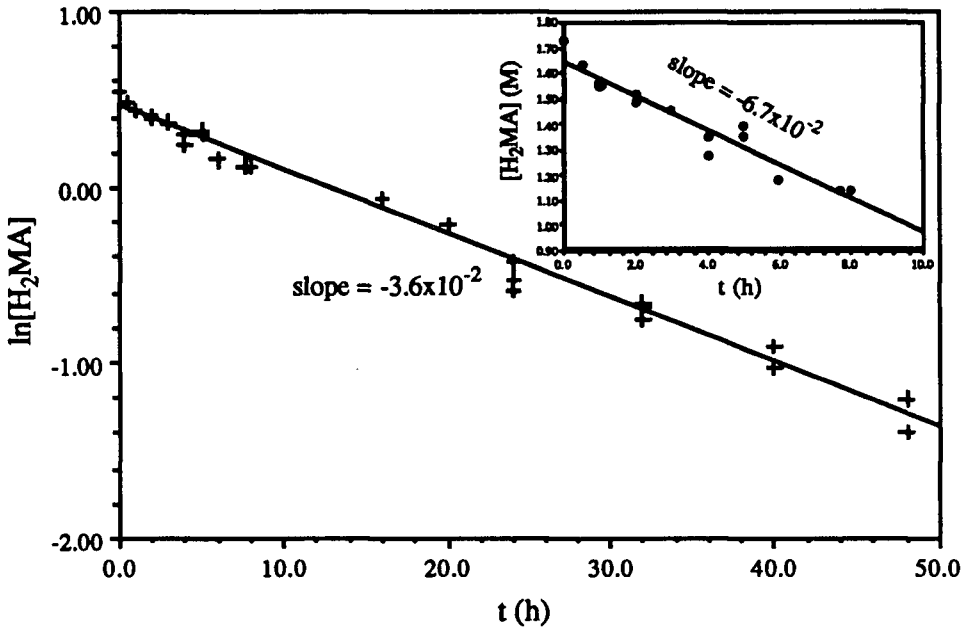

Fig. 6.5. Plot of ln[H_2MA] vs. t (0.0 ≤ t ≤ 48.0 h), $t_{1/2}$ ≅ 19.3 h; inset: plot of [H_2MA] vs. t (0.0 ≤ t ≤ 8.0 h).

6.2.2.2. Catalyst concentration dependence

The $[Cr^{3+}]$ dependence was determined by varying the concentration of Cr^{3+} species, while keeping the concentration of maleic acid relatively constant (Table 6.6, Fig. 6.6).

At low Cr^{3+} concentration, the order approximates to one (Fig. 6.6), while a gradual decrease from the first-order dependence is seen at higher Cr^{3+} concentration and eventually the dependence is approaching zero-order. The decrease in order on Cr is tentatively attributed to the interference of the malic acid product, by coordination of the malate mono-anion to the Cr^{3+} (Sect. 6.2.1); reduction of the effective Cr^{3+} concentration because of the oligomerization is also a possibility.

Table 6.6. Data for Cr^{3+} Concentration Dependence[a]

$[Cr^{3+}]x10^3$ (M)	H_2MA (%, M)	H_2mal (%, M)	H_2FA (%, M)	$\Delta[MA]/\Delta t$ ($M/hx10^2$)
3.0	96.3, 0.830	1.7, 0.015	1.9, 0.016	1.60
7.4	92.2, 0.795	6.0, 0.052	1.7, 0.015	3.35
9.0	91.3, 0.787	6.4, 0.055	2.2, 0.019	3.75
14.4	89.2, 0.769	8.7, 0.075	2.1, 0.018	4.65
18.0	86.6, 0.746	11.5, 0.099	2.1, 0.018	5.80
22.0	84.3, 0.727	13.8, 0.119	1.9, 0.016	6.75
27.0	81.8, 0.705	15.9, 0.137	2.2, 0.019	7.85
36.0	79.2, 0.683	18.0, 0.155	2.8, 0.024	8.95
45.0	78.1, 0.673	18.3, 0.158	3.6, 0.031	9.45
60.8	77.3, 0.666	19.7, 0.170	3.0, 0.026	9.80
65.0	76.1, 0.660	19.9, 0.172	3.9, 0.034	10.1

(a) $[H_2MA]_i$ = 0.862 M, temp.= 100 ± 1°C, t = 2.0 h, pH = 1.5.

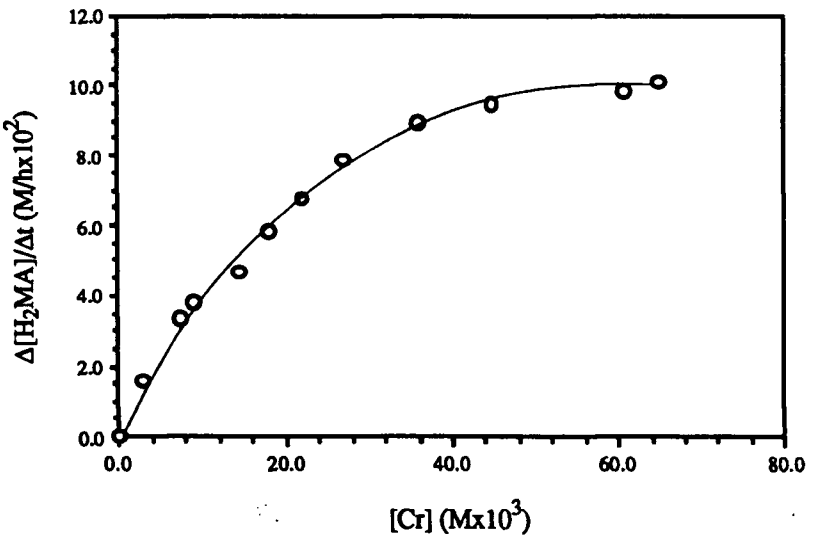

Fig. 6.6. Initial rate of loss of maleic acid as a function of [Cr].

6.2.2.3. pH dependence

The adjustable pH range for kinetic measurements is very narrow in this system because of the formation of a grey, colloidal precipitate, possibly $Cr(OH)_3$, around pH 2.6. For those solutions required with pH > 1.6, the pH levels were initially brought to selected values by addition of solid NaOH; the solutions were then self-buffered by the substrate (maleic acid/maleate conjugate pair action). For those solutions with pH < 1.6 , the pH levels were adjusted using HCl-KCl buffer solution. A ΔpH change of 0.2 between the initial and final solutions was observed (Table 6.7), the unbuffered solutions normally have a ΔpH change of around 0.2 - 0.3. Spectra of some of the 'final' catalysis solutions after 10 h reaction were measured at room temperature; broad maxima, noted at ~415 and ~570 nm, are between the maxima of the maleate and malate complexes. The experimental conditions and work-up procedures were similar to those of the unbuffered experiments, except that aqueous HCl was added to neutralize the added base before the Et_2O extraction. The data are summarized in Table 6.7 and Fig. 6.7.

Table 6.7. pH Dependence Data[a]

pH (initial)	pH (final)	H_2MA (%, M)	H_2mal (%, M)	H_2FA (%, M)
0.87	0.75	65.6, 0.565	25.5, 0.220	8.9, 0.077
1.00	1.07	44.7, 0.385	43.4, 0.374	11.8, 0.102
1.30	1.46	37.9, 0.327	52.7, 0.454	9.4, 0.081
1.77[b]	1.96	54.0, 0.465	36.0, 0.310	10.0, 0.086
1.92[b]	2.12	61.9, 0.533	31.6, 0.272	6.5, 0.056
2.0	2.15	51.7, 0.446	32.5, 0.280	15.9, 0.137
2.35	2.44	84.4, 0.728	9.1, 0.078	6.5, 0.056
2.64	2.60	91.5, 0.789	3.9, 0.034	4.6, 0.040
3.0	2.86	92.3, 0.796	3.5, 0.030	4.2, 0.036

(a) $[H_2MA]_i$ = 0.862 M, $[Cr^{3+}]$ = 3.6×10^{-2} M; temp. = 100 ± 1°C, t = 10.0 h. (b) Buffered by potassium hydrogen phthalate and NaOH solutions.

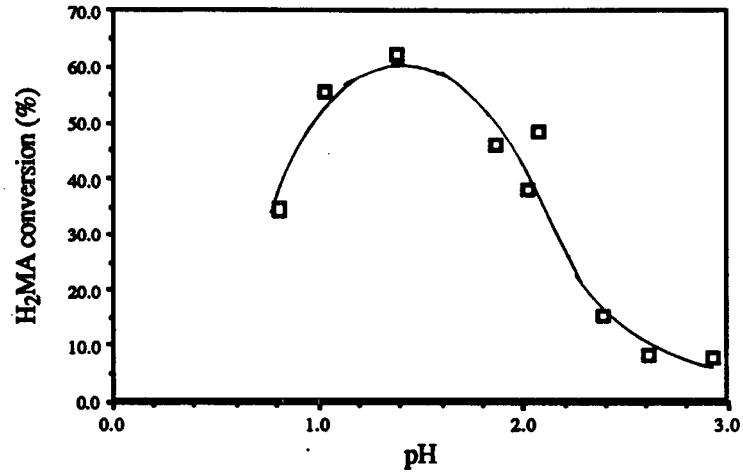

Fig. 6.7. Conversion of maleic acid after 10 h as a function of pH; pH values are averaged between the initial and final values (Table 6.7)

From the data in Fig. 6.7, the rate of catalytic hydration is obviously pH dependent; however, no quantitative information can be obtained from these results. As mentioned previously, in the presence of base the oligomerization becomes more important, and this may explain the drastic reduction of the conversion at higher pH.

6.2.3. Mechanism

There are several possible mechanisms for the formation of malic and fumaric acids. Three of the most plausible ones are discussed below.

The $Cr(H_2O)_6^{3+}$ ion may form a $Cr(\eta^2\text{-olefin})(H_2O)_4^{3+}$ complex analogous to the known $Ru(\eta^2\text{-}H_2MA)$ complex;[18] then free or coordinated H_2O attacks the coordinated C=C, forming a hydroxyalkyl ligand (Scheme 1.12). The alkyl group, as in the case of a fluoroolefin substrate,[19] is cleaved off in a subsequent protonation step. This mechanism is considered unlikely because of the fact that the maleato ligand is coordinated through the oxygen donor of the carboxylic group instead of the olefinic bond, as indicated by the small shift of absorption maxima on coordination of the maleate mono-anion to the $Cr(H_2O)_6^{3+}$species. Other O-bonded maleato complexes have also been isolated (see below).

A second possible mechanism involves the direct formation of a $[C\text{-}Cr]^{3+}$ cation, analogous to a protonated C=C bond. Cleavage of the C-Cr bond yields a zwiterion, and addition of H_2O to this unstable intermediate gives the hydrated product (see Eq. 6.3). This mechanism was proposed by Bzhasso and Pyatnitskii,[2] and was used to explain the formation of fumaric acid and malic acid. This mechanism also accounts for a kinetic dependence on the catalyst concentration that was noted in the present study, but it would predict that Cr^{3+} should catalyze the hydration of fumaric acid; also a fumarate complex would be expected to form during the reaction.

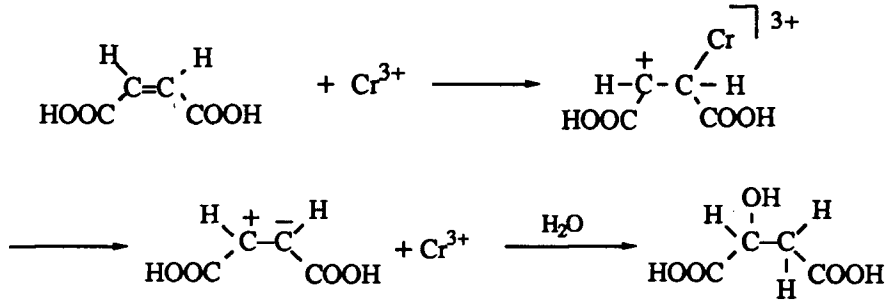

(6.3)

The coordination of carboxylate oxygen to the Cr centre has been demonstrated by Olson and Taube in the stoichiometric aquation of $Cr(H_2O)_5(HMA)^{2+}$ at temperatures of 40 - 60°C,[4] and more recently a similar monomethyl maleate Co(III) complex, $Co(CH_3\text{-}MA)(H_2O)_5^{3+}$, was characterized by Sargeson and coworkers.[20] The experimental conditions in the present study differ from those in the reported stoichiometric reaction in the temperature, pH and the concentration of maleic acid.[4] However, the reactions occurring in these two systems appear to be very much related. The chromium(III) maleato complexes, formed *in situ* by mixing perchloric acid, hexaaquochromium(III) and maleic acid in a 1:1:2 ratio at 40°C for 115 h, were separated by cation exchange chromatography into three species:[4] a chelate $Cr(H_2O)_4(MA)^+$, a 'malato intermediate' (see below), and a monodentate maleate species $Cr(H_2O)_5(HMA)^{2+}$. On aquation at 60°C for 20 h in 0.94 M perchloric acid, each species gave maleic, fumaric and malic acids with the compositions shown in Table 6.8.[4] This intermediate was characterized by an absorption maxima at 417 nm (ε 36.3 $M^{-1}cm^{-1}$) and, from its elution behaviour, was more like a +1 than a +2 complex.[4] This chromic species, giving predominantly malic acid on aquation, was suggested to be the 5-member ring chelate (**57**, see structure in Scheme 6.1) formed by the

hydroxyl and carboxylate groups of malic acid. With knowledge of this structure for **57**, the elution behaviour can be explained by dissociation of the proton on the coordinated hydroxo group (the pK_a of this proton in the Co(III) complex was found to be 2.75 [20]). The scheme presented in the reference 4, showing a conversion of a monodentate maleate species to monodentate fumarate and chelate malate species **57**, seems applicable to the catalytic hydration system. Although the possibility of a "C-Cr^{3+} cation" mechanism cannot be excluded, the similarity between the stoichiometric and catalytic reactions is very evident. Based on the spectroscopic and kinetic results, the catalytic cycle for the hydration of maleic acid is outlined below (Scheme 6.1). In this mechanism, formation of fumaric acid is very slow and irreversible.

Table 6.8. Results of Aquation of Maleato Complexes of Cr^{3+} [4]

Complex (% yield[a])	H_2MA (%)	H_2mal (%)	H_2FA (%)
chelate (6.4)	76	22	1
intermediate (1.6)	28	69	3
monodentate (~92)	87	10	3

(a) The yields are calculated from the data given in ref. 4.

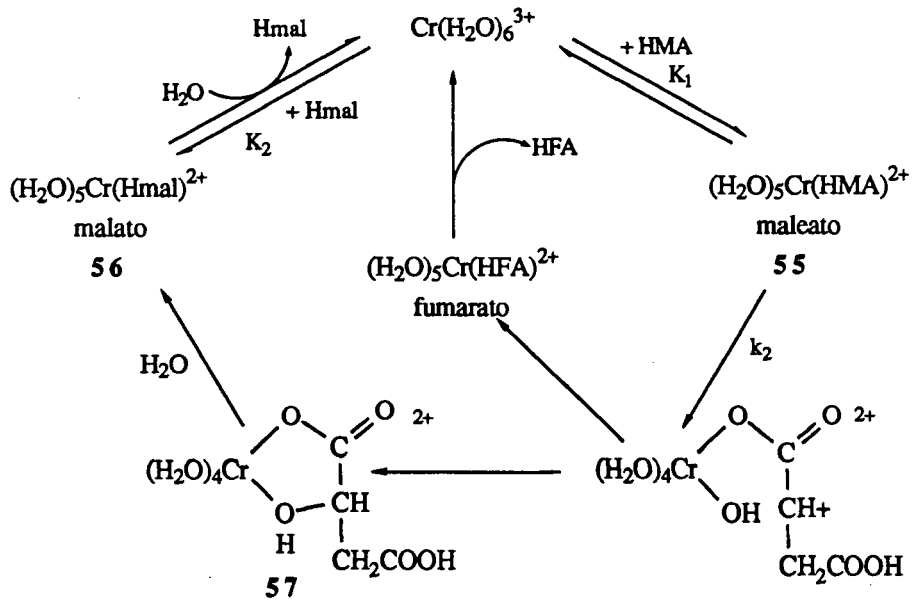

Scheme 6.1. A plausible mechanism for maleic acid hydration catalyzed by the Cr^{3+} aquo ion; the HMA, HFA and Hmal species are monoanions, but the charges are omitted for convenience both in the Scheme and in the derivation of the rate-law.

The rate-law for the disappearance of maleic acid can be derived, assuming that the H^+ transfer from the coordinated water to the double bond of the coordinated maleate is the rate determining step.

$$\text{rate} = k_2[\mathbf{55}] = k_2K_1[Cr][HMA], \qquad \text{where } [Cr] = [Cr(H_2O)_6^{3+}]$$

and as $[Cr]_{tot} = [Cr] + [\mathbf{55}] + [\mathbf{56}] = [Cr]\,(1 + K_1[HMA] + K_2[Hmal])$,

$$\text{rate} = k_2K_1\frac{[Cr]_{tot}[HMA]}{1 + K_1[HMA] + K_2[Hmal]} \tag{6.4}$$

Assuming dissociation of the second proton is negligible for both maleic acid and malic acid under the catalysis condition (pK_{a_2} values are 6.07 and 5.10, respectively), we have

$$K_{a_1} = \frac{[HMA][H^+]}{[H_2MA]} = 10^{-1.8} \quad \text{and} \quad K'_{a_1} = \frac{[Hmal][H^+]}{[H_2mal]} = 10^{-3.4}\text{, and thus}$$

$$[H_2MA]_{tot} = [HMA]\left(\frac{K_{a_1} + [H^+]}{K_{a_1}}\right) \quad \text{and} \quad [H_2mal]_{tot} = [Hmal]\left(\frac{K'_{a_1} + [H^+]}{K'_{a_1}}\right)$$

At the beginning of the reaction, the concentrations of malic acid (and fumaric acid) are very small, and at the pH values used, with knowledge of the K_1 and K_2 values (~10^3 and 10^4 M^{-1}, respectively) and the pK_{a_1} values (see above), it is simple to show that the $K_1[HMA]$ term in the denominator of Eq. 6.4 dominates (i.e. 'all' the Cr is present as **55**). Thus

$$\text{rate} = k_2[Cr]_{tot}$$

The rate is first-order in $[Cr]_{tot}$ concentration, and independent of the maleic acid concentration as found experimentally.

When malic acid has accumulated to a significant amount, it will compete with maleic acid for a coordination site on Cr^{3+}; i.e. $K_2[Hmal]$ and $K_1[HMA]$ become comparable. Under these conditions (assuming that the concentration of free Cr^{3+} is negligible), Eq. 6.4 gives

$$\text{rate} = k_2K_1\frac{[Cr]_{tot}[HMA]}{K_1[HMA] + K_2[Hmal]}$$

The rate expression at the later stages of the hydration is thus

$$\text{rate} = \frac{k_2 K_1 K_{a_1}[Cr]_{tot}[H_2MA]_{tot}(K'_{a_1}+[H^+])}{K_1 K_{a_1}(K'_{a_1}+[H^+])[H_2MA]_{tot} + K_2 K'_{a_1}(K_{a_1}+[H^+])[H_2mal]_{tot}}$$

Approximately, $[H_2mal]_{tot} = [H_2MA]_i - [H_2MA]_{tot}$, where $[H_2MA]_i$ is the initial concentration of H_2MA. Thus,

$$\text{rate} = \frac{A[Cr]_{tot}[H_2MA]_{tot}}{B + C[H_2MA]_{tot}}$$

where $A = k_2K_1K_{a_1}([H^+] + K'_{a_1})$, $B = K_2K'_{a_1}[H_2MA]_i(K_{a_1} + [H^+])$,

$C = K_1K_{a_1}(K'_{a_1} + [H^+]) - K_2K'_{a_1}(K_{a_1} + [H^+])$

The rate is still first-order in chromium, and is between first- and zero-order in maleic acid concentration. At the stage where $K_2[Hmal] > K_1[HMA]$ (Eq. 6.4), the rate then becomes first-order in maleic acid concentration.

The above analysis based on the plausible mechanism shown in Scheme 6.1 is in qualitative agreement with the kinetic results. The rate of the isomerization reaction is very slow compared to the hydration, and no kinetic information is available on the formation of fumaric acid because of the difficulty in measuring the fumaric acid concentration accurately.

6.2.4. Other metal ion catalysts, and the hydration of other olefinic carboxylic acids

Besides Cr^{3+}, Fe^{3+} ion (added as $FeCl_3{\cdot}6H_2O$) was found in the present study and Al^{3+} (added as $Al_2(SO_4)_3{\cdot}18H_2O$) is known from the literature,[2] to catalyze the hydration of maleic acid in a similar fashion. The last two catalyst systems, however, give more isomerization product, fumaric acid. The Al^{3+} catalyst is reported to yield 73.9% malic acid and 26.1% fumaric acid while the Cr^{3+} catalyst yields 88.8 and 11.2% of malic and fumaric acid, respectively, at 170°C.[2] In the present study, the Fe^{3+} catalyst gave a system that analyzed for a mixture of 38.6, 44.0 and 17.4% of H_2MA, H_2mal and H_2FA, respectively, while Cr^{3+} under the same conditions (Table 6.5, 8 h entry) gave a mixture of 66.2, 30.8 and 3.1% of H_2MA,

H_2mal and H_2FA, respectively. Other metal ions, such as, Rh^{3+} (added as $RhCl_3 \cdot 3H_2O$), Rh^{3+}/Rh^{+} (prepared *in situ* from $RhCl_3 \cdot 3H_2O$ using C_2H_4)[21], Ru^{3+} ($RuCl_3 \cdot 3H_2O$), Ru^{2+} (via $TiCl_3$ reduction of $(NH_4)_2RuCl_6$ in 3 M HCl)[22] and Pt^{2+} (K_2PtCl_4), were shown in the present studies to be ineffective for either hydration or isomerization of maleic acid under the same conditions (100°C, closed system).

Among the olefinic carboxylic acids tested with the Cr^{3+} system, maleic acid was the only substrate catalytically hydrated. Fumaric acid, mesaconic acid ($HO_2CC(CH_3)=CHCO_2H$) and aconitic acid ($HO_2CC(CH_2COOH)=CHCO_2H$) were shown in the present work to be unreactive. When the mixture of R, S -malic acid and Cr^{3+} was heated at 100°C for 8 h, no dehydration product, either as maleic acid or fumaric acid, was detected; furthermore, under the same conditions, S-malic acid was not racemized. The replacement of malato ligand by maleate must be facile when maleic acid is present in large excess, however, because under similar experimental conditions, both cis-$K[Cr(MA)_2(H_2O)_2]$ and cis-$K[Cr(mal)_2(H_2O)_2]$ as catalysts gave comparable hydration mixtures after ~ 2 h (Table 6.9).

Table 6.9. Hydration Products of Maleic Acid Using Diaquo- bis(MA) and -bis(mal) Cr^{3+} Complexes as Catalysts

cis-$K[Cr(MA)_2(H_2O)_2]$			cis-$K[Cr(mal)_2(H_2O)_2]$		
$[H_2MA]_i$ = 0.862 M, [Cr] = 1.01×10^{-2} M t = 2.17 h, temp. = 100.0°C			$[H_2MA]_i$ = 0.862 M, [Cr] = 9.52×10^{-3} M t = 2.17 h, temp. = 100.0°C		
$[H_2MA]$	$[H_2mal]$	$[H_2FA]$	$[H_2MA]$	$[H_2mal]$	$[H_2FA]$
86.7%	10.0%	3.3%	84.6%	12.0%[a]	3.4%

(a) Malic acid from the catalyst contributes $9.52 \times 10^{-3} \times 2/[0.862 + (2 \times 9.52 \times 10^{-3})] = 2.2\%$.

6.3. Conclusion

The catalytic hydration of maleic acid by a non-phosphine metal complex was realized at 100°C using Cr^{3+} ion, and the kinetics were studied in some detail in the present work.

Previous workers had reported on such catalytic activity at 170°C.[2] Because of the practical problems of this system (Sect. 6.1), large errors in the kinetic data became inevitable. A temperature variation study was impossible because of the concentration change of the key catalytic species resulting from oligomerization. The maleic acid consumption is first-order in Cr_{total} concentration below approximately 2.7×10^{-2} M, but the initial rate dependence gradually drops off at higher Cr concentrations. This decrease is attributable perhaps partially to the oligomerization and partially to the interference of malic acid (see Scheme 6.1). A pH dependence of the maleic acid conversion is evident. Addition of base causes extensive oligomerization and formation of possibly a hydroxide; the reduction of catalyst concentration at higher pH (2.0 - 3.0) is believed to be responsible for the reduction in conversion. The specific interaction between maleate and Cr involved in the catalysis is not yet clear. Several other metal ions tested showed negative results with maleic acid, and the hydration of fumaric acid and other prochiral olefins using Cr^{3+} was also unsuccessful. Asymmetric synthesis of malic acid from prochiral fumaric acid was thus not pursued further.

Olson and Taube's results[4] provide very useful information in attempts to elucidate the reaction mechanism. The malato ligand of $Cr(malato)(H_2O)_5^{2+}$ can be replaced readily by maleate at the initial stage of reaction. As malic acid accumulates, it becomes more difficult for the product to be released; the rate thus becomes substrate concentration dependent because of the competition of maleic and malic acid for the active $Cr(H_2O)_6^{3+}$ catalyst.

References

1. Kása, Z.; Déak, Gy. *Hung. J. Ind. Chem.,* **1983**, *11*, 313.

2. (a) Bzhasso, N.A.; Pyatnitskii, M.P. *Zh. Prikl. Khim.,* **1969**, *42*, 1610. (b) Bzhasso, N.A.; Pyatnitskii, M.P. *Izv. Vyssh. Ucheb. Zaved., Pishch. Tekhnol.,* **1967**, *5*, 207; through *C.A.* **1968**, *68*, 39013k.

3. Haupt, G.W. *J. Res. Natl. Bur. Stand. (U.S.),* **1952**, *48*, 414.

4. Olson, M.V.; Taube, H. *J. Am. Chem. Soc.,* **1970**, *92*, 3236.

5. Cotton, F.A.; Wilkinson, G. *Advanced Inorganic Chemistry,* 4th ed.; John Wiley and Sons: New York, 1980; p.727.

6. (a) Wood, D.L.; Ferguson, J.; Knox, K.; Dillon, J.F. Jr. *J. Chem. Phys.,* **1963**, *39*, 890. (b) Figgis, B.N. *Introduction to Ligand Fields;* Wiley: New York, 1966; p.209, 222.

7. O'Brien, T.O. In *Chemistry of Coordination Compounds,* Ed. Bailar, J.C. Jr.; Reinhold: New York, 1956; pp.261 - 262.

8. Gates, H.S.; King, E.L. *J. Am. Chem. Soc.,* **1958**, *80*, 5011.

9. Johnson, H.B.; Reynolds, W.L. *Inorg. Chem.,* **1963**, *2*, 468.

10. Swaddle, T.W.; King, E.L. *Inorg. Chem.,* **1965**, *4*, 532.

11. Halpern, J.; Harkness, A.C. *J. Chem. Phys.,* **1959**, *31*, 1147.

12. Cathers, R.E.; Wendlandt, W.W. *J. Inorg. Nucl. Chem.,* **1965**, *27*, 1015.

13. (a) Thompson, M.; Connik, R.E. *Inorg. Chem.,* **1981**, *20*, 2279. (b) Finholt, J.E.; Thompson, M.; Connik, R.E. *Inorg. Chem.,* **1981**, *20*, 4151.

14. Laswick, J.A.; Plane, R.A. *J. Am. Chem. Soc.,* **1959**, *81*, 3564.

15. Stunzi, H.; Marty, W. *Inorg. Chem.,* **1983**, *22*, 2145.

16. Bauer, H.H.; Christian, G.D.; O'Reilly, J.E. *Instrumental Analysis;* Allyn and Bacon: Boston, 1978; pp.178 - 179.

17. Olson, M.V.; Taube, H. *Inorg. Chem.,* **1970**, *9*, 2072.

18. Halpern, J.; Harrod, J.F.; James, B.R. *J. Am. Chem. Soc.,* **1961**, *83*, 753.

19. James, B.R.; Louie, J. *Inorg. Chim. Acta,* **1969**, *3*, 568.

20. Gahan, L.R.; Harrowfield, J.M.; Herlt, A.J.; Lindoy, L.F.; Whimp, P.O.; Sargeson, A.M. *J. Am. Chem. Soc.,* **1985**, *107,* 6231.

21. (a) James, B.R.; Kastner, M.; Rempel, G.L. *Can. J. Chem.*, **1969**, *47*, 349. (b) James, B.R.; Rempel, G.L. *Can. J. Chem.*, **1968**, *46*, 571.

22. Halpern, J.; James, B.R. *Can. J. Chem.*, **1966**, *44*, 495.

Appendix

AI. Structural parameters of $Pt_2Cl_2(\mu\text{-}PN_2)_2$ (HT), 7b.1

Empirical formula	$C_{32}H_{26}Cl_2N_4P_2Pt_2$
Formula weight	989.62
Crystal system	Monoclinic
Lattice parameters:	a = 15.142(5) Å
	b = 9.853(3) Å
	c = 23.74(1) Å
	β = 107.98(3)°
	V = 3369(2) Å^3
Space group	P21/n (#14)
Z value	4
Density calculated	1.95 g/cm^3
Residuals: R; Rw	0.056; 0.069
Goodness of fit indicator	2.09
Maximum shift in final cycle	0.08
Largest peak in final diff. map	4.11 e/Å^3

Intramolecular distances involving the nonhydrogen atoms

atom	atom	distance	atom	atom	distance
Pt(1)	N(3)	2.10(1)	C(6)	C(7)	1.36(2)
Pt(1)	P(1)	2.169(3)	C(7)	C(8)	1.36(2)
Pt(1)	Cl(1)	2.405(4)	C(8)	C(9)	1.36(3)
Pt(1)	Pt(2)	2.574(1)	C(9)	C(10)	1.33(3)
Pt(2)	N(1)	2.08(1)	C(11)	C(12)	1.35(2)
Pt(2)	P(2)	2.169(4)	C(11)	C(16)	1.36(2)
Pt(2)	Cl(2)	2.383(4)	C(12)	C(13)	1.46(3)
P(1)	C(6)	1.83(2)	C(13)	C(14)	1.35(3)
P(1)	C(1)	1.83(2)	C(14)	C(15)	1.26(3)
P(1)	C(11)	1.86(2)	C(15)	C(16)	1.37(3)
P(2)	C(17)	1.80(2)	C(17)	C(18)	1.41(2)
P(2)	C(22)	1.80(2)	C(18)	C(19)	1.35(2)
P(2)	C(27)	1.84(2)	C(19)	C(20)	1.36(3)
N(1)	C(1)	1.36(2)	C(20)	C(21)	1.40(2)
N(1)	C(5)	1.36(2)	C(22)	C(23)	1.36(2)
N(2)	C(6)	1.33(2)	C(23)	C(24)	1.39(2)
N(2)	C(10)	1.37(2)	C(24)	C(25)	1.37(3)
N(3)	C(21)	1.31(2)	C(25)	C(26)	1.34(3)
N(3)	C(17)	1.38(2)	C(27)	C(32)	1.35(2)
N(4)	C(22)	1.38(2)	C(27)	C(28)	1.37(2)
N(4)	C(26)	1.39(2)	C(28)	C(29)	1.31(2)
C(1)	C(2)	1.36(2)	C(29)	C(30)	1.31(3)
C(2)	C(3)	1.38(3)	C(30)	C(31)	1.40(3)
C(3)	C(4)	1.37(3)	C(31)	C(32)	1.39(2)
C(4)	C(5)	1.30(3)			

Distances are in Å. Estimated standard deviations in the least significant figure are given in parentheses.

Torsion and conformation angles

(1)	(2)	(3)	(4)	angle	(1)	(2)	(3)	(4)	angle
Pt(1)	N(3)	C(21)	C(20)	178(2)	Pt(2)	Pt(1)	P(1)	C(1)	39.2(6)
Pt(1)	N(3)	C(17)	C(18)	176(1)	Pt(2)	Pt(1)	P(1)	C(11)	159.8(6)
Pt(1)	N(3)	C(17)	P(2)	-2(1)	Cl(1)	Pt(1)	N(3)	C(21)	39(1)
Pt(1)	P(1)	C(6)	N(2)	118(1)	Cl(1)	Pt(1)	N(3)	C(17)	-143(1)
Pt(1)	P(1)	C(6)	C(7)	-60(1)	Cl(1)	Pt(1)	P(1)	C(6)	91.2(5)
Pt(1)	P(1)	C(1)	N(1)	-29(1)	Cl(1)	Pt(1)	P(1)	C(1)	-147.4(6)
Pt(1)	P(1)	C(1)	C(2)	149(2)	Cl(1)	Pt(1)	P(1)	C(11)	-26.7(6)
Pt(1)	P(1)	C(11)	C(12)	-26(2)	Cl(1)	Pt(1)	Pt(2)	N(1)	-130(1)
Pt(1)	P(1)	C(11)	C(16)	159(1)	Cl(1)	Pt(1)	Pt(2)	P(2)	48(1)
Pt(1)	Pt(2)	N(1)	C(1)	32(1)	Cl(1)	Pt(1)	Pt(2)	Cl(2)	48(3)
Pt(1)	Pt(2)	N(1)	C(5)	-150(1)	Cl(2)	Pt(2)	N(1)	C(1)	-148(1)
Pt(1)	Pt(2)	P(2)	C(17)	44.7(5)	Cl(2)	Pt(2)	N(1)	C(5)	31(1)
Pt(1)	Pt(2)	P(2)	C(22)	-76.7(5)	Cl(2)	Pt(2)	P(2)	C(17)	-135.3(5)
Pt(1)	N(1)	C(1)	C(2)	174(1)	Cl(2)	Pt(2)	P(2)	C(27)	-17.1(6)
Pt(1)	Pt(2)	P(2)	C(27)	162.9(6)	Cl(2)	Pt(2)	P(2)	C(22)	103.3(6)
Pt(2)	N(1)	C(5)	P(1)	-8(2)	Cl(2)	Pt(2)	Pt(1)	N(3)	-37(2)
Pt(2)	N(1)	C(5)	C(4)	-176(2)	Cl(2)	Pt(2)	Pt(1)	P(1)	143(2)
Pt(2)	P(2)	C(17)	N(3)	-37(1)	P(1)	C(6)	N(2)	C(10)	-178(1)
Pt(2)	P(2)	C(17)	C(18)	145(2)	P(1)	C(6)	C(7)	C(8)	179(1)
Pt(2)	P(2)	C(22)	C(23)	-25(2)	P(1)	C(1)	N(1)	C(5)	174(1)
Pt(2)	P(2)	C(22)	N(4)	159(1)	P(1)	C(1)	C(2)	C(3)	-173(2)
Pt(2)	P(2)	C(27)	C(32)	110(2)	P(1)	C(11)	C(12)	C(13)	-179(1)
Pt(2)	P(2)	C(27)	C(28)	-64(1)	P(1)	C(11)	C(16)	C(15)	180(2)
Pt(2)	Pt(1)	N(3)	C(21)	-147(1)	P(1)	Pt(1)	N(3)	C(21)	-146(2)
Pt(2)	Pt(1)	N(3)	C(17)	30(1)	P(1)	Pt(1)	N(3)	C(17)	32(3)
Pt(2)	Pt(1)	P(1)	C(6)	-82.2(5)	P(1)	Pt(1)	Pt(2)	N(1)	-34.2(4)
P(1)	Pt(1)	Pt(2)	P(2)	143.4(1)	N(3)	Pt(1)	P(1)	C(6)	-84(3)
P(2)	C(17)	N(3)	C(21)	176(1)	N(3)	Pt(1)	P(1)	C(1)	38(3)
P(2)	C(17)	C(18)	C(19)	-174(2)	N(3)	Pt(1)	P(1)	C(11)	158(3)
P(2)	C(22)	C(23)	C(24)	-177(1)	N(4)	C(22)	C(23)	C(24)	-1(3)
P(2)	C(22)	N(4)	C(26)	177(1)	N(4)	C(22)	P(2)	C(17)	35(1)

(to be continued)

Tortion and conformation angles

(1)	(2)	(3)	(4)	angle	(1)	(2)	(3)	(4)	angle
P(2)	C(27)	C(32)	C(31)	-168(2)	N(4)	C(22)	P(2)	C(27)	-73(1)
P(2)	C(27)	C(28)	C(29)	176(2)	N(4)	C(26)	C(25)	C(24)	0(3)
P(2)	Pt(2)	N(1)	C(1)	10(4)	C(1)	N(1)	C(5)	C(4)	2(3)
P(2)	Pt(2)	Pt(1)	N(3)	-36.8(3)	C(1)	P(1)	C(6)	C(7)	175(1)
N(1)	C(1)	C(2)	C(3)	5(3)	C(1)	P(1)	C(11)	C(12)	100(1)
N(1)	C(1)	P(1)	C(6)	96(1)	C(1)	P(1)	C(11)	C(16)	-75(1)
N(1)	C(1)	P(1)	C(11)	-158(1)	C(2)	C(1)	N(1)	C(5)	-4(2)
N(1)	C(5)	C(4)	C(3)	-1(4)	C(2)	C(1)	P(1)	C(6)	-87(2)
N(1)	Pt(2)	P(2)	C(17)	67(3)	C(2)	C(1)	P(1)	C(11)	20(2)
N(1)	Pt(2)	P(2)	C(22)	-54(3)	C(2)	C(3)	C(4)	C(5)	2(4)
N(1)	Pt(2)	P(2)	C(27)	-175(3)	C(6)	N(2)	C(10)	C(9)	0(3)
N(1)	Pt(2)	Pt(1)	N(3)	145.6(5)	C(6)	C(7)	C(8)	C(9)	-1(3)
N(2)	C(6)	C(7)	C(8)	1(2)	C(6)	P(1)	C(11)	C(12)	-149(1)
N(2)	C(6)	P(1)	C(1)	-7(1)	C(6)	P(1)	C(11)	C(16)	36(1)
N(2)	C(6)	P(1)	C(11)	-115(1)	C(7)	C(8)	C(9)	C(10)	0(3)
N(2)	C(10)	C(9)	C(8)	0(4)	C(7)	C(6)	N(2)	C(10)	0(2)
N(3)	C(21)	C(20)	C(19)	4(3)	C(7)	C(6)	P(1)	C(11)	67(1)
N(3)	C(17)	C(18)	C(19)	8(3)	C(11)	C(12)	C(13)	C(14)	3(3)
N(3)	C(17)	P(2)	C(22)	89(1)	C(11)	C(16)	C(15)	C(14)	-3(4)
N(3)	C(17)	P(2)	C(27)	-163(1)	C(12)	C(11)	C(16)	C(15)	5(3)
C(12)	C(13)	C(14)	C(15)	-1(4)	C(13)	C(14)	C(15)	C(16)	1(4)
C(13)	C(12)	C(11)	C(16)	-5(3)	C(17)	N(3)	C(21)	C(20)	0(3)
C(17)	C(18)	C(19)	C(20)	-5(4)	C(17)	P(2)	C(27)	C(32)	-128(2)
C(17)	P(2)	C(27)	C(28)	58(1)	C(18)	C(19)	C(20)	C(21)	-1(4)
C(18)	C(17)	N(3)	C(21)	-6(2)	C(18)	C(17)	P(2)	C(22)	-89(2)
C(18)	C(17)	P(2)	C(27)	19(2)	C(22)	C(23)	C(24)	C(25)	1(3)
C(22)	N(4)	C(26)	C(25)	-1(3)	C(22)	P(2)	C(27)	C(32)	-17(2)
C(22)	P(2)	C(27)	C(28)	169(1)	C(23)	C(22)	N(4)	C(26)	1(3)
C(23)	C(22)	P(2)	C(27)	103(1)	C(23)	C(24)	C(25)	C(26)	0(3)
C(27)	C(32)	C(31)	C(30)	-9(4)	C(27)	C(28)	C(29)	C(30)	-6(4)
C(28)	C(29)	C(30)	C(31)	3(4)	C(28)	C(27)	C(32)	C(31)	6(3)
C(29)	C(28)	C(27)	C(32)	1(3)	C(29)	C(30)	C(31)	C(32)	5(4)

The sign is positive if when looking fron atom 2 to atom 3 a clockwise motion of atom 1 would superimpose it on atom 4.

Intramolecular bond angles involving the nonhydrogen atoms

atom	atom	atom	angle	atom	atom	atom	angle
N(3)	Pt(1)	P(1)	172.9(3)	C(5)	N(1)	Pt(2)	120(1)
N(3)	Pt(1)	Cl(1)	88.0(3)	C(6)	N(2)	C(10)	116(1)
N(3)	Pt(1)	Pt(2)	91.4(3)	C(21)	N(3)	C(17)	118(1)
P(1)	Pt(1)	Cl(1)	99.1(1)	C(21)	N(3)	Pt(1)	122(1)
P(1)	Pt(1)	Pt(2)	81.5(1)	C(17)	N(3)	Pt(1)	119.0(9)
Cl(1)	Pt(1)	Pt(2)	173.5(1)	C(22)	N(4)	C(26)	119(2)
N(1)	Pt(2)	P(2)	173.7(3)	N(1)	C(1)	C(2)	121(2)
N(1)	Pt(2)	Cl(2)	90.6(4)	N(1)	C(1)	P(1)	113(1)
N(1)	Pt(2)	Pt(1)	92.8(3)	C(2)	C(1)	P(1)	126(1)
P(2)	Pt(2)	Cl(2)	95.3(2)	C(1)	C(2)	C(3)	117(2)
P(2)	Pt(2)	Pt(1)	81.4(1)	C(4)	C(3)	C(2)	122(2)
Cl(2)	Pt(2)	Pt(1)	176.6(1)	C(5)	C(4)	C(3)	120(2)
C(6)	P(1)	C(1)	107.0(7)	C(4)	C(5)	N(1)	121(2)
C(6)	P(1)	C(11)	101.7(7)	N(2)	C(6)	C(7)	122(1)
C(6)	P(1)	Pt(1)	112.3(5)	N(2)	C(6)	P(1)	120(1)
C(1)	P(1)	C(11)	103.0(7)	C(7)	C(6)	P(1)	118(1)
C(1)	P(1)	Pt(1)	113.4(5)	C(8)	C(7)	C(6)	120(1)
C(11)	P(1)	Pt(1)	118.2(6)	C(7)	C(8)	C(9)	119(2)
C(17)	P(2)	C(22)	106.9(7)	C(10)	C(9)	C(8)	119(2)
C(17)	P(2)	C(27)	103.3(7)	C(9)	C(10)	N(2)	124(2)
C(17)	P(2)	Pt(2)	111.0(5)	C(12)	C(11)	C(16)	122(2)
C(22)	P(2)	C(27)	102.6(8)	C(12)	C(11)	P(1)	120(1)
C(22)	P(2)	Pt(2)	114.9(5)	C(16)	C(11)	P(1)	118(1)
C(27)	P(2)	Pt(2)	117.0(6)	C(11)	C(12)	C(13)	116(2)
C(1)	N(1)	C(5)	120(1)	C(14)	C(13)	C(12)	120(2)
C(1)	N(1)	Pt(2)	120(1)	C(15)	C(14)	C(13)	120(2)
C(14)	C(15)	C(16)	124(2)	C(11)	C(16)	C(15)	118(2)
N(3)	C(17)	C(18)	120(1)	N(3)	C(17)	C(18)	120(1)
N(3)	C(17)	P(2)	113(1)	C(18)	C(17)	P(2)	127(1)
C(19)	C(18)	C(17)	120(2)	C(18)	C(19)	C(20)	120(2)

Intramolecular bond angles involving the nonhydrogen atoms (continued)

atom	atom	atom	angle	atom	atom	atom	angle
C(19)	C(20)	C(21)	119(2)	N(3)	C(21)	C(20)	123(2)
C(23)	C(22)	N(4)	120(2)	C(23)	C(22)	P(2)	121(1)
N(4)	C(22)	P(2)	119(1)	C(22)	C(23)	C(24)	119(2)
C(25)	C(24)	C(23)	121(2)	C(26)	C(25)	C(24)	119(2)
C(25)	C(26)	N(4)	122(2)	C(32)	C(27)	C(28)	121(1)
C(32)	C(27)	P(2)	124(1)	C(28)	C(27)	P(2)	115(1)
C(29)	C(28)	C(27)	117(2)	C(28)	C(29)	C(30)	125(2)
C(29)	C(30)	C(31)	119(2)	C(32)	C(31)	C(30)	116(2)
C(27)	C(32)	C(31)	120(2)				

Angles are in degrees. Estimated standard deviations in the least significant figure are given in parentheses.

AII. The acid-base titration data for $Pd_2Cl_2(\mu\text{-}PN_3)_2(HT)$, **11c**, and $PdCl_2(PN_3)_2$, **4c**, in aqueous solution.

Table AII 1. NaOH titration against HNO_3[a]

vol (mL)	pH	vol (mL)	pH
0.000	2.905	0.618	9.650
0.126	3.030	0.649	9.820
0.262	3.228	0.681	9.950
0.390	3.570	0.778	10.195
0.427	3.725	0.905	10.395
0.455	3.962	1.134	10.615
0.488	4.460	1.382	10.770
0.520	6.795	1.610	10.910
0.552	8.970	1.962	10.990

(a) $[HNO_3] = 9.80\times10^{-4}$ M, $[NaOH] = 4.71\times10^{-2}$ M; ionic strength I = 0.3 M using $NaNO_3$, temp. = 25.0 ± 0.2°C, under N_2 (see Fig. 3.21).

Table AII 2. NaOH titration against HNO_3 and **11c**[a]

vol (mL)	pH	vol (mL)	pH
0.000	2.970	0.682	9.610
0.102	3.075	0.712	9.780
0.166	3.166	0.745	9.910
0.259	3.330	0.807	10.100
0.324	3.490	0.870	10.240
0.394	3.765	0.934	10.345
0.427	3.995	0.996	10.430
0.460	4.442	1.061	10.500
0.490	4.920	1.157	10.590
0.524	5.845	1.316	10.705
0.554	7.075	1.506	10.815
0.584	8.200	1.665	10.885
0.618	8.960	1.859	10.955
0.650	9.360	1.986	10.995

(a) $[HNO_3] = 9.80\times10^{-4}$ M, $[NaOH] = 4.71\times10^{-2}$ M, $[\mathbf{11c}] = 4.98\times10^{-4}$ M; ionic strength I = 0.3 M using $NaNO_3$, temp. = 25.0 ± 0.2°C, under N_2 (see Fig. 3.21).

Table AII 3.NaOH titration against HNO_3[a]

vol (mL)	pH	vol (mL)	pH
0.000	2.890	0.613	9.575
0.129	3.016	0.646	9.760
0.228	3.150	0.709	10.005
0.291	3.266	0.805	10.228
0.387	3.530	0.969	10.454
0.420	3.680	1.166	10.626
0.452	3.895	1.427	10.780
0.483	4.300	1.631	10.870
0.516	6.070	1.828	10.940
0.548	8.770	1.993	10.990
0.580	9.285		

(a) The conditions are exactly the same as described in Table AII 1 (a).

Table AII 4:.NaOH titration against HNO_3 and **11c**[a]

vol (mL)	pH	vol (mL)	pH
0.000	2.830	0.871	8.680
0.101	2.904	0.904	9.055
0.165	2.960	0.936	9.330
0.229	3.022	0.967	9.520
0.293	3.097	1.000	9.700
0.358	3.186	1.033	9.840
0.422	3.295	1.065	9.952
0.486	3.435	1.096	10.040
0.550	3.624	1.162	10.182
0.582	3.750	1.226	10.290
0.614	3.906	1.322	10.420
0.647	4.114	1.423	10.520
0.678	4.422	1.523	10.595
0.710	4.975	1.650	10.685
0.743	6.080	1.810	10.775
0.774	6.560	2.004	10.865
0.808	7.185		
0.840	8.005		

(a) The conditions are exactly the same as described in Table AII 2 (a).

Table AII 5. NaOH titration against HNO_3[a]

vol (mL)	pH	vol (mL)	pH
0.000	2.610	0.611	10.080
0.100	2.715	0.644	10.225
0.150	2.791	0.675	10.333
0.200	2.865	0.707	10.421
0.264	2.980	0.803	10.618
0.329	3.130	0.997	10.860
0.394	3.365	1.250	10.990
0.426	3.555	1.347	11.100
0.450	3.790	1.564	11.202
0.482	4.705	1.724	11.260
0.498	7.145	1.855	11.302
0.516	8.780	1.959	11.335
0.546	9.520	1.999	11.402
0.578	9.875		

(a) $[HNO_3] = 1.98 \times 10^{-3}$ M, $[NaOH] = 9.42 \times 10^{-2}$ M; ionic strength I = 0.3 M using $NaNO_3$, temp. = 25.0 ± 0.2°C, under nitrogen (see Fig. 3.24).

Table AII 6. NaOH titration against HNO_3 and 4c[a]

vol (mL)	pH	vol (mL)	pH
0.000	2.635	0.909	9.27
0.099	2.708	0.941	9.65
0.163	2.765	0.972	9.90
0.260	2.865	1.005	10.07
0.356	2.990	1.038	10.20
0.423	3.100	1.069	10.30
0.579	3.335	1.136	10.47
0.583	3.585	1.200	10.585
0.616	3.770	1.264	10.675
0.650	4.040	1.330	10.752
0.681	4.460	1.417	10.850
0.714	4.940	1.555	10.957
0.740	5.350	1.654	11.020
0.811	6.610	1.749	11.072
0.843	7.38	1.880	11.135
0.875	8.43	1.986	11.180

(a) $[HNO_3] = 1.98 \times 10^{-3}$ M, [4c] = 2.00×10^{-3} M, $[NaOH] = 9.42 \times 10^{-2}$ M; ionic strength I = 0.3 M using $NaNO_3$, temp. = 25.0 ±0.2°C, under N_2.

Table AII 7. NaOH titration against HNO_3 and 4c[a]

vol (mL)	pH	vol (mL)	pH
0.000	2.500	0.888	6.29
0.132	2.607	0.923	7.09
0.230	2.712	0.954	8.15
0.381	2.925	0.991	9.06
0.478	3.120	1.025	9.25
0.575	3.430	1.089	9.590
0.640	3.825	1.155	9.960
0.682	4.320	1.221	10.215
0.716	4.660	1.319	10.440
0.748	4.960	1.448	10.643
0.781	5.270	1.583	10.780
0.824	5.855	1.844	10.965
0.856	5.99	1.972	11.030

(a) The conditions are exactly the same as described in Table AII 6 (see Fig. 3.24)

Table AII 8. NaOH titration against 4c in the absence of HNO_3[a]

vol (mL)	pH	vol (mL)	pH
0.000	2.900	28.83	5.80
2.28	3.03	29.44	6.00
5.09	3.12	29.81	6.20
7.90	3.24	30.35	6.50
11.76	3.50	31.09	6.80
15.73	3.75	31.61	7.03
19.04	4.00	32.31	7.40
21.70	4.30	32.95	7.88
23.45	4.51	33.70	8.45
25.03	4.75	34.70	8.92
25.37	4.85	35.75	9.40
26.09	5.00	36.98	9.60
26.80	5.15	38.21	9.80
27.35	5.30	39.36	9.92
27.85	5.45	40.95	10.10
28.18	5.60	45.45	10.32

(a) $[NaOH] = 1.0 \times 10^{-3}$ M, [4c] = 3.34×10^{-3} M, 10 mL; ionic strength I = 0.3 M using $NaNO_3$; temp. = 25.0 ± 0.2 °C, under N_2 (see Fig. 3.22).

AIII. Kinetic data of the oxidative addition of DMAD to $Pt_2I_2(\mu\text{-}PN_3)_2$ (HT), 9c, in CH_2Cl_2.

Table AIII 1. [9c] = 1.18×10^{-3} M, [DAMD] = 3.58×10^{-2} M, temp. = 34.0°C.

t (s)	A_t (λ = 518 nm)	$-\ln(A_t - A_\infty)$
0.0	0.852	0.681
20.0	0.810	0.768
40.0	0.760	0.882
60.0	0.715	0.997
80.0	0.676	1.109
100.0	0.643	1.214
120.0	0.612	1.324
140.0	0.587	1.423
160.0	0.563	1.528
180.0	0.544	1.619
200.0	0.526	1.715
220.0	0.509	1.814
260.0	0.483	1.988
300.0	0.462	2.154
340.0	0.455	2.313
∞	0.346	

slope = 4.77×10^{-3} s^{-1}, R^2 = 0.996.

Table AIII 2. [9c] = 1.18×10^{-3} M, [DAMD] = 2.39×10^{-2} M, temp. = 34.0°C.

t (s)	A_t (λ = 518 nm)	$-\ln(A_t - A_\infty)$
0.0	0.857	0.671
40.0	0.793	0.805
60.0	0.758	0.887
80.0	0.726	0.968
100.0	0.697	1.047
120.0	0.671	1.124
140.0	0.649	1.194
180.0	0.609	1.336
200.0	0.592	1.402
250.0	0.554	1.570
280.0	0.535	1.666
320.0	0.513	1.790
380.0	0.486	1.960
450.0	0.462	2.154
∞	0.346	

slope = 3.29×10^{-3} s^{-1}, R^2 = 0.996.

Table AIII 3. [9c] = 1.18×10^{-3} M, [DAMD] = 1.19×10^{-2} M, temp. = 34.0°C.

t (s)	A_t (λ = 518 nm)	$-\ln(A_t - A_\infty)$
0.0	0.852	0.681
40.0	0.822	0.742
60.0	0.803	0.783
80.0	0.784	0.826
100.0	0.766	0.868
120.0	0.748	0.911
140.0	0.732	0.952
160.0	0.717	0.992
180.0	0.702	1.033
200.0	0.689	1.070
240.0	0.663	1.149
280.0	0.640	1.224
320.0	0.619	1.298
390.0	0.587	1.423
450.0	0.564	1.523
480.0	0.553	1.575
∞	0.347	

slope = 1.90×10^{-3} s^{-1}, R^2 = 0.999.

Table AIII 4. [9c] = 1.18×10^{-3} M, [DAMD] = 3.58×10^{-2} M, temp. = 29.0°C.

t (s)	A_t (λ = 518 nm)	$-\ln(A_t - A_\infty)$
0.0	0.858	0.717
20.0	0.817	0.805
40.0	0.776	0.901
60.0	0.738	1.000
80.0	0.705	1.090
100.0	0.674	1.190
120.0	0.648	1.280
140.0	0.624	1.370
160.0	0.603	1.457
180.0	0.584	1.542
200.0	0.565	1.635
220.0	0.549	1.720
250.0	0.527	1.852
280.0	0.509	1.973
300.0	0.497	2.064
340.0	0.476	2.244
400.0	0.455	2.465
510.0	0.423	2.937
600.0	0.407	3.297
∞	0.370	

slpoe = 4.28×10^{-3} s^{-1}, R^2 = 0.999.

Table AIII 5. [9c] = 1.18×10^{-3} M, [DAMD] = 2.39×10^{-2} M, temp. = 29.0°C.

t (s)	A_t (λ = 518 nm)	$-\ln(A_t - A_\infty)$
0.0	0.858	0.687
20.0	0.837	0.730
40.0	0.807	0.794
60.0	0.780	0.856
80.0	0.753	0.921
100.0	0.730	0.981
120.0	0.708	1.041
140.0	0.688	1.100
160.0	0.669	1.158
200.0	0.636	1.269
240.0	0.607	1.378
300.0	0.571	1.532
360.0	0.540	1.687
400.0	0.522	1.790
450.0	0.503	1.911
∞	0.355	

slope = 2.74×10^{-3} s^{-1}, R^2 = 0.998.

Table AIII 6. [9c] = 1.18×10^{-3} M, [DAMD] = 1.19×10^{-2} M, temp. = 29.0°C.

t (s)	A_t (λ = 518 nm)	$-\ln(A_t - A_\infty)$
0.0	0.858	0.687
20.0	0.854	0.695
40.0	0.840	0.724
60.0	0.825	0.755
80.0	0.810	0.787
100.0	0.796	0.819
120.0	0.783	0.849
140.0	0.770	0.879
160.0	0.758	0.909
180.0	0.747	0.936
200.0	0.736	0.965
240.0	0.714	1.024
280.0	0.696	1.076
320.0	0.677	1.133
380.0	0.653	1.211
450.0	0.627	1.302
510.0	0.607	1.378
570.0	0.589	1.452
∞	0.355	

slope = 1.38×10^{-3} s^{-1}, R^2 = 0.999.

Table AIII 7. [9c] = 1.18×10^{-3} M, [DAMD] = 3.25×10^{-2} M, temp. = 25.0°C.

t (s)	A_t (λ = 518 nm)	$-\ln(A_t - A_\infty)$
0.0	0.885	0.679
40.0	0.829	0.796
60.0	0.802	0.858
80.0	0.775	0.924
100.0	0.751	0.986
120.0	0.729	1.047
150.0	0.701	1.130
180.0	0.675	1.214
200.0	0.660	1.266
240.0	0.632	1.370
280.0	0.606	1.478
360.0	0.564	1.682
400.0	0.547	1.778
∞	0.378	

slope = 2.74×10^{-3} s^{-1}, R^2 = 0.998.

Table AIII 8. [9c] = 1.18×10^{-3} M, [DAMD] = 1.63×10^{-2} M, temp. = 25.0°C.

t (s)	A_t (λ = 518 nm)	$-\ln(A_t - A_\infty)$
0.0	0.884	0.681
40.0	0.857	0.736
60.0	0.839	0.774
80.0	0.824	0.807
100.0	0.807	0.846
140.0	0.784	0.901
180.0	0.755	0.976
220.0	0.733	1.036
260.0	0.711	1.100
300.0	0.693	1.155
360.0	0.666	1.245
450.0	0.632	1.370
∞	0.378	

slope = 1.55×10^{-3} s^{-1}, R^2 = 0.998.

Table AIII 9. [9c] = 1.45×10^{-4} M, [DAMD] = 5.70×10^{-3} M, temp. = 21.0°C.

t (min)	A_t (λ = 413 nm)	$-\ln(A_t - A_\infty)$
0.0	0.645	1.019
4.0	0.611	1.146
8.0	0.576	1.262
12.0	0.549	1.363
16.0	0.523	1.470
20.0	0.498	1.585
24.0	0.478	1.687
∞	0.293	

slope = 2.76×10^{-2} min^{-1}, R^2 = 0.999.

Table AIII 11. [9c] = 1.18×10^{-3} M, [DAMD] = 2.71×10^{-2} M, temp. = 18.0°C.

t (s)	A_t (λ = 518 nm)	$-\ln(A_t - A_\infty)$
0.0	0.881	0.687
40.0	0.844	0.764
60.0	0.819	0.819
80.0	0.798	0.868
100.0	0.779	0.914
120.0	0.761	0.960
160.0	0.729	1.047
200.0	0.700	1.133
240.0	0.674	1.217
280.0	0.651	1.298
330.0	0.625	1.398
390.0	0.597	1.519
450.0	0.573	1.635
510.0	0.552	1.749
570.0	0.534	1.858
660.0	0.510	2.025
780.0	0.485	2.235
∞	0.378	

slope = 2.00×10^{-3} s^{-1}, R^2 = 0.998.

Table AIII 10. [9c] = 1.45×10^{-4} M, [DAMD] = 8.13×10^{-3} M, temp. = 21.0°C.

t (min)	A_t (λ = 428 nm)	$-\ln(A_t - A_\infty)$
0.0	0.631	1.073
3.0	0.596	1.189
6.0	0.561	1.302
9.0	0.532	1.415
12.0	0.505	1.532
15.0	0.478	1.666
18.0	0.457	1.784
21.0	0.438	1.904
24.0	0.420	2.033
∞	0.289	

slope = 4.01×10^{-2} min^{-1}, R^2 = 1.000.

Table AIII 12. [9c] = 1.18×10^{-3} M, [DAMD] = 2.39×10^{-2} M, temp. = 18.0°C.

t (s)	A_t (λ = 518 nm)	$-\ln(A_t - A_\infty)$
0.0	0.883	0.683
40.0	0.839	0.774
60.0	0.821	0.814
80.0	0.805	0.851
110.0	0.780	0.911
150.0	0.754	0.978
180.0	0.736	1.027
240.0	0.705	1.118
300.0	0.678	1.204
360.0	0.652	1.295
420.0	0.630	1.378
480.0	0.609	1.465
540.0	0.590	1.551
660.0	0.556	1.726
780.0	0.528	1.897
∞	0.378	

slope = 1.49×10^{-3} s^{-1}, R^2 = 0.991.

Table AIII 13. [9c] = 1.18×10^{-3} M, [DAMD] = 1.19×10^{-2} M, temp. = 18.0°C.

t (s)	A_t (λ = 518 nm)	$-\ln(A_t - A_\infty)$
0.0	0.876	0.697
40.0	0.864	0.722
80.0	0.844	0.764
120.0	0.827	0.801
180.0	0.805	0.851
220.0	0.792	0.882
260.0	0.780	0.911
300.0	0.767	0.944
380.0	0.745	1.002
460.0	0.734	1.033
540.0	0.703	1.124
620.0	0.683	1.187
720.0	0.662	1.259
840.0	0.639	1.343
960.0	0.618	1.427
∞	0.378	

slope = 7.64×10^{-4} s^{-1}, R^2 = 0.999.

Table AIII 15. [9c] = 1.18×10^{-3} M, [DAMD] = 3.58×10^{-2} M, temp. = 13.0°C.

t (s)	A_t (λ = 518 nm)	$-\ln(A_t - A_\infty)$
0.0	0.892	0.666
40.0	0.857	0.736
60.0	0.837	0.779
80.0	0.818	0.821
100.0	0.800	0.863
120.0	0.785	0.899
160.0	0.758	0.968
200.0	0.735	1.030
240.0	0.712	1.100
280.0	0.693	1.155
330.0	0.669	1.234
390.0	0.646	1.317
480.0	0.613	1.448
600.0	0.576	1.619
720.0	0.545	1.780
∞	0.378	

slope = 1.48×10^{-3} s^{-1}, R^2 = 0.999.

Table AIII 14. [9c] = 1.18×10^{-3} M, [DAMD] = 4.54×10^{-2} M, temp. = 18.0°C.

t (s)	A_t (λ = 518 nm)	$-\ln(A_t - A_\infty)$
0.0	0.886	0.677
40.0	0.812	0.835
60.0	0.782	0.906
80.0	0.757	0.970
100.0	0.734	1.033
120.0	0.714	1.091
140.0	0.694	1.156
160.0	0.677	1.207
180.0	0.661	1.262
200.0	0.646	1.317
240.0	0.618	1.427
270.0	0.599	1.510
330.0	0.566	1.671
390.0	0.538	1.833
480.0	0.505	2.064
550.0	0.483	2.254
780.0	0.434	2.882
∞	0.378	

slope = 2.75×10^{-3} s^{-1}, R^2 = 0.999.

Table AIII 16. [9c] = 1.18×10^{-3} M, [DAMD] = 2.39×10^{-2} M, temp. = 13.0°C.

t (s)	A_t (λ = 518 nm)	$-\ln(A_t - A_\infty)$
0.0	0.890	0.641
40.0	0.873	0.673
60.0	0.858	0.703
80.0	0.845	0.730
100.0	0.833	0.755
120.0	0.821	0.781
140.0	0.811	0.803
200.0	0.782	0.870
280.0	0.750	0.949
330.0	0.731	1.000
390.0	0.710	1.058
480.0	0.682	1.143
600.0	0.648	1.255
720.0	0.618	1.366
∞	0.378	

slope = 1.05×10^{-3} s^{-1}, R^2 = 0.998.

Table AIII 17. [9c] = 1.18×10^{-3} M, [DAMD] = 1.19×10^{-2} M, temp. = 13.0°C.

t (s)	A_t (λ = 518 nm)	$-\ln(A_t - A_\infty)$
0.0	0.885	0.650
40.0	0.867	0.685
80.0	0.852	0.715
120.0	0.838	0.744
160.0	0.824	0.774
210.0	0.810	0.855
270.0	0.793	0.844
360.0	0.774	0.889
420.0	0.760	0.924
540.0	0.735	0.989
600.0	0.722	1.024
720.0	0.700	1.088
∞	0.378	

slope = 6.08×10^{-4} s^{-1}, R^2 = 0.998.

AIV. Kinetic data of the oxidative addition of DMAD to $Pt_2I_2(\mu\text{-}PN_3)_2$ (HH) **10c** in CH_2Cl_2 (binding of DMAD, k_1).

Table AIV 1. [**10c**] = 1.10×10^{-3} M, [DAMD] = 4.88×10^{-2} M, temp. = 34.0°C.

t (s)	A_t (λ = 500 nm)	$-\ln(A_t - A_\infty^*)$
0.0	0.499	1.162
40.0	0.332	1.924
50.0	0.305	2.129
60.0	0.285	2.313
70.0	0.268	2.501
80.0	0.254	2.688
90.0	0.240	2.919
100.0	0.229	3.147
120.0	0.214	3.576
140.0	0.204	4.017
∞	0.186	

*The lowest absorbance recorded before the subsequent increase of absorbance reading, similarly hereinafter.

slope = 2.00×10^{-2} s^{-1}, R^2 = 0.998.

Table AIV 2. [**10c**] = 1.10×10^{-3} M, [DAMD] = 2.28×10^{-2} M, temp. = 34.0°C.

t (s)	A_t (λ = 500 nm)	$-\ln(A_t - A_\infty^*)$
0.0	0.508	1.146
40.0	0.415	1.492
60.0	0.379	1.666
80.0	0.349	1.839
100.0	0.324	2.010
120.0	0.304	2.172
140.0	0.288	2.323
160.0	0.275	2.465
180.0	0.263	2.617
200.0	0.253	2.765
∞	0.190	

slope = 9.85×10^{-3} s^{-1}, R^2 = 1.000.

TAble AIV 3. [10c] = 1.10×10^{-3} M, [DAMD] = 3.25×10^{-2} M, temp. = 34.0°C.

t (s)	A_t (λ = 500 nm)	$-\ln(A_t - A_\infty^*)$
0	0.501	1.168
30	0.399	1.565
40	0.377	1.677
60	0.336	1.924
80	0.305	2.163
100	0.278	2.430
120	0.258	2.688
140	0.242	2.957
160	0.230	3.219
180	0.219	3.540
200	0.212	3.817
∞	0.190	

slope = -1.31×10^{-2} s^{-1}, R^2 = 0.997

Table AIV 4. [10c] = 1.10×10^{-3} M, [DAMD] = 3.25×10^{-2} M, temp. = 29.0°C.

t (s)	A_t (λ = 500 nm)	$-\ln(A_t - A_\infty^*)$
0.0	0.498	1.158
40.0	0.382	1.619
60.0	0.346	1.820
80.0	0.318	2.010
100.0	0.295	2.198
120.0	0.275	2.397
140.0	0.259	2.590
160.0	0.245	2.797
180.0	0.234	2.996
200.0	0.225	3.194
∞	0.184	

slope = 1.00×10^{-2} s^{-1}, R^2 = 0.999.

Table AIV 5. [10c] = 1.10×10^{-3} M, [DAMD] = 6.50×10^{-2} M, temp. = 29.0°C.

t (s)	A_t (λ = 500 nm)	$-\ln(A_t - A_\infty^*)$
0.0	0.509	1.136
40.0	0.320	2.025
50.0	0.298	2.207
60.0	0.276	2.430
70.0	0.260	2.631
80.0	0.247	2.830
90.0	0.236	3.037
100.0	0.227	3.244
120.0	0.213	3.689
∞	0.190	

slope = 2.20×10^{-2} s^{-1}, R^2 = 0.999.

Table AIV 6. [10c] = 1.10×10^{-3} M, [DAMD] = 4.06×10^{-2} M, temp.= 25.0°C.

t (s)	A_t (λ = 500 nm)	$-\ln(A_t - A_\infty^*)$
0.0	0.488	1.130
30.0	0.384	1.519
40.0	0.359	1.640
50.0	0.340	1.743
60.0	0.323	1.843
70.0	0.308	1.945
80.0	0.294	2.048
100.0	0.270	2.254
120.0	0.250	2.465
140.0	0.235	2.659
160.0	0.222	2.865
∞	0.168	

slope = 9.08×10^{-3} s^{-1}, R^2 = 1.000.

Table AIV 7. [10c] = 1.10×10^{-3} M, [DAMD] = 6.50×10^{-2} M, temp. = 25.0°C.

t (s)	A_t (λ = 500 nm)	$-\ln(A_t - A_\infty^*)$
0.0	0.488	1.106
30.0	0.352	1.704
40.0	0.325	1.864
50.0	0.299	2.048
60.0	0.280	2.207
70.0	0.263	2.375
80.0	0.250	2.526
100.0	0.228	2.847
120.0	0.212	3.170
∞	0.170	

slope = 1.73×10^{-2} s^{-1}, R^2 = 1.000.

Table AIV 8. [10c] = 1.10×10^{-3} M, [DAMD] = 3.25×10^{-2} M, temp. = 21.0°C.

t (s)	A_t (λ = 500 nm)	$-\ln(A_t - A_\infty^*)$
0.0	0.490	1.152
40.0	0.398	1.500
50.0	0.375	1.604
60.0	0.359	1.687
70.0	0.344	1.772
80.0	0.331	1.852
90.0	0.319	1.931
100.0	0.308	2.010
120.0	0.290	2.154
140.0	0.275	2.293
160.0	0.260	2.453
200.0	0.238	2.749
240.0	0.223	3.016
280.0	0.211	3.297
∞	0.174	

slope = 7.58×10^{-3} s^{-1}, R^2 = 0.999

Table AIV 9. [10c] = 1.10×10^{-3} M, [DAMD] = 6.50×10^{-2} M, temp. = 21.0°C.

t (s)	A_t (λ = 500 nm)	$-\ln(A_t - A_\infty^*)$
0.0	0.499	1.124
40.0	0.340	1.833
60.0	0.299	2.129
70.0	0.286	2.244
80.0	0.270	2.408
90.0	0.259	2.538
100.0	0.249	2.674
120.0	0.232	2.957
160.0	0.210	3.502
∞	0.177	

slope = 1.33×10^{-2} s^{-1}, R^2 = 0.999.

Table AIV 10. [**10c**] = 1.10×10^{-3} M, [DAMD] = 6.50×10^{-2} M, temp.= 17.0°C.

t (s)	A_t (λ = 500 nm)	$-\ln(A_t - A_\infty^*)$
0.0	0.493	1.121
30.0	0.356	1.614
40.0	0.328	1.766
50.0	0.307	1.897
60.0	0.290	2.017
70.0	0.274	2.146
100.0	0.239	2.501
140.0	0.213	2.882
180.0	0.192	3.352
∞	0.164	

slope = 1.09×10^{-2} s^{-1}, R^2 = 0.997.

Table AIV 11. [**10c**] = 1.10×10^{-3} M, [DAMD] = 4.07×10^{-2} M, temp.= 17.0°C.

t (s)	A_t (λ = 500 nm)	$-\ln(A_t - A_\infty^*)$
0.0	0.492	1.109
30.0	0.396	1.431
40.0	0.376	1.519
50.0	0.357	1.609
60.0	0.340	1.698
80.0	0.313	1.858
100.0	0.293	1.995
120.0	0.273	2.154
160.0	0.245	2.430
220.0	0.217	2.813
∞	0.159	

slope = 7.14×10^{-3} s^{-1}, R^2 = 0.997.

AV. Kinetic data of the isomerization of $Pt_2I_2(\mu\text{-DMAD})(\mu\text{-PN}_3)_2$ (HH), **28.2** to $Pt_2I_2(\mu\text{-DMAD})(\mu\text{-PN}_3)_2$ (HT), **19**, in CH_2Cl_2 (k_2).

Table AV 1. [**10c**] = 1.10×10^{-3} M, [DAMD] = 2.28×10^{-2} M, temp. = 34.0°C.

t (min)	A_t (λ = 476 nm)	$-\ln(A_\infty - A_t)$
0.0	0.363	1.174
5.0	0.373	1.207
35.0	0.460	1.551
65.0	0.517	1.864
95.0	0.558	2.172
125.0	0.589	2.489
155.0	0.609	2.765
185.0	0.625	3.058
215.0	0.636	3.324
∞	0.672	

slope = 1.01×10^{-2} min^{-1}, R^2 = 0.997.

Table AV 2. [**10c**] = 1.10×10^{-3} M, [DAMD] = 3.25×10^{-2} M, temp. = 34.0°C.

t (h)	A_t (λ = 460 nm)	$-\ln(A_\infty - A_t)$
0.0	0.478	0.872
0.04	0.503	0.929
1.04	0.698	1.609
2.04	0.787	2.198
3.04	0.830	2.688
4.04	0.860	3.270
∞	0.898	

slope = 9.76×10^{-3} min^{-1}, R^2 = 0.997.

Table AV 3. [**10c**] = 1.10×10^{-3} M, [DAMD] = 4.88×10^{-2} M, temp. = 34.0°C.

t (min)	A_t (λ = 460 nm)	$-\ln(A_\infty - A_t)$
0.0	0.451	0.920
3.0	0.469	0.965
28.0	0.568	1.266
53.0	0.634	1.532
78.0	0.685	1.802
103.0	0.715	2.002
128.0	0.745	2.250
153.0	0.765	2.470
178.0	0.782	2.690
203.0	0.795	2.900
∞	0.850	

slope = 9.72×10^{-3} min^{-1}, R^2 = 0.997.

Table AV 4. [**10c**] = 1.10×10^{-3} M, [DAMD] = 3.25×10^{-2} M, temp. = 29.0°C.

t (min)	A_t (λ = 480 nm)	$-\ln(A_\infty - A_t)$
0.0	0.286	1.115
9.0	0.296	1.146
39.0	0.356	1.355
69.0	0.399	1.537
99.0	0.435	1.720
129.0	0.463	1.890
159.0	0.486	2.056
189.0	0.507	2.235
219.0	0.522	2.386
249.0	0.539	2.590
279.0	0.548	2.718
∞	0.614	

slope = 5.72×10^{-3} min^{-1}, R^2 = 0.999.

Table AV 5. [**10c**] = 1.10×10^{-3} M, [DAMD] = 6.50×10^{-2} M, temp. = 29.0°C.

t (min)	A_t (λ = 470 nm)	$-\ln(A_\infty - A_t)$
0.0	0.386	1.013
3.0	0.393	1.033
33.0	0.457	1.231
63.0	0.502	1.398
93.0	0.538	1.556
123.0	0.570	1.720
153.0	0.595	1.871
183.0	0.620	2.048
213.0	0.638	2.198
243.0	0.652	2.333
273.0	0.668	2.477
303.0	0.686	2.740
∞	0.749	

slope = 5.35×10^{-3} min^{-1}, R^2 = 0.999.

Table AV 6. [10c] = 1.10×10^{-3} M, [DAMD] = 6.50×10^{-2} M, temp. = 25.0°C.

t (min)	A_t (λ = 486 nm)	$-\ln(A_\infty - A_t)$
0.0	0.258	1.262
34.0	0.288	1.374
64.0	0.313	1.478
94.0	0.333	1.570
124.0	0.350	1.655
154.0	0.365	1.737
184.0	0.379	1.820
214.0	0.391	1.897
∞	0.541	

slope = 2.86×10^{-3} min^{-1}, R^2 = 0.998.

Table AV 7. [10c] = 1.10×10^{-3} M, [DAMD] = 4.06×10^{-2} M, temp. = 25.0°C.

t (min)	A_t (λ = 476 nm)	$-\ln(A_\infty - A_t)$
0.0	0.295	1.162
30.0	0.327	1.269
60.0	0.353	1.366
90.0	0.377	1.465
120.0	0.398	1.561
150.0	0.416	1.650
180.0	0.433	1.743
210.0	0.446	1.820
240.0	0.459	1.904
∞	0.608	

slope = 2.82×10^{-3} min^{-1}, R^2 = 0.997.

Table AV 8. [10c] = 1.10×10^{-3} M, [DAMD] = 3.25×10^{-2} M, temp. = 21.0°C.

t (min)	A_t (λ = 478 nm)	$-\ln(A_\infty - A_t)$
0.0	0.297	1.162
45.0	0.324	1.252
90.0	0.347	1.336
135.0	0.366	1.411
180.0	0.383	1.483
225.0	0.401	1.565
270.0	0.415	1.635
315.0	0.426	1.693
∞	0.610	

slope = 1.65×10^{-3} min^{-1}, R^2 = 0.996.

Table AV 9. [10c] = 1.10×10^{-3} M, [DAMD] = 6.50×10^{-2} M, temp. = 21.0°C.

t (min)	A_t (λ = 457 nm)	$-\ln(A_\infty - A_t)$
4.0	0.501	0.801
44.0	0.532	0.872
84.0	0.561	0.944
124.0	0.584	1.005
164.0	0.604	1.061
204.0	0.621	1.112
244.0	0.638	1.165
284.0	0.654	1.217
324.0	0.667	1.262
364.0	0.681	1.313
404.0	0.694	1.363
444.0	0.707	1.415
484.0	0.718	1.461
524.0	0.727	1.501
∞	0.950	

slope = 1.37×10^{-3} min^{-1}, R^2 = 0.997.

Table AV 10. [**10c**] = 1.10×10^{-3} M, [DAMD] = 6.50×10^{-2} M, temp. = 17.0°C.

t (min)	A_t (λ = 470 nm)	$-\ln(A_\infty - A_t)$
0.0	0.342	1.016
60.0	0.360	1.070
120.0	0.375	1.112
180.0	0.392	1.165
240.0	0.405	1.207
300.0	0.419	1.255
360.0	0.432	1.302
420.0	0.446	1.355
480.0	0.457	1.398
∞	0.704	

slope = 7.95×10^{-4} min^{-1}, R^2 = 1.000.

Table AV 11. [**10c**] = 1.10×10^{-3} M, [DAMD] = 4.07×10^{-2} M, temp. = 17.0°C.

t (min)	A_t (λ = 478 nm)	$-\ln(A_\infty - A_t)$
0.0	0.275	1.162
80.0	0.301	1.248
160.0	0.320	1.317
240.0	0.337	1.382
320.0	0.351	1.440
400.0	0.366	1.505
480.0	0.379	1.565
560.0	0.392	1.630
∞	0.588	

slope = 7.68×10^{-4} min^{-1}, R^2 = 0.999.

AVI. Kinetic data of the oxidative addition of DMAD to $Pt_2I_2(\mu\text{-}PN_1)_2$ (HH), **10a**, in CH_2Cl_2.

Table AVI 1. [**10a**] = 2.89×10^{-4} M, [DAMD] = 1.08×10^{-2} M, temp. = 35.0°C.

t (min)	A_t (λ = 425 nm)	$-\ln(A_t - A_\infty)$
0.0	0.709	0.904
3.0	0.673	0.997
13.0	0.578	1.295
23.0	0.506	1.599
33.0	0.449	1.931
43.0	0.411	2.235
53.0	0.381	2.564
63.0	0.361	2.865
73.0	0.346	3.170
∞	0.304	

slope = 3.16×10^{-2} min^{-1}, R^2 = 0.997.

Table AVI 2. [**10a**] = 2.89×10^{-4} M, [DAMD] = 8.13×10^{-3} M, temp. = 35.0°C.

t (min)	A_t (λ = 425 nm)	$-\ln(A_t - A_\infty)$
0.0	0.709	0.880
20.0	0.546	1.366
30.0	0.489	1.619
40.0	0.449	1.845
50.0	0.414	2.096
60.0	0.390	2.313
70.0	0.366	2.590
80.0	0.350	2.830
90.0	0.337	3.079
∞	0.291	

slope = 2.39×10^{-2} min^{-1}, R^2 = 0.999.

Table AVI 3. [**10a**] = 2.89×10^{-4} M, [DAMD] = 1.08×10^{-2} M, temp. = 30.0°C.

t (min)	A_t (λ = 425 nm)	$-\ln(A_t - A_\infty)$
0.0	0.723	0.931
2.5	0.703	0.983
17.5	0.586	1.359
32.5	0.502	1.754
47.5	0.447	2.137
62.5	0.408	2.538
77.5	0.384	2.900
∞	0.329	

slope = 2.64×10^{-2} min^{-1}, R^2 = 0.999.

Table AVI 4. [**10a**] = 2.89×10^{-4} M, [DAMD] = 1.63×10^{-2} M, temp. = 30.0°C.

t (min)	A_t (λ = 425 nm)	$-\ln(A_t - A_\infty)$
0.0	0.732	0.919
3.0	0.684	1.047
13.0	0.574	1.423
23.0	0.494	1.826
33.0	0.439	2.244
43.0	0.401	2.688
53.0	0.375	3.170
∞	0.333	

slope = 4.20×10^{-2} min^{-1}, R^2 = 0.998.

Table AVI 5. [**10a**] = 2.89×10^{-4} M, [DAMD] = 1.63×10^{-2} M, temp. = 25.0°C.

t (min)	A_t (λ = 425 nm)	$-\ln(A_t - A_\infty)$
3.0	0.681	0.965
11.0	0.601	1.201
19.0	0.536	1.444
27.0	0.483	1.698
35.0	0.444	1.938
43.0	0.413	2.180
51.0	0.390	2.408
59.0	0.369	2.674
∞	0.300	

slope = 3.05×10^{-2} min^{-1}, R^2 = 1.000.

Table AVI 6. [**10a**] = 2.89×10^{-4} M, [DAMD] = 8.13×10^{-3} M, temp. = 25.0°C.

t (min)	A_t (λ = 425 nm)	$-\ln(A_t - A_\infty)$
3.0	0.683	0.965
15.0	0.619	1.149
27.0	0.563	1.343
39.0	0.519	1.528
51.0	0.476	1.749
63.0	0.446	1.938
75.0	0.420	2.137
87.0	0.399	2.333
∞	0.302	

slope = 1.65×10^{-2} min^{-1}, R^2 = 1.000.

Table AVI 7. [**10a**] = 2.89×10^{-4} M, [DAMD] = 1.63×10^{-2} M, temp. = 20.0°C.

t (min)	A_t (λ = 425 nm)	$-\ln(A_t - A_\infty)$
3.0	0.693	0.949
18.0	0.570	1.332
33.0	0.482	1.737
48.0	0.425	2.129
63.0	0.386	2.526
78.0	0.357	2.976
∞	0.306	

slope = 2.69×10^{-2} min^{-1}, R^2 = 0.999.

Table AVI 8. [**10a**] = 2.89×10^{-4} M, [DAMD] = 1.08×10^{-2} M, temp. = 20.0°C.

t (min)	A_t (λ = 425 nm)	$-\ln(A_t - A_\infty)$
0.0	0.714	0.856
5.0	0.684	0.929
25.0	0.571	1.266
45.0	0.488	1.614
65.0	0.432	1.945
85.0	0.393	2.263
105.0	0.365	2.577
125.0	0.346	2.865
∞	0.289	

slope = 1.63×10^{-2} min^{-1}, R^2 = 0.999.

Table AVI 9. [10a] = 6.63×10^{-4} M, [DAMD] = 1.33×10^{-2} M, temp. = 30.0°C.

t (min)	A_t (λ = 425 nm)	$-\ln(A_t - A_\infty)$
0.0	1.614	0.091
3.5	1.551	0.163
13.5	1.304	0.506
23.5	1.138	0.828
33.5	1.021	1.139
43.5	0.930	1.474
53.5	0.869	1.784
63.5	0.833	2.025
∞	0.701	

slope = 3.26×10^{-2} min^{-1}, R^2 = 1.000.

Table AVI 10. [10a] = 5.31×10^{-4} M, [DAMD] = 1.33×10^{-2} M, temp. = 30.0°C.

t (min)	A_t (λ = 430 nm)	$-\ln(A_t - A_\infty)$
0.0	1.178	0.392
3.5	1.123	0.476
13.5	0.946	0.812
23.5	0.820	1.146
33.5	0.721	1.519
43.5	0.669	1.790
53.5	0.621	2.129
∞	0.502	

slope = 3.25×10^{-2} min^{-1}, R^2 = 1.000.

Table AVI 11. [10a] = 4.09×10^{-4} M, [DAMD] = 1.33×10^{-2} M, temp. = 30.0°C.

t (min)	A_t (λ = 430 nm)	$-\ln(A_t - A_\infty)$
0.0	0.908	
3.5	0.857	
13.5	0.726	
23.5	0.631	
33.5	0.564	
43.5	0.517	
53.5	0.482	
∞	0.390	

slope = 3.23×10^{-2} min^{-1}, R^2 = 1.000.

Table AVI 12. [10a] = 2.83×10^{-4} M, [DAMD] = 1.33×10^{-2} M, temp. = 30.0°C.

t (min)	A_t (λ = 430 nm)	$-\ln(A_t - A_\infty)$
0.0	0.629	
3.5	0.601	
13.5	0.513	
23.5	0.448	
33.5	0.405	
43.5	0.373	
53.5	0.348	
∞	0.285	

slope = 3.17×10^{-2} min^{-1}, R^2 = 1.000.

AVII Kinetics of the oxidative addition of DMAD to $Pt_2I_2(\mu\text{-}PN_2)_2$ (HH), **10b.2/10b.3**, in CH_2Cl_2

Derivation of the rate-law for reactions 4.6 and 4.7:

Because **10b.2** and **10b.3**, **31.1** and **32.1**, as well as **31.2** and **32.2** are three enantiomeric sets, ε(10b.2) = ε(10b.3) etc.

$A_0 = A_0(10b.2) + A_0(10b.3) = \varepsilon(10b.2)([10b.2] + [10b.3])l = \varepsilon(10b.2)[10b.2/10b.3]l = \varepsilon C_i l$

Assuming **31.1/32.1** and **31.2/32.2** are formed in a fixed ratio, at the end of reaction: [31.2/32.2]:[31.1/32.1] = K, and [31.2/32.2] + [31.1/32.1] = C_i; x is the concentration of **10b.2/10b.3** at time t.

$$A_\infty = \varepsilon_{31.1}\frac{C_i}{1+K}l + \varepsilon_{31.2}\frac{KC_i}{1+K}l$$

$$A_t = x\varepsilon_{10b.2}l + \frac{C_i - x}{1+K}\varepsilon_{31.1}l + \varepsilon_{31.2}\frac{K(C_i - x)}{1+K}l$$

$$A_t - A_\infty = x(\varepsilon_{10b.2} - \frac{\varepsilon_{31.1} + K\varepsilon_{31.2}}{1+K})l$$

$$A_0 - A_\infty = C_i(\varepsilon_{10b.2} - \frac{\varepsilon_{31.1} + K\varepsilon_{31.2}}{1+K})l$$

$$\frac{A_t - A_\infty}{A_0 - A_\infty} = \frac{x}{C_i}$$

Thus, for a first-order reaction, a plot of $\ln(A_t - A_\infty)$ vs. t should be a straight line.

Table AVII 1. [**10b.2/10b.3**] = 2.18×10^{-4} M, [DAMD] = 8.13×10^{-3} M, temp. = 25.0°C.

t (min)	A_t (λ = 425 nm)	$-\ln(A_t - A_\infty)$
0.0	0.798	0.732
3.3	0.703	0.952
5.0	0.669	1.044
8.0	0.630	1.162
13.0	0.559	1.419
18.0	0.514	1.625
23.0	0.471	1.870
28.0	0.441	2.087
33.0	0.415	2.323
38.0	0.396	2.538
∞	0.317	

slope = 4.55×10^{-2} min^{-1}, R^2 = 0.999.

Table AVII 2. [**10b.2/10b.3**] = 2.18×10^{-4} M, [DAMD] = 8.13×10^{-3} M, temp. = 35.0°C.

t (min)	A_t (λ = 425 nm)	$-\ln(A_t - A_\infty)$
0.0	0.819	0.757
2.5	0.708	1.027
6.5	0.600	1.386
10.5	0.532	1.704
14.5	0.479	2.048
18.5	0.445	2.354
22.5	0.422	2.631
∞	0.350	

slope = 8.08×10^{-2} min^{-1}, R^2 = 0.998.

Table AVII 3. [**10b.2/10b.3**] = 2.18×10^{-4} M, [DAMD] = 8.13×10^{-3} M, temp. = 15.0°C.

t (min)	A_t (λ = 425 nm)	$-\ln(A_t - A_\infty)$
0.0	0.788	0.633
3.0	0.704	0.805
13.0	0.559	1.197
23.0	0.484	1.483
33.0	0.427	1.772
43.0	0.385	2.056
53.0	0.352	2.354
63.0	0.329	2.631
∞	0.257	

slope = 2.99×10^{-2} min^{-1}, R^2 = 0.996.

Table AVII 4. [**10b.2/10b.3**] = 2.18×10^{-4} M, [DAMD] = 8.13×10^{-3} M, temp. = 30.0°C.

t (min)	A_t (λ = 425 nm)	$-\ln(A_t - A_\infty)$
0.0	0.794	0.699
2.5	0.696	0.919
7.5	0.581	1.259
12.5	0.506	1.565
17.5	0.450	1.877
22.5	0.413	2.154
27.5	0.386	2.419
32.5	0.366	2.674
37.5	0.352	2.900
∞	0.297	

slope = 6.02×10^{-2} min^{-1}, R^2 = 0.996.

Table AVII 5. [10b.2/10b.3] = 2.18×10^{-4} M, [DAMD] = 8.13×10^{-3} M, temp. = 20.0°C.

t (min)	A_t (λ = 425 nm)	$-\ln(A_t - A_\infty)$
0.0	0.815	0.656
3.0	0.723	0.851
13.0	0.567	1.306
23.0	0.475	1.720
33.0	0.420	2.087
43.0	0.380	2.477
53.0	0.354	2.847
∞	0.296	

slope = 3.93×10^{-2} min^{-1}, R^2 = 0.997.

Table AVII 6. [10b.2/10b.3] = 2.18×10^{-4} M, [DAMD] = 4.07×10^{-3} M, temp. = 20.0°C.

t (min)	A_t (λ = 425 nm)	$-\ln(A_t - A_\infty)$
0.0	0.806	0.669
3.0	0.743	0.801
15.0	0.626	1.103
27.0	0.549	1.366
39.0	0.488	1.640
51.0	0.447	1.877
63.0	0.412	2.137
75.0	0.387	2.375
87.0	0.369	2.590
∞	0.294	

slope = 2.07×10^{-2} min^{-1}, R^2 = 0.996.

Table AVII 7. [10b.2/10b.3] = 2.18×10^{-4} M, [DAMD] = 1.62×10^{-2} M, temp. = 20.0°C.

t (min)	A_t (λ = 425 nm)	$-\ln(A_t - A_\infty)$
0.0	0.791	0.650
2.5	0.669	0.916
7.5	0.527	1.355
12.5	0.440	1.766
17.5	0.338	2.674
22.5	0.350	2.513
27.5	0.324	2.900
32.5	0.309	3.219
∞	0.269	

slope = 7.88×10^{-2} min^{-1}, R^2 = 0.998.

Table AVII 8. Activation parameters of reaction 4.6 and 4.7.

T(K)	k ($\times 10^2$ M^{-1}s^{-1})	1/T($\times 10^3$ K^{-1})	ln k/T
288.15	5.80	3.47	-8.511
293.15	8.06	3.41	-8.199
298.15	9.33	3.35	-8.070
303.15	12.3	3.30	-7.810
308.15	16.6	3.25	-7.526

AVIII. Kinetic data of the oxidative addition of DMAD to $Pt_2I_2(\mu\text{-}PN_2)_2$ (HH), **10b.1**, in CH_2Cl_2.

Table AVIII 1. [**10b.1**] = 1.99×10^{-4} M, [DAMD] = 8.13×10^{-3} M, temp. = 25.0°C.

t (min)	A_t (λ = 425 nm)	$-\ln(A_t-A_\infty)$
0.0	0.712	0.764
2.5	0.643	0.924
6.5	0.572	1.121
10.5	0.521	1.291
14.5	0.473	1.483
18.5	0.438	1.650
22.5	0.407	1.826
26.5	0.383	1.988
30.5	0.361	2.163
∞	0.246	

slope = 4.37×10^{-2} min^{-1}, R^2 = 0.999.

Table AVIII 2. [**10b.1**] = 1.99×10^{-4} M, [DAMD] = 4.07×10^{-3} M, temp. = 25.0°C.

t (min)	A_t (λ = 425 nm)	$-\ln(A_t-A_\infty)$
0.0	0.713	0.819
3.7	0.665	0.934
13.7	0.576	1.191
23.7	0.512	1.427
33.7	0.461	1.666
43.7	0.424	1.884
53.7	0.394	2.104
63.7	0.370	2.323
∞	0.272	

slope = 2.29×10^{-2} min^{-1}, R^2 = 0.999.

Table AVIII 3. [**10b.1**] = 1.99×10^{-4} M, [DAMD] = 1.62×10^{-2} M, temp. = 25.0°C.

t (min)	A_t (λ = 425 nm)	$-\ln(A_t-A_\infty)$
0.0	0.706	0.730
2.5	0.597	0.986
6.5	0.489	1.328
10.5	0.415	1.655
14.5	0.363	1.973
18.5	0.327	2.273
22.5	0.300	2.577
26.5	0.280	2.882
∞	0.224	

slope = 7.85×10^{-2} min^{-1}, R^2 = 0.999.

Table AVIII 4. [**10b.1**] = 1.99×10^{-4} M, [DAMD] = 1.22×10^{-2} M, temp. = 25.0°C.

t (min)	A_t (λ = 425 nm)	$-\ln(A_t-A_\infty)$
0.0	0.727	0.753
2.5	0.641	0.955
7.5	0.528	1.302
12.5	0.449	1.645
17.5	0.401	1.931
22.5	0.361	2.254
27.5	0.332	2.577
∞	0.256	

slope = 6.37×10^{-2} min^{-1}, R^2 = 0.999.

Table AVIII 5. **[10b.1]** = 1.99×10^{-4} M, [DAMD] = 2.04×10^{-2} M, temp. = 25.0°C.

t (min)	A_t (λ = 425 nm)	$-\ln(A_t - A_\infty)$
0.0	0.707	0.730
2.5	0.589	1.011
7.5	0.419	1.640
12.5	0.337	2.189
17.5	0.288	2.765
22.5	0.261	3.324
27.5	0.245	3.912
∞	0.225	

slope = 1.15×10^{-1} min^{-1}, R^2 = 1.000.

Table AVIII 6. **[10b.1]** = 1.99×10^{-4} M, [DAMD] = 2.44×10^{-2} M, temp. = 25.0°C.

t (min)	A_t (λ = 425 nm)	$-\ln(A_t - A_\infty)$
0.00	0.725	0.724
2.12	0.598	1.027
5.12	0.482	1.419
8.12	0.408	1.784
11.12	0.350	2.207
14.12	0.323	2.489
17.12	0.298	2.847
∞	0.240	

slope = 1.21×10^{-1} min^{-1}, R^2 = 0.998.

Table AVIII 7. **[10b.1]** = 1.99×10^{-4} M, [DAMD] = 2.71×10^{-2} M, temp. = 25.0°C.

t (min)	A_t (λ = 425 nm)	$-\ln(A_t - A_\infty)$
0.00	0.718	0.709
2.12	0.571	1.064
5.12	0.453	1.483
8.12	0.380	1.871
11.12	0.331	2.254
14.12	0.296	2.659
17.12	0.276	2.996
∞	0.226	

slope = 1.31×10^{-1} min^{-1}, R^2 = 0.998.

Table AVIII 8. **[10b.1]** = 1.99×10^{-4} M, [DAMD] = 3.26×10^{-2} M, temp. = 25.0°C.

t (min)	A_t (λ = 425 nm)	$-\ln(A_t - A_\infty)$
0.00	0.707	0.717
2.12	0.551	1.103
5.12	0.412	1.645
8.12	0.338	2.129
11.12	0.294	2.590
14.12	0.266	3.058
17.12	0.250	3.474
∞	0.219	

slope = 1.61×10^{-1} min^{-1}, R^2 = 0.998.

AIX

1.Calculation of the ΔG^o and ΔH^o values for Eq. 6.1,[a] and the ΔG values at different temperatures.

	maleic acid + H_2O ⟶		R, S-malic acid
Standard states:	crystalline	liquid	crystalline
ΔG_f^o (kcal/mol)	-149.40	-56.75	-211.45[b]
ΔH_f^o (kcal/mol)	-188.94	-68.37	-264.27

ΔG^o = -5.3 kcal/mol

ΔH^o = -6.96 kcal/mol

According to the Gibbs-Helmholtz equation:

$$\left[\frac{\partial(\Delta G/T)}{\partial T}\right]_P = -\frac{\Delta H^o}{T^2}$$

ΔG values at 100 and 170°C are calculated to be -4.9 and -4.5 kcal/mol, respectively.

(a) The ΔG_f^o and ΔH_f^o values are taken from: 1) Dean, J.A. *Handbook of Organic Chemistry*, McGraw-Hill: New York, 1987; S-22, S-26. 2) Kaye, G.W.C.; Laby, T.H. *Tables of Physical and Chemical Constants*, 15th ed.; Longman: London, 1986; p.268.

(b) The ΔG_f^o value for R, S-malic acid is unavailable; the value used in calculation is that for S-malic acid.

2. Visible absorption spectral parameters of $CrCl_3 \cdot 6H_2O$ solutions at various concentrations[a]

Table AIX 1. Visible absorption spectral data for $CrCl_3 \cdot 6H_2O$ solutions at various concentrations

[Cr] (M)	410 nm	572 nm	$\varepsilon_{410}/\varepsilon_{572}$
0.007	0.148	0.128	1.16
0.014	0.277	0.240	1.16
0.021	0.372	0.319	1.17
0.028	0.485	0.418	1.16
0.035	0.605	0.523	1.16

(a) Solutions in this series of experiments had been heated for 30 min at 100°C prior to the measurements; the ionic strength and acidity of the solutions were held relatively constant using 0.02 M HNO_3 and 0.20 M KNO_3; pH = 2.0.

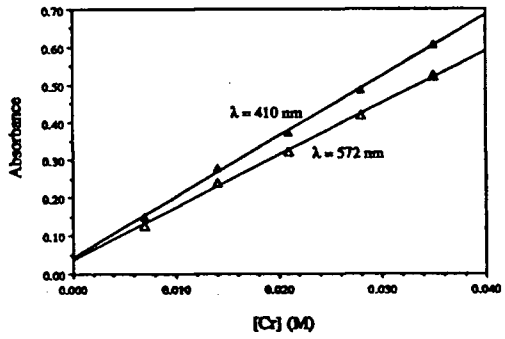

Fig. A 1. Plot of absorbance against [Cr] for $CrCl_3 \cdot 6H_2O$ solutions.

3. Determination of compositions and formation constants of maleato and malato Cr^{3+} complexes in aqueous solution at 100°C.

Table AIX 2. Absorbances at various Cr/[H_2MA] ratios[a]

V_{Cr} (mL)	V_{H_2MA} (mL)	$[Cr]_i/([Cr]_i + [H_2MA]_i)$	A_{572}
5.0	0.0	1.0	0.47
4.0	1.0	0.8	0.58
3.5	1.5	0.7	0.60
3.0	2.0	0.6	0.61
2.5	2.5	0.5	0.54
2.0	3.0	0.4	0.52
1.5	3.5	0.3	0.47
1.0	4.0	0.2	0.30
0.0	5.0	0.0	0.0

(a) $[Cr^{3+}]_i = [H_2MA]_i = 0.035$ M. Absorbances (A) were recorded at r.t, after the solutions were heated at 100°C for 30 min. The solution pH (~2.0) and ionic strength were held relatively constant using 0.02 M HNO_3 and 0.20 M KNO_3.

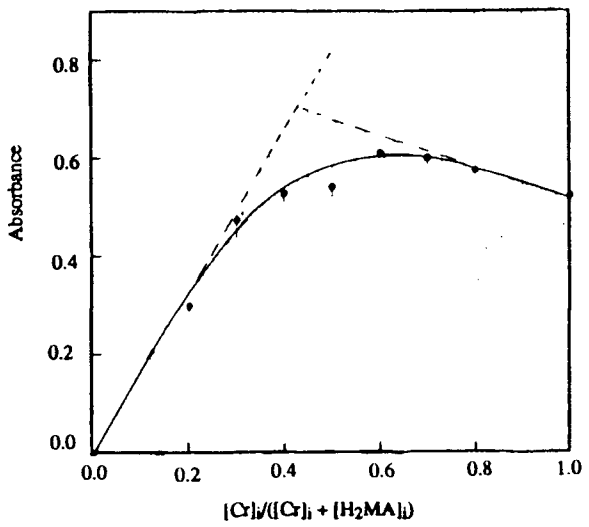

Fig. A.2. Job's plot; absorbance at 572 nm vs. $[Cr]_i/([Cr]_i + [H_2MA]_i)$; data from Table AIX 2.

Table AIX 3. Formation constants calculated based on the data from Fig. A.2 at selected molar ratios, pH = 2.0.

$\frac{[Cr]_i}{[Cr]_i + [H_2MA)]_i}$	$\frac{[Cr(HMA)]_{eq.}}{[Cr]_{eq.} + [Cr(HMA)]_{eq.}}$ (%)	K_1
0.50	71.6	8.3×10^2
0.45	76.9	7.6×10^2
0.40	81.7	7.6×10^2
0.35	87.0	9.0×10^2

$K_1 = 8.1 \times 10^2\ M^{-1}$

Table AIX 4. Absorbances at various [Cr]/[H_2mal] ratios[a]

V_{Cr} (mL)	V_{H_2mal} (mL)	$[Cr]_i/([Cr]_i + [H_2mal]_i)$	A_{562}
5.0	0.0	1.0	0.44
4.0	1.0	0.8	0.56
3.5	1.5	0.7	0.56
3.0	2.0	0.6	0.57
2.5	2.5	0.5	0.57
2.0	3.0	0.4	0.52
1.5	3.5	0.3	0.42
1.0	4.0	0.2	0.30
0.5	4.5	0.1	0.17
0.0	5.0	0.0	0.0

(a) $[Cr^{3+}]_i = [H_2mal]_i = 0.035$ M. Absorbances (A) were recorded at r.t, after the solutions were heated at 100°C for 30 min. The solution pH (~2.0) and ionic strength were held relatively constant using 0.02 M HNO_3 and 0.20 M KNO_3.

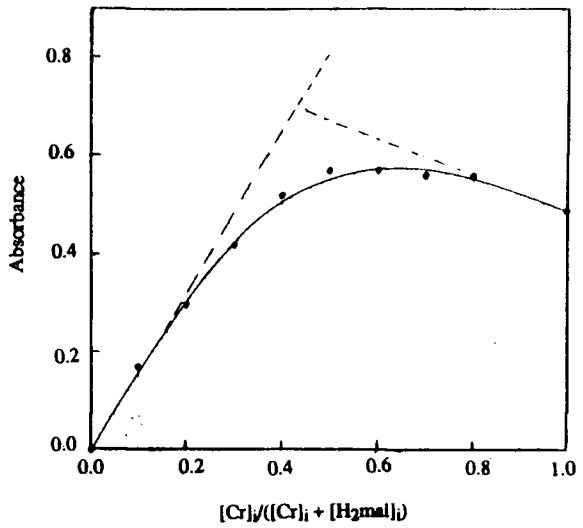

Fig. A.3. Job's plot; absorbance at 562 nm vs. $[Cr]_i/([Cr]_i + [H_2mal]_i)$; data from Table AIX 4.

Table AIX 5. Formation constants calculated based on the data from Fig. A.3 at selected molar ratios, pH = 2.0.

$\frac{[Cr]_i}{[Cr]_i + [H_2mal)]_i}$	$\frac{[Cr(Hmal)]_{eq.}}{[Cr]_{eq.} + [Cr(Hmal)]_{eq.}}$ (%)	K_2
0.50	67.9	9.8×10^3
0.45	72.6	8.8×10^3
0.40	76.9	8.5×10^3
0.35	82.4	9.6×10^3

$K_2 = 9.2 \times 10^3\ M^{-1}$

Table AIX 6. Absorbances at various $[Cr]/[H_2mal]$ ratios[a]

V_{Cr} (mL)	V_{H_2mal} (mL)	$[Cr]_i/([Cr]_i+[H_2mal]_i)$	A_{562}
4.0	1.0	0.8	0.58
3.5	1.5	0.7	0.63
3.0	2.0	0.6	0.64
2.5	2.5	0.5	0.62
2.0	3.0	0.4	0.53
1.5	3.5	0.3	0.48
1.0	4.0	0.2	0.31
0.5	4.5	0.1	0.19

(a) $[Cr^{3+}]_i = [H_2mal]_i = 0.035$ M. Absorbances (A) were recorded at r.t, after the solutions were heated at 100°C for 30 min. The solution pH (~2.4) and ionic strength were held relatively constant by 0.01 M HNO_3 and 0.20 M KNO_3.

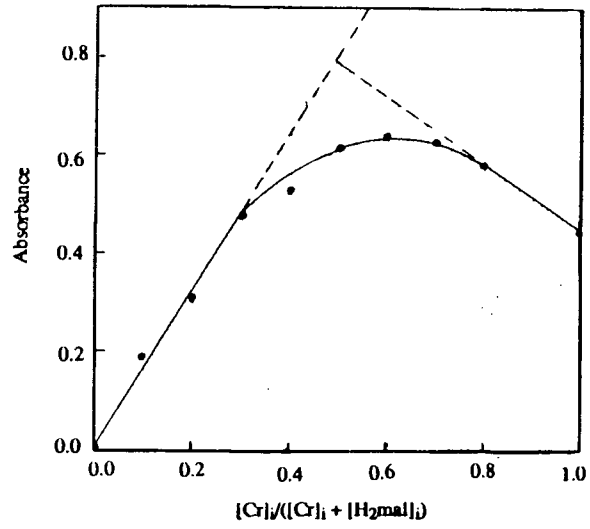

Fig. A.4. Job's plot; absorbance at 562 nm vs. $[Cr]_i/([Cr]_i + [H_2mal]_i)$; data from Table AIX 6.

Table AIX 7. Formation constants calculated based on the data from Fig. A.3 at selected molar ratios, pH = 2.4.

$\frac{[Cr]_i}{[Cr]_i + [H_2mal)]_i}$	$\frac{[Cr(Hmal)]_{eq.}}{[Cr]_{eq.} + [Cr(Hmal)]_{eq.}}$ (%)	K_2
0.50	76.5	8.7×10^3
0.45	81.0	7.2×10^3
0.40	87.7	9.0×10^3
0.35	93.0	1.1×10^4

$K_2 = 9.0 \times 10^3\ M^{-1}$

Sample calculation for the formation constant:

The equilibrium concentration for the malate monoanion [Hmal] is calculated using the K'_{a_1} expression, i.e.

$$[Hmal] = \frac{K'_{a_1}[H_2mal]_{tot}}{K'_{a_1} + [H^+]}$$

Thus,

$$K_2 = \frac{[Cr(Hmal)]}{[Cr][Hmal]} = \frac{[Cr(Hmal)](K'_{a_1} + [H^+])}{K'_{a_1}[Cr][H_2mal]_{tot}}$$

$[Cr] = [H_2mal]_{tot} = C_i - [Cr(Hmal)]$, where C_i is the initial concentration for both [Cr] and $[H_2mal]_{tot}$ as they are mixed in a 1:1 ratio. From the Job's plot, the percentage of the undissociated complex at the equilibrium is determined to be 76.5%, i.e. another 23.5% Cr^{3+} is present as the aquated ion.

Therefore, based on the data in Table AIX 6,

$$K_2 = \frac{0.765 \times 0.0175(10^{-3.4} + 10^{-2.4})}{(0.235 \times 0.0175)^2 \times 10^{-3.4}}$$
$$= 8.7 \times 10^3\ (M^{-1})$$

Similarly, at other molar ratios, K_2 values are calculated and given in Table AIX 7, the averaged K_2 value is $9.0 \times 10^3\ M^{-1}$.